Biochemical and biophysical characterization of the human TIM/TIPIN/CRY complex - a potential direct link between the circadian clock and the cell cycle

Dissertation

Zur Erlangung des Grades

Doktor der Naturwissenschaften

Am Fachbereich Biologie

Der Johannes Gutenberg-Universität Mainz

Tim Albert Grimmelsmann

Mainz, 2020

Abbreviations

ACN	Acetonitrile
ADP	Adenosine diphosphate
AEBSF	4-(2-aminoethyl)benzenesulfonyl fluoride hydrochloride
AEX	Anion exchange chromatography
APS	Ammonium persulfate
ATM	Ataxia Telangiectasia Mutated
ATP	Adenosine triphosphate
ATR	*Ataxia telangiectasia and Rad3-related protein*
BER	Base excision repair
bHLH	Basic-Helix-Loop-Helix
BMAL1	Brain and muscle ARNT-like 1
BS3	Bis-sulfosuccinimidyl suberate
CAEX	Cation exchange chromatography
CBD	CRY-binding-domain
cDNA	Complementary DNA
CEP131	Centrosomal Protein 131
CHAPS	3-[(3-cholamidopropyl)dimethylammonio]-1-propanesulfonate
CHK	Checkpoint kinase
CK	Casein kinase
CLOCK	Circadian Locomotor Output Cycles Kaput
CRY	Cryptochrome
CryoEM	Cryogenic electron microscopy
CT	Circadian time
CTD	C-terminal domain
CV	Column volume
DDR	DNA-damage response
DLS	Dynamic light scattering
Dmax	Maximal dimension
DMF	Dimethyl formamide
DMSO	Dimethyl sulfoxide
DOL	Degree of labeling
dsDNA	Double stranded DNA
E-Box	Enhancer box
EDTA	Ethylenediaminetetraacetic acid
FA	Formic acid
FAD	Flavin-adenin-dinucleotide
FASP	Familial advanced sleep phase
FBXL3	F-box/Leucine rich repeat protein 3
FDR	False discovery rate
FP	Fluorescence polarization
FPC	Fork-protection complex
FPLC	Fast protein liquid chromatography
γ-H2AX	Phosporylated H2A protein

GraFix	Gradient fixation
GRE	Glucocorticoid responsive elements
HU	Hydroxyurea
IMAC	Immobilized metal ion affinity chromatography
IPTG	Isopropyl β-D-1-thiogalactopyranoside
K_D	Dissociation constant
kDa	Kilodalton
LB	Luria Bertani Medium
MALS	Multi-angle light scattering
MES	2-(*N*-morpholino)ethanesulfonic acid
MOPS	3-(*N*-morpholino)propanesulfonic acid
MS	Mass Spectrometry
MW	Molecular weight
MW_{MALS}	MW determined by MALS analysis
MW_{PREP}	MW determined by preparative SEC
MW_{SEC}	MW determined by analytical SEC
NanoSPR	Nano Surface plasmon resonance
NER	Nucleotide excision repair
NHEJ	Non-homologous end joining
NLS	Nuclear localization site
PARP1	Poly ADP-ribose polymerase 1
PAS	PER-ARNT-SIM
PBL	Phosphate binding loop
PBS	Phosphate buffered saline
PCR	Polymerase chain reaction
PER	Period
PHR	Photolyase homology region
PMSF	Phenylmethylsulfonyl fluoride
PSM	Peptide spectrum matches
Rg	Radius of gyration
Rh	Hydrodynamic radius
RNAi	RNA interference
RT	Room temperature
SAXS	Small-angle X-ray scattering
SCN	Suprachiasmatic nucleus
SEC	Size exclusion chromatography
SILAC	Stable Isotope Labeling by Amino acids in Cell culture
SLIC	Sequence and ligation independent cloning
SOC	Super optimal broth with added glucose
ssDNA	Single stranded DNA
TAD	Transactivation domain
TAE	Tris-acetate-EDTA buffer
TB	Terrific broth
TCEP	Tris(2-carboxyethyl)phosphin
TEMED	Tetramethylethylenediamine
TIM	TIMELESS
TIPIN	TIMELESS-interacting protein

TTFL	Transcription-translation feedback loop
TTP	TIM/TIPIN complex
WT	Wild-type
X-Gal	5-bromo-4-chloro-3-indolyl-β-D-galactopyranoside
XLMS	Crosslink Mass Spectrometry
XPA	Xeroderma pigmentosum group A
YFP	Yellow fluorescent protein
YLPM1	YLP motif-containing protein 1

Table of Contents

1 Zusammenfassung

Die innere Uhr beeinflusst das Verhalten vieler Lebensformen und ist funktionell verbunden mit der DNA Replikation und der zellulären Reaktion auf DNA Schäden. Circadiane Regulatoren können auf diese Prozesse Einfluss nehmen, indem sie die Biosynthese von daran beteiligten Proteinen steuern oder direkt mit diesen interagieren. Der zentrale circadiane Repressor CRY interagiert mit dem TIM/TIPIN Komplex, der in die Signaltransduktion von stockenden Replikationsgabeln und DNA Schäden involviert ist. CRY kann TIMs Fähigkeit, die CHK1 Kinase zu aktivieren, beeinflussen. Nach Aktivierung der CHK1 Kinase, aktiviert CHK1 Prozesse wie den Zellzyklusarrest in der S-Phase und DNA Reparatur. Es ist unklar, wie die Interaktion von CRY und TIM/TIPIN reguliert ist und ob es sich um eine direkte Interaktion handelt oder ob sie Teile eines gemeinsamen großen Komplexes sind.

Mit isolierten Proteinen konnten wir zeigen, dass CRY TIM/TIPIN direkt band und einen trimeren Komplex bildete. Wir haben beobachtet, dass sich die beiden CRY Paraloge (CRY1 und CRY2) in ihrer Affinität zu TIM/TIPIN unterschieden und dass CRY2 mit einer höheren Affinität band. Dieser Effekt war möglicherweise auf die flexiblen C-terminalen Anhänge von CRY zurückzuführen, die sich zwischen CRY1 und CRY2 stark unterscheiden. Wir vermuten, dass dieser Unterschied auf unterschiedliche Interaktionen des CRY Anhangs mit einer bisher funktionell unbeschriebenen Proteinschleife von TIM zurückzuführen ist. Diese Proteinschleife war für die Bindung an CRY nicht essentiell und ihre Deletion verursachte, dass die CRY Proteine TIM/TIPIN mit gleicher Affinität banden. Mit Hilfe von *Small-Angle X-Ray Scattering* und Crosslink Massenspektrometrie Daten erstellten wir ein hypothetisches Modell für einen CRY/TIM Komplex. Initiale *Pulldown* Experimente konnten Kandidatenproteine identifizieren, welche durch die TIM Proteinschlaufe beeinflusst werden könnten.

Die Beobachtung des direkten trimeren Komplexes zwischen CRY und TIM/TIPIN deutet an, dass diese Proteine eine direkte Verbindung zwischen der inneren Uhr und der zellulären Reaktion auf DNA Schäden und Replikationsstress darstellen. Unterschiedliche Bindungsaffinitäten zwischen den CRY Paralogen und TIM/TIPIN lassen funktionelle Unterschiede vermuten und geben einen Hinweis auf die funktionelle Bedeutung der C-terminalen CRY Anhänge. Die TIM Proteinschleife wurde bisher nicht funktionell beschrieben, und ihr Effekt auf die CRY Bindung könnte ein weiteres regulatorisches Detail darstellen. Die

im *Pulldown* identifizierten Kandidatenproteine könnten als Ausgangspunkt für eine weitere funktionelle Charakterisierung der TIM Proteinschlaufe dienen.

2 Abstract

The circadian clock controls the behavior of many lifeforms and is functionally connected to DNA replication and DNA damage response. Central circadian regulators influence cell cycle and DNA damage response by altering protein expression of regulatory factors or by interacting with them. The central circadian repressor CRY interacts with the TIM/TIPIN complex, that is involved in signaling of stalled replication forks and DNA damage. CRY affects TIMs' ability to activate the CHK1 kinase which in turn leads to activation of cell cycle checkpoints and repair of DNA damage. It is not clear how the interaction is achieved, whether there is a direct interaction of both proteins or if they are parts of a larger complex.

With purified proteins we showed that CRY bound TIM/TIPIN in a direct manner and formed a stoichiometric trimeric complex. We found that the two human CRY paralogs (CRY1 and CRY2) differ in their affinity to TTP and that CRY2 bound with higher affinity. This was possibly due to the highly variable tails between CRY1 and CRY2 as most divergent feature between CRY1 and CRY2. We furthermore confirmed data from literature, that the TIM N-Terminus is sufficient to bind CRY. A functionally undescribed loop within TIM was dispensable for CRY binding, but caused both CRYs to bind with different affinities, indicating a further regulatory detail. Using Small-Angle X-Ray scattering and Crosslink MS, we created a hypothetical model to visualize the interaction of CRY and TIM. Initial pulldown experiments identified candidate proteins that might be affected by the TIM loop.

The observation of a direct trimeric complex of TTP/CRY indicates that CRY and TIM/TIPIN functionally connect the circadian clock with signaling of DNA damage and replication stress. Different binding affinities of CRY1 and CRY2 to TTP give a hint in order to understand functional differences between the CRY paralogs and indicate functional importance of the C-terminal CRY tails. The TIM loop was not functionally described before and its effect on CRY binding could indicate an additional regulatory detail. The candidate proteins identified in a TIM loop dependent pulldown could serve as a starting point for functional characterization of the TIM loop.

3 Introduction

3.1 Circadian Clocks

Circadian clocks are internal timekeepers that generate a 24 h 'circadian' (lat. Circa diem – about a day) rhythm. This internal clock allows organisms to adapt their behavior and physiology to 24-hour day-night changes. The importance of circadian clocks is underlined by the Nobel Prize for Physiology or Medicine in 2017, which was awarded to Jeffrey C. Hall, Michael Rosbash and Michael W. Young for describing molecular mechanisms controlling circadian rhythms. Circadian rhythms are found in all lifeforms; from unicellular organisms like the Cyanobacterium *S. elongates* to multicellular organisms such as the fruit fly *D. melanogaster* and mammals such as mice and humans. One of the classical examples of circadian rhythmicity, which was already observed in the 18th century, is the plant *Mimosa pudica*, that shows leaf movement in a day and night rhythm. This regular movement is continued even in the absence of light and dark shifts (Bass, 2012). Mice show a clear pattern of resting and activity distributed over day and night times. This activity is also continued in constant dark conditions and it is accompanied by a variety of physiological effects, such as blood pressure, release of stress hormones and body temperature (Sheward *et al*, 2010).

One reason for the evolutionary development of circadian clocks is an 'escape from light' hypothesis. It suggests that organisms have developed a circadian clock to anticipate light and dark phases of the day to protect sensitive processes from UV radiation and protect DNA integrity (Shostak, 2017). In addition, a molecular clock can increase fitness of the organism by allowing to prepare for changing environmental conditions, instead of merely reacting to acute stimuli. For example, in the liver the expression of genes involved in gluconeogenesis and energy metabolism precedes the onset of activity in order to be prepared for energy storage. A similar effect can be observed for glucose transporters before the onset of feeding time (Langmesser & Albrecht, 2006).

Signals that appear and disappear in a 24h fashion can entrain the circadian clock; they act as 'Zeitgeber' (german for time cues). The most important 'Zeitgeber' is light. In mammals, light is received by the photo pigment Melanopsin, which is present in the retina of the eye. Before the discovery of Melanopsin, rods and cones were considered the only light sensitive parts of

the mammalian eye. This idea was questioned by a study on blind persons that were unable to form visual images. Surprisingly, those persons are able to sense light to control melatonin secretion (Czeisler *et al*, 1995). Those light sensitive cells are called intrinsically photosensitive retinal ganglion cells (ipRGC). Mice that are genetically depleted of those cells, but could otherwise form normal vision, are unable to synchronize their circadian clock to light (Güler *et al*, 2008).

The light signal that is perceived in the retina is transferred to the so-called "master clock". In the early 1970s, it was shown that the selective destruction of the suprachiasmatic nucleus (SCN) in the hypothalamus of the brain leads to a complete loss of the circadian rhythmicity (Stephan & Zucker, 1972; Moore & Eichler, 1972). Later, the confirmation that the SCN is the location of the master clock was confirmed by experiments, which showed the restoration of the rhythm in arrhythmic animals upon transplantation of SCN cells (Ralph *et al*, 1990).

In addition to the master clock in the SCN, in most organs there are peripheral clocks that are synchronized by the SCN. Those peripheral clocks display autonomous rhythms in isolation (Dibner *et al*, 2010), but still receive input from the SCN *in vivo*. Circadian oscillators of individual cells and tissues respond differently to entrainment, control different physiological outputs and interact with each other and the system as a whole (Balsalobre *et al*, 1998; Nagoshi *et al*, 2004; Yoo *et al*, 2004). The clock mechanics are almost identical to those in the master clock.

In contrast to the master clock, the peripheral clocks receive inputs from their physiological environment (e.g. food intake). Signal transfer from the SCN to peripheral clocks is organized by the nervous system that innervates peripheral organs and through hormonal pathways. The most prominent candidates are the glucocorticoids, which are released in a rhythmic pattern. Glucocorticoid responsive elements (GRE) are present in regulatory regions of many clock genes (*Bmal1, Cry1, Per1, Per2*) (Reddy *et al*, 2007; Yamamoto *et al*, 2005; So *et al*, 2009). In contrast to the SCN clock, peripheral clocks are sensitive to temperature and can be reset by temperature pulses (Brown *et al*, 2002; Buhr *et al*, 2010). It was observed that food intake during the resting phase completely reverses the clock gene expression in the liver, heart, kidney and pancreas (Damiola, 2000). In addition, peripheral clocks can be entrained by scheduled feeding, leading to food anticipation activities such as an increased arousal and activity during the time before feeding (Stephan, 2002; Stephan *et al*, 1979; Mistlberger, 1994).

There are studies that link circadian misalignments with diseases such as cancer. In a study, female flight attendants, which are exposed the frequent time shifts by travel through different time zones, have an increased risk of developing breast cancer (Pukkala *et al*, 1995). In addition, people working in shifts show an increased risk of developing different kinds of cancers as well (Filipski & Lévi, 2009). A chronic jet-lag also increases mortality in aged mice (Davidson *et al*, 2006).

3.1.1 Molecular clock

After light perception, the information is transferred to the master clock. The master clock creates a transcription-translation-feedback-loop (TTFL) by the activity of two central regulatory complexes, the transcriptional activator Circadian Locomotor Output Cycles Kaput (CLOCK) (Gekakis, 1998)) and Brain and Muscle ARNT-Like 1 (BMAL1) (Bunger et al. 2000) as well as the transcriptional repressors Cryptochrome and Period (CRY and PER) (Tei *et al*, 1997; Zheng *et al*, 1999; Zylka *et al*, 1998; Kume *et al*, 1999). CLOCK and BMAL1 form a heterodimeric transcription factor, that translocates into the nucleus and binds to E-box elements in promotor regions of the genome. The CLOCK/BMAL1 complex activates the transcription of *Cry* and *Per* genes, which form the repressive arm of the feedback loop, and of other clock controlled genes (*Ccg*). The CRY and PER proteins also form a heterodimer, translocate into the nucleus, where they bind to CLOCK/BMAL1 leading to inhibition of their transcriptional activation in the late afternoon/evening. After ubiquitination, CRY and PER are degraded by the proteasome, finally closing the loop by allowing another round of transcriptional activation by CLOCK/BMAL1. In addition, the CRY and PER complexes are tightly regulated by kinases and phosphatases (CKIα, CKIδ, CKIε, PP1, PP5), that control the rate of nuclear entry and degradation relative to their phosphorylation status. A genome wide analysis in mouse liver by chromatin-immunoprecipitation sequencing (ChiP-Seq) identified 4,600 and 5,900 binding sites for CLOCK and BMAL1 and even 16,000 and 10,000 binding sites for CRY1 and CRY2, respectively, which explains the large impact of the circadian clock on the behavior of the whole organism (Koike *et al*, 2012). 4-17% of all the genes expressed in various mouse organs show cycling of mRNA products (Zhang *et al*, 2014).

A second TTFL is created by the nuclear receptors reverse strand of ERB (REV-ERB) and the retionoic-acid related orphan receptor (ROR). ROR is a transcriptional activator of *Bmal1* expression, that competes with REV-ERB, a negative regulator, for binding at ROR responsive

elements (RRE) in the promotor of *Bmal1* (Guillaumond *et al*, 2005; Preitner *et al*, 2002; Sato *et al*, 2004; Ueda *et al*, 2002). This allows fine tuning of *Bmal1* expression (Figure 1).

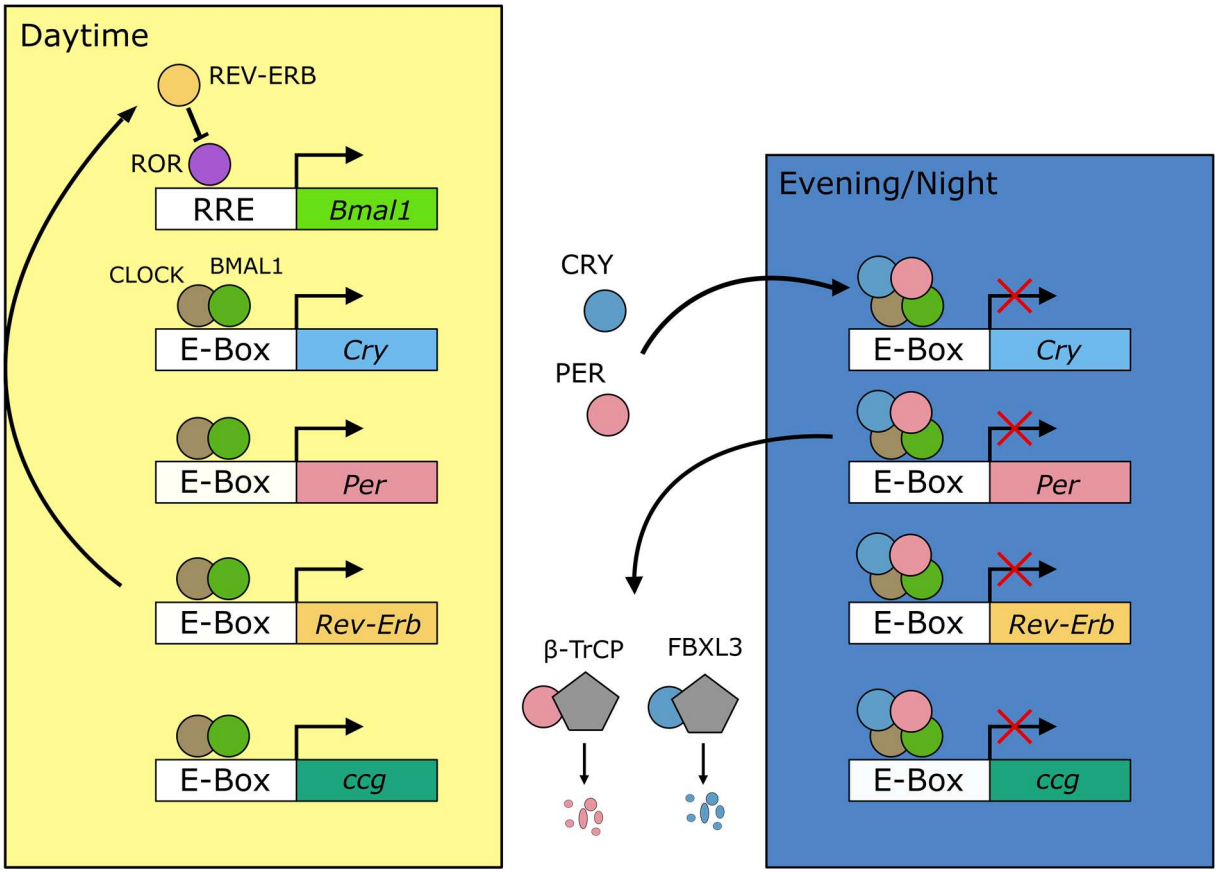

Figure 1: Overview of the circadian clock of mammals. The heterodimeric transcription factor CLOCK/BMAL1 translocates into the nucleus and binds to E-Box elements in promotor regions of many genes. This activates transcription of *Cry* and *Per* genes. The CRY and PER proteins form a heterodimer, which is imported into the nucleus and binds to CLOCK/BMAL1 to repress transcription. After E3 ligase mediated degradation of PER and CRY, the repression is relieved and the cycle can start again. *Rev-Erb* is another gene under CLOCK/BMAL1 control. The REV-ERB protein competes with ROR for the binding, which regulates rhythmic expression of *Bmal1*. Figure inspired by (Rosensweig & Green, 2018).

The circadian entrainment of the clock is signaled by Ca^{2+} influx into the SCN cells. This triggers a set of signaling kinases involving calmodulin-dependent protein kinase II (CaMKII), mitogen-activated protein kinases (MAPK), protein kinase A (PKA) leading to phosphorylation of cAMP response element binding protein (CREB). Phosphorylated CREB can bind to cAMP response elements (CRE) in promotor regions of *Per1* and *Per2* genes, which are also activated by binding of CLOCK/BMAL1 to E-box elements in their promotor regions (Golombek & Rosenstein, 2010).

3.1.2 The activating complex

CLOCK/BMAL1 form a heterodimeric basic Helix Loop Helix (bHLH) transcription factor, that binds to the CACGTG E-Box sequence in the genome. The structure is asymmetric and both proteins interact with each other *via* their PER-ARNT-SIM (PAS-A, PAS-B) domains (Huang *et al*, 2012). CLOCK and BMAL1 contain unstructured C-terminal regions that are important for regulation of their activity.

At CT0, the beginning of the subjective day, the circadian phase starts with CLOCK/BMAL1 being bound to DNA. CRY1 is bound to CLOCK/BMAL1 as well, independently of PER (Stratmann *et al*, 2010; Ye *et al*, 2011). CRY1 delays CLOCK/BMAL1 activated transcription, creating a so-called transcriptionally inactive, poised state. After CRY1 dissociation, the acetyltransferases p300/CBP (CREB binding protein) bind to CLOCK/BMAL1, which act as coactivator. This leads to histone acetylation and provides an accessible chromatin structure for transcription to begin (Curtis *et al*, 2004; Hosoda *et al*, 2009). In addition, CLOCK was also reported to have an intrinsic histone acetylation activity (Doi *et al*, 2006; Hirayama *et al*, 2007). CLOCK/BMAL1 interact with mixed lineage leukaemia 1 (MLL1). MLL1 is important for CLOCK recruitment to DNA (Katada & Sassone-Corsi, 2010) and is furthermore involved in rhythmic trimethylation (H3K4me3), a histone marker that is associated with high promotor activity. In this pre-initiation complex RNA polymerase II (RNAPII) binds in a hypophosphorylated state, which is later phosphorylated at its C-terminal domain (CDT) to initiate transcription (Jones *et al*, 2004; Chapman *et al*, 2007).

3.1.3 The repressive complex

In the late afternoon, early night, the repressive complex forms. It is large and contains at least 25 proteins. In addition to the core repressors CRY and PER, it consists of many other proteins such as Non-POU domain-containing octamer-binding protein (NONO), WD repeat-containing protein 5 (WDR5) (Brown, 2005), the probable helicase senataxin (SETX) (Padmanabhan *et al*, 2012) and the nucleosome remodeling and histone deacetylation complex (NuRD) (Kim *et al*, 2014). NONO is involved in RNA processing and WDR5 is a member of the histone methyltransferase complex. SETX was shown to be involved in transcriptional termination. PER antagonizes the action of SETX, thereby inhibiting termination at 3' termination sites and thus blocking another round of transcription by RNAPII (Padmanabhan *et al*, 2012). CLOCK/BMAL1 associate with chromodomain helicase DNA binding protein 4 (CHD4) and metastasis-associated 1 family member 2 (MTA2), components of the NuRD complex, that do

not constitute a functional complex. However, the repressive complex with PER contains methyl-CpG-binding domain protein 2 (MBD2), GATA zinc finger domain containing protein 2A (GATAD2A), histone deacetylase 1 (HDAC1) and retinoblastoma binding protein p48 (RBAP48), that reconstitute a functional NuRD complex, which deacetylates histones, leading to repression (Kim *et al*, 2014). Polycomb repressive complex 2 (PRC2) can be recruited as well, which leads to trimethylation of H3K27 to inhibit gene expression (Etchegaray *et al*, 2006).

The repressive complex is largely influenced by its core components PER and CRY. Their degradation and translocation to the nucleus is what controls formation of the repressive complex and the circadian phase. The degradation of PER is mediated by casein kinase 1 (CKI) dependent phosphorylation. Phosphorylation results in association with the E3-Ligase β-transducin repeat-containing protein (β-TrCP), which causes ubiquitination and subsequent proteasomal degradation (Camacho et al. 2001; Eide et al. 2005; Akashi et al. 2002; Miyazaki et al. 2004). PER2 can be phosphorylated by CKII as well (Tsuchiya *et al*, 2009). In contrast, a phosphorylation at Ser662 and four other serines located downstream leads to stabilization of PER2 (Hirano *et al*, 2016; Vanselow *et al*, 2006; Shanware *et al*, 2011). Protein phosphatase 1 (PP1) dephosphorylates PER2 and counteracts the CKI mediated degradation (Gallego *et al*, 2006). Protein phosphatase 5 (PP5) indirectly stabilizes PERs by preventing auto-phosphorylation of CKI, which leads to its inhibition (Budini *et al*, 2009). PER1, CRY1 and CRY2 can be de-ubiquitinated by USP-2 (Ubiquitin carboxyl-terminal hydrolase 2) increasing their stability (Scoma *et al*, 2011; Yang *et al*, 2012). The *tau* mutation in CKIε (isoform ε of CKI) causes shortening of the circadian period (Lowrey, 2000). It is described as a gain-of-function mutation, that leads to destabilization of PER proteins, by targeting it for β-TrCP degradation mediated degradation. $CKI\varepsilon^{tau}$ asymmetrically targets PER proteins, not CRY (Meng *et al*, 2008).

CRY1 is phosphorylated by AMP-activated protein kinase (AMPK) at Ser71, which induces ubiquitination of CRY by F-box/leucine rich-repeat protein 3 (FBXL3) and subsequent degradation (Lamia *et al*, 2009). FBXL3 competes with FBXL21 for CRY binding, which leads to a stabilization of CRY (Yoo *et al*, 2013). Dual-specificity tyrosine-phosphorylation regulated kinase 1A (DYRK1A) phosphorylates CRY2 at Ser557, which is followed by phosphorylation of Ser553 by Glycogen synthase kinase 3-β (GSK-3β). This sequential phosphorylation results in degradation of CRY2 mediated by an unknown E3 ligase (Kurabayashi *et al*, 2010; Harada

et al, 2005). Phosphorylation of CRY1 at Ser588 by an unknown kinase leads to its stabilization as this modification blocks FBXL3 binding (Gao *et al*, 2013).

The compounds KL001 and Longdaysin lead to a period lengthening through stabilization of CRY and PER, respectively, by blocking their degradation. KL001 competes with FBXL3 for the Flavin adenine dinucleotide (FAD) binding pocket in CRY and Longdaysin inhibits CKI activity, which is responsible for PER degradation (Hirota *et al*, 2012, 2010).

3.1.4 The CRY/PER complex

PER is a large protein of 1257 amino acids, that consists mainly of unstructured regions, which allow interactions with multiple partners (Cortese *et al*, 2008). The only structured parts are the PAS domains (*Figure 2*), which span amino acids 191-315 (PAS-A) and 329-435 (PAS-B) (Gustafson & Partch, 2015). PAS domains form a large family of conserved structures, that facilitate various functions, such as sensing of light, redox potential, oxygen levels and protein binding (Taylor & Zhulin, 1999). The PAS domains of PER mediate its binding to the PAS domains of CLOCK/BMAL1, they are essential for the complex formation. The PAS domains are implicated in recruitment of PER to the repressive complex as deletion of PAS-B reduces the amount of co-precipitated PER2 with CLOCK/BMAL1 (Chen *et al*, 2009). The binding site for CRY is located at the C-Terminus of PER2. Several elements of CRY are involved in binding of PER2, creating a large interface between both proteins. Furthermore, CRY and PER harbor a Zn^{2+} ion in their interface which is coordinated by cysteines and histidines. Upon binding, the CRY-binding domain (CBD) of PER2 adopts a partially helical structure (Schmalen *et al*, 2014; Nangle *et al*, 2014). The binding site for the kinases CKI_{δ} and CKI_{ε} are indicated by KB1 and KB2 (Figure 2), that have a SYQ and LT motif (Lee *et al*, 2004) and are very conserved across phyla. The multisite phosphorylation area (P) lies in between both binding sites and controls the activity of PER (Toh, 2001).

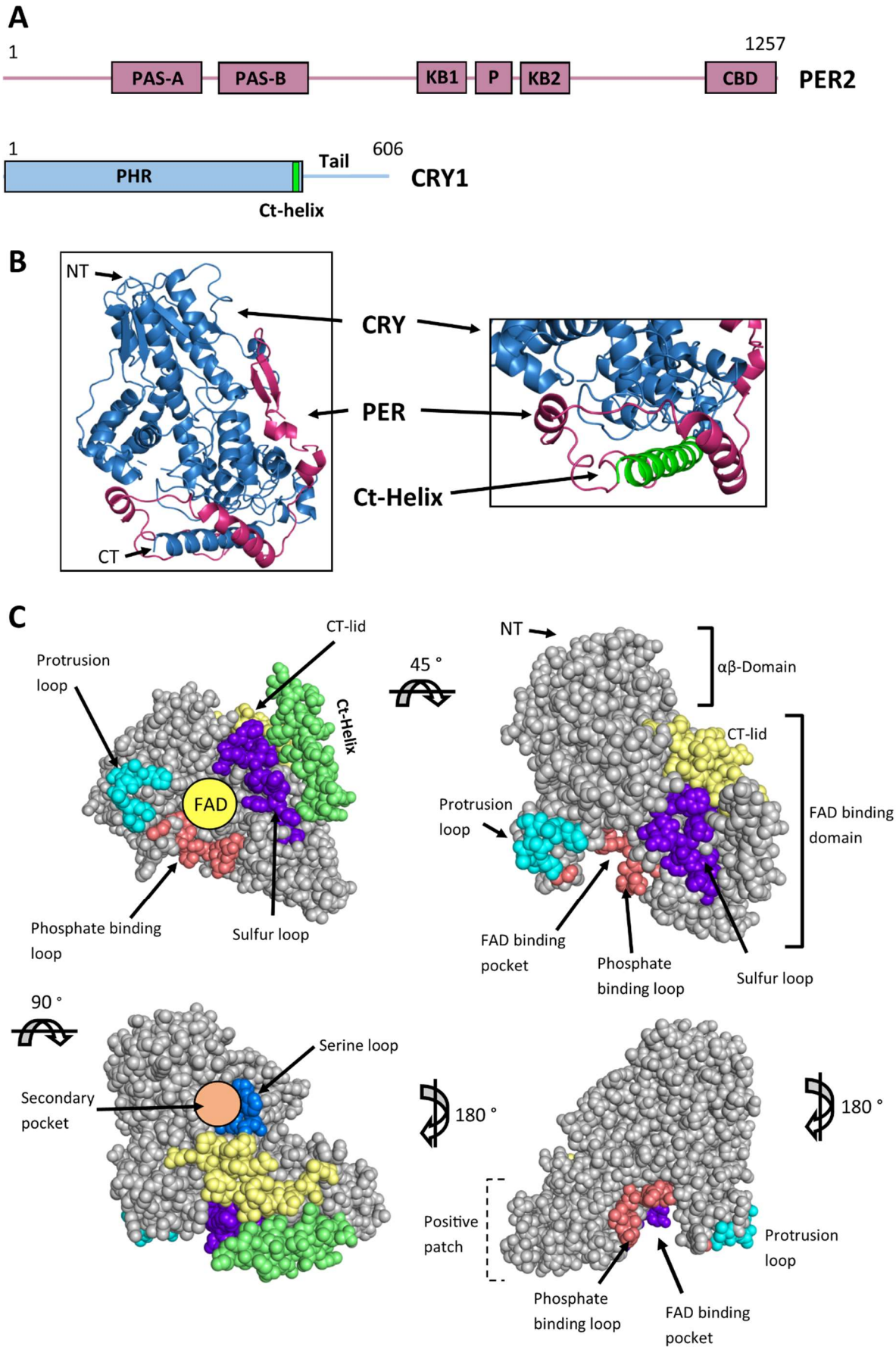
A
1
1257
PAS-A
PAS-B
KB1
P
KB2
CBD
PER2
1
606
Tail
PHR
CRY1
Ct-helix
B
NT
CRY
PER
Ct-Helix
CT
C
CT-lid
Protrusion loop
Ct-Helix
FAD
Phosphate binding loop
Sulfur loop
45 °
NT
αβ-Domain
CT-lid
Protrusion loop
FAD binding domain
FAD binding pocket
Phosphate binding loop
Sulfur loop
90 °
Serine loop
Secondary pocket
180 °
180 °
Positive patch
Protrusion loop
Phosphate binding loop
FAD binding pocket

Figure 2: Schematic overview about the different functional domains of the mammalian PER and CRY proteins. A) PER is a mostly unstructured protein, but contains the conserved PER-ARNT-SIM (PAS) domains as folded parts and a CRY binding domain (CBD), which folds upon CRY binding. It contains two kinase binding sites for $CKI_{\delta,\varepsilon}$ (KB1, KB2) and phosphorylation sites (P) in between them. CRY contains the photolyase homology region (PHR) and an unstructured C-terminal tail. The PHR contains a C-terminal α-helix (Ct-helix, helix22) which facilitates interactions with many partners. B) Structural overview of the mCRY1-PHR/mPER2-CBD complex (left, blue/red), with a zoom of the CT-helix (right, green). C) Overview of functionally relevant loops in the CRY structure. In dCRY, the phosphate binding loop and the protrusion loop create a lid to effectively trap FAD in the FAD binding pocket. The sulfur loop contains electron-rich residues (Met331, Cys337) that appear to affect the photoreduction and dark recovery time in dCRY (Czarna *et al*, 2013). In inactive dCRY its C-Terminus is trapped in a cavity formed by the phosphate binding loop, the protrusion loop and the C-terminal lid. The secondary pocket and the serine loop trap the antenna chromophore in photolyases. Figure was prepared using PDB-ID: 4CT0.

3.1.5 Structure of CRY

CRY consists of two parts: the photolyase homology region (PHR), and a C-terminal extension called CRY 'tail'. The PHR of CRY consists of a N-terminal αβ-domain and a helical FAD binding domain, that are connected by an unstructured linker. The PHR, as the name suggests, shares a large homology with the photolyases, a group of light sensitive enzymes responsible for repair of DNA photolesions. Photolyases use flavine adenine dinucleotide (FAD) as a cofactor, and, absorbing light energy sets off an electron transfer cascade that leads to split of the pyrimidine photoproducts (Müller & Carell, 2009). In contrast, CRY in *D. melanogaster* (dCRY) is a light sensitive protein that is essential for photoentrainment of the circadian clock. It senses blue light by FAD, which triggers an electron transfer leading to a structural rearrangement of its C-Terminus. In the inactive state the helix in its C-Terminus is bound to a cavity in the PHR created by the phosphate binding loop (PBL; originally named after the phosphate binding property of the 6-4 photolyase in *A. thalina*), the protrusion loop (an extended surface loop close to the phosphate binding loop) and the C-terminal lid (Zoltowski *et al*, 2011; Czarna *et al*, 2013). Photoactivated dCRY binds to dTIMELESS (dTIM), one of the central repressors of the *D. melanogaster* clock. dTIM is subsequently degraded and the transcriptional repression is abolished, which allows for another round of transcriptional activation (Merbitz-Zahradnik & Wolf, 2015). Such an effect was not observed for mammalian CRY. However, findings suggest FAD binding of mammalian CRY. It was observed that FAD could lead to a stabilization of CRY by a light-independent mechanism (Xing *et al*, 2013; Hirano *et al*, 2017), possibly by competing with FBXL3, which specifically targets the FAD

binding pocket. Although, it was reported that human CRY1 showed photoreduction of FAD by blue light after overexpression in living insect cells (Hoang *et al*, 2008) and human CRY2 was also considered to have light dependent magnetoreceptive function (Foley *et al*, 2011). Finally, the function of the cofactor pocket and FAD binding is not very well understood in mammals.

Mammalian CRY binds FAD with low affinity 16 – 64 μM (Kutta *et al*, 2017). This is explained by structural differences that surround the FAD binding pocket. mCRY adopts a more open conformation of the FAD binding pocket compared to dCRY. This is caused by two loops adjacent to the FAD binding pocket: The phosphate binding loop, that is partially disordered in mCRY and the protrusion loop which is shortened by seven residues compared to dCRY (Czarna *et al*, 2013; Zoltowski *et al*, 2011). Although it was reported that mammalian CRY comprises conserved residues inside the FAD binding pocket that are important for Cofactor binding.

There is a secondary pocket in CRY that corresponds to the antenna chromophore binding pocket in photolyases. It was indicated to be involved in binding of CLOCK/BMAL1 (Michael *et al*, 2017), and indeed in a low resolution CryoEM structure it was found that an extended loop of the PAS-B domain of CLOCK can target the secondary pocket of CRY1 (Fribourgh *et al*, 2019). This is underlined by the finding that mutations in the neighboring serine loop shortens then circadian period by 1 h (Nangle *et al*, 2014).

One important feature of CRY is the C-terminal helix (helix 22), which is a binding hot-spot in CRY functions. This helix22 is essential for core clock function (Chaves *et al*, 2006) and binds BMAL1-TAD (Czarna *et al*, 2011). It is wrapped by the PER2 C-Terminus as two crystal structures demonstrate (Schmalen *et al*, 2014; Nangle *et al*, 2014) and it is also bound by the E3 ligase FBXL3 (Xing *et al*, 2013). Furthermore, there is information that mammalian TIMELESS (TIM) binds to the C-terminal helix as well (Engelen *et al*, 2013).

The CRY tail was described to be important for nuclear import, as both CRY tails contain an import signal. Deletion of the tail or mutation of the nuclear localization signal (NLS), however, does not lead to an exclusive cytoplasmic localization. This was only achieved after additional deletion of the helix22 (Chaves *et al*, 2006). The tail stabilizes CRY and determines the period length by affecting the import rates of CRY (Li *et al*, 2016). The CRY1 tail contains a phosphorylation site Ser588, that causes stabilization and nuclear import of CRY1 (Gao *et al*, 2013). In contrast, dual phosphorylation of Ser557 by DYRK1A and Ser553 by GSK-3β in the

CRY2 tail leads to its destabilization and subsequent degradation (Harada *et al*, 2005; Kurabayashi *et al*, 2010)

3.1.6 Differences between CRY1 and CRY2

Deletion of single CRY1$^{-/-}$ or CRY2$^{-/-}$ does not disrupt the circadian rhythm. However, single knockout of CRY1 causes shortening of the period, whereas knockout of CRY2 causes lengthening of the period (Van Der Horst *et al*, 1999; Vitaterna *et al*, 1999). Ultimately, the circadian period is determined by the ratio of CRY1/CRY2 (Li *et al*, 2016). CRY1 is a more potent transcriptional repressor than CRY2 (Khan *et al*, 2012), which is consistent with the finding that CRY1 bound with a 20 fold higher affinity to the PAS domains of CLOCK/BMAL1 than CRY2 (Fribourgh *et al*, 2019). CRY1 and CRY2 are important for main circadian repression with PER, but CRY1 has an additional function in late repression as indicated by their expression peaks in circadian time and the observation that CRY1 can bind to CLOCK/BMAL1 independently of PER. In addition, the expression of CRY1 is delayed compared to CRY2 and PER and it is recruited to the DNA bound CLOCK/BMAL1 complex in two distinct phases: as part of the PER/CRY repressive complex at CT 16-20 and the majority at CT0-4 as part of the late repressive complex (Aryal *et al*, 2017; Lee *et al*, 2001; Ukai-Tadenuma *et al*, 2011; Koike *et al*, 2012).

In contrast to CRY1, CRY2 is described to facilitate the ubiquitination and degradation of c-Myc, a transcription factor regulating cellular proliferation, in a FBXL3 dependent fashion. CRY2 enhances the FBXL3 c-Myc interaction. In this function CRY1 is not able to substitute CRY2 (Huber *et al*, 2016).

CRY1 and CRY2 are structurally very similar (Figure 64). CRY2, however, carries an additional N-terminal polypeptide that slows down its degradation (Li *et al*, 2016). The most variable part is the C-terminal tail that shows substantial differences (see Figure 64).

3.2 Mammalian TIM

The TIMELESS (TIM) protein was first described in *D. melanogaster* as one of the main circadian repressors. In the *D. melanogaster* circadian clock, the activating complex consists of CLOCK (CLK) and CYCLE (CYC), which form a heterodimer to bind E-Boxes in the genome

to activate transcription of the genes *per* and *tim*. Period (dPER) and TIMELESS (dTIM) proteins slowly accumulate during the day. After sunset, they are phosphorylated and they translocate to the nucleus, where they bind to CYC/CLK to repress gene expression (Merbitz-Zahradnik & Wolf, 2015). However, the paralog of dTIM, dTIMEOUT, seems to be closer related to mammalian TIM. dTIMEOUT is crucial in DNA metabolism, chromosomal integrity, but was also reported in light entrainment of the circadian clock (Benna *et al*, 2010). The exact role of the mammalian TIM ortholog in the circadian clock is still under debate. So far, TIM was described mostly as member of the fork protection complex (FPC) with functions during DNA replication, under replication stress and DNA damage but there are also findings connecting mammalian TIM to the circadian clock (Barnes, 2003; Field *et al*, 2000; Sangoram *et al*, 1998; Unsal-Kaçmaz *et al*, 2005; Kang & Leem, 2014).

3.2.1 DNA Replication

In order for organisms to grow, cells need to divide, and pass a whole cell cycle, during which the genetic information is copied and distributed among the two daughter cells. The cell cycle is divided in 4 specific phases: The first gap phase (G1) after mitosis is a growth phase and during the synthesis-phase (S-phase), the cellular DNA is replicated. Then a second gap phase (G2) follows and finally the replicated DNA is distributed between the two nascent cells that subsequently separate in the mitosis-phase (M-phase). Transition between the phases is tightly controlled by cellular checkpoints, that check for e.g. DNA damage during the interphase (G1, S, G2) and if the mitosis is proceeding normally (Vermeulen *et al*, 2003). During the S-Phase the DNA is replicated. The DNA replication machinery is a large complex (also called replisome), that consists of many proteins. The core replication machinery notably consists of the helicase complex minichromosome maintenance 2-7 (MCM2-7), the GINS (japanese: *go-ichi-ni-san,* acronym referring to SLD5, PSF1, PSF2, PSF3) complex, cell division cycle 45 (CDC45), replication protein A (RPA), the Polymerases α (α primase), the Polymerases δ and ε and proliferating cell nuclear antigen (PCNA) (Johnson & O'Donnell, 2005).

MCM2-7, which depends on GINS and CDC45, starts to unwind the DNA double strand and separates the two strands (MacNeill, 2010). The nascent single stranded DNA (ssDNA) is covered by RPA for protection and to avoid formation of secondary structures which could block fork progression (Chen & Wold, 2014). Polymerase α synthesizes RNA primers, which the Polymerase δ and ε use as starting point to synthesize the nascent DNA strand. PCNA, the

'polymerase clamp' inhibits dissociation of the polymerases from the DNA, which increases their processing speed (Kelman Z, 1997). DNA polymerases can only synthesize DNA in 5'-3' direction, which creates a problem for the replication of the lagging strand since it moves 'in the wrong direction'. In order to deal with this problem, the lagging strand DNA is replicated in 'Okazaki fragments' (Langston & O'Donnell, 2006). Synthesis of each fragment is initiated by the synthesis of a short ~12 nucleotide RNA primer by Polymerase α that can be used as starting point for lagging strand synthesis (Lehman & Kaguni, 1989). The fragments are later fused by a DNA ligase. After full assembly of the replisomes, the DNA is replicated in opposite directions starting from one replication origin.

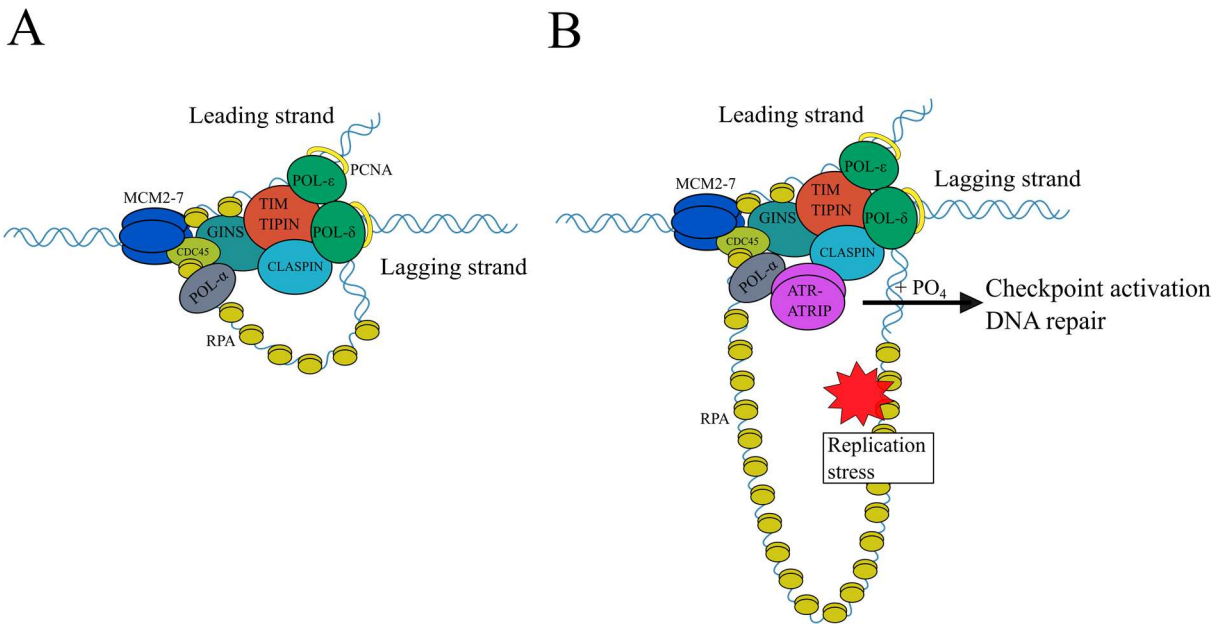

Figure 3: Schematic and simplified representation of the DNA replication under normal and replication stress. A) The replication complex consists of the MCM2-7 helicase, GINS, CDC45, the Polymerases α, δ, ε, the sliding clamp PCNA and the TIM/TIPIN complex. MCM2-7 separates the template strand into ssDNA, which is covered by RPA. The Polymerase ε synthesizes the leading strand. POL-α synthesizes primers, which the POL-δ uses as starting points to synthesizes the lagging strand in fragments. The Okazaki fragments are later joined by a DNA ligase. B) Under replication stress, ssDNA accumulates, as result of uncoupling of helicase and polymerase activity. This leads to accumulation of RPA, that leads to recruitment of downstream signaling kinases, such as ATR/ATRIP. ATR phosphorylates CHK1 in a TIM/TIPIN and CLASPIN dependent manner, which leads to regulation of cell cycle progression and feeds back to the regulation of DNA replication.

3.2.2 Replication Stress

During replication, the replisomes reach points in the DNA that are difficult to replicate; e.g. points that contain secondary structures, a lot of DNA binding proteins or DNA damages. This

causes slowing or stalling of replication forks and constitutes a stress for the replication process. During the S phase, the replication machinery competes with other proteins involved in transcription, chromatin remodeling, DNA repair or sister chromatid cohesion for access to DNA. During replication stress replication forks can collapse leading to genomic instability, including mutations, double strand breaks (DSB) and genomic rearrangements (Leman & Noguchi, 2012).

The cell has several ways to cope with replication stress. When replication stress is detected, signaling pathways, such as the ATR-CHK1 pathway, are activated. Stalled or slowed replication forks accumulate ssDNA, because the helicase continues to separate dsDNA, while the Polymerase is inhibited (Feng *et al*, 2006; Sogo, 2002). The accumulating ssDNA is covered by RPA, which leads to recruitment of the ATR-ATRIP complex (Figure 3 B, Figure 4 A). ATR is a phosphorylation activated kinase, which phosphorylates downstream checkpoint kinase 1 (CHK1. CHK1 phosphorylates a number of downstream targets that lead to an arrest in cell cycle progression and facilitates DNA repair (Zhang & Hunter, 2014; Cimprich & Cortez, 2008). Phosphorylation of CHK1 is assisted by CLASPIN as a scaffolding protein, which binds components of the replisome, such as CDC45, POL-ε and branched replication fork-like DNA (Serçin & Kemp, 2011). In addition to the ATR pathway, there is the ATM pathway, which acts more specifically on double strand breaks (Kim *et al*, 1999). Similar to ATR, ATM is activated by phosphorylation (Bakkenist & Kastan, 2003). ATM phosphorylates CHK2, which, together with ATM, phosphorylates p53 to stop cell cycle progression in order to repair DNA damage or apoptosis in case of severe damage (Shieh *et al*, 2000; Wahl & Carr, 2001). The PSF3 subunit of the GINS complex was also shown to be phosphorylated by ATR and ATM kinases, suggesting a regulation of the helicase activity (Matsuoka *et al*, 2007).

3.2.3 Functions of TIM/TIPIN

TIM is tightly bound to its partner TIM interacting protein (TIPIN). TIPIN was identified by a yeast-2-hybrid screen of a cDNA library. Both proteins are co-expressed and TIM promotes translocation of TIPIN to the nucleus (Gotter, 2003). TIM and TIPIN stabilize each other and the loss of one partner by RNAi leads to the loss of the other partner (Chou & Elledge, 2006). Depletion of TIPIN and TIM compromises the cells' ability to respond and survive to DNA damage and replication stress (Chou & Elledge, 2006). TIM and TIPIN in combination with CLASPIN are also referred to as the 'Fork protection complex' (FPC).

The FPC associates with the replisome at the onset of S-phase and travels with it along the replicated DNA by associating with replisome components such as the MCM2-7 helicase and the DNA Polymerase-δ and ε (Gotter *et al*, 2007; Numata *et al*, 2010). The FPC binds RPA as well, which is important to locate TIM/TIPIN (TTP) at ssDNA (Kemp *et al*, 2010)

Depletion of TIM/TIPIN leads to an accumulation of ssDNA in yeast and mammalian cells (Sommariva *et al*, 2005; Noguchi *et al*, 2004; Smith *et al*, 2009), which is indicative of an unrestricted helicase activity while the replication fork is stalled. This also causes an activation of the ATR-CHK1 pathway, which suggests that TIM/TIPIN might stabilize the replisome by bridging between the helicase and the polymerases, to couple the unwinding of the DNA with the synthesis of the daughter strands.

Interestingly, TTP was shown to restrict the activity of the MCM2-7/GINS/CDC45 complex and on the other hand, to increase the activities of Polymerase-α, ε, δ (Cho *et al*, 2013; Aria *et al*, 2013). This is consistent with the observation that depletion of TIM leads to a strong decrease in replication fork progression. In TIM depleted cells, the fork progresses only at half speed compared to a control (Unsal-Kacmaz *et al*, 2007).

Depletion of TTP also leads to an accumulation of γ-H2AX foci, an indicator of double strand breaks (DSB) (Chou & Elledge, 2006). The importance of TTP is underlined by the observation that its expression is increased prior and during the S-phase (Gotter *et al*, 2007) and that a reduction of TTP levels impedes S-phase progression (Yoshizawa-Sugata & Masai, 2007; Unsal-Kacmaz *et al*, 2007). TIPIN binds to RPA (Gotter *et al*, 2007; Ali *et al*, 2010; Nakaya *et al*, 2010), which is important for delay in cell cycle progression, recruitment of DNA repair factors, stabilization of replication forks (Sancar *et al*, 2004).

TTP was reported to be involved in preservation of telomere length by cooperating with telomeric repeat binding factors TRF1 and TRF2, as TIM depletion caused rapid shortening of telomeric repeats (Leman *et al*, 2012). TIM cooperates with RNA-Polymerase I transcription termination factor 1 (TTF1) in coordination of DNA transcription and replication activity at highly transcribed genes (Akamatsu & Kobayashi, 2015).

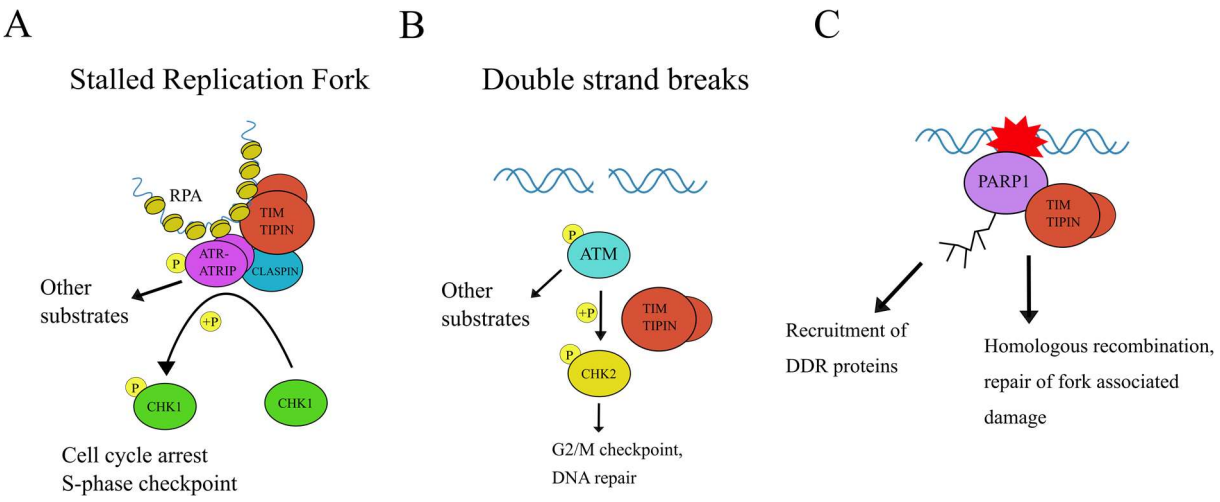

Figure 4: Overview of DNA damage signaling that involves TIM. A) The TTP complex is involved in signaling of replication stress. A stalled replication fork leads to accumulation of ssDNA, which is bound and protected by RPA. RPA together with TTP and other proteins lead to activation of ATR/ATRIP, a signaling kinase that phosphorylates CHK1 and other substrates to activate the S-phase checkpoint and DNA repair processes. B) DBS are signaled by ATM. ATM dependent phosphorylation of CHK2 depends on TTP. C) PARP1 recruits TTP to DNA damage sites. TIM binds the catalytic domain of PARP1, but the recruitment is independent of the enzymatic activity of PARP1. PARP1 and TTP are suggested to work in facilitating homologous recombination repair.

3.2.4 TIM/TIPIN in replication stress

TTP participates in replication stress response in various ways. It interacts with core components of the ATR-CHK1 pathway. It binds ATR-ATRIP and CHK1, which leads to accumulation of CHK1 at ssDNA to facilitate CHK1 phosphorylation by ATR (Figure 4A) (Unsal-Kaçmaz *et al*, 2005; Kemp *et al*, 2010). Those interactions are stimulated after inducing replicative stress by UV irradiation or hydroxyurea (HU) and CHK1 phosphorylation is reduced after knockdown of TTP (Yoshizawa-Sugata & Masai, 2007). In order to facilitate the phosphorylation of CHK1, TIM/TIPIN interacts with CLASPIN, that is important for scaffolding (Kemp *et al*, 2010; Serçin & Kemp, 2011). A depletion of TTP during replication stress causes a reduction of CLASPIN accumulation in the nucleus (Yoshizawa-Sugata & Masai, 2007). It was observed, that TIM and CLASPIN are overexpressed in some cancer cells to cope with the cells replication stress (Bianco *et al*, 2019) without hyperactivating the ATR-CHK1 checkpoint, but to promote fast reassembly of the FPC to favor restart of replication forks (Pasero & Tourrière, 2019). The TTP binds directly to RPA (Gotter *et al*, 2007; Ali *et al*, 2010; Witosch *et al*, 2014; Nakaya *et al*, 2010). RPA can sense DNA damage and interacts with DNA repair proteins, such as xeroderma pigmentosum group A (XPA) (He *et al*, 1995; Matsuda

et al, 1995; Burns *et al*, 1996) and uracil DNA glycosylase 2 (UNG2) (Nagelhus *et al*, 1997; Otterlei, 1999) to facilitate nucleotide excision repair (NER) and base excision repair (BER). RPA is also involved in the repair of double strand breaks by homologous recombination (Park *et al*, 1996; Sugiyama *et al*, 1998).

An additional way for cells to deal with replication stress is fork rotation. During DNA replication, the DNA helicase needs to unwind the two strands of the template DNA strand. This unwinding causes compensatory coiling in the region ahead of the helicase. Normally, topoisomerases can relax coiled DNA. However, accumulation of overwinding can prevent progress in DNA replication (Bermejo *et al*, 2007). The region ahead of the helicase is relaxed at the expense of generating double stranded intertwines behind the fork, which can be relaxed by topoisomerases as well (Bermejo *et al*, 2012). TTP was shown to be able to restrain these processes (Schalbetter *et al*, 2015) and unrestricted fork rotation can lead to significantly elevated levels of DNA damage.

TIM is important for ATM dependent signaling of DSBs as well. It affects the activation of CHK2 and G2/M checkpoint (Figure 4B). Depletion of TIM causes attenuation of CHK2 phosphorylation and reduces accumulation of the downstream acting protein p53. However, TIM is not required for phosphorylation and activation of ATM itself (Yang *et al*, 2010).

TIM binds poly ADP-ribose polymerase 1 (PARP1) and is recruited to DNA damage sites (Figure 4C) (Xie *et al*, 2015). PARP1 PARylates itself and other proteins, which leads to recruitment of proteins involved in DNA repair. The binding of TIM, however, is independent of the PARP1 enzymatic activity (Xie *et al*, 2015). The interaction of PARP1 and TIM is suggested to promote repair of DSBs by homologous recombination repair and non-homologous-end-joining (Xie *et al*, 2015; Young *et al*, 2015; Urtishak *et al*, 2009). PARP1 can also activate the ATM pathway, that causes slowing or stalling of the cell cycle after detection of DSBs (Ray Chaudhuri & Nussenzweig, 2017).

3.2.5 Structure of the TIM/TIPIN complex

Human TIM is a large protein consisting of 1207 amino acids. Secondary structure prediction proposes a predominant helical fold (Figure 66). In 2014, a low resolution CryoEM envelope of the pentameric TTP-RPA complex was published (Witosch *et al*, 2014). The TTP-RPA complex is a 150 Å protein with a horseshoe conformation and a central cavity (Figure 5). TTP

is the component of the complex that is responsible for the horseshoe (U-shape) conformation as seen in 2D class averages of TTP and TTP-RPA (Witosch *et al*, 2014). The combination of antibody analysis of the TTP-RPA complex and crystal structures of the RPA complex (Fan & Pavletich, 2012) allowed to position the RPA trimer in the TTP-RPA CryoEM envelope. The RPA trimer is positioned on the side of the complex. It forms a separate smaller horseshoe, in which RPA14, RPA32D and RPA70C are located in the upper limb and RPA70AB in the bottom limb of the horseshoe (Figure 5C). In the TTP-RPA structure it was not possible to clearly position TIM and TIPIN. However, antibody analysis of TIPIN suggests that it is located on the top of the large horseshoe structure.

Two partial crystal structures of TIM were published. The crystal structure of TIM N-Terminus (1-463ΔL) revealed a globular, mostly helical conformation, which is consistent with the secondary structure prediction. However, TIM contains two loops, that are not resolved, likely due to structural flexibility: A 100 residue loop (residues 239-330, 'TIM loop') and a shorter loop (residues 173-183, 'secondary loop') (Holzer *et al*, 2017). A C-terminal crystal structure is mostly helical as well, as a bundle 5 helices with a loop, that is involved in its homodimerization and binding of PARP1 (Xie *et al*, 2015). Initially, 4 hypothetical NLS sites were identified in the sequence of TIM. However, only the C-terminal NLS (residues 1175-1190) is relevant for nuclear translocation (Engelen *et al*, 2013). The minimal binding site for CRY1 was found to span residue 1-309 (Engelen *et al*, 2013). Interactions of TIM with MCM2-7 subunits, ATR, CHK1 and POL-δ, ε were reported, but a detailed characterization of interacting sites is still lacking (Numata *et al*, 2010).

Human TIPIN is much smaller compared to TIM and consists of 301 amino acids. A secondary structure prediction shows that it is mostly helical (Figure 67). It contains a proline-rich region at the N-Terminus, which likely is disordered. The RPA binding site spans residues 185-218, and it has a sequence similarity with XPA and UNG2 (Ali *et al*, 2010).

The binding site of TIPIN to TIM was first located between residues 64-140 (Yoshizawa-Sugata & Masai, 2007) and later confirmed spanning residues 67-143 (Ali *et al*, 2010). The fact, that this binding site does not overlap with the RPA binding site (185-218) is consistent with the observation that a pentameric complex between TIM, TIPIN, and RPA could be purified and structurally characterized (Witosch *et al*, 2014).

Furthermore, Crosslink Mass Spectrometry (XLMS) data on the TIM/TIPIN complex suggests that TIPIN residues 57-160 interact with TIM, which was also confirmed by pulldown assays

(Holzer *et al*, 2017). The binding site for TIPIN within TIM can be between residues 1-267 or 267-573 (Yoshizawa-Sugata & Masai, 2007) and XLMS located crosslinks between residues 427 and 1085. In pulldown experiments, a C-terminally truncated TIM 1-814 is sufficient to interact with TIPIN (Holzer *et al*, 2017).

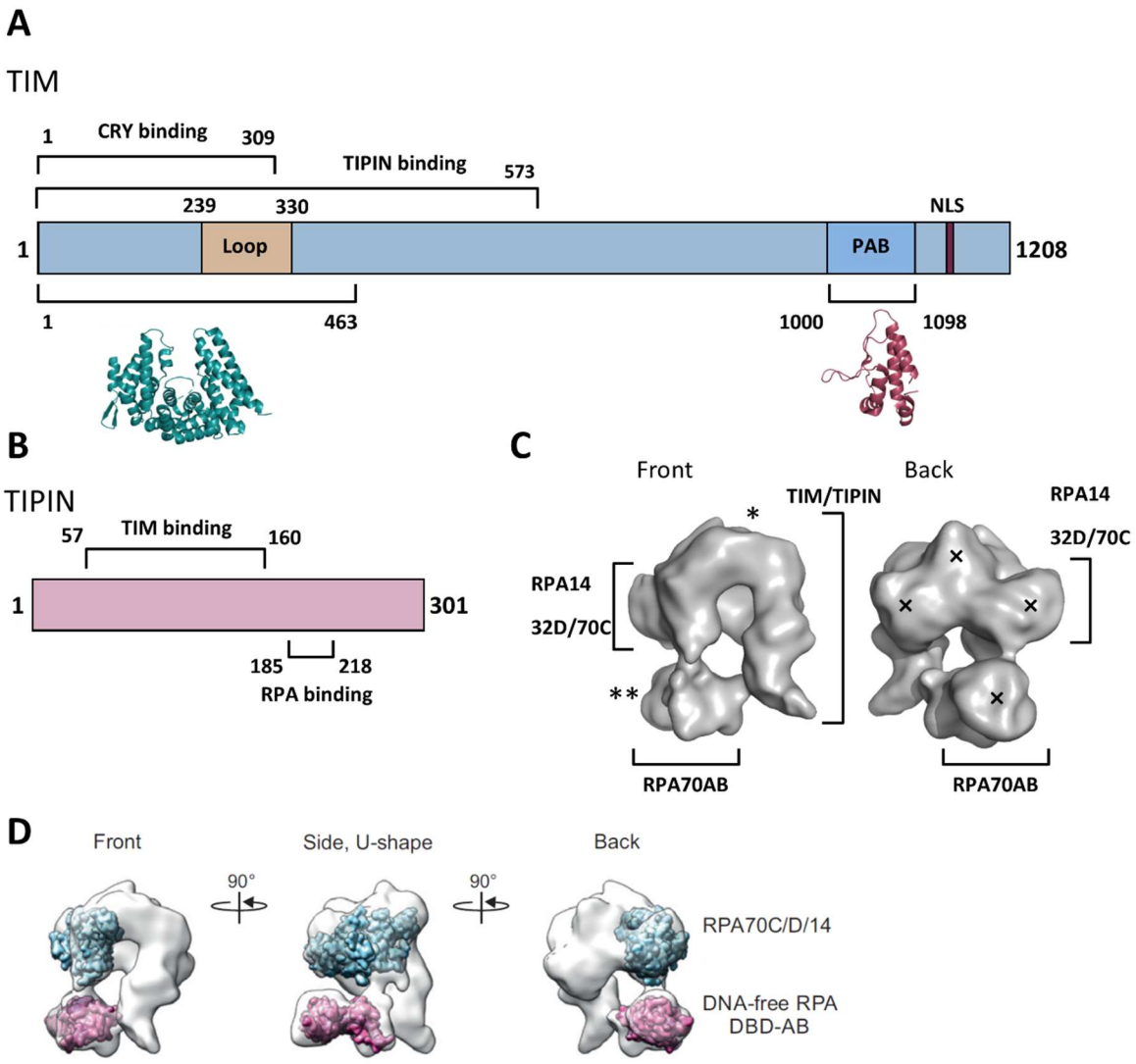

Figure 5: Overview about TIM and TIPIN. A) TIM is a large protein containing a CRY and TIPIN binding site in its N-terminus. It contains a flexible and supposedly unstructured ~100 residue long loop (residues 239-330). On its C-Terminus, it contains the PARP1 binding site (PAB). There are two partial crystal structures of TIM: A N-terminal 1-463-ΔL (ΔL= Δloop) and a C-terminal 1000-1098 structure. B) TIPIN contains a large N-terminal binding site for TIM and smaller binding site for RPA close to its C-Terminus. C) CryoEM structure of the TTP-RPA complex. The pentameric complex adopts an overall horseshoe conformation with a central cavity. Asterisks indicate the position of antibodies in antibody analysis of TIPIN (*) and RPA (**). Based on EMDB entry EMD-2789. Four distinct domains on the back side of the structure are marked by (x). D) Positioning of RPA in the TTP-RPA CryoEM envelope. Adapted from (Witosch *et al*, 2014).

3.3 Connection between the circadian clock, DNA Replication and DNA damage

TIM can be seen as a factor that couples the circadian clock with DNA replication and cell cycle control. There are studies that describe an interconnection between both processes, as well as TIM being involved in this regulation. TIM exists in two isoforms (Li *et al*, 2000), one full length isoforms that showed cycling behavior of protein (Barnes, 2003), and another isoform comprised of 475 C-terminal residues, that has a stable expression. TIM knockdown causes reduced expression of *Per1,2,3* and an increase of *Cry1,2* expression (Barnes, 2003). In addition, it caused a lack of circadian firing of neurons in the SCN (Barnes, 2003). Furthermore, TIM knockdown represses the transcription activities of CLOCK/BMAL1 (Kume *et al*, 1999; Sangoram *et al*, 1998). Nucleotide excision repair (NER), which is regulated by ATR (Auclair *et al*, 2009) exhibits daily rhythms. Protein levels of XPA, a central protein for the assembly of NER incision complexes, are in phase with BMAL1 and anti-phase with CRY1/2 (Kang *et al*, 2009). XPA can be phosphorylated by ATR, which increases its nuclear localization, so it can bind more effectively to DNA damage sites (Wu *et al*, 2007). In agreement with that is the observation that CRY deficient mice do not show any time dependent NER activity leading to the assumption that time-controlled NER is dependent on CRY expression (Kang *et al*, 2010). In fact, in non-dividing human fibroblasts (to remove effect of the cell cycle), synchronized by dexamethasone addition, DNA damage induction and repair efficiency are influenced by the phase of the circadian rhythm. They occur at a circadian time at which the chromatin is the most relaxed, which is controlled by the clock through rhythmic modification of histones (Bee *et al*, 2015).

Another example is the connection of PER to DNA damage signaling. PER1 binds to ATM and CHK2 kinases of the DSB signaling pathway in human cancer cells. This interaction is enhanced after IR treatment. PER1 promotes the phosphorylation and activation of CHK2 (Gery *et al*, 2006). PER2 can form a complex with p53, a target of ATM, that can induce a cell cycle arrest or apoptosis as response to DNA damage, and modulates its ubiquitination (Gotoh *et al*, 2015). PER1 and PER2 are implicated to act tumor suppressive (Fu *et al*, 2002; Gery *et al*, 2006).

Indeed, TIM can associate with the circadian repressors CRY1 and CRY2 (Field *et al*, 2000; Unsal-Kaçmaz *et al*, 2005; Kang & Leem, 2014). CRY1 was proposed to be a time-gated

mediator of TIM-activated ATR DNA damage response (DDR), as it positively affects phosphorylation of the ATR checkpoint markers p53 and CHK1. The interaction of TIM and CRY1 under genotoxic stress is increased (Kang & Leem, 2014). TIM is proposed to mediate between circadian clock by interacting with CRY2 and the cell cycle by actively engaging in cell cycle checkpoint control (Unsal-Kaçmaz *et al*, 2005).

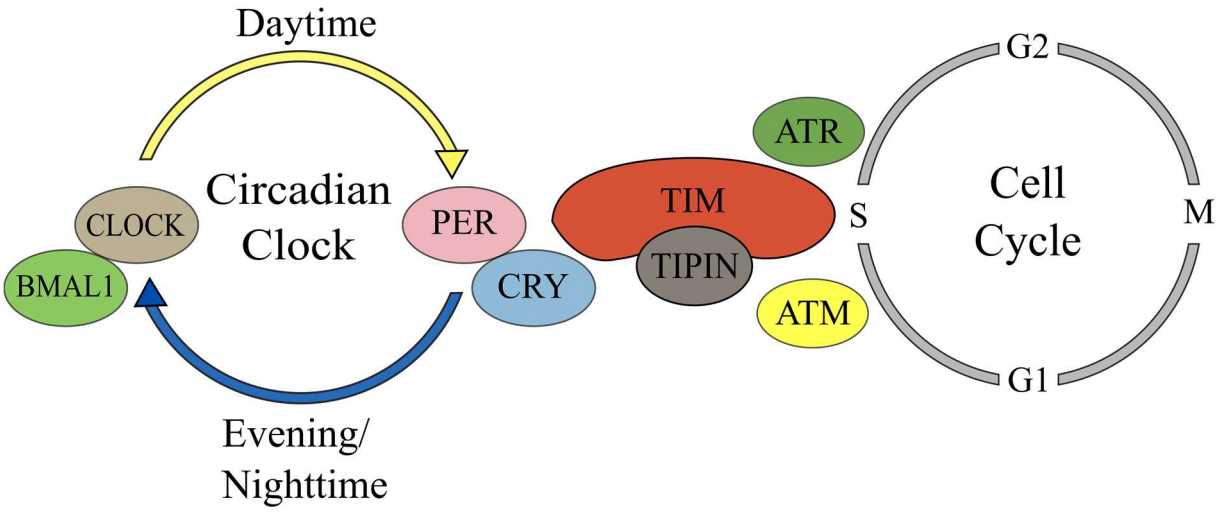

Figure 6: TIM-TIPIN connects the circadian clock and the cell cycle by interacting with the central clock proteins CRY1/2 and the replisome proteins and is involved signaling of DNA damage. TIM-TIPIN can trigger cell cycle arrest and DNA repair by interacting and regulating the signaling kinases ATM and ATR. Figure inspired by (Unsal-Kaçmaz *et al*, 2005).

DNA damage was shown to have an effect on the stability of the two paralogs CRY1 and CRY2. While DNA damage results in a stabilization of CRY1 by phosphorylation and subsequent deubiquitination by HAUSP, CRY2 is destabilized by an increased interaction with FBXL3 (Papp *et al*, 2015). Since the ratio of CRY1/CRY2 alters the period length (Li *et al*, 2016), it could explain why cells show an advancing of the circadian phase after DNA damage by ionizing radiation (Oklejewicz *et al*, 2008).

Additionally, familiar advanced sleep phase (FASP), a phenotype/disease, that was formerly associated with mutations in core clock proteins or the direct regulators (PER2, CK1δ) (Toh, 2001), also appears with a TIM mutation, which weakens the interaction between TIM and CRY2 (Kurien *et al*, 2019).

3.4 Aims of the Thesis

TTP and CRY were thought to have distinct roles in the cell: TTP as a protective complex of the replication fork and CRY as a member of the central repressive complex in the circadian clock. Lately, more and more data supports a closer connection between both processes and an interaction between TTP and CRY was observed. However, a direct binding between the two proteins has not been shown yet and it is still not fully understood how exactly the processes are coupled. Multiple questions are open on a potential link between replication regulation and the circadian clock and could rely on the existence of a direct interaction between TTP and CRY.

The first aim of this work was to prove a direct interaction between these two partners *in vitro* using purified protein. To this end, expression and purification procedures of both partners had first to be established. Once the direct interaction confirmed the complex, it should be biochemically and biophysically characterized using a combination of methods such as size exclusion chromatography, multiangle light scattering, or pulldown experiments to shed light on the structural features involved in binding. These binding studies notably revealed that the CRY tail and a TIM loop were involved in binding. This interaction was then characterized by affinity measurements using Nano Surface plasmon resonance (NanoSPR) and Fluorescence polarization experiments. Finally, an integrative structural biology approach combining Crosslink Mass Spectrometry, Small-angle x-ray scattering and Negative Stain Electron Microscopy was used to further characterize the complex. To further support the data, we conducted interaction analysis with partial TIM constructs. We wanted to answer the question whether there is a distinct TTP/CRY complex *in vitro* to confirm the proposed direct link of replication protection and the circadian clock *via* TTP and CRY.

A better understanding of the TTP/CRY complex and thereby the connection of the circadian clock and DNA replication could help to grasp what ultimately leads to the physiological and psychological disorders related to circadian misalignment.

4 Materials and Methods

4.1 Materials

List of Instruments

Table 1: List of equipment used in this thesis.

Instrument	**Manufacturer**
Centrifuges	Beckmann-Coulter, Avanti J-HC, Rotor JS-5.0
	Sorvall, RC 6+, Rotors: F10S 6x500Y, F21S 8x50Y
	Beckmann-Coulter, Optima XE-100, Ultracentrifuge
	Thermo Scientific, Hareus Fresco 21
	Eppendorf, Centrifuge 5415 C
	Eppendorf, Centrifuge 5810 R
FPLC	GE Äkta prime plus
	Biorad NGC Quest
	GE Äkta micro
Microscope cell culture	Leica DM750
Ultrasonicator	Branson, Ultrasonics Sonifier 450
Microvolume spectrometer	Nanodrop 2000c – Thermo Fischer
PCR cycler	MWG Biotech, Primus
	Biometra, TP professional standard
Gel Imaging system	BioRad XRS+
Incubators	Infors HT, Multitron pro
	Infors HT, Multitron Standard
Incubator Insect Cells	Thermo Fisher Forma Steri-Cult 3308
Plate reader	Tecan Spark20M
	Tecan Infinite 200 pro
Water purification system	Thermo Fisher, Barnstead GenePure xCAD Plus
MALS/DLS	Wyatt miniDAWN TREOS/QELS (DLS)
	Wyatt T-rEX (rI)

Consumables and Chemicals

Standard chemicals, such as buffers, salts, etc. were obtained from Applichem (AppliChem GmbH, Darmstadt), Carl Roth (Carl Roth GmbH + Co. KG, Karlsruhe), Merck (Merck KGaA, Darmstadt), Roche Diagnostics (Mannheim, Germany), Serva (SERVA Electrophoresis GmbH, Heidelberg), Sigma Aldrich (Sigma-Aldrich Chemie GmbH Munich, Germany) and VWR (VWR International GmbH, Darmstadt).

Columns and Chromatography resins

Table 2: Columns and resins that were used during this thesis for protein purification and buffer exchange. Most columns are by GE Healthcare (München, Germany) - GE

Column Type	**Resin Type**
Size Exclusion Chromatography	HiLoad Superdex200 16/600 pg HiLoad Superdex75 16/600 pg Superdex200 10/300 GL Superdex75 10/300 GL Superdex200 Increase 10/300 GL Superose6 Increase 5/150 GL
Ion-Exchange	5 mL HiTrap SPHP 5 mL HiTrap QHP
Affinity chromatography	5 mL, 1 mL HisTrap 1 mL GSTrap Glutathion-Sepharose 4 fast Flow NiNTA Resin, Superflow (Novagen, Merck KGaA, Darmstadt) 7 mL Heparin (in XK16 column)
Desalting	HiTrap Desalting, G-25 Sephadex Zeba Micro Spin 0.5 mL (Thermo Fisher Scientific, Massachusetts, USA)

In the text, the acronyms S200 and S75 will be used for Superdex200 und Superdex75, respectively.

Enzymes

Table 3: Overview of enzymes that were used in this thesis.

Enzyme	**Source**
His-Prsc (6xHis-3C protease)	Protein Production core facility at IMB
GST-Prsc (GST-3C protease)	Protein Production core facility at IMB
Sm nuclease (Benzonase substitute)	Protein Production core facility at IMB
HF DNA Polymerase (Phusion substitute, Fusion of Pfu-Sso7)	Protein Production core facility at IMB
Taq DNA Polymerase	Protein Production core facility at IMB
Dpn-1	New England Biolabs (Ipswich, USA)
RecA	New England Biolabs (Ipswich, USA)

Software

For analysis of FP and NanoSPR data the Prism 5 (Graphpad software, San Diego, USA) was used. For alignments of DNA and protein sequences Clustal Omega was used (Madeira *et al*, 2019). Different services from the Expasy server were used: Protparam, Translate (Gasteiger, 2003) and Swiss-model (Waterhouse *et al*, 2018). To create 3D models of structures we used Pymol version 2.2.3 (Schrodinger LLC, New York, USA) and Chimera version 1.14 (Pettersen *et al*, 2004). For analysis of SAXS data the ATSAS 3.0.0.3 software package was used (Franke *et al*, 2017). XLMS data was visualized with xiVIEW (Graham *et al*, 2019).

DNA Sequencing

DNA was sequenced using the *Lightrun* and *Supremerun* services provided by GATC (Eurofins Genomics, Ebersberg, Germany). 10 µL of sample with DNA concentration of 40-50 ng/µL and a primer concentration of 5 µM was shipped to GATC.

Media for cultivation of *E. coli* and insect cells

Table 4: Solutions and Media used to cultivate *E. coli* and insect cells.

Medium/Solution	**Composition**
LB Luria	10 g/L NaCl 10 g/L Tryptone 5 g/L Yeast extract, pH 7.0
LB Lennox	5 g/L NaCl 10 g/L Tryptone 5 g/L Yeast extract, pH 7.0
SF900II SFM	Serum free medium for insect cell culture, Gibco (Life Technologies)
TB Medium	12 g/L Tryptone 24 g/L Yeast extract 4 g/L Glycerol 0.017 M KH_2PO_4 0.072 M K_2HPO_4
SOC Medium	2% (w/v) Tryptone 0.5% (w/v) Yeast extract 10 mM NaCl 10 mM $MgSO_4$ 2.5 mM KCl 0.4% Glucose pH 7.2

Antibiotics and Agar plates

To select the *E. coli* strains on agar-plates and in liquid culture, antibiotics were added to the solution. The following working concentrations were used:

Table 5: Overview of antibiotics used in this thesis and their working concentrations.

Antibiotic	**Working concentration**
Ampicillin	100 µg/mL
Chloramphenicol	34 µg/mL
Gentamycin	7 µg/mL
Kanamycin	30 µg/mL
Streptomycin	50 µg/mL
Tetracyclin	10 µg/mL

15 g/L Agar-Agar stock (in LB Luria) was dissolved by heating and the antibiotics were added at ~50 °C. 25 mL of solution were poured into each petri dish (92 mm diameter).

To prepare Bacmid selection plates, Gentamycin, Tetracyclin, Kanamycin at their working concentration, IPTG (40 µg/mL) and X-Gal (100 µg/mL) were added to Agar solution.

Cells and Organisms

Table 6: Overview of *E. coli* strains used in this thesis.

***E. coli* strain**	**Genotype**	**Purpose**
DH5alpha	F$^-$ *endA1 glnV44 thi-1 recA1 relA1 gyrA96 deoR nupG purB20* φ80d*lacZ*ΔM15 Δ(*lacZYA-argF*)U169, hsdR17($r_K^- m_K^+$), λ$^-$	Cloning and amplification of plasmids
Omnimax	F′ {*pro*AB *lac*I^q *lac*ZΔM15 *Tn*10(Tet^R) Δ(*ccdA*B)} *mcr*A Δ(*mrr hsd*RMS-*mcr*BC) Φ80(*lac*Z)ΔM15 Δ(*lac*ZYA-*arg*F)U169 *end*A1 *rec*A1 *sup*E44 *thi*-1 *gyr*A96 *rel*A1 *ton*A *pan*D	Cloning
ccdB Survival	F$^-$*mcr*A Δ(*mrr-hsd*RMS-*mcr*BC) Φ80*lac*ZΔM15 Δ*lac*X74 *rec*A1 *ara*Δ139 Δ(*ara-leu*)7697 *gal*U *gal*K *rps*L (Str^R) *end*A1 *nup*G *fhu*A::*IS2*	Amplification of pCoofy plasmids, that contain a *ccdB* gene
Rosetta	F$^-$, *ompT*, *hsdS$_B$*(r_B-, m_B-), *gal*, *dcm (DE3)* / pRARE (C*am^R*)	Protein expression

Rosetta 2	F^- *ompT hsdS*$_B$ (r_B^- m_B^-) *gal dcm* (DE3) pRARE2 (Cam^R)	Protein expression
BL21DE3	F^- *ompT gal dcm lon hsdS*$_B$($r_B^-m_B^-$) λ(DE3 [*lacI lacUV5-T7p07 ind1 sam7 nin5*]) [*malB*$^+$]$_{K-12}$(λ^S)	Protein expression
NEB Shuffle®	*F′ lac, pro, lacI*^{q} */ Δ(ara-leu)7697 araD139 fhuA2 lacZ::T7 gene1 Δ(phoA)PvuII phoR ahpC* galE (or U) galK λatt::pNEB3-r1-cDsbC (Spec*^{R}*, lacI*^{q}*) ΔtrxB rpsL150(Str*^{R}*) Δgor Δ(malF)3*	Protein expression
DH10Bac	F-, *mcrA*, Δ(*mrr-hsd*RMS-*mcr*BC), φ80*lac*ZΔM15, ΔlacX74, *deo*R, *rec*A1, *end*A1, *ara*D139, Δ(*ara*, *leu*)7697, *gal*U, *gal*Kλ$^-$*rps*L, *nup*G/bMON14272/pMON7124	Creation of recombinant Bacmids, integrates Casette with *gene of interest* into Bacmid backbone

Table 7: Insect cell lines that were used in this thesis.

Cell line	**Description**
Hi5	Originated from ovarian tissue of cabbage looper, *Trichoplusia ni.* Used for protein expression
Sf9	Derived from pupal ovarian tissue of the fall army worm, *Spodoptera frugiperda*. Used for expression and amplification of recombinant baculoviruses

Vectors and Expression constructs

Table 8: Vectors that were used for protein expression in this thesis.

Name	**Tag**	**Antibiotic resistance**	**Cleavage site**	**Host**
pCoofy1	6xHis	KAN	3C	*E. coli*
pCoofy3	6xHis-GST	KAN	3C	*E. coli*
pCoofy4	6xHis-MBP	KAN	3C	*E. coli*
pCoofy6	6xHis-Sumo	KAN	Sumo	*E. coli*
pBeto1	6xHis	AMP	3C	*E. coli*
pBeto3	6xHis-GST	AMP	3C	*E. coli*
pGEX6p2	GST	AMP	3C	*E. coli*
pCoofy27	6xHis	AMP	3C	Insect cells
pCoofy28	6xHis-GST	AMP	3C	Insect cells
pCoofy27mod	6xHis (C-term.)	AMP	-	Insect cells
pFB CHis	6xHis (C-term.)	AMP	-	Insect cells

Table 9: Expression constructs that were used during this thesis. PHR – photolyase homology region; TIM-ΔL – TIM with deletion of the loop; TIM-SL – TIM with a shortened loop; TIM-N – N-terminal TIM residues 1-463, TIM-BD – TIM bending domain.

Name	Residues	Vector	Tag	Comment
hCRY1	1-586	pCoofy27mod	CT-6xHis	
hCRY1 tail	492-586	pCoofy3	6xHis-GST	
hCRY1 PHR	1-496	pCoofy27	6xHis	
hCRY2	1-593	pCoofy27mod	CT-6xHis	
hCRY2 PHR	1-512	pCoofy27	6xHis	
hCRY2 PHR	1-512	pCoofy28	6xHis-GST	
hCRY2 tail	511-593	pCoofy1	6xHis	
mCRY1 PHR	1-496	pFB CHis	CT-6xHis	I. Schmalen
mCRY1 PHR	1-496	pFB (6preHis)	6xHis	I. Schmalen
hTIM	1-1207	pCoofy1	6xHis	
hTIM-ΔL	1-1207 Δ239-330	pCoofy1	6xHis	
hTIM-SL	1-1207 Δ274-303	pCoofy1	6xHis	
hTIM 827-935	827-935	pCoofy3	6xHis-GST	
hTIM 997-1207	997-1207	pCoofy3	6xHis-GST	
hTIM-N	1-463	pCoofy6	6xHis-Sumo	
hTIM-N-ΔL	1-463 Δ239-330	pCoofy1	6xHis	Replaced with GSTGST linker
hTIM-N-SL	1-463 Δ274-303	pCoofy1	6xHis	
hTIM-loop	229-344	pCoofy1	6xHis	
hTIM-N	1-463	pCoofy6-Gly	6xHis-Sumo	+1 Gly after Sumo
hTIM BD	520-680	pCoofy1	6xHis	
hTIPIN	1-301	pBeto1	6xHis	
hTIPIN	1-301	pCoofy3	6xHis-GST	
mTIPIN	1-278	pEC-K-3C-GST	GST	J. Witosch

Most experiments were done with the human CRY1/2, TIM and TIPIN proteins. From here on, a shortened version of the protein names e.g. CRY1 is used. It refers to the human ortholog, unless otherwise mentioned.

Oligonucleotides

Oligonucleotides were ordered as salt-free from Eurofins Genomics (Ebersberg, Germany). For cloning of constructs the SLIC method (4.2.4) was used that requires a sequence homologous to the vector, which is added by PCR.

Table 10: Oligonucleotides used in this thesis. Small letters indicate the sequences that are added to the gene of interest, which are homologous to vector sequences at the insertion sites used in SLIC. Capital letters indicate the sequences that are complementary to the gene of interest.

Name	Sequence 5'-3'
hCRY1_fl_3C_fw	aagttctgttccaggggcccATGGGGGTGAACGCCGTGCA
hCRY1_fl_ccdB_r	ccccagaacatcaggttaatggcgCTAATTAGTGCTCTGTCTCTGGACTT
hCRY1pC27m_fw	ggcgcggatctcggtccgaaaccATGGGGGTGAACGCCGTGCA
hCRY1_AAALE_rev	ctcgagtgcggccgcATTAGTGCTCTGTCTCTGGACTTTAGGACC
hCRY1ctHisNLink	tcagtgatggtgatggtgatgATTAGTGCTCTGTCTCTGGACTTTAGG
hCRY1_fw_ctail_492_3C	AagttctgttccaggggcccTCACGATATAGAGGACTAGGTCTTCTGG
hCRY1 1-496 LP1	aagttctgttccaggggcccGGGGTGAACGCCGTGCACT
hCRY1 1-496 LP2	ccccagaacatcaggttaatggcgTCATCCTCTATATCGTGAAAGCT
hCRY2_fl_3C_fw	aagttctgttccaggggcccATGGCGGCGACTGTGGCGAC
hCRY2_fl_ccdB_r	ccccagaacatcaggttaatggcgTCAGGCATCCTTGCTCGGCAGCTCT
hCRY2pC27mfw	ggcgcggatctcggtccgaaaccatgATGGCGGCGACTGTGGCGAC
hCRY2_AAALE_rev	ctcgagtgcggccgcGGCATCCTTGCTCGGCAGCTCTGG
hCRY2ctHisNLink	tcagtgatggtgatggtgatgGGCATCCTTGCTCGGCAGCTCTGG
hCRY2_fw_511_3C	AagttctgttccaggggcccTCGCGCTACCGGGGACTCTGTC
hCRY2 3C start	aagttctgttccaggggcccATGGCGGCGACTGTGGCGAC
hCRY2 ccdB end 512	ccccagaacatcaggttaatggcgTTAGCGCGAAAGCTGCTGGTAAATCTGCTT
hTIM_fw_229_3C	aagttctgttccaggggcccCAGAACCCCGAGCAGCTGGCGGG
hTIM_rev_344_ccdB	ccccagaacatcaggttaatggcgTTAGTCTCTGAGGAAGAGCCTCACATTGAG
hTIM_fw_238_3C	aagttctgttccaggggcccGGGCAGGGACGCTTAGCTCAGGAGC
hTIM_rev_332_ccdB	ccccagaacatcaggttaatggcgTTA GCGCTGAATGGACAGCTCTCG
TIM 997 FW 3C	aagttctgttccaggggcccGGTAGCTTAGTCCTTTCAAATGAAAACCTTGGT
hTIM 827 FW 3C	aagttctgttccaggggcccGAGGCTCATCTTCGGGAGCTGTACC
hTIM ccdB rev 935	ccccagaacatcaggttaatggcgTCACCCCAGAGCCAAGAGTTTATCCACT
hTIM_fw_glylinker_sumo_3C	gtgttccagcagcagaccggtggaggaGACTTGCACATGATGAACTGTG
AAALE_His_rev	tcagtgatggtgatggtgatgCTCGAGTGCGGCCGC
CTHis_slic_rev	ccccagaacatcaggttaatggcgTCAGTGATGGTGATGGTGATG
LP1_pC27mod_fw	catggtttcggaccgagatccgcgcc
LP2_pC27_mod_rev	cgccattaacctgatgttctggggaatataagcttgcg

4.2 Molecular Biology Methods

Templates

DNA templates for human CRY1, CRY2, TIM and TIPIN were obtained from Addgene. The plasmids for human TIM, TIPIN, and variations (TIM-N-ΔL, TIM-N, TIM-N-SL) were cloned into expression vectors by Dr. Roberto Orrù.

4.2.1 Preparation of competent cells

To prepare chemically competent cells for transformation, cells from a permanent stock were streaked out on an agar plate. After 16 h, a single colony was picked to inoculate a pre-culture (10 mL in LB Luria). The main culture (100 mL) was inoculated at OD_{600} = 0.1. It was grown at 37 °C to an OD_{600} of 0.6. After 5 min incubation on ice, cells were pelleted (3200 x g, 10 min, 4 °C) and suspended in 8 mL chilled Tbf1 buffer. The cells were pelleted, suspended in 10 mL Tbf2 buffer and incubated for 15 min on ice. 50 µL aliquots were prepared and snap-frozen with liquid N_2. Competent cells were stored at -80 °C.

Later during this work, competent cells were prepared using the $CaCl_2$ method, which replaces the Tbf buffers with simpler $CaCl_2$ solutions. The preparation of the cells was done in the same way.

Table 11: Solutions that were used to prepare chemically competent cells.

Solution	**Components**
Tbf1	30 mM $C_2H_3KO_2$ K-acetate, 100 mM RbCl, 10 mM $CaCl_2$, 50 mM $MnCl_2$, 15 % Glycerol, pH adjusted to 5.8 with acetic acid
Tbf2	10 mM MOPS, RbCl, CaCl2, 15% Glycerol, pH adjusted to 5.8
Ca1	100 mM $CaCl_2$
Ca2	100 mM $CaCl_2$, 10% Glycerol

4.2.2 Transformation

Chemically competent *E. coli* cells (4.2.1) were thawed on ice. 1 µL of plasmid DNA (50-500 µg DNA) was transferred into the cell suspension. After co-incubation for 10 min, a heat shock was conducted for 45 sec at 42 °C. After 2 min on ice, 500 µL of LB Luria was added and the cells were incubated under agitation at 37 °C for 1 h. Cells were pelleted (7000 x g, 2 min) and resuspended in 100 µL LB Luria and were streaked on agar plates containing selective antibiotics. The agar plates were grown 16 h at 37 °C.

Co-transformation of TIM and TIPIN

The TIM plasmid (pBeto1) was transformed in *E. coli* (4.2.2). One colony was picked and a 1 mL culture in LB Luria (in a 1.5 mL reaction tube) was grown for 7 h at 37 °C. The cells were

made chemically competent for an additional transformation using the $CaCl_2$ method. Briefly, the cells were sedimented and resuspended in 500 µL of cold Ca1 solution and incubated for 5 min on ice. Then, cells were sedimented again and resuspended in 50 µL of cold Ca2 solution. 1 µL of the TIPIN plasmid (pCoofy1) was added and after co-incubation for 5 min on ice a heat shock was performed. Cells were streaked on agar plates containing antibiotics to select both plasmids.

4.2.3 Amplification and Isolation of plasmids

The plasmid was transformed into the *E. coli* strain DH5alpha. 5 mL of LB Luria were inoculated with a single colony and grown for 16 h at 37 °C. The cells were collected by centrifugation (10 min, 3200 x g, 4 °C). Plasmids were isolated using commercial kits such as *Spin Miniprep* (Qiagen, Venlo, the Netherlands) and *Nucleospin plasmid* (Macherey & Nagel, Düren, Germany).

4.2.4 Sequence and ligation independent cloning

For cloning of expression vectors the sequence and ligation independent cloning (SLIC) method was used (Scholz *et al*, 2013). It is based on recombination of complementary DNA stretches within insert and vector by the enzyme RecA. The pCoofy backbone carries a *ccdB* gene to reduce background of the original plasmid.

4.2.5 PCR

To amplify the gene of interest and to add complementary overhangs for SLIC, a PCR was used. The reaction was set up on ice, and the polymerase was added last. The annealing temperature was adjusted to the theoretical melting temperature of the set of primers, which was calculated using the *Snapgene viewer* software. As starting condition an annealing temperature 5 °C below the theoretical melting temperature was used. For amplification of genes and vector linearization different protocols were used. After the PCR, a sample of the reaction was analyzed by agarose gel electrophoresis (4.2.8).

4.2.5.1 Amplification of Insert

Table 12: PCR reaction conditions for amplification of gene insert.

Component	Final concentration
Forward primer	1 µM
Reverse Primer	1 µM
dNTPs	1.6 mM
Phusion HF buffer (NEB)	1 x
Template Vector	25 ng
Phusion, HF DNA-Polymerase	0.6 U
ddH_20	Ad 50 µL

Table 13: PCR program to amplify gene inserts.

Temp [°C]	Time [sec]	Cycle
98	30	
98	30	30x
60	30	
72	40	
72	120	
4	∞	

4.2.5.2 Linearisation of pCoofy vectors:

Table 14: PCR reaction conditions for linearisation of vector backbones.

Component	Final concentration
Forward Primer LP1	1 µM
Reverse Primer LP2	1 µM
dNTPs	1.6 mM
Phusion GC buffer (NEB)	1 x
DNA Template	25 ng
Phusion, HF DNA Polymerase	0.6 U
ddH_20	Ad 50 µL

Table 15: PCR program for linearisation of vector backbones.

Temp [°C]	Time [min]	Cycle
98	3	
98	0.5	30x
72	1.5	
72	10	
4	∞	

PCR product cleanup

After PCR, the amplicons were cleaned up to remove PCR residuals such as oligonucleotides and PCR buffer components. The *NucleoSpin* PCR cleanup kit by Macherey & Nagel (Düren, Germany) was used according to the manufacturer's instructions.

4.2.6 Recombination of Insert and Vector

An excess of the purified amplicon was incubated with the linearized vector for 1 h at 37 °C. Alternatively, the incubation was done 16 h at room temperature. The ratios of amplicon and vector were varied.

Table 16: Conditions of recombination reaction of amplicons and linearized vectors in SLIC. For optimization of reaction conditions, the molar ratios of vector and insert were varied between 1:1 and 1:7.

Vector	100 ng
Insert	1:3 mol. excess (alt. 1:1-1:7 ratios used)
RecA buffer	1x
RecA	2 ng
ddH_2O	Ad 10 µL

After recombination, 5 µL were transformed into the competent *E. coli* strains DH5alpha or Omnimax (4.2.2). Colonies were screened by colony PCR (4.2.7). Plasmids isolated from positive colonies were sequenced.

4.2.7 Colony PCR

The colonies were screened for the plasmid of interest by PCR. Colonies were picked and re-suspended in 50 µL H_2O. 10 µL were kept separately for later inoculation of cultures. The rest was boiled (5 min, 95 °C) and spun (5 min, 21000 x g, 4 °C). 5 µL of the supernatant was used as template for colony PCR. The same PCR program as for the amplification of the insert was used (4.2.5). The reaction volume was 25 µL.

4.2.8 Agarose Gel Electrophoresis

PCR products were analyzed by agarose gel electrophoresis. 0.5-2% (w/v) agarose was dissolved in hot TAE buffer (40 mM Tris pH 7.6, 20 mM acetic acid, 1 mM EDTA). The agarose was cooled to approx. 50 °C, SYBR safe DNA stain (Invitrogen, Carlsbad, USA) was added 1:20.000 (v/v) and the warm agarose was poured into a gel tray, supplied with a comb to create wells for the samples. The solidified gel was run in TAE buffer at 120 V for 25 min. For documentation the gel was analyzed using the BioRAD XRS+ (BioRAD, Hercules, California, USA) in SYBR safe mode. To analyze small DNA fragments (smaller than 400 bp) agarose concentrations of 1.5-2% were used. In agarose gel electrophoresis, DNA ladders (1 kb and 100 bp Ladder) by Genecraft (Manchester, UK) were used.

4.2.9 Protein expression in *E. coli*

The vector was transformed (4.2.2) into the *E. coli* expression strain. An overnight culture (16 h, 37 °C) in LB Luria was inoculated. It was used to inoculate a large scale expression culture at OD_{600} of 0.1-0.2. The cells were grown under constant agitation (Table 17) at 37 °C. After reaching the desired cell density the temperature was reduced to 18 °C and the expression was induced by adding IPTG (Table 18). *E. coli* cultures grown in LB Luria were induced at an OD_{600}=0.6-0.8 and cultures in TB Medium at OD_{600}=1.0-1.2. The expression conditions were varied depending on the protein of interest (Table 18). After 16 h of expression, the cells were harvested by centrifugation (15 min, 3200 x g) and the pellets were stored at -80 °C. For expression in TuneAIR flasks 0.0001% (v/v) AntiFoam (Sigma Aldrich, GmbH Munich, Germany) was added.

Table 17: Agitation speeds used to culture cells in different flasks

Flask	**Agitation speed (rpm)**
5 L Erlenmeyer flask	160
5 L Erlenmeyer flask (baffled)	130
1 L TuneAIR flask	200

Table 18: Overview of expression conditions in *E. coli* for different proteins.

Protein	Host	Vector	Medium	IPTG [µM]	Expression Temp.	Flask
CRY1 tail	Rosetta	pCoofy3	LB Luria	300	18 °C	Erlenmeyer flask
CRY2 tail	Rosetta	pCoofy1	TB	200	18 °C	TuneAIR
TIPIN	Rosetta	pCoofy3	TB	100	18 °C	TuneAIR
mTIPIN	Rosetta	pEC-K-3C-GST	TB	100	18 °C	TuneAIR
TIM/TIPIN	Rosetta/ Rosetta2	pBeto1/pCoofy1	TB	100	18 °C	TuneAIR
TIM-N	Rosetta2	pCoofy6	TB	300	18 °C	TuneAIR
TIM-N-ΔL	Rosetta2	pCoofy1	TB	100	18 °C	TuneAIR
TTP-SL	Rosetta	pCoofy1/pBeto1	TB	100	18 °C	TuneAIR
TTP-ΔL	Rosetta	pCoofy1/pBeto1	TB	100	18 °C	TuneAIR
TIM 238-332	BL21 DE3	pCoofy3	LB Lennox	500	18 °C	Erlenmeyer
TIM 520-680	Rosetta	pCoofy1	TB	200	18 °C	TuneAIR
TIM 997-1207	Rosetta	pCoofy3	TB	200	18 °C	Erlenmeyer
TIM 827-935	NEB Shuffle	pCoofy3	LB Luria	200	18°C	Erlenmeyer

4.2.10 Protein expression in Insect cells

For expression of CRY we used the Bac-to-Bac Baculovirus expression system (Invitrogen, Carlsbad, USA) for insect cells. The advantages of insect cell expression are that the protein translation machinery is more similar to mammalian cells, therefore allowing better folding of proteins, and in addition it permits posttranslational modifications similar to the mammalian system. The insect cell cytoplasmic environment allows proper formation of disulfide bonds, unlike the reducing environment in *E. coli.*

The gene of interest is cloned into a donor plasmid (e.g. pCoofy27-29, pFB) using SLIC (see 4.2.4). This donor plasmid is then transformed into *E. coli* DH10Bac that facilitates the transposition of the expression cassette into the viral Bacmid. The Bacmid is transfected into insect cells. The successfully transfected cells produce recombinant baculoviruses and express the protein of interest under a viral promotor. Since one infected insect cell produces many viruses, the viral titer can be amplified by infection of more cells. For the large scale expression, an amplified baculovirus stock is used to infect the culture.

4.2.10.1 General maintenance of Insect cells

Cells were grown in serum-free SF900II medium at 27 °C under constant agitation of 90 rpm. The cells were split regularly and a density between $0.2x10^6$ and $1x10^6$ was maintained. Stocks were cultured in a volume of 30 mL in standard Erlenmeyer flasks. No antibiotics were used in the insect cell culture. Cells were counted using a Hemocytometer. Cells were stained by mixing 1:1 with Trypanblue solution (0.4% (w/v) Trypanblue in PBS buffer (8 g/L NaCl, 0.2 g/L KCl, 1.4 g/L Na_2HPO_4, 0.24 g/L KH_2HPO_4, pH 7.4)) to differentiate between living and dead cells. The dead cells stain blue while the living cells remain white.

4.2.10.2 Freezing and thawing of insect cells

Cells were pelleted by centrifugation (5 min, 500 x g) and resuspended at a density of $5*10^6$ cells/mL in SF900II SFM + 10% DMSO. 1 mL aliquots were prepared in cryogenic vials and were frozen using a freezing container (*Mr. Frosty*, Nalgene, ThermoFisher, Massachusetts, USA), filled with isopropanol, to ensure a steady cooling rate of -1 °C/min. The cells were frozen over night at -80 °C and were transferred to a liquid N_2 container or in a -150 °C freezer for long term storage.

Thawing of cells:

The vials were quickly thawed in hand. One vial of frozen cells was diluted in 20 mL of SF900II SFM in a suspension culture. After 2-3 of days of adaptation, the cells started to divide 1 x per 24 h.

4.2.10.3 Production of recombinant Bacmids

Chemically competent DH10Bac (+YFP) cells were transformed with 1 µL of vector (100-500 ng) suitable for Bacmid production (pCoofy27-29, pFB). After incubation for 10 min, a 45 sec heat shock at 42 °C was performed and the cells were put on ice for 2 min. 500 µL of SOC medium was added and the cells were incubated 4 h at 37 °C under constant agitation. Afterwards, cells were pelleted and resuspended in 150 µL SOC medium. 150 µL of cells were plated on Bacmid selection plates in different dilutions: 1:1, 1:10, 1:100 and 1:1000. The plates were incubated for 48 h at 37 °C until positive and negative colonies could be identified by

their white or blue color, respectively. This makes use of the enzymatic activity of β-Galactosidase to screen for successful transposition of the expression cassette into the Bacmid. The cassette integrates into the *lacZ* gene, which encodes the β-Galactosidase, making it non-functional. X-Gal present in the Bacmid selection plates cannot be cleaved, which leaves it colorless. As control, white colonies were again streaked out on Bacmid selection plates and incubated over night at 37 °C. White colonies were used to inoculate 5 mL over-night cultures (50 µg/mL Kanamycin, 10 µg/mL Tetracyclin, 7 µg/mL Gentamycin).

The Bacmids were isolated using the following protocol: Cells were collected by centrifugation (3200 x g, 10 min). To isolate the Bacmids, buffers of the *Spin Miniprep* Kit (Qiagen, Venlo, the Netherlands) were used. Cells were resuspended in 300 µL P1 buffer, then mixed with 300 µL P2 buffer and were inverted multiple times. Afterwards 300 µL of buffer N3 were added and incubated 2 min on ice. The lysate was cleared by centrifugation (21000 x g, 10 min, 4 °C). The supernatant was transferred to a sterile reaction tube containing 700 µL isopropanol, the tube was inverted multiple times and spun at 21000 x g for 10 min. The supernatant was discarded; the pellet was washed with 200 µL 20% ethanol. The pellet was spun again 21000 x g, 10 min and the supernatant was removed and replaced with 50 µL 70% ethanol. The ethanol was removed and the pellet was air dried. The pellet was carefully resuspended in 5 µL ddH_20, by tapping the tube.

4.2.10.4 Transfection of insect cells

Sf9 cells were transfected inside six-well plates. Five wells were filled with 3 mL of SF900II SFM with 10^6 Sf9 cells. One well was filled with 3 mL of medium as a control for sterility. The plate was incubated 20 minutes at 27 °C to allow cells to attach to the surface.

For transfection, two solutions were prepared: Solution A: The isolated Bacmid (4.2.10.3) was diluted with 50 µL SF900II SFM. Solution B: 50 µL of SF900II SFM was mixed with 3 µL of the transfection reagent FuGENE (Promega, Wisconsin, USA) by thoroughly pipetting up and down. Solution B was incubated for 5 min at room temperature.

Both solutions were mixed and incubated at room temperature for 30 min. After incubation 400 µL of SF900II SFM was added and gently mixed. 250 µL of the solution was used to transfect one well. The cells were incubated 4-5 days at 27 °C. To judge success of transfection, the cells were checked for YFP fluorescence. In case of standard DH10Bac cells, successful transfection

was judged by size of the cells, their shape and growth. The supernatant was harvested after 5 days. The cells were washed-off the surface of the 6-well plate. Cells and supernatant were separated by centrifugation (10 min, 3200 x g). The P_0 Virus was stored in the dark at 4 °C.

4.2.10.5 Amplification of P_1 Virus:

50 mL Sf9 cells at $0.5*10^6$ cells/mL was infected with 1 mL of P_0 Virus. The cells' growth, viability and diameter was monitored. During the infection the cell growth stops, the cell diameter increases and the viability decreases. After 4-5 days, when the viability fell below 70%, the culture was harvested. The virus containing supernatant was separated from cells by centrifugation. The virus was stored in the dark at 4 °C.

4.2.10.6 Expression in Insect cells

To determine the ideal ratio of virus in expression culture, an expression test with P_1 virus was done. 50 mL culture (Hi5 or Sf9) at $0.5*10^6$ cells/mL was infected with different volumes of virus (50-500 µL). During the test, a sample of 10^6 cells was collected every day to analyze the expression level of the target protein. The samples were analyzed by SDS-PAGE.

For large scale expression, 1 L insect cells were cultivated in a 3 L Fernbach Flasks (Corning Inc., Corning, USA). Once the density of the culture reached 10^6 cells/mL, the cells were infected with 5 mL of P_1 Virus. To improve expression 2 mM Glutamine (Life Technologies, ThermoFisher, Massachusetts, USA) was added. After 48 h, the culture was harvested by centrifugation at 3200 x g. The pellets were frozen and stored at -80 °C.

Table 19: Expression conditions of different CRYs in insect cells.

Protein	Expression host	Vector	Medium
CRY1	Hi5/Sf9	pCoofy27mod	SF900II SFM
CRY2	Sf9	pCoofy27mod	SF900II SFM + 2 mM Glutamine
mCRY1 PHR Ct-His	Hi5/Sf9	pFB CHis	SF900II SFM
mCRY1 PHR Nt-His	Sf9	pFB	SF900II SFM

4.3 Biochemical Methods

4.3.1 Determination of Protein and DNA concentrations

To determine concentration of purified protein, the microscale UV spectrometer Nanodrop 2000c was used. The protein concentration is determined by the Lambert-Beer-law based on the absorbance at 280 nm and the theoretical extinction coefficient, which was calculated using the Protparam service (4.1). The A260/A280 ratio was calculated as an indicator for nucleic acid contamination.

Protein concentrations of cell extracts (SILAC pulldowns) were determined by a Bradford assay. 1 mL of Bradford solution (QuickStart 1x Protein Dye (Biorad, Hercules, California, USA)) was mixed with 2 µL protein extract. After 5 min at RT, the absorbance at 595 nm was measured. The concentration was calculated using a calibration curve and the Lambert-Beer-law.

DNA concentrations were measured using the Nanodrop 2000c spectrophotometer. The absorbance of sample was measured at 260 nm. The concentration is calculated by $conc.\ ng/\mu L = A260 * 50$ µg/mL, in which an OD_{260}=1 corresponds to a dsDNA concentration of 50 µg/mL. The ratios A260/A280 and A260/A230 were taken into account to assess the sample purity.

4.3.2 Gel electrophoresis

4.3.2.1 Polyacrylamide gels

Gels were prepared using a casting system for 10 gels. The resolving solution was transferred into the casting chamber and was topped with 30% isopropanol to create an even surface between stacking and resolving gel. After 20 min, when the polymerization reaction was completed, the isopropanol was removed and the stacking solution was added. Afterwards, the combs to create the wells were inserted. For 10 gels 60 mL resolving solution and 20 mL stacking solution was used. After polymerization, Gels were stored at 4 °C.

Table 20: Composition of stacking and resolving solutions for the preparation of polyacrylamide gels.

Component	**Stacking gel 4 %**	**Resolving Gel 10 %**
BisTris pH 6.5	250 mM	300 mM
Acrylamid-Bisacryalmid 37.5:1 (v/v)	4 %	10 %
APS (w/v)	0.08 %	0.06 %
TEMED (v/v)	0.01 %	0.05 %
ddH_20	ad 20 mL	ad 60 mL

For electrophoresis a MOPS running buffer (resolving large MW proteins) or a MES running buffer (resolving smaller MW proteins) were used:

Table 21: Composition of SDS-PAGE running buffer to resolve large and small proteins.

Component	**MOPS buffer**	**MES buffer**
MOPS	50 mM	-
MES	-	50 mM
Tris	50 mM	50 mM
EDTA pH 7.5	1 mM	1mM
SDS (w/v)	0.1 %	0.1 %
Sodium bisulfate ($NaHSO_4$)	5 mM	5 mM

The gels were run at 110 mA for 30 min. For Crosslink MS experiments pre-casted NuPAGE 4-12% Bis-Tris gels (Invitrogen, Carlsbad, USA) were used and were run at 150 V for 90 minutes in MOPS buffer. The gels were stained with a Coomassie solution (0.1 % (w/v) Coomassie R250, 30% (v/v) methanol, 10% (v/v) Acetic acid) for 10 min. Gels were destained with destaining solution (30% (v/v) MeOH, 10% (v/v) acetic acid) or alternatively in ddH_20.

As protein marker the Roti-Mark Standard and Roti mark prestained (Carl Roth, Karlsruhe, Germany) were used.

Gradient gels:

To analyze crosslinked proteins (see 4.3.10 and 4.3.11), gradient gels were casted. A 4-10% acrylamide gradient was created by using a gradient mixer that evenly mixes the acrylamide solutions (4% and 10%, Table 20). Before preparing the gradient, TEMED (0.04% v/v) and APS (0.04 % w/v) were added to both solutions.

4.3.3 Protein purification

All buffers were prepared using ultrapure water and the pH was adjusted at room temperature. All buffers were filtered through at 0.4 µm filter. Buffers for SEC were degassed using a vacuum pump.

Table 22: Buffers used for protein purifications. All buffers were prepared with ultrapure water and were filtered. Buffers for SEC were degassed. The pH was adjusted at room temperature. LYS – Lysis buffers; HSB – high salt buffer; AB – ATP wash buffer; EB – elution buffer; IEX – ion exchange buffer; AEX – anion exchange buffer; DB – dialysis buffer; SEC – size exclusion buffer; HIS1 – buffer to reduce salt concentration before ion exchange chromatography of TTP; WB – wash buffer.

Name	**Components**
LYS1	50 mM Tris pH 7.1, 300 mM NaCl, 10% (v/v) Glycerol, 3 mM β-Me, 20 mM Imidazole
LYS2	50 mM Tris pH 8, 250 mM NaCl, 10% (v/v) Glycerol, 2 mM β-Me, 5 mM Imidazole
LYS3	100 mM Tris pH7.5, 400 mM NaCl, 10% (v/v) Glycerol, 1 mM β-Me, 20 mM Imidazole
LYS4	50 mM Tris pH 7.4, 400 mM NaCl, 10% (v/v) Glycerol, 1 mM β-Me, 20 mM Imidazole, 100 mM Urea
LYS5	25 mM Hepes pH 7.2, 150 mM KCl, 5 mM Imidazole
LYS6	50mM Tris pH 7.5, 150 mM NaCl, 30 mM Imidazole, 5 mM $MgCl_2$
HSB1	50 mM Tris pH 7.1, 750 mM NaCl, 10% (v/v) Glycerol, 3 mM β-Me, 20 mM Imidazole
HSB2	50 mM Tris pH 8, 1 M NaCl, 5% (v/v) Glycerol, 2 mM β-Me, 5 mM Imidazole
HSB3	50 mM Tris pH 7.5, 1 M NaCl, 5% (v/v) Glycerol, 1 mM β-Me, 20 mM Imidazole
HSB4	50 mM Tris pH 7.5, 750 mM NaCl, 10% (v/v) Glycerol, 3 mM β-Me, 10 mM Imidazole

HB5	25 mM Hepes pH 7.2, 750 mM KCl, 5 mM Imidazole
HSB6	50 mM Tris pH 7.5, 1 M NaCl, 5% (v/v) Glycerol, 2 mM β-Me
AB1	50 mM Tris pH 7.1, 200 mM NaCl, 5% (v/v) Glycerol, 3 mM β-Me, 20 mM Imidazole, 2 mM ATP, 50 mM KCl, 10 mM Mg_2SO_4
AB2	50 mM Tris pH 7.5, 200 mM NaCl, 5% (v/v) Glyceroel, 1 mM β-Me, 20 mM Imidazole, 2 mM ATP, 50 mM KCl, 10 mM $MgSO_4$
AB3	50 mM Tris pH 7.5, 200 mM NaCl, 5% (v/v) Glycerol, 3 mM β-Me, 10 mM Imidazole, 5 mM ATP, 50 mM KCl, 10 mM $MgSO_4$
EB1	50 mM Tris pH 7.1, 200 mM NaCl, 5% (v/v) Glycerol, 3 mM β-Me, 500 mM Imidazole
EB2	50 mM Tris pH 8, 250 mM NaCl, 5% (v/v) Glycerol, 2 mM β-Me, 500 mM Imidazole
EB3	50 mM Tris pH 7.5, 200 mM NaCl, 5% (v/v) Glycerol, 1 mM β-Me, 500 mM Imidazole
EB4	50 mM Tris pH 7.4, 200 mM NaCl, 5% (v/v) Glycerol, 1 mM β-Me, 500 mM Imidazole
EB5	25 mM Hepes pH 7.2, 150 mM KCl, 300 mM Imidazole
EB6	50 mM Tris pH 7.5, 150 mM NaCl, 500 mM Imidazole
EB7	50 mM Tris pH 7.4, 200 mM NaCl, 5% (v/v) Glycerol, 2 mM β-Me, 400 mM Imidazole
IEX1	50 mM Tris pH 7.5, 50 mM NaCl, 5% (v/v) Glycerol, 2 mM β-Me
IEX2	50 mM Tris pH 7.5, 1 M NaCl, 5% (v/v) Glycerol, 2 mM β-Me
AEX1	50 mM Tris pH 7.5, 50 mM NaCl, 5% (v/v) Glycerol, 2 mM β-Me
AEX2	50 mM Tris pH 7.5, 1 M NaCl, 5% (v/v) Glycerol, 2 mM β-Me
AEX3	25 mM Hepes pH 7.2, 1 M KCl
DB1	25 mM Tris pH 8, 150 mM NaCl, 5% (v/v) Glycerol, 3 mM β-Me
DB2	25 mM Tris pH 7.5, 125 mM NaCl, 5% (v/v) Glycerol, 1 mM β-Me
DB3	50 mM Tris pH 7.2, 300 mM NaCl, 5% (v/v) Glycerol, 10 mM β-Me
SEC1	25 mM Hepes pH 7, 150 mM NaCl, 2 mM DTT
SEC2	25 mM Hepes pH 7.5, 125 mM NaCl, 5% (v/v) Glycerol, 2 mM DTT
SEC3	25 mM Hepes pH 7, 150 mM NaCl, 1 mM β-Me
SEC4	25 mM Hepes pH 7.2, 125 mM KCl
SEC5	50 mM Tris pH 7.5, 150 mM NaCl, 3 mM β-Me
SEC6	25 mM Hepes pH 7.5, 125 mM NaCl, 5% (v/v) Glycerol, 2 mM β-Me
HIS1	50 mM Tris pH 7.5, 5% (v/v) Glycerol, 1 mM β-Me, 20 mM Imidazole
WB1	50 mM Tris pH 7.5, 150 mM NaCl, 30 mM Imidazole

4.3.3.1 Human CRY1/2

The cell pellet was resuspended (1:10 w/v) in LYS1. The suspension was supplemented with 1 mM PMSF, 0.5 mM AEBSF, 5 mM CHAPS, 2 mM $MgCl_2$, Sm-Nuclease (1 µL per g of cells) and 1 protease inhibitor tablet, which inhibits a broad spectrum of different proteases (cOmplete by Roche, or Pierce protease inhibitor, Thermo Fisher Scientific). After 30 min stirring, cells were lysed by ultrasonication (9 mm horn, output: 6, Duty cycle: 50%, 3x 1.5 min) and the lysate was cleared by centrifugation (92000 x g, 45 min, 4 °C). The protein was purified by

Immobilized metal affinity chromatography (IMAC). The lysate was loaded on a 5 mL HisTrap column using a FPLC system. If Hi5 cells were used for expression, the lysate could not be cleared by centrifugation. In this case 1 mL (dry volume) Ni^{2+}-NTA resin was added to the lysate and was coincubated for 1 h at 4 °C while stirring. The resin was separated from the lysate by centrifugation (300 x g, 2 min) and washed with LYS1. The resin was then transferred to a gravity flow column and was washed with 10 column volumes (CV) HSB1 and 10 CV AB1. The protein was eluted with 100% EB1. The protein was subjected to a cation exchange chromatography (CAEX, 5 mL HiTrap SPHP) using IEX1 buffer to dialyze and load the protein and IEX2 for a gradient elution (50 mL gradient). The protein was filter concentrated (MW cut-off 30 kDa) and size exclusion chromatography was conducted with S200 16/600 column in SEC1 buffer. The final product was filter-concentrated and flash-frozen.

The purification of CRY2 was done in an analogous manner compared to CRY1. The only difference was the buffer pH during the affinity chromatography (50 mM Tris pH 7.5)

The purification of mCRY1-PHR was done as described before (Schmalen *et al*, 2014).

4.3.3.2 CRY1 tail (492-586)

The pellet was resuspended (1:5 w/v) in LYS1, supplemented with 1 mM PMSF, 2 mM $MgCl_2$, 10 µL Sm-Nuclease and was lysed by sonication (9 mm horn, 4x 1.5 min, Output: 6, Duty cycle: 50%). The lysate was cleared by centrifugation (64000 x g, 45 min, 4 °C). It was loaded onto a 5 mL HisTrap column, was washed with HSB2 and eluted in a gradient with EB2. The protein was dialyzed against DB1 and cleaved with GST-3C protease (ratio 1:150). The protein was subjected to a S75 (16/600) run in DB1 and the remaining GST was removed by a GSTrap column. Finally, the protein was subjected to another S75 run, filter concentrated and stored at -80 °C.

4.3.3.3 CRY2 tail (511-593)

The pellet was resuspended in (1:5 w/v) LYS3. The suspension was supplemented with 1 mM PMSF, 0.5 mM AEBSF, 2 mM $MgCl_2$, Sm-Nuclease (1 µl/g pellet) and was lysed by ultrasonication (9 mm horn, Output: 6; Duty cycle 50%, 3x 1.5 min). The lysate was cleared (43000 x g, 45 min) and loaded on a HisTrap column and washed with HSB3 and AB2. After elution, the 6xHis-tag was cleaved with His-3C (mol. ratio 1:100) during an overnight dialysis.

His-3C and 6xHis-tag were removed by HisTrap column. The protein was run on SEC (S75, 16/600, in DB2 buffer) and filter concentrated.

4.3.3.4 TTP complexes

The TIM/TIPIN complexes (TTP, TTP-ΔL, TTP-SL) were purified in a similar way compared to (Justine Witosch, PhD Thesis) with a few modifications. Briefly, the cells were resuspended (1:4 w/v) in LYS3. The suspension was supplemented with 1 mM PMSF, 1 mM AEBSF, 1 tablet protease inhibitor (Roche cOmplete or alternatively Thermo fisher Pierce) and 25 µL Sm Nuclease. After 30 min stirring, cells were lysed by ultrasonication (9 mm horn, 2x 3 min, Duty cycle: 50%, Output: 6). After clearing (43000 x g, 45 min, 4 °C) the lysate was diluted to 500 mL with LYS3 and was loaded on a 5 mL HisTrap column at 4 mL/min. The column was washed with 8 CV HSB3, AB2 and 5% EB3. After elution with 100% EB4, the protein was diluted 1:3 with HIS1 for loading onto an anion exchange column (5 mL Q-HP). After washing with AEX1 and gradient elution with AEX2 the 6xHis-tag was cleaved in dialysis against SEC2 (1:100 mol. ratio, His-3C protease). TTP was run on a S200 16/600 column in SEC2 and was filter concentrated.

4.3.3.5 TIPIN

Cells were resuspended in LYS4 (1:4 w/v) and were lysed by ultrasonication (9mm horn, Output: 6, Duty cycle: 50%, 3x 2 min). 1 mM PMSF, 0.5 mM AEBSF, 20 µL Sm nuclease, 2 mM $MgCl_2$ were added. The lysate was cleared by centrifugation (30 min, 43000 x g), diluted 1:2 with LYS4 and loaded onto a 5 mL HisTrap column. After washing with HSB4, AB3 and 5% EB4, the protein was eluted with 100% EB5. It was dialyzed against DB3 and cleaved (His-3C protease, 1:100 w/w). The solution was supplemented with 10 mM Imidazole and the 6xHis-GST tag was removed by HisTrap column. The flow-through was run on a S200 16/600 column. The protein was filter concentrated, flash-frozen and stored at -80 °C.

mTIPIN was purified according to a previous protocol (Witosch, 2014). The tag was severed in dialysis against DB3.

4.3.3.6 TIM-N-ΔL

Cells were resuspended in 1:4 (w/v) LYS5, supplemented with of 1 mM PMSF, 0.5 mM AEBSF, 2 mM $MgCl_2$, 25 µL Sm Nuclease. The cells were lysed by ultrasonication (9 mm horn, Duty cycle: 50%, Output: 6, 3x 1.5 min). The lysate was cleared at 43000 x g and was loaded onto a 5 mL HisTrap column. The protein was washed with HSB5 and eluted with EB5. Finally, the protein was run on a S200 16/600 with SEC4 and was filter concentrated.

TIM-N-SL was obtained from Dr. Roberto Orrù, who purified it under similar conditions to TIM-N-ΔL.

4.3.3.7 TIM-N-Sumo

Cells were resuspended in 1:5 (w/v) LYS5 (addition of 1 mM PMSF, 0.5 mM AEBSF, 2 mM $MgCl_2$, 25 µL Sm Nuclease). They were lysed using an ultrasonifier (9 mm horn, output: 6, 4x 1.5 min, Duty Cycle: 50%). The lysate was cleared (43000 x g, 45 min) and was loaded onto a 5 mL HisTrap column. The protein was washed with HSB5 buffer, and eluted in a 20 CV gradient of EB5. The eluate was dialyzed against SEC4 and was loaded to an AEX (HiTrap Q-HP), from which it was eluted with a 20 CV gradient of AEX3. Finally, the protein was subjected to a S200 16/600 column, filter concentrated and flash frozen.

4.3.3.8 TIM 520-680

The cells were resuspended in 1:5 (w/v) LYS6, 1 mM PMSF, 20 µL Sm Nuclease were added and the cells were lysed by ultrasonication (9 mm horn, Output: 6, Duty cycle: 50%, 3x 1.5 min). After clearing (43000 x g, 45 min), the supernatant was loaded to a 5 mL HisTrap column. The column was washed with WB1 and eluted in a gradient with EB6. TIM 520-680 was filter concentrated and loaded to a S200 16/600 column for SEC, which was run in SEC5. The central fractions were pooled, filter concentrated and flash frozen.

4.3.3.9 TIM997-1207

The cells were lysed in 1:5 (w/v) LYS3 using sonication (9 mm horn, Output: 6, 3x 2min, Duty cycle: 50%). The lysate was cleared (64000 x g, 45 min) and loaded to a 5 mL HisTrap column. It was washed with lysis buffer and HSB6. After elution with EB7, it was cleaved during dialysis against SEC6 (GST-3C protease, 1:60 mol. ratio). The GST-Prsc and GST-tag were removed by a GSH column. Afterwards the protein was loaded to a S75 16/600 column. The protein was subjected to another HisTrap column to remove residual 6xHis-GST and was run on another S75 16/600 run before filter concentration and flash freezing with liquid N_2.

4.3.4 Fluorescence polarization

To determine binding affinities, we used a fluorescence polarization (FP) assay. In fluorescence polarization the principle is, if a fluorescent molecule is excited with plane polarized light, light is emitted in the same polarized plane if the molecule did not move during the fluorescence lifetime. As molecules in solution rotate and tumble, the orientation of the molecule is changed, which leads to a difference in polarization of the emitted light (Figure 7). Typically, the polarization is calculated as ratio of vertically and horizontally polarized intensity.

$$P = \frac{I_{||} - I_{\perp}}{I_{||} + I_{\perp}}$$

Where $I_{||}$ is the intensity of parallel polarized light, and $I_{\perp}$ the intensity of perpendicularly polarized light. A stationary molecule does not tumble during the fluorescent lifetime; therefore, the emitted light is polarized in the same plane as the absorbed light. Due to tumbling the emitted light changes its polarization. The change in polarization can be related to molecular size, as larger molecules tumble slower than small molecules. Due to protein binding, the size of the protein changes, leading to a change in polarization of the emitted light (Lea & Simeonov, 2012).

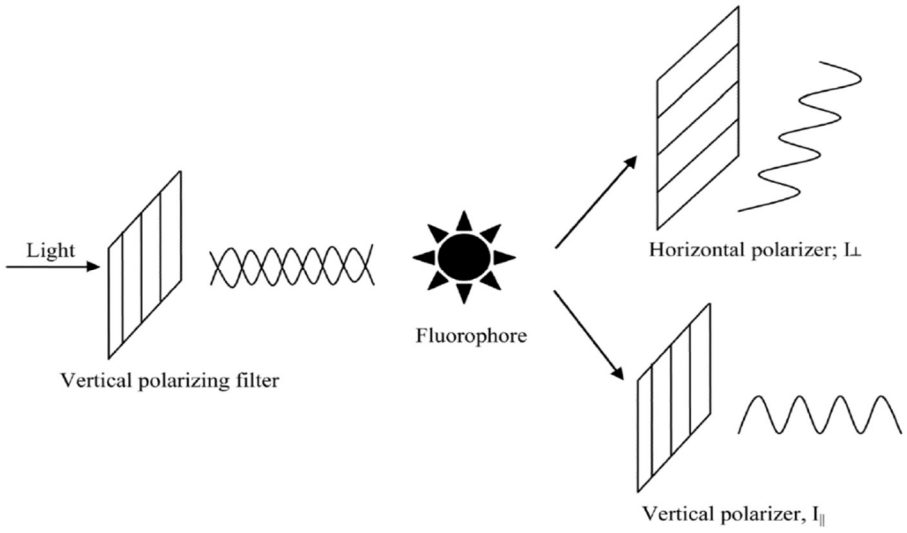

Figure 7: Principle of fluorescence polarization, Figure adapted from (Lea & Simeonov, 2012)

CRY1/2 were labeled on their C-terminal 6xHis-tag and CRY1-PHR (mCRY1 1-496 NT His) on the N-terminal 6xHis tag with Ni^{2+}NTA-Atto647N (Sigma Aldrich GmbH Munich, Germany) dye in PBS buffer. The proteins were labeled in the dark, 30 min on ice and 15 min at RT. The unbound excess of dye was removed by a desalting column (Zeba spin 0.5 mL, Thermo Fisher Scientific), following the manufacturers' instructions. Briefly, the columns were equilibrated with PBS buffer, the protein solution and a 15 µL stacker of PBS were added. The column was spun 3 min at 1500 g. Absorbance at 280 nm and 647 nm were measured in a microscale UV-spectrometer and the protein absorbance was corrected by absorbance of the $^{2+}$NTA-Atto-647N label at 280 nm.

$$A_{prot} = A_{280} + A_{max} * CF_{280}$$

A_{prot} is the corrected protein absorbance at 280 nm; A_{280} the raw absorbance without correction; A_{max} is the absorbance at 647 nm; CF_{280} is the correction factor for the absorbance of the dye at 280 nm (0.03), provided by the manufacturer. The protein concentration was calculated using A_{prot}.

The degree of labeling (DOL) was calculated using the following formula:

$$DOL = \frac{A_{max} * \varepsilon_{prot}}{(A_{280} - A_{max} * CF_{280}) * \varepsilon_{max}}$$

The DOL for CRY1 was on average 1.4, the DOL for CRY2 was 1.6. The degree of labeling for CRY1-PHR was 0.4.

The buffer of the ligands (cleaved TTP, TTP-ΔL, TTP-SL) was changed to PBS. The ligand was prepared in a dilution series in which the protein was mixed 1:1 in each step of the series. The labeled protein was added in a 1:1 volume ratio afterwards. The final concentration of labeled CRY in the reaction was 50 nM in a volume of 20 µL. The samples were transferred to a 384 well plate (Greiner, black well, flat bottom, transparent bottom plate) and the assay was conducted at 25 °C using the Tecan Spark20M plate reader, utilizing filters with transmission maxima at 625/35 nm and 665/08 nm. K_D values were obtained by Prism 5 (Graphpad software, San Diego, USA) by fitting the following equation to the data, accounting for ligand depletion.

$$Y = offset + a * \frac{(K_D + X + r) - \sqrt{(K_D + X + r)^2 + 4 * r * X}}{2 * r}$$

Offset is the offset from the x-axis (y-intercept), *a* is the signal change, *X* is the variable ligand concentration and *r* is the constant concentration of the receptor. FP data was analyzed with the simpler equation from 4.3.5 as well (Figure 70).

4.3.5 Nanoparticle Surface Plasmon Resonance (NanoSPR)

Nanoparticle surface plasmon resonance (NanoSPR) is a label free method to measure protein binding. With NanoSPR, the change in SPR on nanoparticles is measured. The SPR signal changes due to protein binding near the particles surface. The gold nanoparticles are functionalized with DNA-Ni^{2+}NTA linker to act as binding receptors (Figure 8 a). The nanoparticles are distributed in a flowcell and the location of each particle is recorded. This approach allows to assay multiple receptors in the same experiments (Figure 8 b). Due to protein binding the SPR of each nanoparticle-protein sensor changes and is recorded individually, based on the recorded particle location. For each receptor 80-200 particles are observed and the wavelength shift is averaged (Ahijado-Guzmán *et al*, 2014). The NanoSPR was measured in collaboration with the Lab of Prof. Sönnichsen at JGU Mainz. We would like to thank Dr. Rubén Ahijado-Guzmán and Dr. Weixiang He for assistance with the measurement and data analysis.

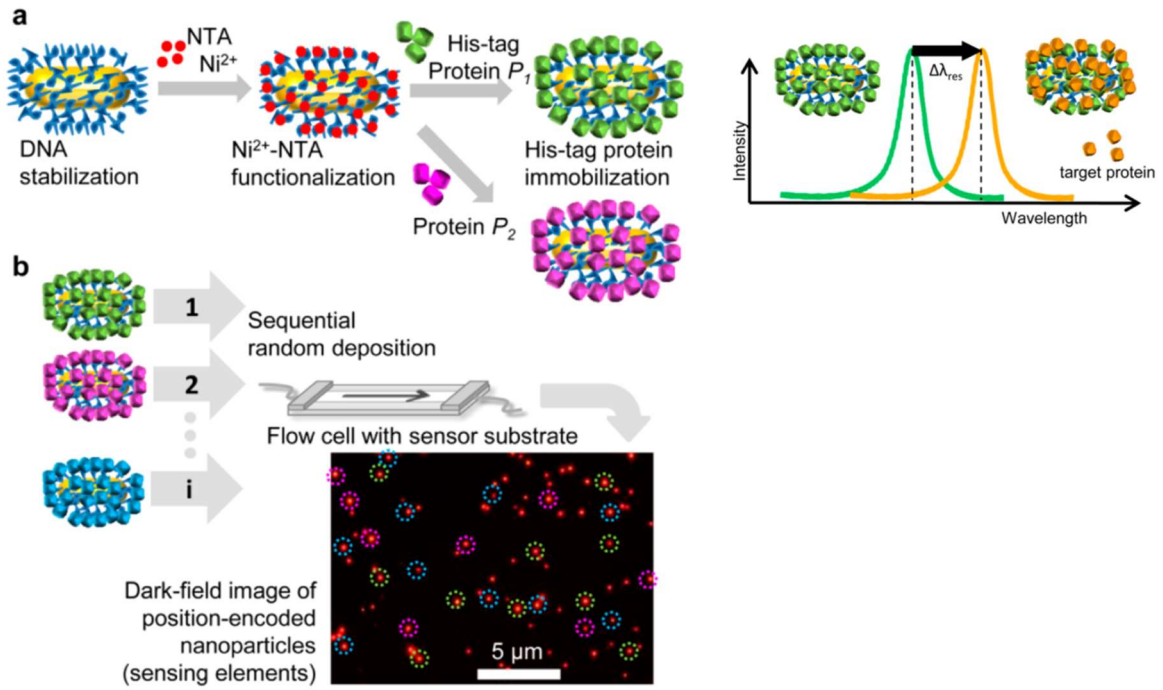

Figure 8: Principle of NanoSPR. A) Gold nanoparticles are functionalized with Ni^{2+}-NTA linker to bind 6xHis tagged proteins (receptor). Binding of the target protein (ligand) to the protein receptor alters the plasmon resonance wavelength. B) The protein bound nanoparticles are deposited sequentially into the flow cell and the position of each particle is recorded. Figure adapted from (Ahijado-Guzmán *et al*, 2014)

The receptors (CRY1 Ct-6xHis, CRY2 Ct-6xHis, CRY1-PHR (mCRY1 1-496 Nt-6xHis)) were diluted with 1x PBS to a concentration of 1 µM. The buffer of the ligands (TTP, TTP-ΔL, TTP-SL) was exchanged to PBS (see 4.3.4) and the protein concentrations were adjusted to 10-30 µM. The nanoparticles were prepared as described in (Ye *et al*, 2013; Ahijado-Guzmán *et al*, 2017). The particles were independently functionalized in solution with 6xHis-tagged CRY, thus making a library of particle-protein receptor conjugates. Each batch of functionalized nanoparticles was flushed separately into the flowcell and the position of each particle was recorded as described (Ahijado-Guzmán *et al*, 2014). By this we created a library of nanosensors and their functionalization. Each nanoparticle-receptor sensor has a characteristic plasmon resonance wavelength (λ_{res}), which shifted due to molecular binding events near the nanoparticle surface (Ahijado-Guzmán *et al*, 2014). To obtain statistics over many nanoparticles-receptor responses, we used an imaging detection method that allowed for the sequential investigation of many particles within the field of view simultaneously as described (Ye *et al*, 2018). The immobilized nanoparticle-receptors were illuminated under dark-field geometry and only the scattered light of the nanoparticles entered the spectrometer at a given

time to spectrally resolve each nanoparticle spectra. To carry out titration experiments, 100 µL of a protein solution (TTP, TTP-ΔL, TTP-SL) was flushed into the flowcell at a flow rate of 50 µL/min, and the plasmon resonance wavelength shift ($\Delta\lambda_{res}$) of every particle (80-200 particles for each protein receptor) was recorded every 60-90 sec at this TTP concentration until an equilibrium value ($\Delta\lambda_{max}$) was reached. This process was repeated for 8-10 different TTP concentrations. K_D values were obtained by fitting a one-site-specific binding model to the data in Prism 5 (Graphpad software, San Diego, USA).

$$Y = \frac{B_{max} * X}{K_D + X}$$

B_{max} is the maximum specific binding and the K_D is the ligand concentration at which half of the binding sites are saturated in equilibrium. X is the ligand concentration.

4.3.6 Analytical SEC

For analytical SEC to test interactions, the proteins were co-incubated 30-60 min, and run on a S75 10/300 or S200 10/300 column at 4 °C at a flow rate of 0.3 mL/min. Typically, the amount of injected protein was 200-600 µg. The absorbance at 260 and 280 nm was recorded as chromatogram.

Calibration of SEC columns:

The S200 10/300 column was calibrated using the *Gelfiltration protein standard* (Biorad, Hercules, California, USA). The run was done at 0.3 mL/min in 25 mM Hepes pH 7.5, 150 mM NaCl, 2 mM β-Me. A linear regression of the retention volumes and the logarithm of the molecular weights (MW) was calculated. Based on linear regressions, MWs were calculated using the retention volumes of proteins on analytical (MW_{SEC}) and preparative (MW_{PREP}) SEC columns (Figure 69).

4.3.7 SAXS (small angle x-ray scattering), MALS (multi angle light scattering) and DLS (dynamic light scattering)

In order to determine structural parameters of the proteins, we used SAXS in combination with MALS and DLS. These methods use protein in solution, no labeling or other modifications are

required. With a combined SEC-SAXS approach, the protein sample is fractionated by SEC before entering the SAXS flow cell, which is advantageous for heterogeneous or unstable samples. This is combined with a MALS-DLS measurement to independently assess the MW and hydrodynamic radius (R_h) (Graewert *et al*, 2015) to complement SAXS data. The synchrotron SAXS data was collected at beamline P12 operated by EMBL Hamburg at the PETRA III storage ring (DESY, Hamburg, Germany). We would like to thank Dr. Nelly Hajizadeh for the assistance in using the beamline and data analysis.

75 µL protein (4-9 mg/mL) was run on a S200 10/300 GL SEC column in the following buffer: 25 mM Hepes pH 7.5, 125 mM NaCl, 5% (v/v) Glycerol, 2 mM TCEP. After SEC the sample was split, half of the sample was directed to MALS, DLS modules and the other half to the X-ray beamline for SAXS data collection (Graewert *et al*, 2015). The MALS and DLS data was analyzed using the Astra 7.1 software.

SAXS data, $I(s)$ vs s, where $s = 4\pi\sin\theta/\lambda 2$ is the scattering angle and the X-ray wavelength (1.24 Å = 10 keV) were collected. Each run consisted of 50 min of data collection, with 3000 frames being collected at an exposure time of 1 sec. The primary 2D data underwent standard automated processing (radial averaging), and buffer subtraction was performed using CHROMIXS (Panjkovich & Svergun, 2018), combined with additional manual and statistical evaluation (e.g., for radiation damage) using the ATSAS software package (Franke *et al*, 2017) to produce the final 1D SAXS profiles.

Briefly, radius of gyration (R_g) values can be extracted by linear approximation of the Guinier region. Alternatively, the R_g can be calculated by Fourier transforming the scattering intensity, which results in a distance distribution function P(r). Plotting the distance distribution over the molecule radius, the curve shows characteristic shapes that are indicative of certain molecule shapes. E.g. a bell shaped curve indicates a globular protein, elongated proteins show a shifted bell shape or multi-subunit proteins show multiple shoulders (Mertens & Svergun, 2010). To do this method the D_{max} (max. particle diameter) was determined using GNOM (Konarev *et al*, 2003). Based on SAXS data MW were calculated using a Consensus Bayesian assessment described in (Hajizadeh *et al*, 2018).

After extraction of SAXS parameters, *ab initio* models were calculated using GASBOR and MONSA. In GASBOR the protein is represented by dummy residues (DR). The protein contains as many dummy residues as there are residues in the protein. The program starts with a random distribution of DRs within a spherical volume of the diameter D_{max}. In each iteration

of the algorithm the distribution of DRs is altered and the *in silico* scattering pattern of this distribution is calculated and compared with the experimental scattering (using CRYSOL (Svergun *et al*, 1995)). The algorithm works on minimizing the difference of *in silico* scattering and experimental scattering (Svergun *et al*, 2001; Mertens & Svergun, 2010).

MONSA is a version of DAMMIN, that can be used to calculate *ab initio models* of complexes. In addition to the scattering data of the complex it uses scattering data of smaller subunits of the complex (Svergun and Nierhaus, 2000). The DAMMIN (Dummy Atom Model Minimization) algorithm starts with a spherical volume (D_{max}) of densely and uniformly packed beads. Each bead is randomly assigned as solvent or solute. In each iteration the *in silico* scattering of the model is changed and compared to the experimental scattering. DAMMIN searches to minimize the scattering differences. The constraints are that the shape must be compact and the beads need to be connected (Svergun *et al*, 2001).

For the prediction of TIM-N-ΔL homodimers the PDBePISA service was used ('Protein interfaces, surfaces and assemblies' service PISA at the European Bioinformatics Institute. (http://www.ebi.ac.uk/pdbe/prot_int/pistart.html) (Krissinel & Henrick, 2007). Graphical overlays of SAXS models were generated by Chimera version 1.14 (Pettersen *et al*, 2004) using the embedded *molmap* and *fit in map* functions.

4.3.8 Protein pulldowns of CRY with TIM-N-ΔL/SL

For protein pulldowns the following buffers were used:

Table 23: Buffers used for pulldown experiments with CRY and TIM-N-ΔL/SL. PD – pulldown buffer.

Name	Component
PD1	50 mM Tris pH 7.5, 250 mM NaCl, 2 mM β-Me, 20 mM Imidazole
PD2	50 mM Tris pH 7.5, 250 mM NaCl, 2 mM β-Me, 50 mM Imidazole
PD3	50 mM Tris pH 7.5, 250 mM NaCl, 2 mM β-Me, 500 mM Imidazole

100 µL Ni-NTA resin (Novagen, Merck KGaA, Darmstadt, Germany) was equilibrated with PD1. 100 µg of CRY1/2 was used as bait and 1.5x mol. excess of prey TIM-N-ΔL/TIM-N-SL was added. Protein and beads were incubated for 1 h at 4 °C while rotating. The resin was washed five times with 500 µL PD1 and five times with 500 µL PD2. The protein was eluted with 50 µL PD3 and analyzed by SDS-PAGE.

4.3.9 Pulldowns with TTP/TTP-ΔL using SILAC extract and MS

In SILAC (Stable Isotope Labeling by Amino acids in Cell culture) the cells are cultured in medium containing light, medium or heavy Arg and Lys. A SILAC approach has the advantage, that three samples can be analyzed at the same time. Three cell extracts are prepared (light, medium, heavy) and are permutated for three pulldown experiments, thus having triplicate samples (Ong, 2003).

U2OS cells were grown in DMEM medium (Life technologies, Thermo Fisher Scientific, Massachusetts, USA) (free from the amino acids Lysine and Arginine) that was supplemented with isotopically labeled heavy Arg-10 and Lys-8 (Cambridge Isotope Laboratories, Tewksbury, Massachusetts, USA), medium Arg-6 and Lys-4 (Cambridge Isotope Laboratories) or light Arg-0 and Lys-0 (Sigma Aldrich GmbH Munich, Germany). Two 15 cm diameter plates of each condition with confluent U2OS cells were harvested. The medium was removed and the cells were washed twice with cold PBS buffer (10 mL). All liquid was removed and 500 µL of modified RIPA buffer (50 mM Tris pH 7.5, 150 mM NaCl, 1 mM EDTA, 1% NP-40, 0.1% Na-deoxycholate), supplemented with 1x Roche cOmplete protease inhibitor, was added. Cells were scraped off the plates and were transferred to a reaction tube and 3 mM $MgCl_2$, 23 U/mL Sm Nuclease were added. The cells were incubated on ice for 45 min and gently mixed. The lysate was cleared by centrifugation (16000 x g, 15 min, 4 °C). The protein concentration was measured in a Bradford assay (4.3.1).

25 µL magnetic Ni^{2+}-NTA coupled Dynabeads (Thermo Fisher Scientific, Massachusetts, USA) that bind 6xHis-tagged proteins, were used per condition. For all washing steps the beads were immobilized using a magnetic rack. The beads were washed with washing buffer (25 mM Tris pH 7.5, 100 mM NaCl, 0.02% Tween20). As bait 100 µg of protein (TTP, TTP-ΔL) were diluted in 500 µL washing buffer (0.2 mg/mL) and incubated for 30 min at 4 °C while tubes were rotated. Unbound bait protein was washed-off by washing 3x with 300 µL washing buffer (beads were carefully resuspended with a pipet). 1200 µg cell lysate (light, medium, or heavy) was added to the beads in a total volume of 500 µL (2.4 mg/mL) and incubated for 2.5 h at 4 °C while mixing. Afterwards, the beads were washed with 1 mL, 2x with 800 µL, and with 250 µL washing buffer. The beads were combined and eluted with 30 µL 1x LDS buffer (NuPAGE, Thermo Fisher Scientific, Massachusetts, USA) for 10 min at 70 °C. Samples were analyzed by the Proteomics core facility at IMB Mainz.

4.3.10 Crosslink Mass Spectrometry

Crosslink Mass Spectrometry (XLMS) is a technique to combine protein crosslinking with Mass Spectrometry analysis. This is especially interesting for protein complexes and can serve as an additional tool to gain insights into structural orientations and distance restrains within the protein complex. The purified protein complex is chemically crosslinked involving reactive residues such as lysine. The linked protein complex is then digested with specific proteases such as trypsin, and the resulting peptides are identified by mass spectrometry. By identification of crosslinked peptides the location of crosslinks can be determined, which can indicate closeness within a protein-protein complex (Petrotchenko & Borchers, 2010; Rappsilber, 2011).

TTP and CRY were mixed in a 1:2-2.5 molar ratio (~2 mg protein in total) and were incubated for 30 min on ice. The complex and the CRY excess were separated on a S200 10/300 GL column in 25 mM Hepes pH 7.5, 125 mM NaCl and the fractions were analyzed on a SDS-PAGE. Fractions corresponding to the trimeric complex were pooled and filter-concentrated to 2 mg/ml. The proteins were crosslinked with 0.2 mg/mL BS3 (bis-(sulfosuccinimidyl)suberate) (Thermo Fisher Scientific, USA), which was dissolved in dimethylformamide (DMF) directly before the reaction. BS3 contains an amine-reactive *N*-hydroxysulfosuccinimide (NHS) ester at both ends of a 11.4 Å spacer arm, that reacts with primary amines such as in lysines.

After 45 min at 37 °C the reaction was stopped by adding 50 mM Ammonium-bicarbonate for 15 min at 37 °C. The crosslinked sample was analyzed on a 4-10% Bis-Tris gradient gel in MOPS buffer (4.3.2). To prepare samples for MS analysis, the crosslinked protein was loaded on NuPAGE 4-12% gradient gels. The gel was stained and bands corresponding to the expected MW were excised. The samples were dried by washing with 100% acetonitrile (ACN) and were shipped to a collaborator (Prof. Rappsilber lab at TU Berlin). The peptide processing and MS data collection and analysis was done by Fränze Müller and Dr. Zhuo Angel Chen.

The excised gel bands were further reduced, alkylated and digested by Trypsin, as previously described (Maiolica et al, 2007). Resulting peptides were extracted from gel bands, concentrated and desalted using C18 Stage Tips (Rappsilber et al, 2007). Peptides were dried down and resuspended in SEC buffer (30% (v/v) ACN, 0.1% (v/v) trifluoroacetic acid) and SEC was performed previously described (Leitner et al, 2012). 16-50 µg of peptides were fractionated using a S3.2/300 column (GE Healthcare) at a flow rate of 40 µl/min. Afterwards, peptides were dried down and resuspended in 2% v/v ACN, 0.1% v/v formic acid (FA) to a final protein concentration of 0.75 µg/µL.

LC-MS/MS analysis was performed using the Orbitrap Fusion™ Lumos mass spectrometer (Thermo Fisher Scientific, USA) with a "high/high" acquisition strategy (high resolution on MS1 and MS2). 1 µg peptides were injected for data-dependent acquisition (DDA) and data-independent acquisition (DIA) experiments. The peptide separation was carried out on an EASY-Spray column (50 cm x 75 µm ID, PepMap C18, 2 µm particles, 100 Å pore size, Thermo Fisher Scientific, Germany). Peptides were separated as previously described (Müller *et al*, 2018) and precursor ions were detected and fragmented and detected in the Orbitrap at 30,000 resolution (Kolbowski *et al*, 2017). In DIA mode, precursor ions were acquired using an MS1 master scan (*m/z* range: 400-1200, max. injection time: 60 ms, AGC target: 4×10^5, detector: Orbitrap, resolution: 60,000), following 53 multiplexed DIA scans (MSX-DIA, two windows in parallel) for MS2 within a fragmentation range of *m/z* 120-1200 using an isolation window width of *m/z* 15 and a max. injection time of 80 ms. Ions in the selected *m/z* window were isolated in the quadrupole, fragmented using HCD (normalized collision energy 30%), and detected in the Orbitrap at 30K resolution.

The raw mass spectrometric data files were processed into peak lists using MSconvert (v. 3.0.9576)(Holman *et al*, 2014). Xi (v. 1.6.731) (Mendes et al, 2019) was used for database searches. The database comprised the sequences of human TIM, TIPIN, CRY1 and CRY2 separately, and the reverse sequence of each of these proteins as decoys. Search parameters were: MS tolerance: 3 ppm, MS/MS tolerance: 10 ppm, enzyme: trypsin, missed cleavages: 3, missing isotope peaks: 3, crosslinker: BS3, fixed modification: carbamidomethylation of cysteine, variable modification: oxidation of methionine and modification by BS3 with the second NHS ester hydrolysis or amidated, with BS3 reaction specificity at lysine, serine, threonine, tyrosine and N-termini of proteins. In a crosslink analysis, the false discovery rate (FDR) was calculated considering residue-pair and peptide spectrum matches (PSM), which were estimated using xiFDR (v. 1.0.22.46) (Fischer & Rappsilber, 2017) following the equation valid for heterobifunctional crosslinkers: FDR = (TD-DD)/TT (Fischer & Rappsilber, 2018) where TT is the number of observed target-target matches, TD the number of observed target-decoy matches and DD the number of decoy-decoy matches. Filtering was applied to only use crosslink PSMs within proteins. Identification with 2% residue-pair FDR was used.

4.3.11 Crosslinking of TTP/CRY2 by Gradient Fixation for single particle EM

In order to obtain a high resolution structure by CryoEM, one needs to have good 2D classes of the particle to know the particle shape. CryoEM images are typically very noisy, due to the low electron dose that is used for imaging of vitrified CryoEM samples. To overcome this problem and to gain signal, tens to hundreds of thousands of images are averaged. In addition to that, the relative particle orientations are unknown and need to be determined. To solve this, each experimental particle image is compared to a reference in all different directions. These low resolution references are often generated by single particle EM (Nogales & Scheres, 2015).

Table 24: Buffers for preparation of crosslinked TTP/CRY2 complex for EM analysis.

Buffer/Solution	**Components**
GraFix buffer	25 mM Hepes pH 7.5, 125 mM NaCl
Heavy solution	30% w/v sucrose, 0.15% glutaraldehyde in GraFix buffer
Light solution	10% w/v sucrose in GraFix buffer
Cushion solution	25 mM Hepes pH 7.5, 125 mM NaCl, 5% sucrose

TTP and CRY2 were chemically crosslinked using the GraFix method (Stark, 2010). TTP and CRY2 were mixed at 1:1.2 molar ratio and diluted with GraFix buffer to a final concentration of 2 mg/mL, 200 µL for each tube. A glutaraldehyde (0-0.15%) and a sucrose gradient (10-30% w/v) inside the GraFix buffer were prepared. A gradient of heavy (30% sucrose, 0.15% glutaraldehyde) and light (10% sucrose) solution (Table 24) were prepared inside a centrifuge tube (Beckman Ultraclear 14 mL thin-walled tubes) using a gradient mixer. On top of the sucrose gradient, 300 µL of cushion solution and the protein were added. The reaction was performed during centrifugation (16 h, 12 °C, 36000 rpm, 217000 x g) using the SW40Ti Rotor inside the Beckman Optima Ultracentrifuge. Afterwards, the gradient was fractionated into 250 µL fractions that were collected in a 96 well plate (Greiner, flat bottom, black plate). The crosslinking reaction was quenched by adding 80 mM Tris pH 7.5. The protein containing fractions were identified by the tryptophane fluorescence (Excitation 280 nm, Emission 330 nm) of the protein using a Tecan Infinite200 pro plate reader. The protein containing fractions were analyzed on a 4-10% Bis-Tris gradient gel. Fractions with a protein band of 240 kDa were pooled, filter concentrated and stored at -80 °C.

The crosslinked TTP/CRY2 complex was subjected to a SEC (Superose6 5/150) to separate aggregates. It was run in 25 mM Tris pH 7.5, 50 mM NaCl. Using this sample, glow-discharged (PELCO easiGlow Glow Discharge Cleaning System) copper grids (TEM grids, 3 mm, 400 mesh, regular, Sigma Aldrich GmbH Munich, Germany) were prepared with 3 µL sample (0.6 mg/mL), washed with 3 µL of uranyl formate, and stained for 30 sec with uranyl-formate (2% w/v). Afterwards excess stain was removed using filter paper.

The data was collected at the MPI of Biophysics (Frankfurt) on a Tecnai Spirit Microscope using the automated data collection software Leginon (Suloway *et al*, 2005) at 26000x magnification and a RIO16 (Gatan) camera at 120 kV at a pixel size of 4.34 Å. For calculating the initial 2D classes 260000 particles were used. 2D classes of particles were calculated using the software CisTEM (Grant *et al*, 2018). Dr. Susann Kaltwasser assisted with data collection and calculated the 2D classes.

5 Results

5.1 Protein Purifications

To perform all the experiments described in this thesis, several proteins were purified (Figure 9). Initially, the interaction of the full length TTP complex and the CRY was analyzed. After the publication of a crystal structure of the N-terminus of TIM (Holzer *et al*, 2017), N-terminal TIM constructs were created. The ΔL variant of TIM was cloned based on the crystal structure that suggested flexibility. In the SL variant the TIM loop is shortened by 30 residues. The C-terminal CRY tails were purified in order to analyze the effect of the CRY tails independently of the CRY-PHR. For analysis of TIM C-terminal interactions, the C-terminal TIM constructs were created.

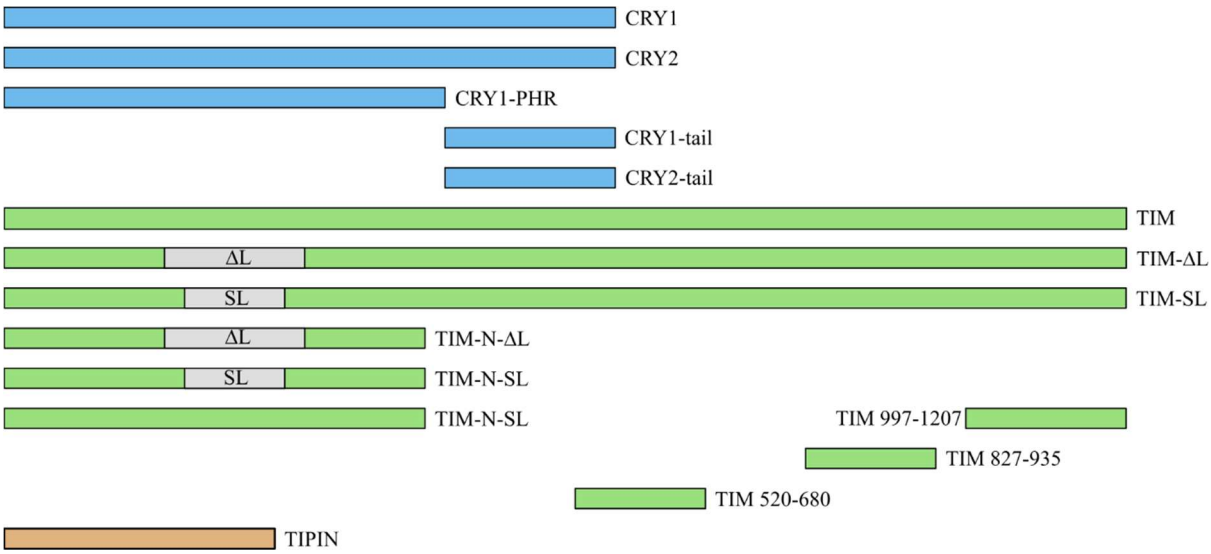

Figure 9: Overview of different CRY and TIM/TIPIN constructs that were used in this study. We worked with full length human CRY1/2. CRY1-PHR is the mouse homolog. Additionally, two C-terminal CRY constructs were used that contain the disordered CRY tails. Full length human TIM and two deletion constructs TIM-ΔL and TIM-SL were used. In TIM-ΔL, the loop was replaced with a –GSTGST- linker; in TIM-SL, the loop was shortened by 30 residues. We created two N-terminal variants of the deletion constructs for TIM. We used two C-terminal TIM constructs and a construct, that spans a short central part of TIM (residues 520-680). For exact construct borders see Table 9.

5.1.1 CRY1

CRY1 was obtained in a two-step purification. First, it was supplied to an IMAC column, which resulted in a clear enrichment of the target protein. Afterwards the protein was cleaned up by SEC, from which it exited as narrow peak with only minor impurities (Figure 10). Occasionally, an anion-exchange-chromatography was conducted before SEC to improve purity. The final protein yield was approximately 10 mg from 1 L of Hi5 insect cell culture. The corresponding MW determined by calibration of the preparative SEC S200 16/60 column (MW_{PREP}) (Figure 69) of CRY1 was 67 kDa, which was consistent with the theoretical MW (MW_{THEO}, calculated using the *Expasy Protparam* server (Gasteiger, 2003)) of 67 kDa. The MW determined by MALS (MW_{MALS}) (Table 26), was 80 kDa, indicating a monomer. Analytical SEC on the S200 10/300 column (MW_{SEC}) showed a MW of only 30 kDa (5.7.1).

5.1.2 CRY2

CRY2 was purified in a similar way as CRY1. After initial IMAC, CRY2 was cleaned up by CAEX and was then supplied to a SEC (Figure 10). 20 mg of CRY2 with minor impurities were obtained from 1 L of Sf9 culture. CRY2 has a theoretical MW of 67.9 kDa based on its amino acid sequence. The observed MW_{PREP} was 82 kDa, which is consistent with the measured MW_{MALS} (85 kDa, see 5.4). An analytical SEC showed a MW_{SEC} of 58.1 kDa (Figure 49), slightly smaller than a monomer. This data suggests that CRY2 was a monomer under used conditions.

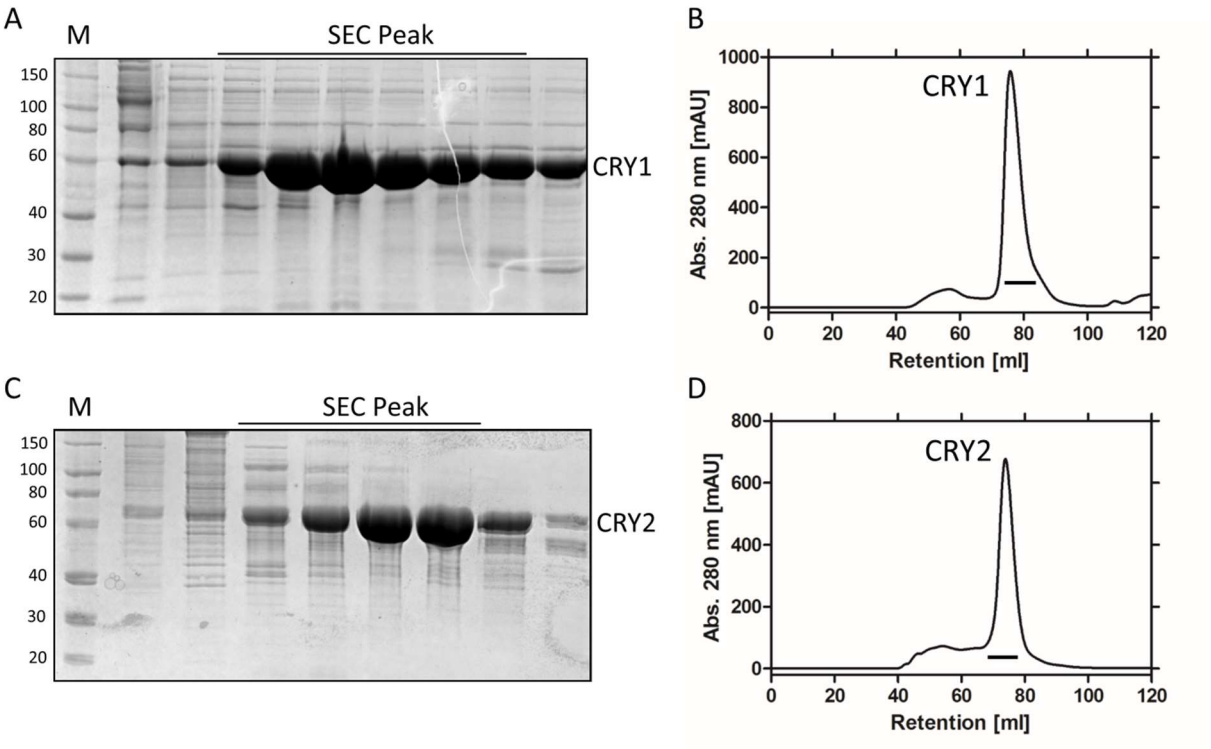

Figure 10: Purification of CRY1 (A, B) and CRY2 (C, D). Final preparative SEC using the S200 16/600 column. A, C) SDS-PAGE shows sample fractions of the SEC peak. B, D) Chromatograms show the absorbance at 280 nm as function of the retention volume. Bar on bottom of the peak indicates the fractions that were pooled as final product. M – protein standard in kDa.

5.1.3 Purification of C-terminal CRY tails

To assess the role of the C-terminal CRY tails in the interaction of CRY and TTP, they were expressed in *E. coli* and purified. The tails are flexible and start after the highly conserved C-terminal helix of CRY (Figure 11).

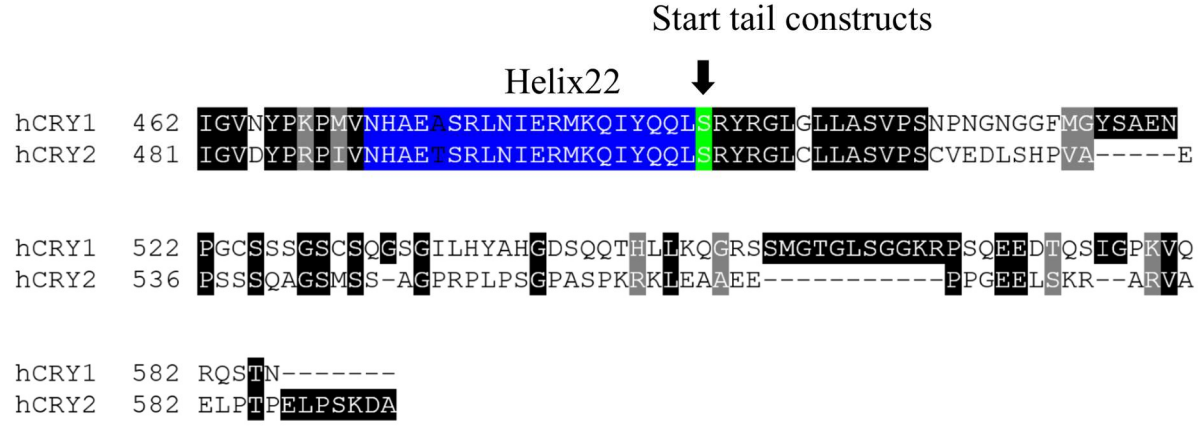

Figure 11: Alignment of CRY1 and CRY2 C-Termini including the C-terminal helix (blue) and the flexible tails. Sequences were aligned using the T-coffee server. CRY1 helix22 472-492; CRY2: 490-510. CRY1 tail: 492-586; CRY2 tail: 511-593. Assignment of helix based on available crystal structures: PDB-ID 4i6g, 4i6e, 4i6j, 4mlp, 5t5x, 4k0r, 4ct0. Note: The C-terminal helix of mCRY1 in complex with mPER2-CBD (PDB ID: 4ct0) is extended by 4 residues. The exchanged amino acid A476T between CRY1 and CRY2 in helix22 is directed inwards to the protein and not exposed to the solvent.

CRY1 tail

The CRY1 tail was expressed as 6xHis-GST fusion protein. The first step was an IMAC, followed by dialysis during which the His-GST-tag was severed. A single SEC did not effectively remove all the residual His-GST, due to its vast excess. Remaining GST was trapped by a GSH column. The CRY1 tail did not bind the column and was collected as flowthrough. Then, a SEC was carried out and resulted in a final product with minor impurities (Figure 12). The estimated MW_{PREP} was 63.6 kDa, which did not fit to the theoretical MW of 9.7 kDa, likely due to observed disorder of the CRY1 tail (Czarna *et al*, 2011).

CRY2 tail

The CRY2 tail was expressed as 6xHis-fusion protein. The purification consisted of three steps. First, the protein was enriched with an IMAC, then the tag was cleaved during dialysis. Finally, the protein was cleaned up by SEC. The final CRY2 tail contained few impurities (Figure 12). The estimated MW_{PREP} was 32.2 kDa, which did not agree to the theoretical MW of 8.4 kDa. The increased MW was consistent with the observation for CRY1 tail and was likely a consequence of the protein disorder.

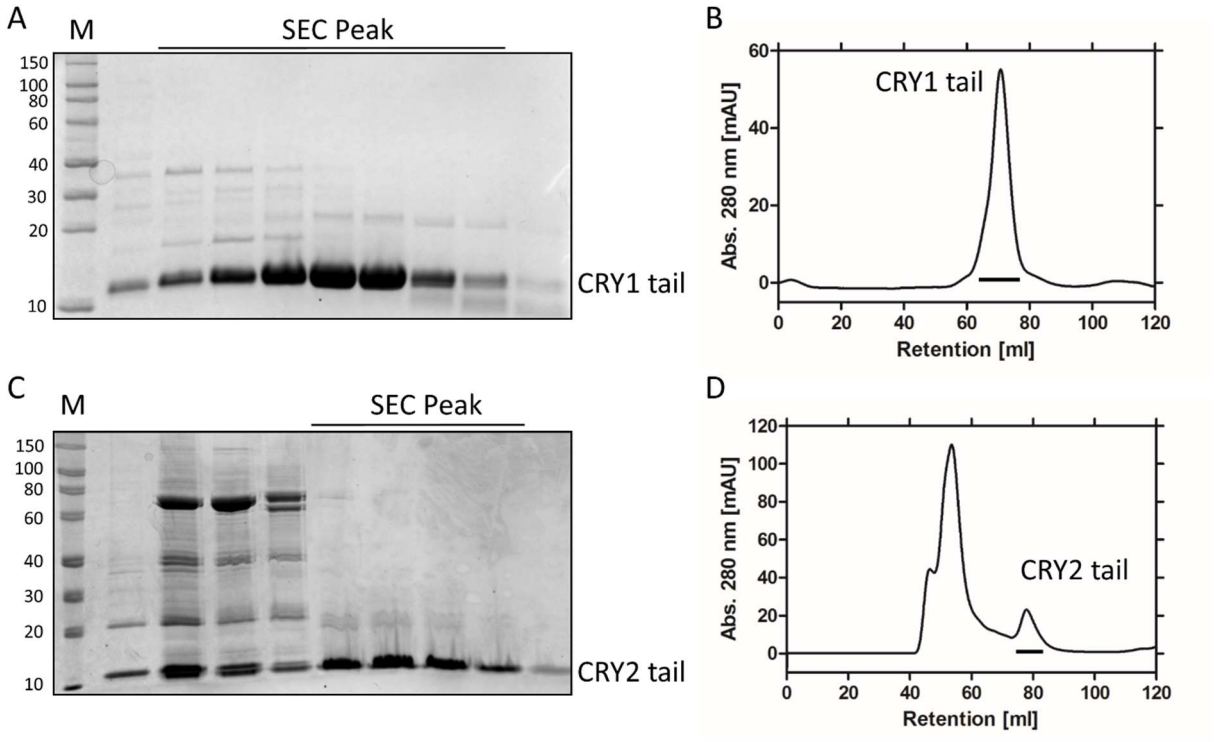

Figure 12: Purification of CRY tails (CRY1 492-586 and CRY2 511-593) by SEC. A, C) SDS-PAGE of peak fractions. B, D) Chromatograms of final SEC. Bars on the top of the SDS-PAGE and the bottom of the chromatograms indicate fractions that were pooled as final product. M – protein standard in kDa.

5.1.4 Purification of TIMELESS/TIPIN

Purification of single full length TIMELESS (TIM) from *E. coli* has not been done successfully yet. Expression and purification of mouse TIM from insect cells leads to formation of large soluble aggregates (Witosch, 2014). But as co-expression, TIM and TIPIN form a complex and stabilize each other, which improves their behavior during purification.

Expression and purification of TTP and modified TTP variants (TTP-SL, TTPΔL) were carried out under similar conditions. Here for simplicity, only the purification of TTP-ΔL is shown (Figure 13). TTP-ΔL, TTP-SL behaved slightly better in terms of less protein degradation and better stability. Briefly, the protein was enriched by an IMAC, afterwards an anion exchange chromatography removed DNA and chaperones present after initial IMAC. As final step the protein was subjected to SEC. TTP-ΔL migrated as a narrow single peak and contained only minor impurities at 70 and 25 kDa.

To compare differences between the TTP variants, MWs were obtained by SEC and MALS (Table 25). For TTP the MW_{SEC} and the MW_{MALS} were in good agreement. However, the MW

estimates were almost twice the MW_{THEO}, suggesting a dimer. TTP-SL, that was shortened by 30 residues, showed a reduction of its MW_{SEC} by approx. 30 %. A similar reduction was observed for its MW_{MALS}. This suggested a TTP-SL monomer. TTP-ΔL had a similar MW_{SEC} compared to TTP-SL, indicating a monomer as well.

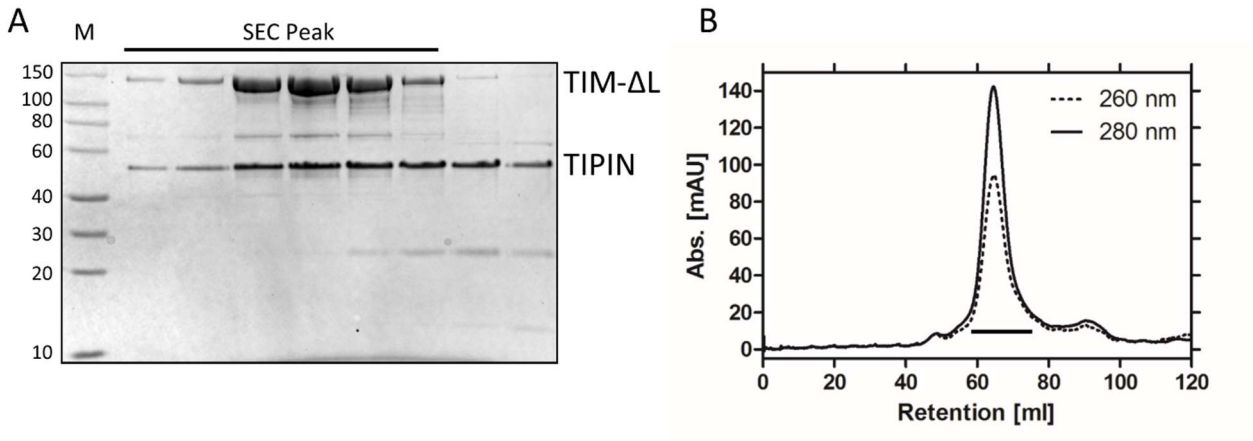

Figure 13: Purification of TTP-ΔL: Final SEC: A) SDS-PAGE of SEC fractions. Numbers indicate the MW of Std. proteins. B) Chromatogram shows the absorbance at 280 and 260 nm as function of the retention volume on a S200 16/600 column. The bar below the peak indicates the fractions that were pooled as final product.

Table 25: MW estimation of TTP, TTP-SL and TTP-ΔL by SEC and MALS. The MW_{THEO} was calculated by the Expasy protparam server using the amino acid sequence. The MW_{PREP} was determined by a SEC run on a calibrated S200 16/600 column. The MW_{PREP} of TTP is an average of 4 runs. The MW_{MALS} was measured in a SEC-MALS setup at the DESY Hamburg using the same samples as for the SAXS data collection.

	MW_{THEO}	**MW_{PREP}**	**MW_{MALS}**
TTP	177 kDa	317 ± 77 kDa	308 kDa
TTP-SL	174 kDa	227 kDa	195 kDa
TTP-ΔL	167 kDa	220 kDa	n.d.

5.1.5 TIM-N-ΔL

To analyze if the N-terminus of TIM would be sufficient to bind CRY (5.3) we cloned the N-Terminus based on a recent study (Holzer *et al*, 2017). We created two constructs: TIM-N-Sumo and TIM-N-ΔL, in which a 100 residue loop was replaced by the residues GSTGST as a linker. It was reported that this construct is more stable and can be more readily expressed and

purified. In comparison to TIM-N-Sumo, the TIM-N-ΔL construct showed an improvement in expression.

TIM-N-ΔL was purified in two steps: an IMAC using a HisTrap column and an additional SEC. The final protein yield of the purification was 17 mg from 2 L of *E. coli* culture with few impurities. The protein could not be concentrated very well; it precipitated at a concentration of 9 mg/mL. The large shoulder left of the main peak, contained large oligomers/aggregates of TIM-N-ΔL and impurities. The migration behavior in SEC indicated a TIM-N-ΔL dimer. The MW_{PREP} was twice the size (93.6 kDa) compared to the MW_{THEO} of 45.5 kDa. Additional analytical SEC obtained a MW_{SEC} of 97 kDa (Figure 49). The dimerization was confirmed by an MW_{MALS} of 92 kDa (Table 26).

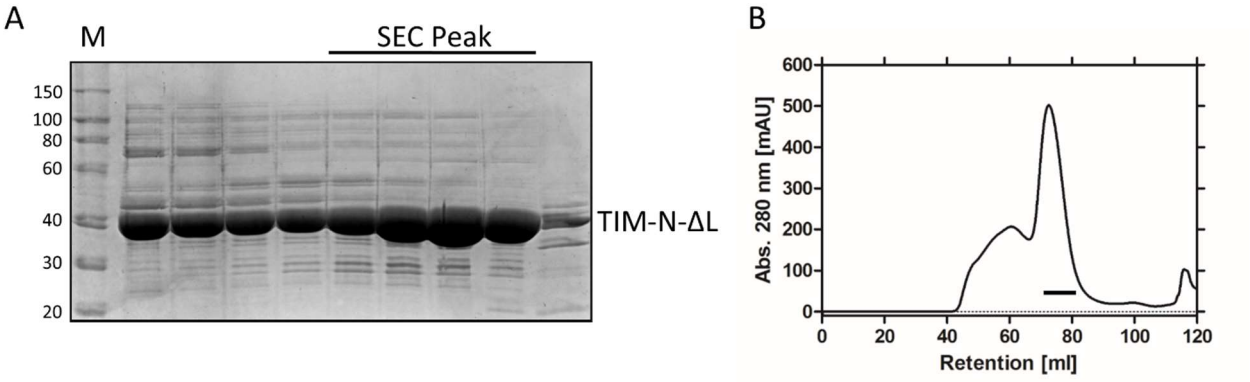

Figure 14: Purification of TIM-N-ΔL. Final SEC with S200 16/600 A) SDS-PAGE shows fractions of the SEC run. B) Chromatogram shows the UV absorbance at 280. Bar indicates fractions pooled for final product. M – protein standard.

5.1.6 TIM-N-Sumo

The first purification attempts of TIM-N-Sumo showed that the Sumo-tag was not cleaved by the sumo protease (not shown). Therefore, we added an additional Glycin behind the Sumo-tag to allow for better accessibility and flexibility for Sumo protease. However, this did not improve the cleavage. The protein was enriched by IMAC and further purified by anion-exchange before SEC (Figure 15). There were small and large MW impurities. TIM-N-Sumo was the most abundant protein in the sample. The main peak had a MW_{PREP} of 590 kDa, because of its low retention. The MW_{THEO} of this construct was 65 kDa. Analytical SEC suggested a MW_{SEC} of

350 kDa (Figure 49). The large MW could have been caused by oligomerization, protein impurities and the disordered nature of the TIM loop.

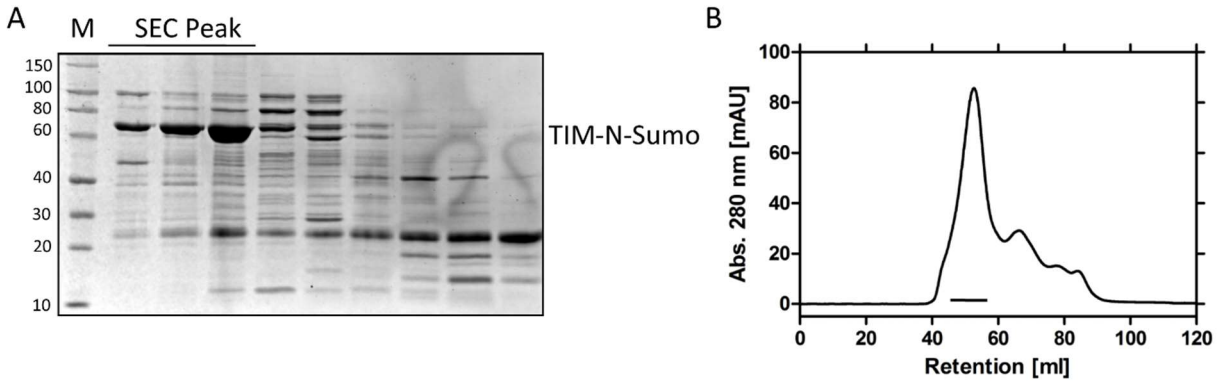

Figure 15: Purification of TIM-N-Sumo. As final step TIM-N-Sumo was run on a S200 16/600 column. A) Analysis of fractions by SDS-PAGE. B) The chromatogram shows Abs. 280 nm as function of the retention volume. Bar inside peak indicates the pooled fractions. M - Protein standard in kDa.

5.1.7 TIPIN

Human TIPIN was expressed and purified following conditions described for mTIPIN (Witosch, 2014) with a few alterations. The protein was enriched by IMAC, then the tag was cleaved during a dialysis. It was further enriched by an AEX. Afterwards, the protein was subjected to a SEC, but pure TIPIN could not be obtained, there was a 70 kDa contamination (Figure 16). Cleaved TIPIN migrated at 50 kDa in SDS-PAGE which was a little higher than expected by its MW_{THEO} of 34.5 kDa, but this was consistent with the migration within the TTP complex (Figure 13) and also with mTIPIN (Witosch, 2014). The protein yield was low: 100 µg protein was obtained from 2 L of *E. coli* culture. The MW_{PREP} was 200-500 kDa, due to a wide SEC peak with a low retention (Figure 16). The MW_{PREP} was much larger than the MW_{THEO} of 34.5 kDa, indicating formation of large oligomers, which was observed for mTIPIN as well (Figure 49 and (Witosch, 2014)). To collect sufficient TIPIN for analytical SECs, mTIPIN was prepared in addition.

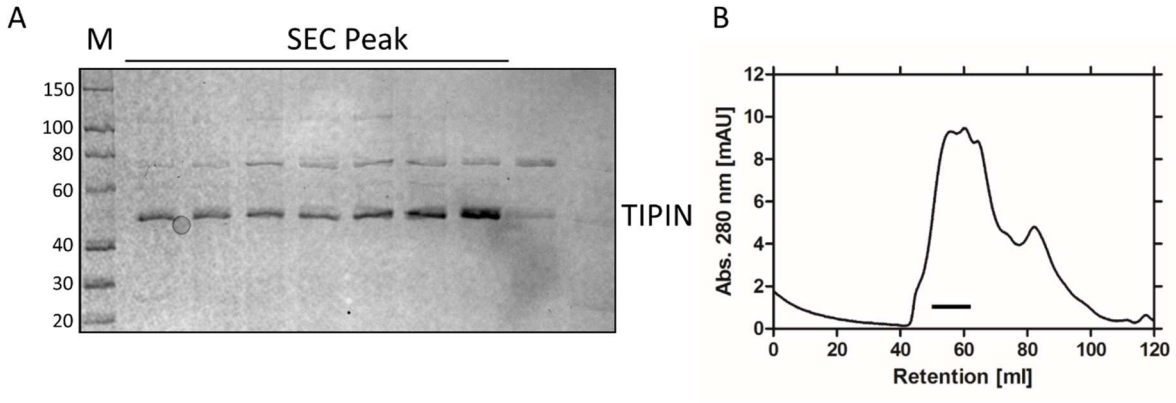

Figure 16: Purification of TIPIN: Final SEC on a S200 16/600 column. A) SDS-PAGE of SEC fractions. B) Chromatogram shows absorbance at 280 nm in SEC. M - protein standard in kDa. Black bars indicate the fractions combined in the final protein sample.

5.1.8 TIM 520-680

TIM 520-680 was well expressed in *E. coli*. The protein was enriched by IMAC and was injected to final SEC. The protein left as single peak with a little shoulder on the right (Figure 17). The retention volume corresponded to a MW_{PREP} of 17.3 kDa which represented a monomer in comparison with its MW_{THEO} of 19.3 kDa. The MW_{SEC} (Figure 49) was in agreement with the MW_{PREP}. It was 26 kDa and corresponds to a monomer. The final yield was 50 mg of protein from 2 L *E. coli* culture.

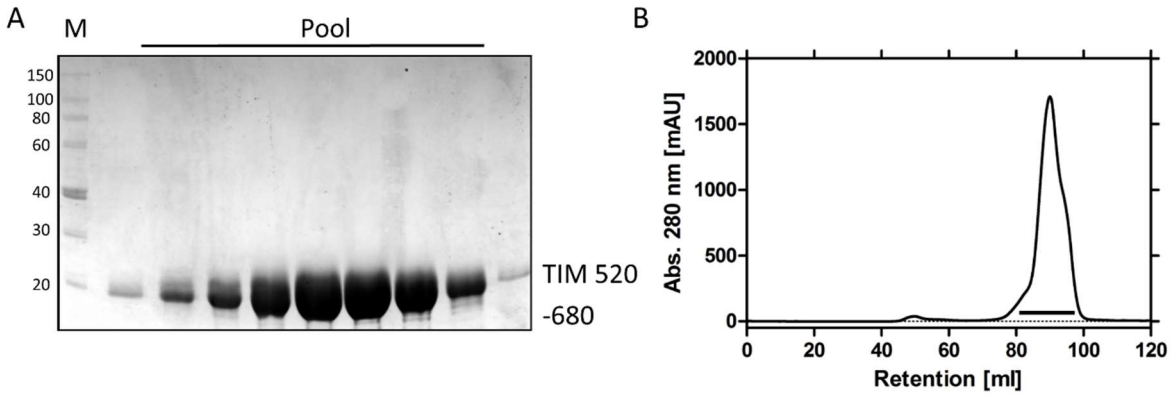

Figure 17: Purification of TIM 520-680. SEC as final step of the purification. The protein was subjected to a S200 16/600 column. A) Shows the SDS-PAGE of representative fractions of the SEC. B) Chromatogram of the SEC shows absorbance at 280 nm as function of the protein retention. Bar indicates the pooled fractions. M - protein standard in kDa.

5.1.9 TIM 997-1207

TIM 997-1207 was purified to test the interaction with CRY1/2 and their tails. It was expressed as 6xHis-GST fusion and was enriched by IMAC. The 6xHis-GST tag was severed during a dialysis. To remove the 6xHis-GST from the sample, the protein was subjected to a GSH column and was run on a SEC. Since the tags were not removed completely, the protein was loaded to a HisTrap column. Finally, the protein was run on another SEC, which showed only minor impurities (Figure 18). The peaks suggested a MW_{PREP} of 70 kDa and 120 kDa, which was larger than the theoretical MW of 23.7 kDa, suggesting trimers and pentamers. Analytical SEC (Figure 49) indicated dimers and tetramers of TIM997-1207 instead.

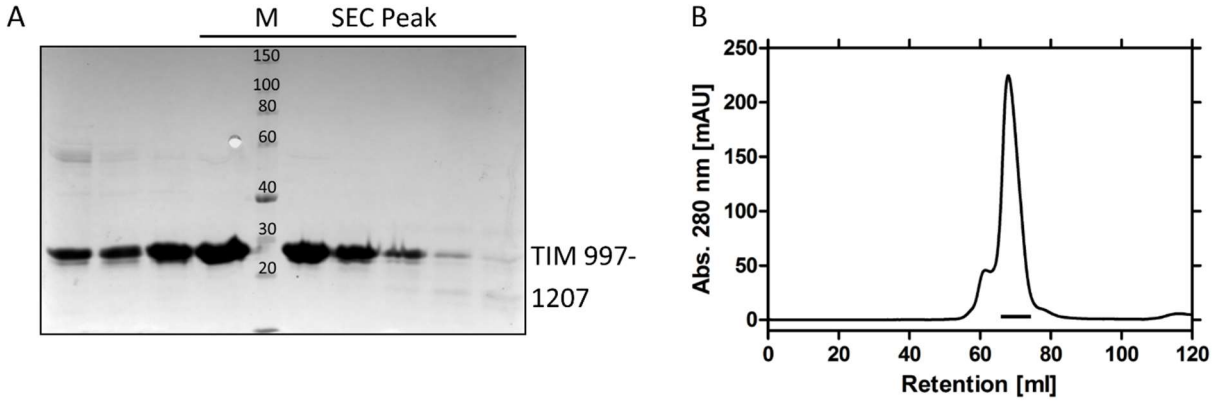

Figure 18: Purification of TIM 997-1207 by SEC with a S75 16/600 column. A) SDS-PAGE shows analyzed SEC fractions. B) The corresponding chromatogram shows Abs. 280 nm as function of the retention volume of the protein. Bar indicates the pooled SEC fractions. M – protein standard in kDa.

5.1.10 TIM 825-935

We purified TIM 827-935 to test its binding to CRY, as XLMS data showed crosslinks between in that region of TIM (5.6). The protein was expressed as 6xHis-GST fusion and was enriched using IMAC. The 6xHis-GST tag was cleaved, but it was not efficiently removed by a HisTrap column. SEC separated some impurities from the target protein (Figure 19), but the final sample was contaminated with GST and His-3C. Based on analytical SEC, the protein had a MW_{SEC} of 16 kDa, therefore, it appeared to be monomeric in comparison with its MW_{THEO} of 12.6 kDa.

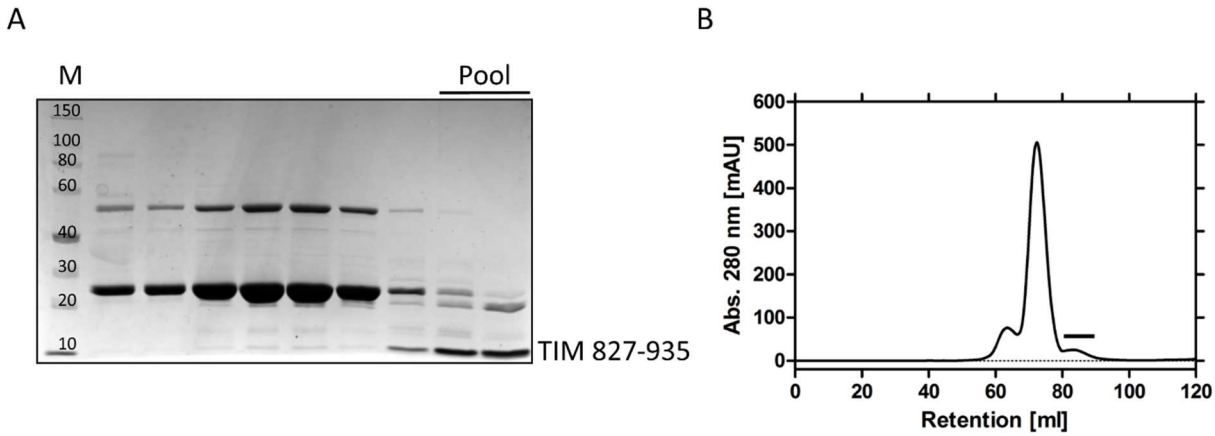

Figure 19: Purification of TIM 827-935. Final SEC using a S75 16/600 column. A) SDS-PAGE shows the final purity of the protein after SEC B) The corresponding chromatogram shows Abs. 280 nm as of the protein. The bar indicates the fractions that were pooled. M – protein standard in kDa.

5.2 CRY1/2 bound TTP directly and formed a trimeric complex

Evidence for an interconnection of TIM with the circadian clock and the findings that CRY and TIM co-precipitate in IP experiments (Kang & Leem, 2014; Unsal-Kaçmaz *et al*, 2005) prompted us to analyze interactions of TIM and CRY. Since was is not possible to purify stable full-length TIM (Witosch, 2014), the TTP complex was used for experiments instead of TIM.

First, the direct interaction of TTP and CRY1/2 was assessed by analytical SEC. TTP was mixed with an excess of CRY1/2 and the proteins were separated by SEC. CRY1 and CRY2 showed a similar behavior with TTP. Two species were formed (Figure 20). The larger species (peak 1) contained TTP and CRY1/2. CRYs did not show this migration behavior when analyzed individually (blue curve), they migrated much faster in presence of TTP. The second protein species (peak 2) contained the unbound excess of CRY1/2. This indicated that CRYs bound to TTP directly and formed a complex *in vitro*.

The stoichiometry of the complexes was determined by MALS analysis (Table 26). The MW_{MALS} of the complexes were 238 kDa for TTP/CRY1 and 249 kDa for TTP/CRY2 (Figure 20 C), which was in agreement with the MW_{THEO} (245 kDa), indicating trimeric complexes with

one molecule of each protein. Similar to the MW_{SEC} analyses for TTP, the MW_{SEC} of the TTP/CRY complexes were larger compared to the MW_{THEO}.

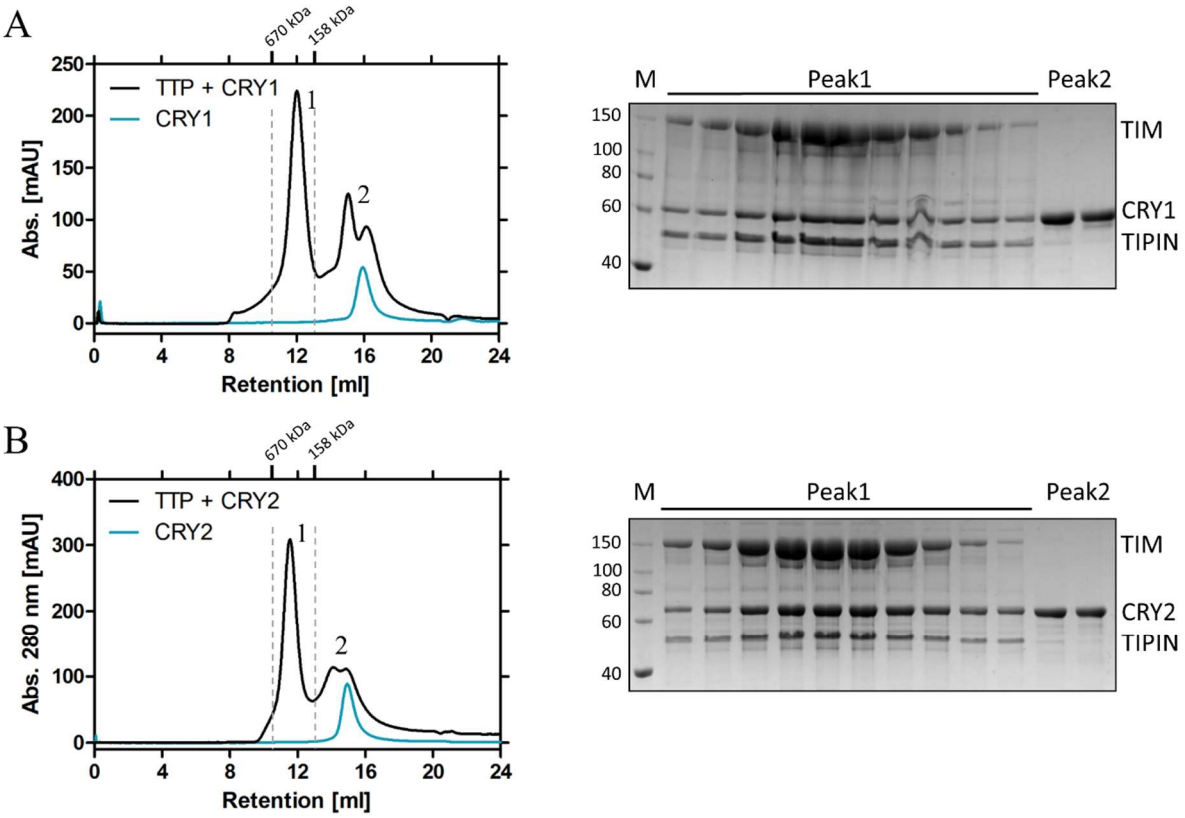

C

	MW_{THEO}	MW_{SEC}	MW_{MALS}
TTP/CRY1	245 kDa	386 kDa	238 kDa
TTP/CRY2	245 kDa	523 kDa	249 kDa

Figure 20: Interaction studies on CRY and the TTP complex. A 2-2.5-fold excess of CRY was mixed with TTP and after 30 min incubation the complexes were analyzed on SEC. A) SEC analysis of the TTP/CRY1 complex. Chromatogram of the SEC (left) shown as overlay of the TTP+CRY1 SEC and the individual CRY1 SEC. SDS-PAGE of representative fractions (right). Dashed lines indicate retention volume of standard proteins. B) SEC analysis of the TTP/CRY2 complex and individual CRY2. SDS-PAGE shows representative fractions (right). M – protein standard in kDa. C) MW estimations of the TTP/CRY1 and TTP/CRY2 complexes by SEC and MALS.

5.2.1 Determination of dissociation constants for TTP/CRY

To characterize the binding, we conducted label-free NanoSPR measurements to obtain K_D values for TTP and CRY1/2 (Figure 21). CRYs were immobilized on nanoparticles that were functionalized to bind 6xHis-tagged proteins. The particles were sequentially flushed with increasing TTP concentrations. CRY1 bound with a K_D of 0.78 µM and CRY2 with a K_D 0.13

µM (CRY2). Based on the findings of (Engelen *et al*, 2013), who found that the C-terminal helix within the PHR region of CRY1 is sufficient for binding to TIM, we measured the affinity for the CRY1-PHR (residues 1-496, excluding the tail) as well. It showed an affinity of 0.48 µM, intermediate between CRY1 and CRY2. The binding affinities were additionally analyzed by a fluorescence polarization (FP) assay in which the CRYs were labeled with a fluorescent dye (Figure 21 B). The FP assay confirmed the K_D values obtained by NanoSPR with slight variations. The K_D of CRY1-PHR to TTP was slightly lower compared to NanoSPR.

The well folded PHR of CRY1 and CRY2 have a high sequence similarity, and the C-terminal helix, which is essential for the interaction with TIM (Engelen *et al*, 2013), is almost identical. The tails, in contrast, show a high sequence variability (Figure 11) and could be involved in the affinity differences between the different CRYs.

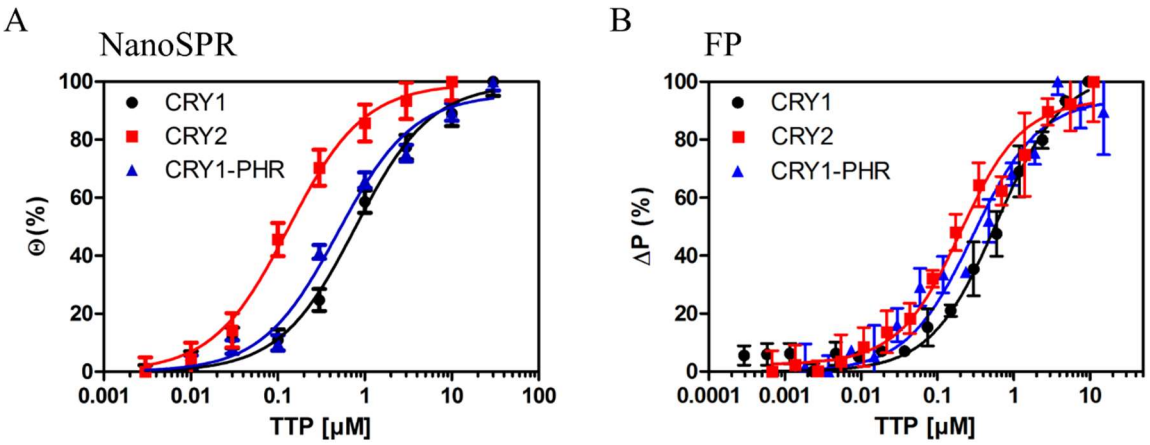

C

	NanoSPR	FP
CRY1	0.78 ± 0.11 µM	0.71 ± 0.11 µM
CRY2	0.13 ± 0.01 µM	0.18 ± 0.05 µM
CRY1-PHR	0.48 ± 0.08 µM	0.36 ± 0.1 µM

Figure 21: Determination of K_D values for CRY and TTP binding. (A) NanoSPR: The CRYs were used as receptors in label-free NanoSPR and were bound to nanoparticles. Increasing concentrations of TTP were titrated to the particles until saturation was reached. The plasmonic resonance wavelength shift for each TTP concentration was recorded. Shown are the normalized plasmonic resonance wavelength shifts as a mean of 80 – 200 single particles (mean ± S.E.M.) n=1 (B) FP assay: CRYs were fluorescently labeled on the 6xHis-tag using the Ni-NTA-atto647 dye. Labeled CRY was titrated with TTP in increasing concentrations. The FP assay was done in duplicates for CRY1 and in triplicates for CRY2 and CRY1-PHR. Data was analyzed using a one-site specific binding model. Here, CRY1-PHR = mCRY1-PHR with N-terminal 6xHis-tag.

To confirm the K_D of TTP/CRY1-PHR, we performed a competition assay of TTP with an CRY1-PHR/mPER 1132-1252. The C-Terminus of mPER2 binds to the C-terminal helix of CRY1 (Schmalen *et al*, 2014), so it could compete with TIM for binding, as TIM binds to the C-terminal helix as well (Engelen *et al*, 2013).

Both complexes were mixed at an equimolar ratio and the sample was analyzed by SEC. There were two peaks: the first peak contained TIM and TIPIN and the second peak contained mCRY1-PHR/mPER2 1132-1252. The slight double band of TIPIN was likely a gel artefact of the SDS gel, as the marker bands show a similar effect. There was no displacement of mPER2 1132-1252 by TTP. Therefore, this data was consistent with the K_D differences of TTP/CRY1-PHR (0.48 µM ± 0.08 µM) and mCRY1-PHR/mPER2 1132-1252 (0.028 µM) (Schmalen *et al*, 2014).

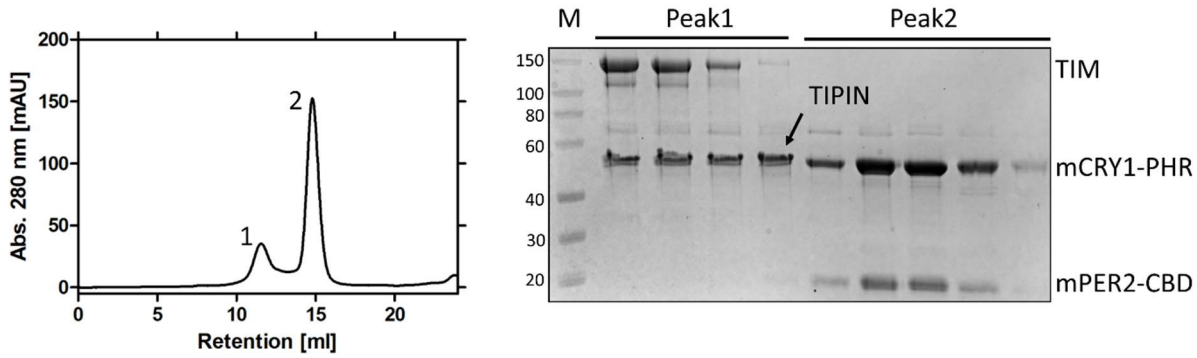

Figure 22: Competition experiment of TTP and mCRY1-PHR/mPER2-CBD for CRY binding: mCRY1-PHR/mPER2-CBD and TTP were mixed in an equimolar ratio, were incubated 30 min, and were separated by SEC. The chromatogram (left) shows the abs. 280 nm. SEC fractions of the different species were analyzed by SDS-PAGE (right). M – protein standard in kDa.

5.3 The TIM Loop

The crystal structure of the TIM N-Terminus shows a well folded, globular protein with predominantly helical secondary structure. It contains a 100 residue long loop that is not resolved (Figure 5A, Figure 9), likely because of disorder in that region (Holzer *et al*, 2017). This loop is of unknown function and has not been investigated yet. After replacement of the loop with a short linker, the construct (TIM 1-463Δloop) has an increased stability compared to TIM 1-463 and it could be readily expressed and purified. Combined with the finding that residues 1-309 of the TIM N-Terminus are sufficient to bind mCRY1 in Co-IP (Engelen *et al*,

2013) we decided to use TIM1-463 (TIM-N) for further characterization of the TIM/CRY interaction. We also were interested to see the effect of the TIM loop on the TIM/CRY interaction.

We created three N-terminal TIM constructs (Figure 9): TIM-N-Sumo contained the complete loop, in TIM-N-ΔL (Δ239-330) the loop was deleted and replaced by a short linker and TIM-N-SL (Δ274-303) contained a 30 residues shortened loop (Table 9, Figure 68). This 30 residue stretch was reported to be highly modified by PTMs in high-throughput screens (Figure 71, (Hornbeck *et al*, 2015)). Firstly, we tested binding of TIM-N-Sumo to CRY1 by SEC. TIM-N-Sumo bound to CRY1 (Figure 23) as both proteins co-migrated (peak1) and CRY1 bound to TIM-N-Sumo showed a faster migration than unbound CRY1 excess (peak2, blue curve).

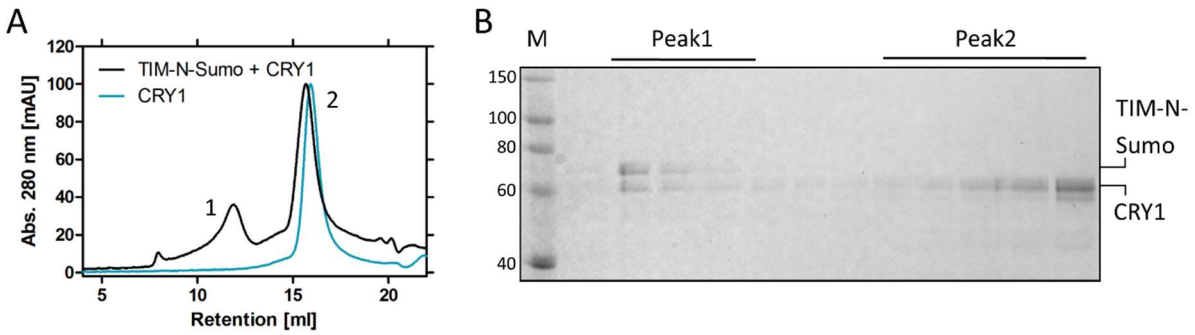

Figure 23: Interaction analysis of CRY1 and TIM-N-Sumo by SEC. A 2-fold excess of CRY1 was mixed with TIM-N-Sumo, incubated 30 min on ice and was analyzed by SEC. SEC chromatogram (A) of TIM-N-Sumo (black curve) is shown as an overlay with the SEC of individual CRY1 (blue curve). Numbers indicate the dominant peaks. SEC fractions were analyzed by SDS-PAGE (B). M - MW of standard proteins in kDa.

To judge the effect of TIM loop deletion or shortening on CRY binding, we conducted protein pulldowns using 6xHis-tagged CRY1/2 as bait and TIM-N-ΔL/TIM-N-SL as prey. The pulldown showed co-elution of both TIM constructs with CRY1 and CRY2, therefore direct binding was concluded (Figure 24). The control showed that the TIM proteins did not bind to the bead material independently of CRY1/2.

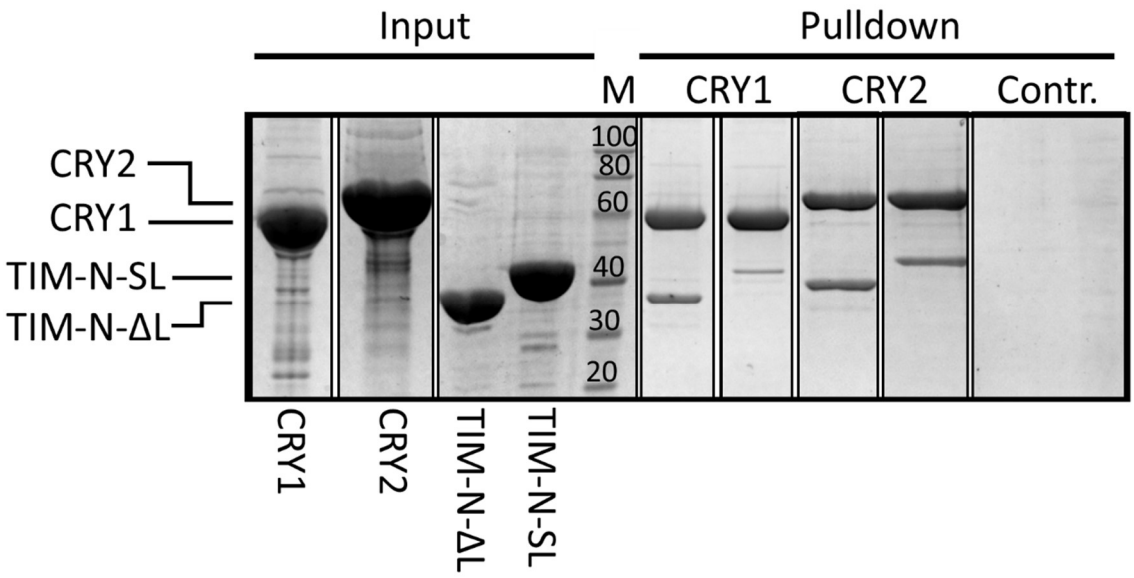

Figure 24: Protein pulldown of TIM-N-SL and TIM-N-ΔL with CRY1/2 as bait. 6xHis-tagged CRY1/2 and untagged TIM-N-ΔL/SL constructs were incubated with Ni-NTA agarose beads for 1 h. After washing, the beads were eluted with 300 mM imidazole and analyzed on a SDS-PAGE. Shown are input samples of CRY1, CRY2, TIM-N-ΔL, TIM-N-SL before the pulldown. Control refers to the experiment done without bait to check for unspecific binding of TIM. M - MW marker of standard proteins in kDa.

To further characterize the interaction of CRY1/2 and TIM-N-ΔL, we tested binding in SEC (Figure 25). The chromatograms showed one predominant peak (peak1) which contained TIM-N-ΔL as well as CRY1 and CRY2, respectively. It was accompanied by an additional peak of CRY1 and CRY2 excess (peak2). TIM-N-ΔL showed binding to CRY1/2. Deletion of the TIM loop did not eliminate binding to CRY, which confirmed the protein pulldowns (Figure 24).

The MW_{SEC} for CRY1/TIM-N-ΔL was estimated to be 165 kDa, which suggested a higher stoichiometry than 1:1. The MW_{SEC} for CRY2/TIM-N-ΔL was estimated to be 332 kDa. The CRY1/TIM-N-SL and the CRY1/TIM-N-ΔL complexes were analyzed by MALS (4.3.7). CRY1/TIM-N-ΔL showed a MW_{MALS} of 138 kDa, and CRY1/TIM-N-SL 170 kDa, which suggested a 2:1 interaction of a TIM-N-ΔL/SL dimer with a CRY monomer (Table 26).

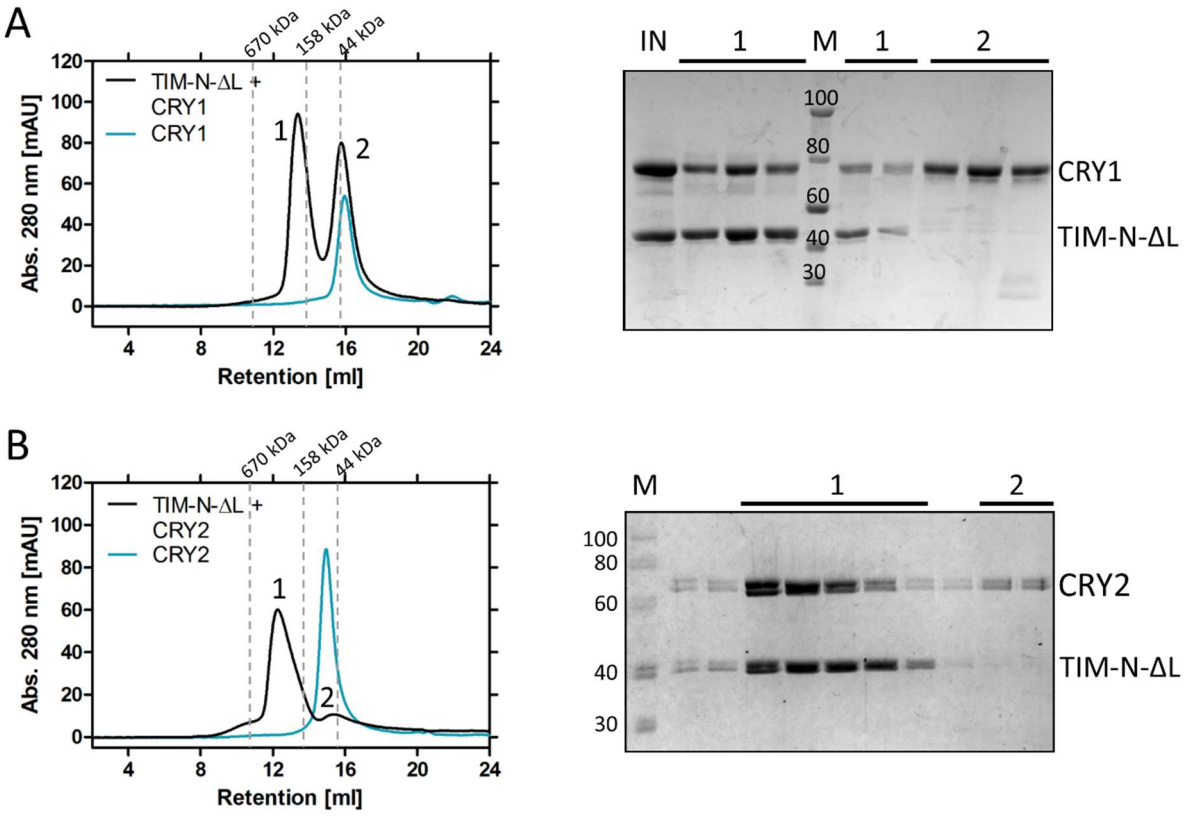

Figure 25: Analytical SEC of TIM-N-ΔL with CRY1 (A) and CRY2 (B). 2-fold and 1.2-fold excess of CRY1 and CRY2 was incubated with TIM-N-ΔL for 30 min and analyzed by SEC. Chromatograms of the combined TIM-N-ΔL and CRY runs (black curve) are shown as overlay with individual CRY SEC runs. Numbers indicate dominant SEC peaks. Dashed lines indicate the retention of standard proteins. Note: the double bands in (B) were a due to heterogeneities of the gel, since the standard proteins showed double bands as well. M – standard proteins in kDa; IN – input sample before SEC.

To confirm that binding of TIM-N-ΔL to CRY1/2 was not an artificial effect of the homodimerization of TIM N-Terminus, we expressed and purified TIM-ΔL/TIPIN (TTP-ΔL) (Figure 13). The interaction of TTP-ΔL with CRY was tested by SEC (Figure 26 A, B). Both CRYs co-migrated with TTP-ΔL (peak 1, black curve) and showed a shift in retention volume compared to their individual SECs (blue curves). In peak2 there was some unbound CRY1 and CRY2 as well as TIPIN. The MW_{SEC} estimation differed from the theoretical molecular weights (MW_{THEO}) by a factor of 2 (Figure 26 E), which was observed for the trimeric complexes of CRY1/2 and TTP before as well (Figure 20 C).

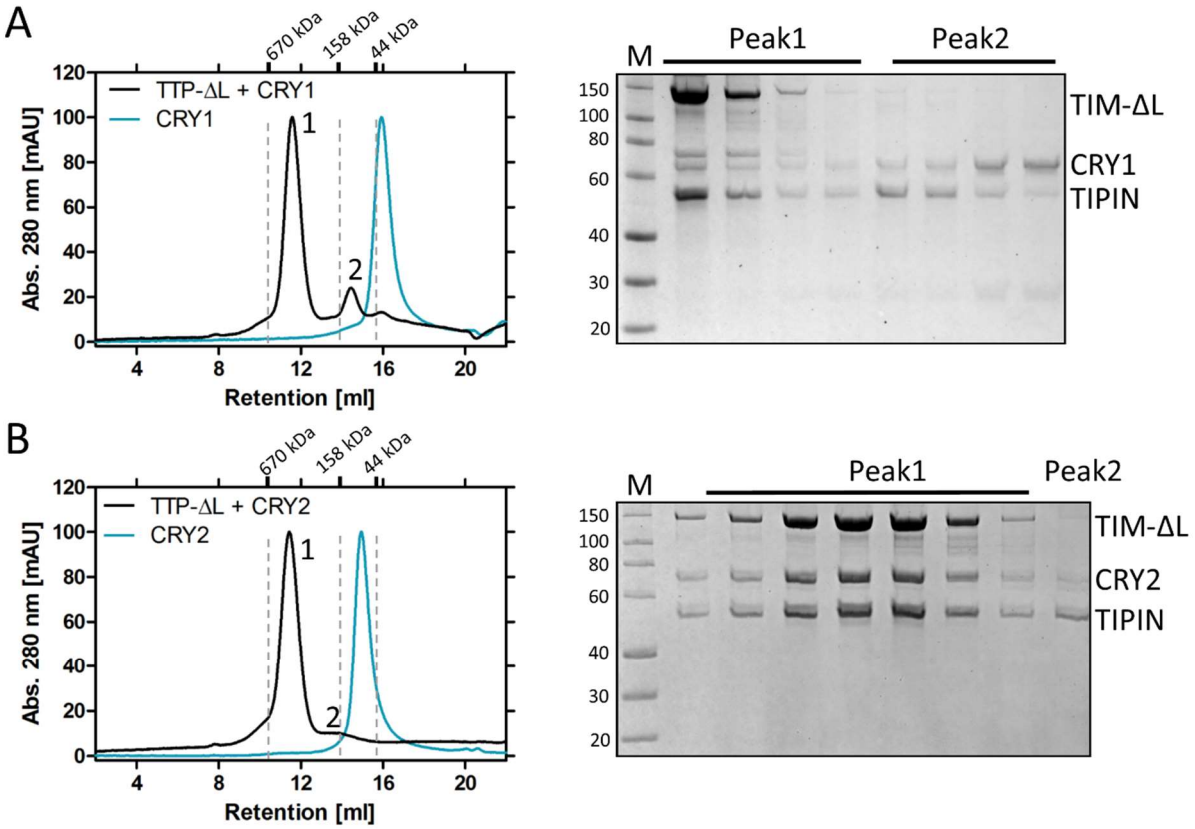

C

	MW_{THEO}	MW_{SEC}
CRY1/TTP-ΔL	234 kDa	460 kDa
CRY2/TTP-ΔL	235 kDa	498 kDa

Figure 26: Interaction analysis of TTP-ΔL with CRY by SEC. CRY1 (A) and CRY2 (B) were incubated with equimolar amounts of TTP-ΔL and were analyzed by SEC. SEC runs are shown as overlay of the TTP-ΔL + CRY chromatogram and the chromatogram of the individual CRY SECs. Dashed lines indicate retention volume of standard proteins. The numbers indicate analyzed protein peaks on SDS-PAGE. Chromatograms were normalized for better comparability. C) MW_{THEO} and MW_{SEC} of the trimeric TTP-ΔL/CRY complexes. MW_{THEO} was calculated based on the amino acid sequence using the Protparam (Expasy server (Gasteiger, 2003) MW_{SEC} was determined by a calibration curve. M – protein MW standard.

5.3.1 TTP loop variants showed altered binding to CRY

In 5.2.1 we determined K_D values for CRY to TTP using NanoSPR and FP, which showed a difference between CRY1 and CRY2. In addition to that, the TIM loop was not essential for the binding of CRY to TIM (Figure 24, Figure 25). Since no function of the TIM loop has been described yet and because it is located within the CRY-interacting N-terminal region (TIM 1-463), we wondered whether the TIM loop could affect the binding affinity of CRY1 and CRY2

to TTP. Here we used TTP-ΔL and TTP-SL to assess the effect of TIM loop deletion and TIM loop shortening on the CRY binding affinity.

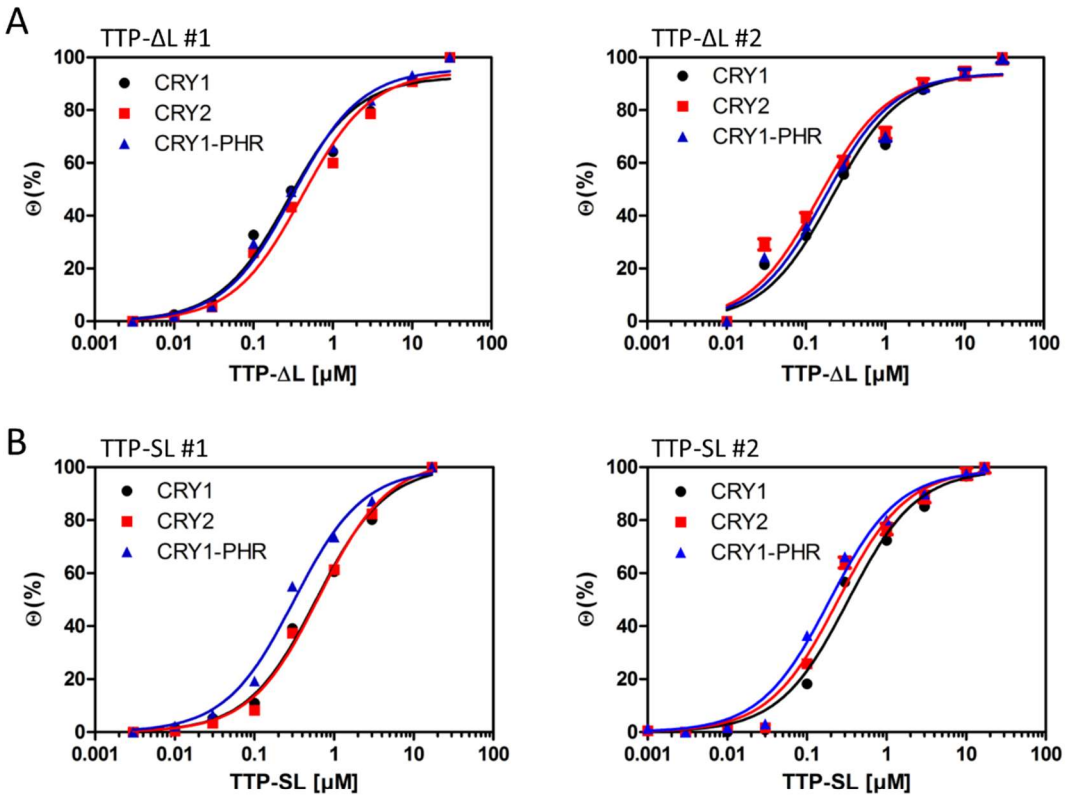

C

	TTP-ΔL #1	TTP-ΔL #2	TTP-SL #1	TTP-SL #2	TTP (NanoSPR)	TTP (FP)
CRY1	0.27 ± 0.06 µM	0.21 ± 0.05 µM	0.60 ± 0.08 µM	0.32 ± 0.06 µM	0.78 ± 0.11 µM	0.71 ± 0.1 µM
CRY2	0.41 ± 0.07 µM	0.14 ± 0.04 µM	0.65 ± 0.08 µM	0.24 ± 0.04 µM	0.13 ± 0.01 µM	0.18 ± 0.05 µM
CRY1-PHR	0.31 ± 0.05 µM	0.17 ± 0.04 µM	0.31 ± 0.04 µM	0.19 ± 0.03 µM	0.48 ± 0.08 µM	0.36 ± 0.1 µM

Figure 27: NanoSPR of TTP-ΔL/TTP-SL and CRYs. Functionalized nanoparticles were coated with CRY1, CRY2 and CRY1-PHR (mCRY1-PHR, N-terminal 6xHis-tag) as receptors. TTP-ΔL (A) and TTP-SL (B) were stepwise titrated to the CRY bound nanoparticles at increasing concentrations. The SPR was measured for 60-90 sec at every concentration until the signal was stabilized. Every datapoint represents the average normalized wavelength shift observed on 80-200 nanoparticles (mean ± SEM). Due to small errors, error bars are hardly visible in the curve. To extract K_D values, a one-site specific binding model was fitted to the data. (C) Overview of measured K_D values, including K_Ds with TTP (gray). Errors indicate errors related to the fit of data.

TIM loop deletion (TTP-ΔL) caused the K_D values for CRY1 and CRY2 to become similar (Figure 27 A, C). This was different to wild-type TTP, that showed a higher affinity for CRY2 and a lower affinity to CRY1 compared to CRY1-PHR that lacked the tail (Figure 21, Figure 27). Hence, TIM loop deletion resulted in an increased affinity for CRY1, that bound with a

similar affinity compared to CRY1-PHR. Shortening of the loop (TTP-SL) caused the affinities for full-length CRY1 and CRY2 to be in the same range, but they were lower compared to CRY1-PHR. Taken together, these results suggest, that the TIM loop might affect the CRY1 and CRY2 binding affinity differentially via the non-conserved CRY1 and CRY2 tails.

Note, that in the first NanoSPR replicates (#1) of TTP-ΔL and TTP-SL, CRY1-PHR showed an affinity similar to the values obtained for wild-type TTP (K_D = 0.31 μM). The second replicates in contrast, (#2) showed reduced K_D values for CRY1-PHR (0.17 μM for TTP-ΔL, 0.19 μM for TTP-SL). Collectively, K_Ds obtained in the second replicate of the TTP-ΔL and TTP-SL affinity measurements seemed reduced by approximately 50% compared to the first. Qualitatively, however, the two measurement series agree showing that i) loop deletion and loop shortening both lead to similar TTP binding affinities of the two full-length CRY1 and CRY2 proteins and ii) loop deletion results in similar affinities of CRY1, CRY2 and the CRY-PHR, whereas loop shortening leads to somewhat lower affinities of full-length CRY1 and CRY2 compared to the CRY-PHR.

To test binding of the isolated TIM loop to CRY, we attempted expression and purification of the TIM loop individually. After successful expression as 6xHis-GST fusion protein, it was very unstable and degraded rapidly during the purification attempts (not shown). Therefore, a successful purification could not be completed.

5.4 Structural analysis by SAXS

For structural characterization of the TIM/CRY complexes, we collected SAXS data which allows to determine structural parameters and low resolution modeling of proteins in solution. Sample was analyzed in a SEC-SAXS setup in which it was run on SEC, and then was split in two parts for parallel collection of SAXS and MALS, DLS data. The structural parameters can be found in Table 26. The R_g values were calculated using two different approaches: Linear approximation of the Guinier region and the distance distribution function P(r). Both values were in good agreement with each other. Comparison of the maximum dimension (D_{max}) of the single proteins and the complexes fits to the relative size differences of the proteins and protein complexes. The R_g/R_h ratios suggested that most analyzed proteins had a close to globular shape, since the characteristic R_g/R_h ratio of a globular protein is 0.7 (Receveur-Brechot & Durand, 2012). A fully denatured protein has a ratio of 1.4. By comparison of the theoretical

MW_{THEO} with experimental Bayesian MW and MW_{MALS}, the stoichiometry was estimated (Table 26).

Table 26: Biophysical parameters determined by SEC-SAXS and MALS/DLS. After passing the SEC column, the sample was split for SAXS and MALS/DLS data collection. The R_g, was calculated from the distance distribution P(r) and the Guinier analysis. D_{max} was determined by the distance distribution P(r). The MW was determined using the MALS measurement and Bayesian interference (MW and Credibility interval of >92% probability of finding the MW in the given range) of SAXS. The R_g/R_h ratio is a shape factor that indicates shape of the protein. The R_h was determined by DLS. MW_{THEO} was calculated by Expasy protparam.

Structural Parameters	**CRY1**	**TIM-N-ΔL**	**TIM-N-SL**	**TIM-N-ΔL/CRY1**	**TIM-N-SL/CRY1**	**TTP/ CRY1**	**TTP/ CRY2**
R_g (nm) [P(r)]	3.3	3.3	3.4	4.6	5.1	5.7	5.7
R_g (nm) [Guinier]	3.2	3.1	3.5	5.0	4.8	5.4	5.4
D_{max} (nm)	14	11	11.7	20.7	22	21.6	21.4
R_h (nm)	3.9	4.2	4.7	5.2	5.7	6.8	7
R_g/R_h	0.8	0.8	0.7	0.9	0.9	0.8	0.8
MW determination							
MW_{THEO} [kDa]	67	43	50	113	117	245	245
MW_{MALS} [kDa]	80	92	103	138	170	238	249
Bayesian MW [kDa]	67 (63-71)	79 (73-87)	114 (106-121)	169 (151-176)	208 (194-264)	318 (221-327)	318 (221-327)

5.4.1 SAXS Analysis of CRY1

The Guinier analysis (Figure 28 A, Table 26) resulted in an R_g of 3.2 nm, which was in close agreement with the R_g value determined by the distance distribution P(r). The ratio R_g/R_h of 0.8 indicates a slight elongation of the particle. Bayesian MW determination and MW_{MALS} indicated a CRY1 monomer. Kratky analysis and the P(r) function showed particle compactness by peak symmetry, but the P(r) function showed tailing of the curve at higher r values indicating extendedness of the particle or slight aggregation (Figure 28 B, C). With GASBOR an *ab initio* model was calculated (Figure 28 D), which had a good fit to the data ($\chi 2 = 1.6$). The model had an overall compact shape, that was slightly elongated with a narrow extension at the bottom. In comparison with the crystal structure of mCRY1-PHR (Czarna *et al*, 2013), there was a clear

overlap of the bulky region of the SAXS envelope and the mCRY1-PHR (Figure 28 D). The narrow extension could represent the CRY tail which was not present in the crystal structure. Hence, comparing the experimental scattering of full length CRY1 with the *in silico* scattering of mCRY1-PHR resulted in a non-ideal fit ($\chi 2 = 5.6$).

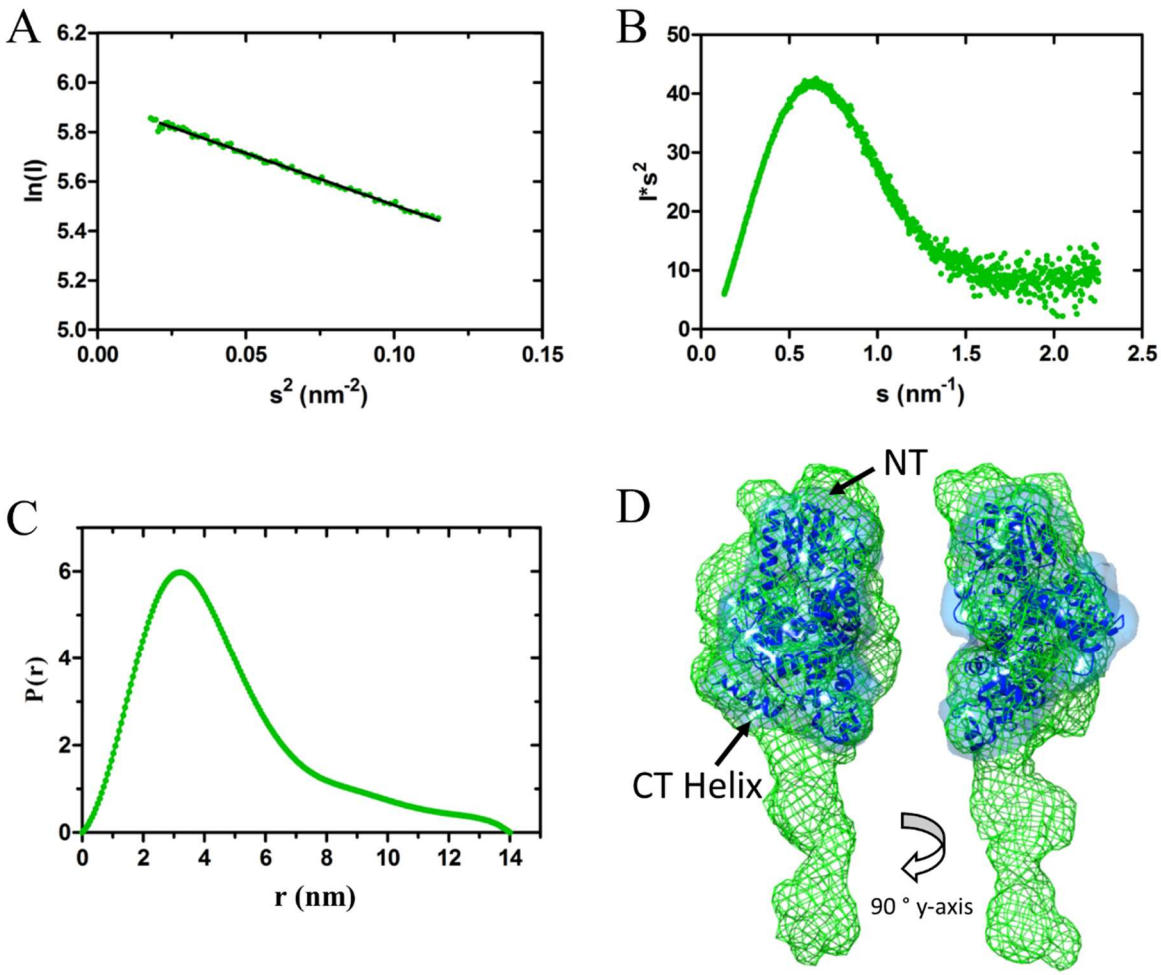

Figure 28: SAXS analysis of CRY1. A) Guinier plot of CRY1. The region used for linear approximation is indicated as green shade. B) Kratky plot showing a folded and compact shape C) Distance distribution analysis with GNOM. A D_{max} of 14 nm was determined. D) GASBOR model of CRY1 (green) with χ^2 of 1.6. An overlay of the CRY1 SAXS model and a crystal structure of mCRY1-PHR (blue, PDB: 4K0R) is shown.

5.4.2 SAXS analysis of TIM-N-ΔL and TIM-N-SL

The Guinier regions of TIM-N-ΔL and TIM-N-SL showed a similar R_g (Table 26, Figure 29), as both constructs were of similar size and differed only by the disordered TIM loop. The R_g determined by distance distribution analysis was in agreement as well. The D_{max} values were

11 nm and 11.7 nm, respectively, TIM-N-SL showed a slightly higher maximal dimension than TIM-N-ΔL. MW determination revealed dimers for both proteins. The particles were compact, which was seen in the Kratky plot and the distance distribution P(r) (Figure 29 B, C). The protein did not show aggregation, as can be seen by the slow and steady approaching of the P(r) curve to zero and the absence of tailing.

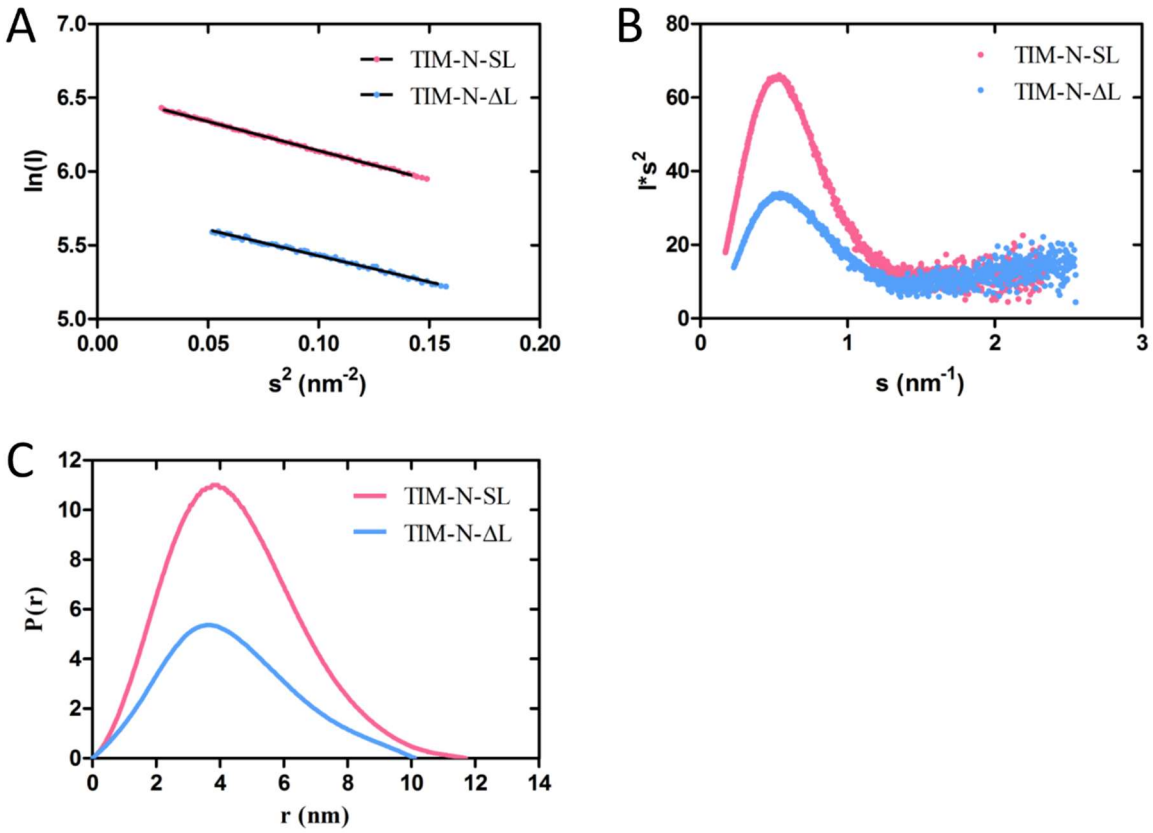

Figure 29: SAXS analysis of TIM-N-ΔL and TIM-N-SL dimers. A) Guinier plots showing the region used for linear approximation of TIM-N-ΔL (blue) and TIM-N-SL (pink). B) Kratky plots showing compactness and folding of the proteins. C) Distance distribution P(r) using the software GNOM was used to determine the D_{max} values for TIM-N-ΔL and TIM-N-SL.

We calculated *ab initio* models of the TIM-N-ΔL and TIM-N-SL dimers using GASBOR (Figure 30 A). The TIM-N-ΔL model was compact and seemed to be slightly extended and with a symmetrical shape. In the top view, it appeared as two roughly triangular shaped objects that were directed towards each other on their side. From the front view the envelope appeared bent, indicating the two TIM-N-ΔL monomers were oriented towards each other in an angled position (Figure 30, Front). The GASBOR model had a good fit to the scattering data ($\chi 2$ = 1.15, CRYSOL).

The *ab initio* model of TIM-N-SL showed a similar shape with a few differences. The GASBOR model showed an excellent fit to the scattering data ($\chi 2 = 1.0$). In the front view, TIM-N-SL possessed an additional bulk on the top, which was not present in TIM-N-ΔL (Figure 30 A, front view, *). The bottom area was similar in shape, however, the additional top bulk made the envelope appear more roundish, which was consistent with the R_g/R_h value of TIM-N-SL compared to TIM-N-ΔL (Table 26). The top view of TIM-N-SL showed a symmetrical shape as well, as if two TIM-N-SL monomers would have been stacked together after one was rotated by 180° (Figure 30 A, Top view). In contrast to the TIM-N-ΔL model, the TIM-N-SL monomers in the TIM-N-SL model did not appear in an angled position towards each other. In a side view, the TIM-N-SL model appeared more roundish compared to the TIM-N-ΔL model, which appeared flat on top.

In an overlay it is visible that both models shared a large similarity, with a few patches that were different between the models. First, the additional bulk in TIM-N-SL (Front view, *), which made TIM-N-SL appear less flat on top, secondly, the almost triangular shape of TIM-N-ΔL made the model wider compared to TIM-N-SL. Since the both TIM-N constructs differed only in the TIM loop which was deleted in TIM-N-ΔL, but just shortened in TIM-N-SL, the additional bulk visible in TIM-N-SL likely contained the 70 residues, present in the shortened TIM loop.

In order to model the TIM1-463 crystal structure into the SAXS envelopes, an *in silico* TIM-N-ΔL dimer structure was predicted using the PDBePISA service (Krissinel & Henrick, 2007). The available TIM1-463 (ΔL) crystal structure only contained a monomer (Holzer *et al*, 2017) and it is therefore not known, how two TIM-N monomers would arrange in a dimer. The dimer model was chosen which contained the largest interface and had a symmetrical orientation of the monomers (Figure 30 B). In this model, the C-terminal helices of the TIM1-463 form a helix bundle consisting of four helices. Both monomers are oriented towards each other at an angle of approximately 150°. The loop positions were located on the opposite side of the C-terminal Helices, but adjacent to one another on the same surface in TIM1-463 (Figure 30 B, bottom).

The *in silico* TIM-N-ΔL dimer and the TIM-N-ΔL GASBOR model had a high overlap (Figure 30 C). The *in silico* TIM-N-ΔL dimer is assembled in way similar to the shape of the GASBOR model. This is underlined by a $\chi 2$ of 1.67, obtained by CRYSOL. However, the *in silico* dimer contains β-turns that stick out of the envelope (Figure 30, arrows) and next to it, there are two small bulks that appear to be hollow.

In a superposition of the *in silico* TIM-N-ΔL dimer with the TIM-N-SL envelope, the *in silico* dimer was oriented in a way that the TIM loop would be located in the additional bulks present in the TIM-N-SL envelope (Figure 30 D, *). In this orientation, two β-turns were not covered by the model and were stuck out of the surface (bold arrows). In addition, there were bulks on the left and right side (dashed arrows), which were hollow and not filled by the *in silico* TIM-N-ΔL dimer structure.

Rotating the *in silico* TIM-N-ΔL dimer in a position that closer fits the GASBOR TIM-N-SL envelope (Figure 30 E) caused the *in silico* dimer to be mostly covered by the TIM-N-SL envelope. The bulks on the bottom left and right side (dashed arrows) of TIM-N-SL were filled by the *in silico* dimer. In this position, however, the top bulks (*) were hollow, because the C-terminal helices did not fill the void completely and the partial TIM loop would be positioned in the bottom. In the bottom, there was no additional volume, that could harbor the TIM loop. This ill-fitting was underlined by a $\chi 2$ of 8 (CRYSOL). This indicates, that the TIM-N-SL dimer might assemble in different way than the TIM-N-ΔL dimer as the *in silico* dimer only showed a good fit to the TIM-N-ΔL data.

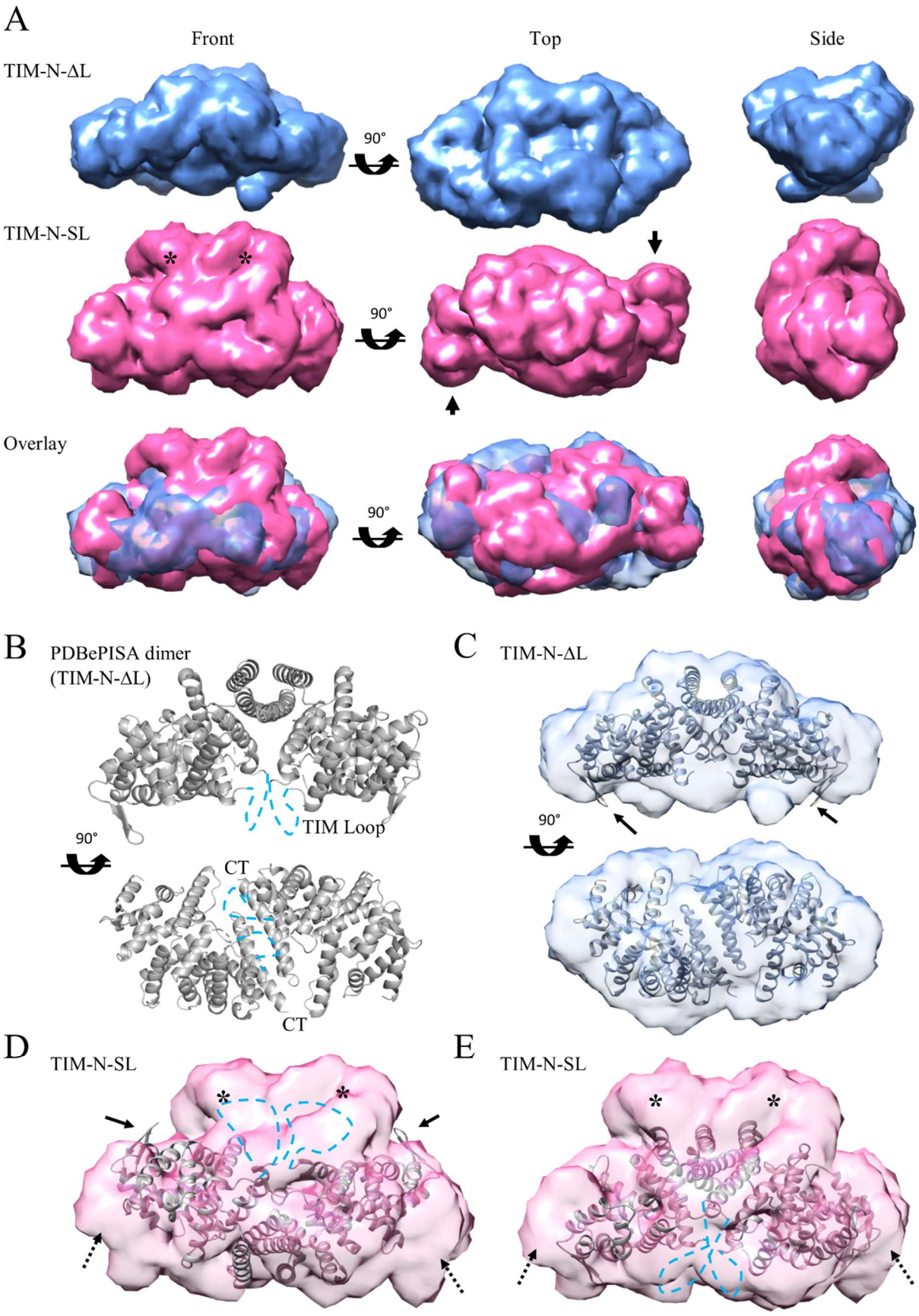

Figure 30: Structural modeling of TIM-N-ΔL and TIM-N-SL using SAXS data. A) *Ab initio* GASBOR models of TIM-N-ΔL (blue) and TIM-N-SL (pink) in different orientations. B) An

in silico TIM-N-ΔL dimer (grey) was created using PDBePISA (Krissinel & Henrick, 2007). Dashed lines (light blue) indicate the position at which the TIM loop would be positioned in a full length TIM-N. C) Overlay of the TIM-N-ΔL model (light blue) with the *in silico* TIM1-463 dimer (grey). Black arrows indicate parts of the dimer are not covered by the GASBOR model. D, E) Overlay of the TIM-N-SL GASBOR model (pink) with the *in silico* TIM1-463 dimer (grey). Arrows indicate parts of the superposition at which both structures diverge from one another.

5.4.3 SAXS analysis of the TIM-N-ΔL/CRY1 and TIM-N-SL/CRY1 complexes

Complexes of TIM-N-ΔL/TIM-N-SL and CRY1 were reconstituted and analyzed in SEC-SAXS. The R_g, D_{max} and R_h values of both complexes were very similar (Table 26) and indicated slight elongation of the protein complexes. The values of TIM-N-SL/CRY1 were slightly larger compared to TIM-N-ΔL/CRY1, which attributed to the 70 residues in the shortened TIM loop. The slight increase in particle radii and dimensions (R_h, R_g, D_{max}) in TIM-N-SL/CRY1 compared to TIM-N-ΔL/CRY1 was observed for single TIM-N-SL before as well (Figure 29). The Kratky plot and distance distribution function revealed a compact shape in both cases (Figure 31 B, C). The MW_{MALS} was 138 kDa for TIM-N-ΔL/CRY1, which indicated a 2:1 complex of 2x TIM-N-ΔL (2x 43 kDa) and 1x CRY1 (67 kDa), since this was closer to the 2:1 stoichiometry of 153 kDa, than a 1:1 stoichiometry of 108 kDa and was consistent with the Bayesian MW (Table 26). The MW_{MALS} for TIM-N-SL/CRY1 was 170 kDa, indicating a 2:1 stoichiometry of 2x TIM-N-SL and 1x CRY1 (2x 50 kDa + 1x 67 kDa). The Bayesian MW was larger than a 2:1 stoichiometry, but smaller than a clear 2:2 stoichiometry. But the credibility interval was large and differences in other structural parameters were not observed between TIM-N-SL/CRY1 and TIM-N-ΔL/CRY1 (Table 26, Figure 31), indicating both complex to have a 2:1 stoichiometry.

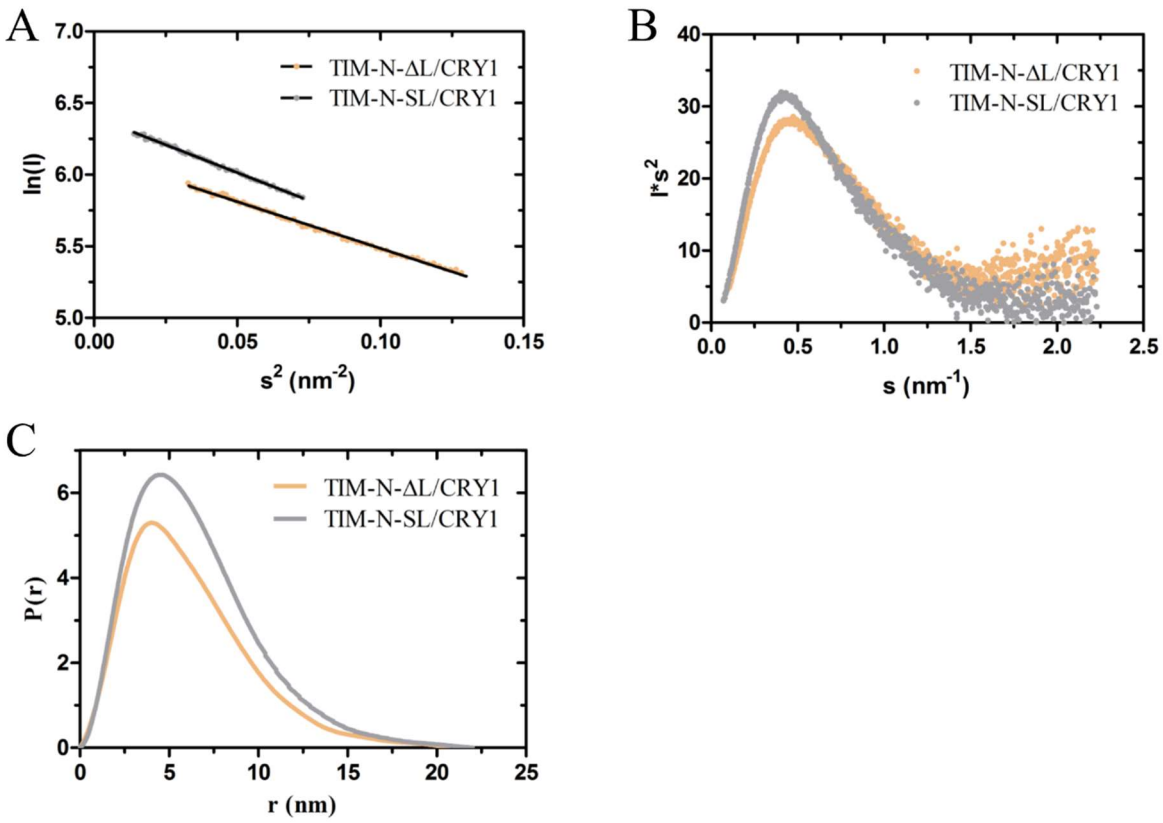

Figure 31: SAXS analysis TIM-N-ΔL/CRY1 and TIM-N-SL/CRY1. A) Guinier plot of TIM-N-ΔL/CRY1 (light brown) and TIM-N-SL/CRY1 (grey) complexes. B) Kratky plot of the complexes shows a peak, indicating protein folding. C) Distance distribution analysis P(r) by GNOM shows similar maximal dimension D_{max} of 20.7 nm and 22 nm.

Both complexes were modeled with MONSA, which used data of the TIM-N-ΔL/SL/CRY1 complexes and single CRY1 data (Figure 32 A, B). The low resolution models (38-39 Å) of TIM-N-ΔL/CRY1 and TIM-N-SL/CRY1 showed $\chi 2$ values of 2.5 and 1.5. Both models had a similar association of the C-Terminus of CRY1 with TIM-N-ΔL and TIM-N-SL (Figure 32 A, B, C), which were dimers, based on MW determination (Table 26). The models were elongated, with a central swelling in TIM-N-ΔL/TIM-N-SL, which was in agreement to their R_g/R_h ratios indicating slight elongation. The partial MONSA model for CRY1 was similar to the CRY1 model determined earlier by GASBOR which had a globular and compact CRY1-PHR and an extension (Figure 28 D, Figure 72). TIM-N-ΔL and TIM-N-SL had a bent shape and appeared broadened at their top, which associated with CRY1. At the bottom, both models were tapered. Both TIM-N models had similar sizes in complex with CRY1, however TIM-N-ΔL was wider at the top (Figure 32D, *) and had an additional pin that was associated with CRY1 in the TIM-N-ΔL/CRY1 complex (Figure 32 D, dashed arrow). At the top TIM-N-SL showed a longer straight edge compared to TIM-N-ΔL (Figure 32 D, solid arrows).

In complex with CRY1, TIM-N-ΔL and TIM-N-SL did not appear symmetrical and show a different shape compared to their dimer models (Figure 32 E, F). TIM-N-ΔL was more asymmetrical showing a larger bulk (*), and an additional pin on top (dashed arrow), which were not observed in TIM-N-ΔL alone (Figure 32 E). But overall both models seemed to have a similar curvature in shape.

The shape of TIM-N-SL from the TIM-N-SL/CRY1 complex was similar to TIM-N-SL alone (Figure 32 F). The bottom part in complex with CRY1 appeared more tapered and extended, thereby creating a slight asymmetry. However, the TIM-N-SL dimer in complex with CRY1 was superposed well with the TIM-N-SL dimer from the individual measurement. In the superposition the straight edge on the back side of TIM-N-SL can be fit into the additional bulk that was present due to the shortened loop (Figure 32 F, black arrows).

This data indicated that the C-terminal portion of CRY1 was associated to TIM-N-DL/SL and the binding site within TIM might be located adjacent to the TIM loop. The N-Terminus of CRY1 did not appear to associate to TIM.

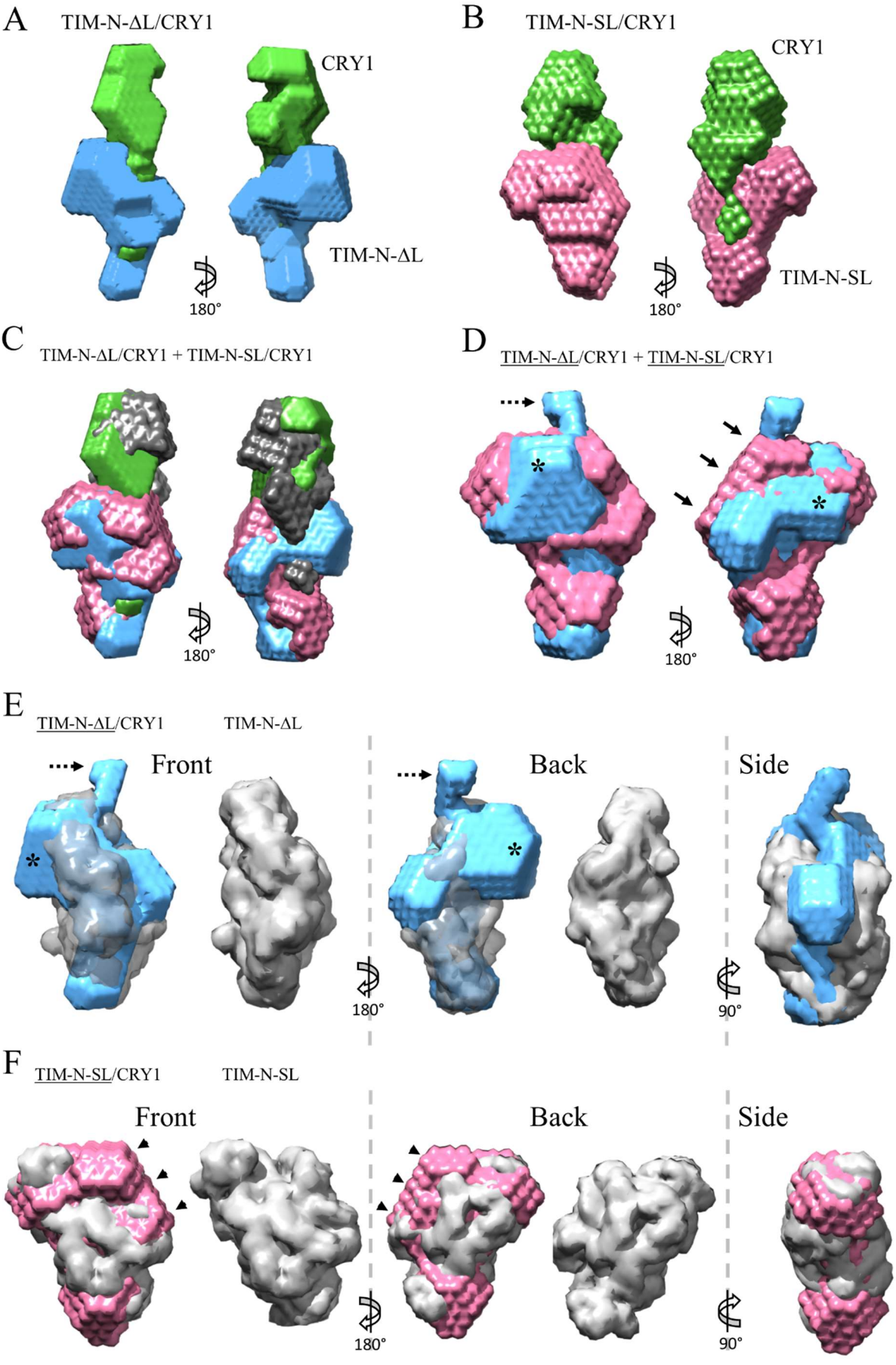
A
TIM-N-ΔL/CRY1
CRY1
TIM-N-ΔL
180°
B
TIM-N-SL/CRY1
CRY1
TIM-N-SL
180°
C
TIM-N-ΔL/CRY1 + TIM-N-SL/CRY1
180°
D
TIM-N-ΔL/CRY1 + TIM-N-SL/CRY1
180°
E
TIM-N-ΔL/CRY1
TIM-N-ΔL
Front
Back
Side
180°
90°
F
TIM-N-SL/CRY1
TIM-N-SL
Front
Back
Side
180°
90°

Figure 32: MONSA modeling of TIM-N-ΔL/CRY1 and TIM-N-SL/CRY1 complex. A) MONSA model of the TIM-N-ΔL/CRY1 complex with CRY1 (green) and TIM-N-ΔL (blue). B) MONSA model of TIM-N-SL/CRY1. CRY1 is shown in green, TIM-N-SL (rose). C) Overlay of the TIM-N-ΔL/CRY1 and the TIM-N-SL/CRY1 complex. Here CRY1 from the TIM-N-SL/CRY1 complex is colored dark grey. D) Superposition of the TIM-N-ΔL and TIM-N-SL from the MONSA models of their complexes with CRY1. In the superposition the major differences are highlighted: an additional pin indicated by a dashed arrow, a more voluminous bulk in TIM-N-ΔL (*) and a longer straight edge on the back side of TIM-N-SL (black arrows). E, F) Comparison of the TIM-N-ΔL and TIM-N-SL portions from the MONSA models of their complexes with CRY1 and the GASBOR models of the single TIM-N-ΔL and TIM-N-SL dimers. The highlights refer to the same parts as in D).

5.4.4 SAXS analysis of the TTP/CRY1 and TTP/CRY2 complexes

The TTP/CRY complexes were analyzed by SAXS. The determined values R_g, R_h and D_{max} for TTP/CRY1 and TTP/CRY2 were very similar (Table 26, Figure 33). The MW_{MALS} values were similar and suggested a 1:1:1 stoichiometry of TIM/TIPIN/CRY. The Bayesian MW showed a large MW with a large credibility interval, but no difference between TTP/CRY1 and TTP/CRY2. This indicated CRY1 and CRY2 associate with TTP the same way. The SAXS data quality was low, hence no *ab initio* modelling was done.

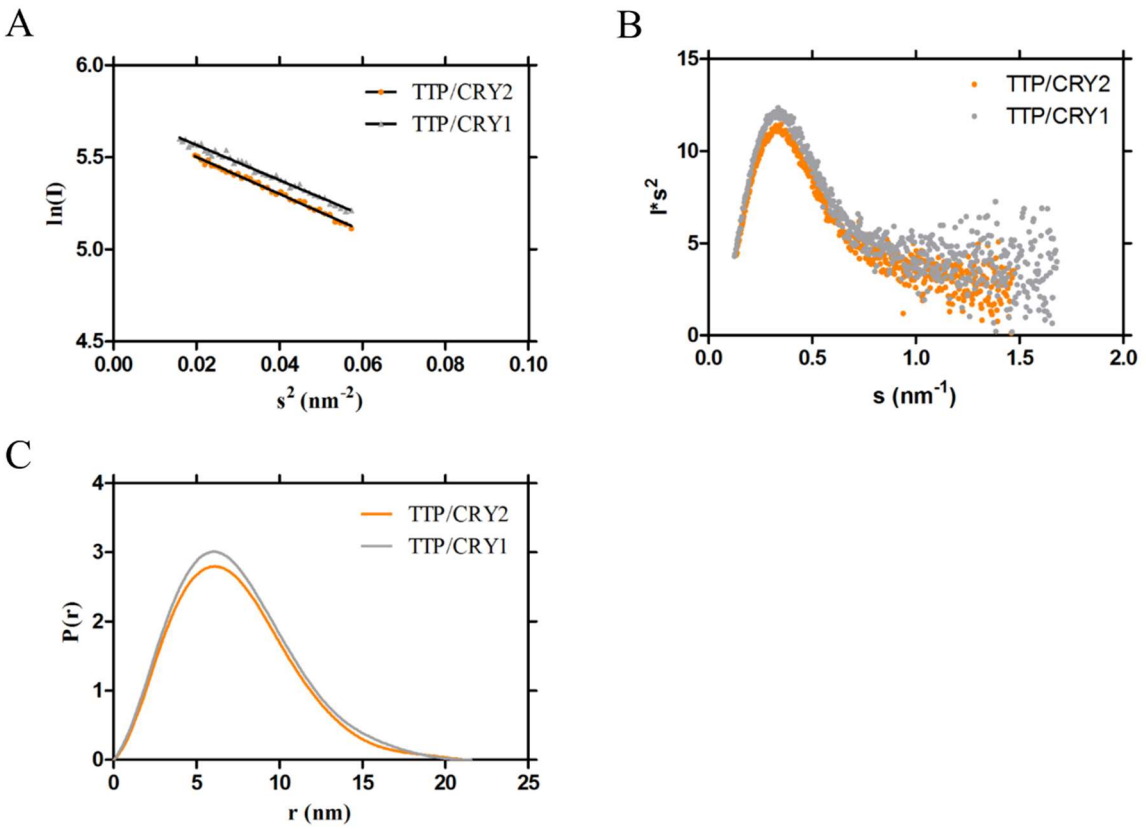

Figure 33: SAXS analysis of TTP/CRY1 and TTP/CRY2 dimers. A) Guinier plots showing the region used for linear approximation of TTP/CRY1 (grey) and TTP/CRY2 (orange). B) Kratky plots showing compactness and folding of the proteins. C) Distance distribution P(r). The software GNOM was used to determine the D_{max} values of 21.4 nm and 21.6 nm for TTP/CRY1 and TTP/CRY2, respectively.

5.5 Single particle Electron Microscopy of the TTP/CRY2 complex

In order to prepare sample collection for CryoEM, we collected single particle Electron Microscopy images of the TTP/CRY2 complex. Negative stain EM data can be used to determine 2D classes (class averages of different particle orientations) that are necessary for automatized particle picking in CryoEM data. This is necessary, because CryoEM images typically have a low contrast.

We used the TTP/CRY2 complex, because of the K_D value compared to TTP/CRY1. In former experiments TTP/CRY2 dissociation was observed during the preparation of EM grids. To

avoid dissociation, the complex was crosslinked using the GraFix method (Stark, 2010). Afterwards, before preparation of the grids, the complex was run on SEC to remove heterogeneities from the crosslinking reaction and to transfer the protein to the low salt EM buffer.

The TTP/CRY2 sample was heterogeneous, e.g. contained aggregation. The aggregation of particles increased with time. The grids that were prepared immediately after the SEC were the most homogenous, but already were affected by aggregation. However, a few spots on the grid allowed data collection. These images were used to calculate 2D classes. 40 different 2D class averages were calculated, that showed a high variability (Figure 34). They varied in size and shape. Some were small and round, some were larger and elongated, some had a dumbbell-like shape.

Based on the observations made during the sample preparation, the conditions of the trimeric TTP/CRY2 complex sample need further optimization to allow a more stable complex to allow single particle EM and CryoEM data collection.

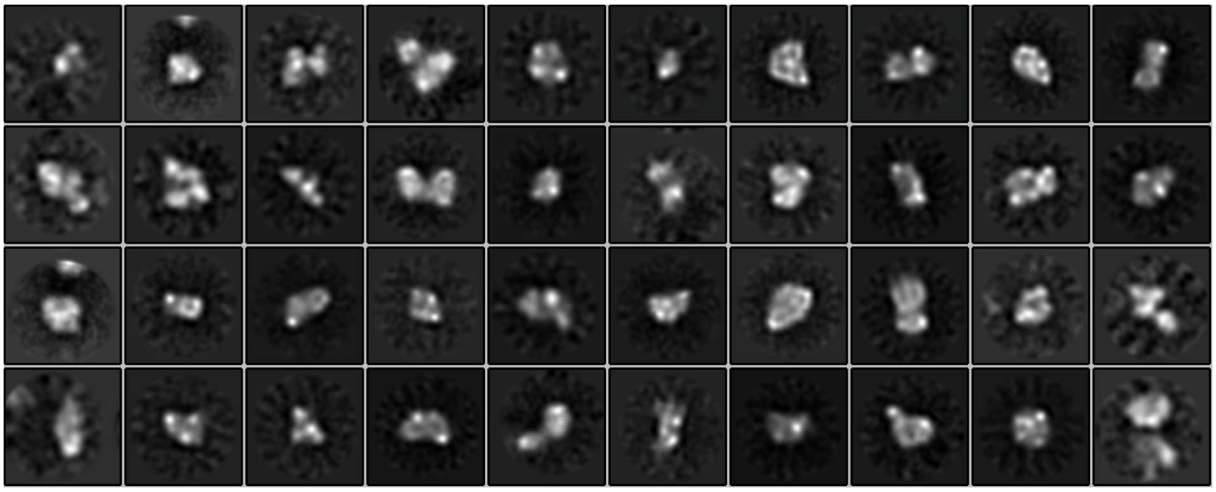

Figure 34: 2D class averages of the TTP/CRY2 complex. The trimeric complex was crosslinked with the GraFix method, was transferred to EM buffer by SEC and was stained with uranyl-formate. Automatized data collection was done using the software Leginon. 2D class averages were calculated from 260.000 particles using the CisTEM software.

5.6 Crosslink Mass Spectrometry (XLMS) analyses of TTP and TTP/CRY complexes

In order to obtain additional information about the interactions of TIM, TIPIN and CRY, we crosslinked their complexes and identified the crosslinked peptides by Mass spectrometry. First, the trimeric complexes were reconstituted in SEC. Then, the protein was chemically crosslinked using the BS3 crosslinker. BS3 contains two reactive N-hydroxysuccinimide (NHS)-esters that react with primary amines in solvent exposed lysines and protein N-Termini. The two reactive groups are separated by a 11.4 Å linker. BS3 has a side reactivity towards Thr, Ser and Tyr that can account for 16-28% of crosslinks (Schneider *et al*, 2018). To remove over-crosslinked and unlinked material, the samples were run on a SDS-PAGE and the bands corresponding to a crosslinked dimer/trimer (172 kDa/245 kDa) were excised (Figure 35) and analyzed by MS.

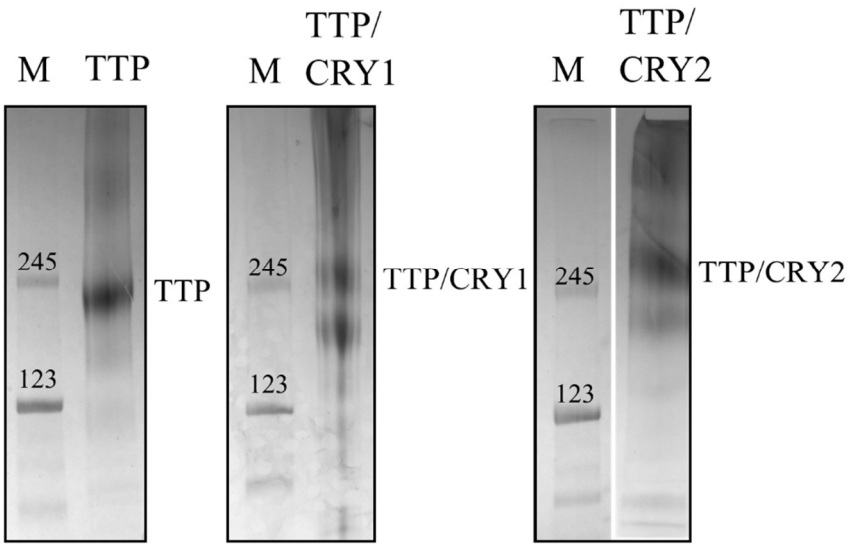

Figure 35: SDS-PAGE of crosslinked TTP and TTP/CRY complexes for MS analysis. TTP was mixed with an excess of CRY1/2 and incubated 30 min on ice. Afterwards, the excess of CRY was separated by SEC. Protein complexes were crosslinked at 2 mg/mL with 0.2 mg/mL BS3 for 45 min at 37 °C. Samples were run on SDS-PAGE to separate over-crosslinked and unlinked material. The labeled bands were excised for MS analysis. M – protein standard in kDa.

5.6.1 Crosslink MS analysis of TIM/TIPIN complex

5.6.1.1 Intramolecular Links of TIM and TIPIN

The intramolecular crosslinks were widely distributed all over TIM and TIPIN (Figure 36). In TIM, there was an accumulation of crosslinks between the TIM loop (residues S247 – K313) and the C-Terminus (K1066 - K1196), which indicated structural closeness. The TIM loop was linked to a region preceding the C-Terminus (PCT) and showed a few links to the N-Terminus as well. The centrally located residues K511 and K528 were linked to the PCT, the C-Terminus and the TIM Loop. The PCT was widely linked to the C-Terminus of TIM. The TIM loop and the C-Terminus showed various links within their regions (Figure 36).

TIPIN showed two main sites of crosslinking: K66-K141 (site 1) and S194-T233 (site 2). These two sites were heavily linked with each other (Figure 36). The region in between these site as well as the N- and C-Termini were not linked (except S294 in the C-Terminus).

Due to the lower number of intramolecular links identified in the second experiment (184 vs. 423 links), there were fewer exact matches (black links) in the crosslinks in TIM. However, the crosslinked regions of TIM and TIPIN were reproduced between both experiments.

The intramolecular crosslinks within TIM indicated that its C-Terminus and the N-terminal loop can be closely located. It indicated that the residues K511, K528 might be close to the C-Terminus as well. The PCT region might be sandwiched between N- and C-Terminus as links to both ends indicate. The C-Terminus and PCT might be closely located as the large number of crosslinks illustrated. Heavy crosslinking within this region might also indicate structural flexibility.

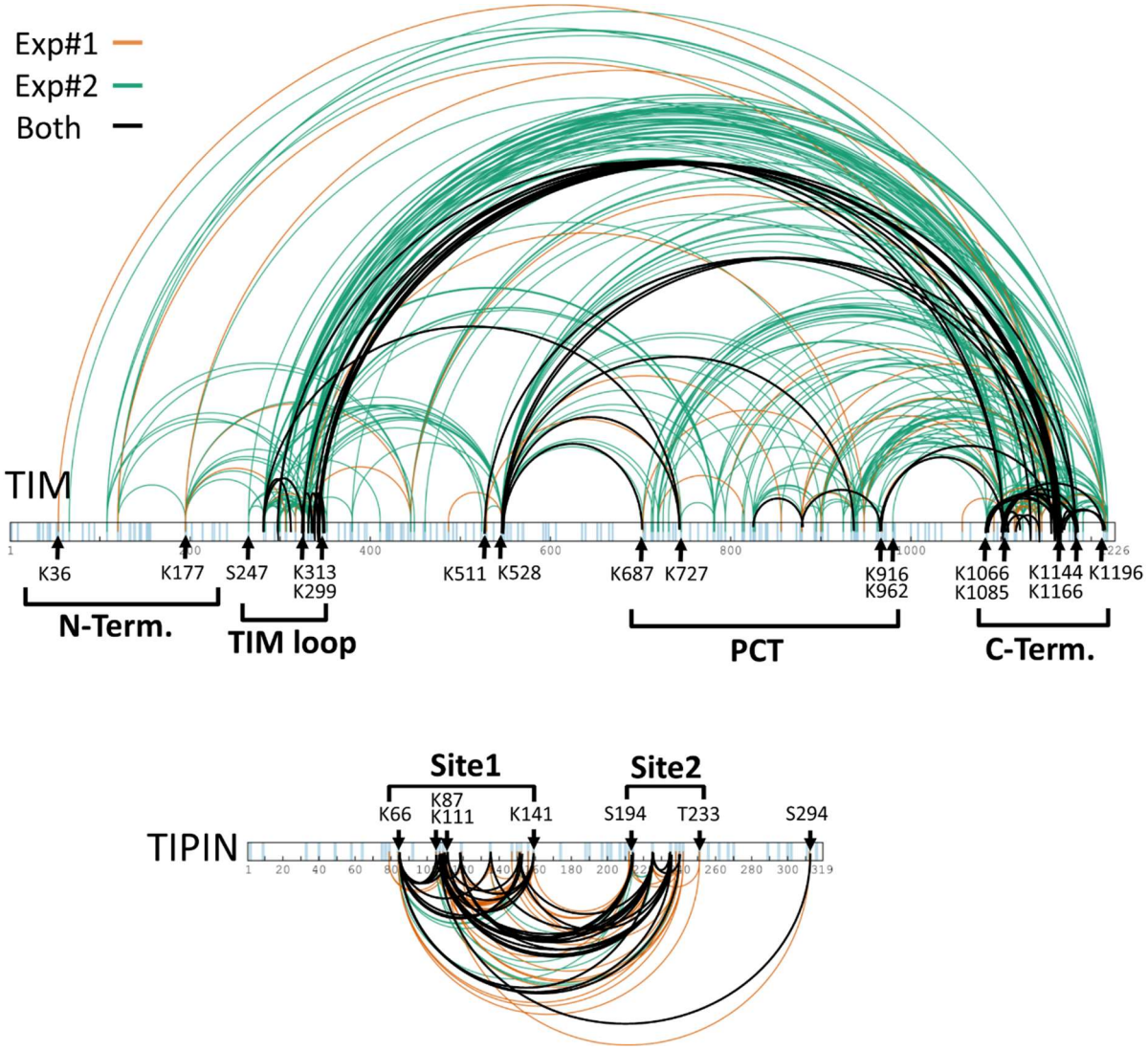

Figure 36: Crosslink MS analysis of TTP. TTP was crosslinked with BS3 (Figure 35). The complex was digested with Trypsin and the crosslinked peptides were analyzed by MS. Representation of intramolecular crosslinks of TIM (top) and TIPIN (bottom). The crosslinks are colored differently (orange: experiment #1, green: experiment #2, black: reproducible links from both experiments). A list of reproducible links is shown in the appendix. Blue dashes inside the protein indicate the crosslinkable residues Lys, Ser and Thr. Labels and highlights indicate crosslinking regions. Note: The analysis and database search was done using the amino acid sequence including the 6xHis-tag and 3C site of the expression construct, which leads to an 18 residue shift in the plot. The highlights are corrected by the shift and show the wild-type residue numbers that can be found in the Uniprot database. TIPIN is zoomed 2x compared to TIM. PCT – preceding C-terminal region.

5.6.1.2 Intermolecular Crosslinks between TIM and TIPIN

Intermolecular links between TIM and TIPIN were found at similar sites as intramolecular links (Figure 37). In TIPIN, site1 (K66-K141) showed an accumulation of links to the TIM C-

Terminus (K1066-K1196, Figure 37) and to the PCT region (K685 – K962). The TIM loop was linked to site1 as well. There were additional links to the N-Terminus of TIM and centrally located residues K427 and K528, but the first half of TIM was linked more scarcely than the PCT and C-Terminus. Site2 was linked to the C-Terminus of TIM and the PCT. It contained few links to the N-Terminus and the TIM loop as well. Especially the linkage of Site1 to the C-Terminus of TIM showed a strong single crosslink reproducibility between both experiments.

The distribution and density of links indicated an association of TIPIN and the TIM C-Terminus and PCT with some flexibility that could allow crosslinks between TIPIN and the TIM N-Terminus as well.

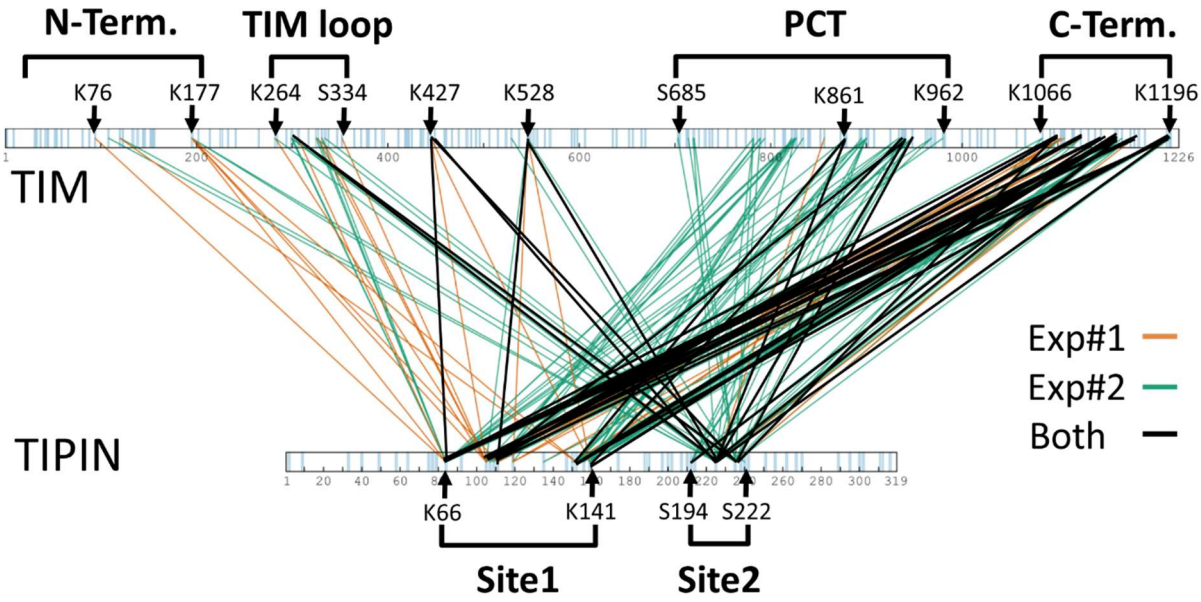

Figure 37: Intermolecular crosslinks between TIM and TIPIN from two experiments. The identified crosslinks of the different experiments are colored differently (orange: experiment #1, green: experiment #2, black: identified in both experiments). The labels and highlights indicate crosslinked regions and highlight certain residues. Blue dashes inside the protein indicate the crosslinkable residues Lys, Thr, Ser. Note: The analysis and MS database search was done using the amino acid sequence including the 6xHis-tag and 3C site of the construct, which leads to an 18 residue shift in the representation. The highlights are corrected by the shift and represent the wild-type residue numbers. TIPIN is zoomed 2x compared to TIM. A table with reproducible crosslinks is shown in the appendix. PCT – preceding C-terminal region.

5.6.2 Crosslink MS Analysis of the TTP/CRY1 complex

5.6.2.1 Intramolecular Crosslinks within TTP/CRY1

The pattern of intramolecular crosslinks in TTP within the trimeric TTP/CRY1 complex (Figure 38) was in principle reproducible when compared to dimeric TTP (Figure 36), but overall more individual intramolecular crosslinks were observed within the proteins of the TTP/CRY1 complex. Briefly, the TIM loop showed many links to the C-Terminus and the PCT region. It displayed links to central TIM regions (K528, K427) as well. K528 in addition, was heavily linked to the TIM C-Terminus (Figure 38). TIPIN was almost exclusively linked inside its two crosslinking sites (site1 and site2). There were a few single intramolecular crosslinks in the C-Terminus of TIPIN.

CRY1 showed an accumulation of crosslinks in its C-terminal tail (S555-K579) (Figure 38, Figure 39). The flexible tail was linked to K442, K468, K485 in a region containing the positively charged patch and the C-terminal helix. It showed links to helices flanking the phosphate binding loop (S285, K247, K228). It contained further links to residues in the CRY1 αβ-domain (K114, K115, K89, K22, G2) and links to K159, K151 and K137 (Figure 38, Figure 39).

5.6.2.2 Intermolecular Crosslinks in the TTP/CRY1 complex

The intermolecular crosslinks between TIM and TIPIN were conserved between the TTP and TTP/CRY1 sample. Briefly, the C-Terminus and the PCT of TIM were predominantly linked to site1 and site2 in TIPIN (Figure 38). The N-terminal half of TIM was linked to both sites as well, but with a lower density. In the N-terminal half, the TIM loop showed the densest accumulation of links to both sites of TIPIN.

TIM/CRY1

The CRY1 αβ-domain (G2, T131, Y133) was linked to the PCT and the C-Terminus (Figure 40 A, Figure 41 A). K228, which is close to the phosphate binding loop (PBL, residues 235-250) was linked to the to the secondary loop in the TIM N-Terminus (Figure 40 A, Figure 42), the PCT and the C-Terminus. The positive patch and the C-terminal helix of CRY1 (K442,

K485) were linked to the TIM C-Terminus. The CRY1 tail (S562, K579) was linked to TIM C-Terminus (K1085 and S1039) and the TIM Loop as well as central K427.

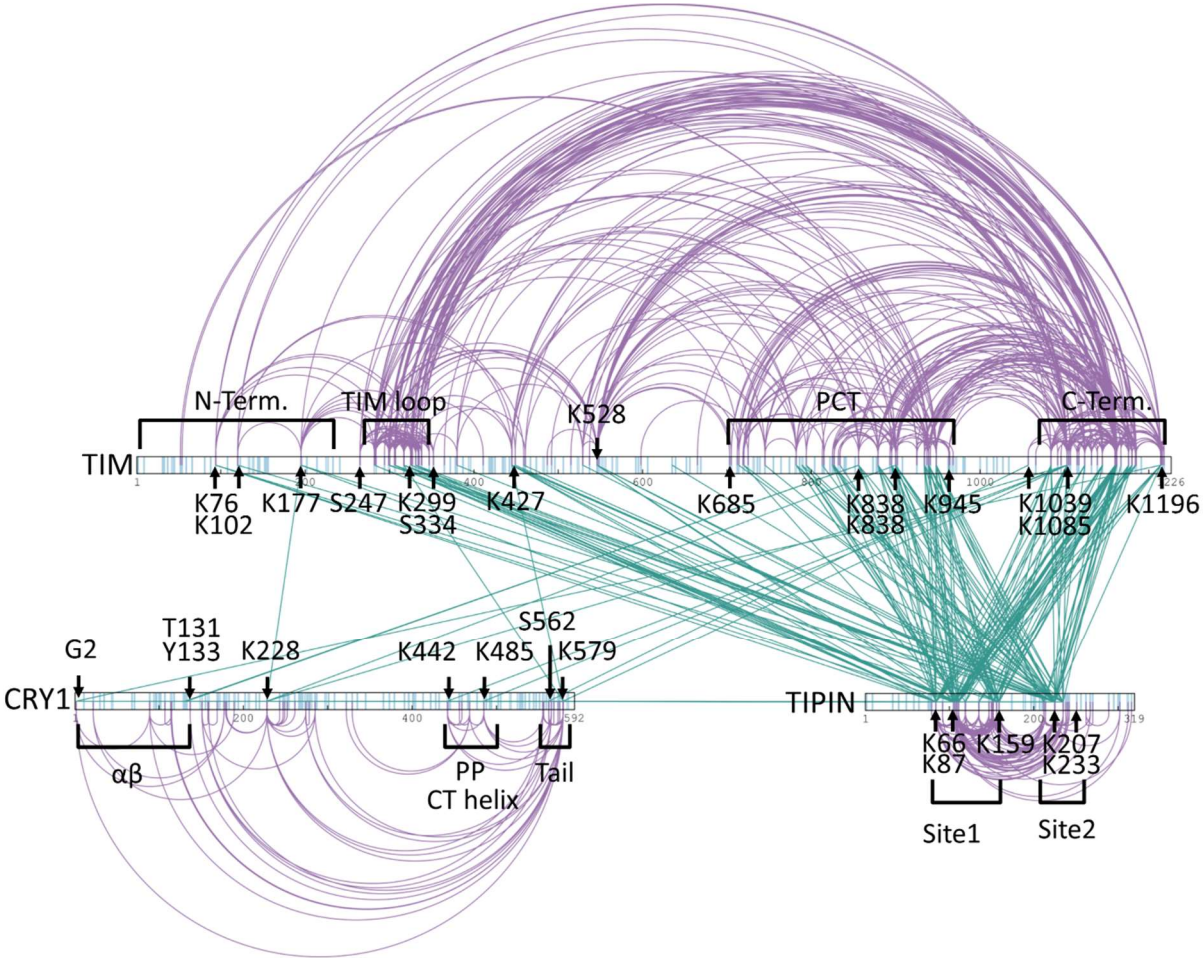

Figure 38: Chemical crosslinks within the TTP/CRY1 complex. The complex was reconstituted in SEC and was crosslinked with BS3. It was loaded on a SDS-PAGE and the band corresponding to the trimer was excised and prepared for MS analysis (see Figure 35). Purple lines: intramolecular links within individual proteins; green lines: intermolecular links between different proteins. Blue bars indicate residues that are linkable with BS3 (Lys, Thr, Ser). Note: For Database search the amino acid sequences that include the 6xHis tag and 3C sites were used, which caused an 18 residue shift in TIM, TIPIN. The highlights and labels refer to the corrected residues numbers.

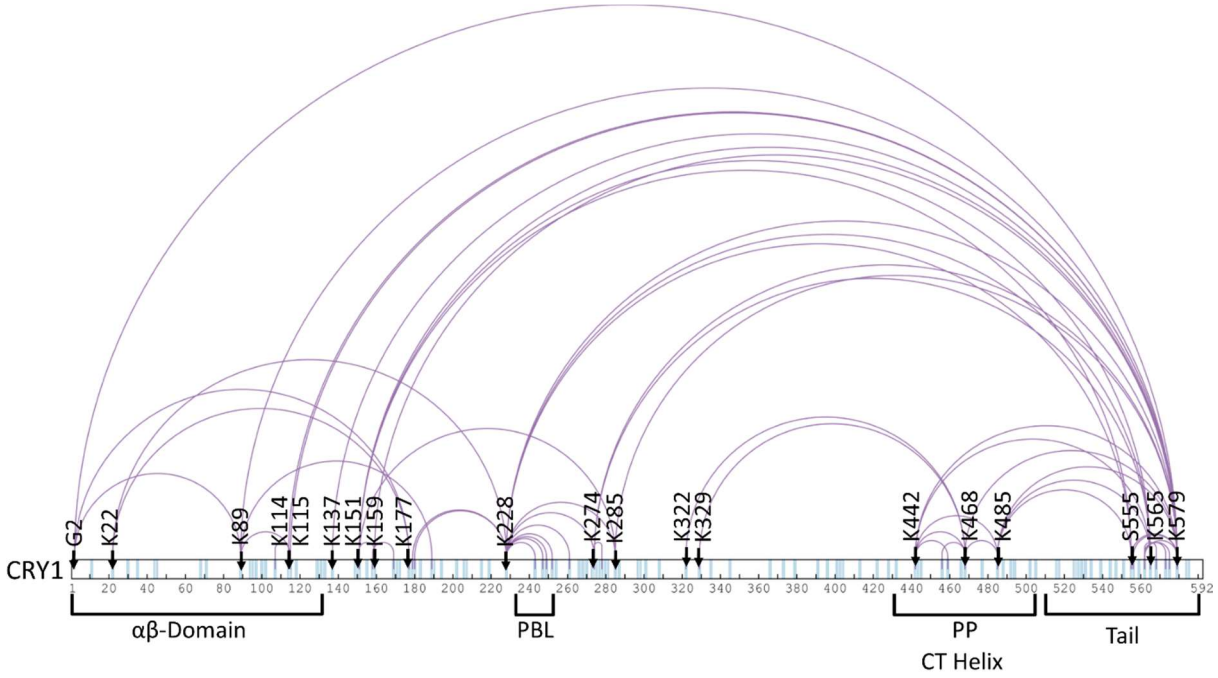

Figure 39: Intramolecular crosslinks of CRY1 within the TTP/CRY1 complex. The complex was reconstituted in SEC and was crosslinked with BS3 for 45 min at 37 °C. It was loaded on a SDS-PAGE and the band corresponding to the trimer was excised and prepared for MS analysis (see Figure 35). Blue bars indicate residues that are linkable with BS3.

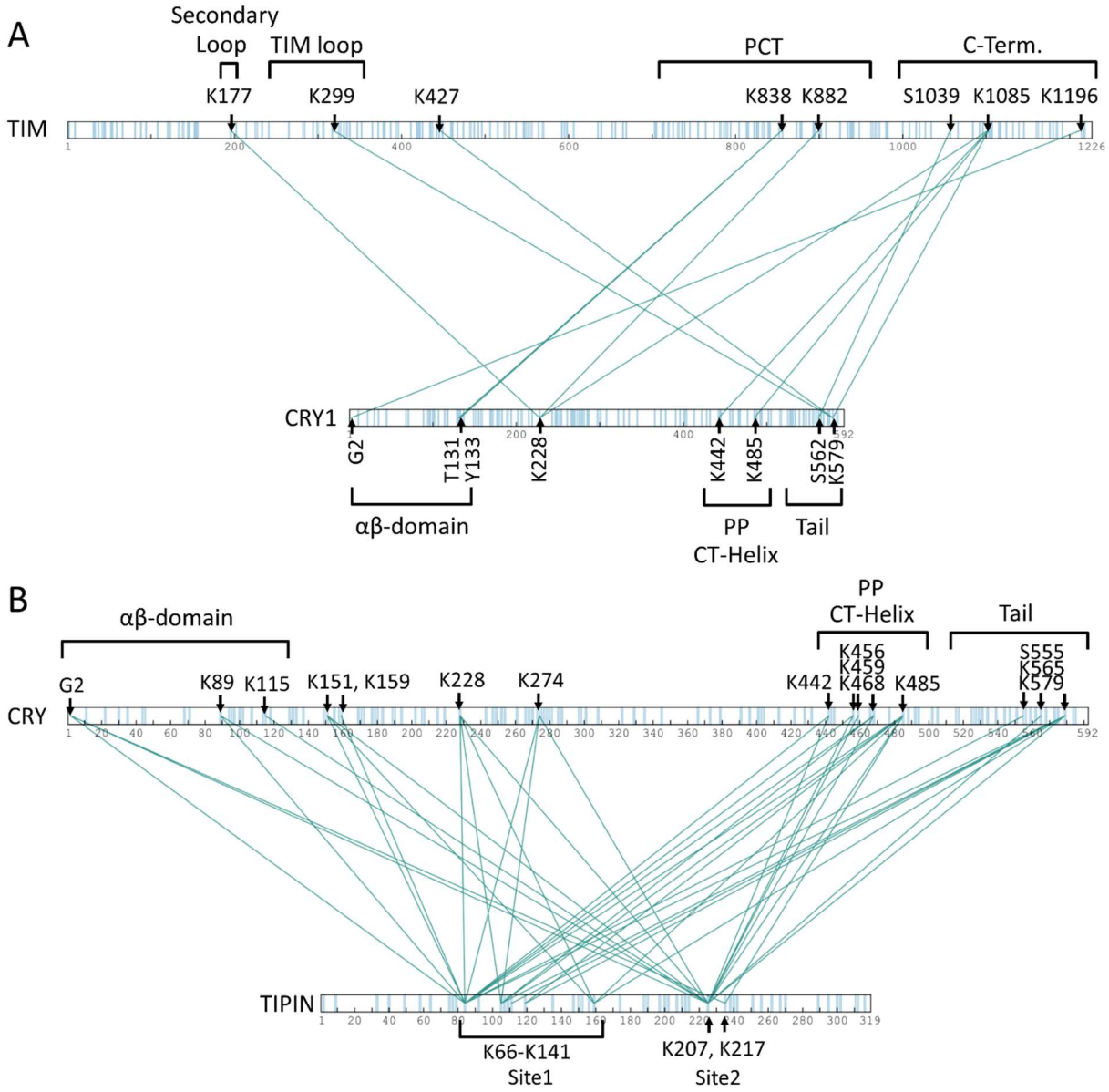

Figure 40: Intermolecular crosslinks within the trimeric TTP/CRY1 complex. The complex was reconstituted, run on a SEC and was crosslinked with BS3. The crosslinks in the complex were analyzed by MS. A) Crosslinks of TIM and CRY1 B) Crosslinks of CRY1 and TIPIN. Blue bars indicate crosslinkable residues. Note: The residue numbers of TIM and TIPIN in the plot are shifted by 18 residues due to the N-terminal 6xHis tag and a 3C site, which were part of the expression construct and were used in the MS database search. The highlights were corrected by the shift and refer to the wild-type residue numbers.

The links of TIPIN to CRY1 were found within the two crosslinking sites of TIPIN (K66-K141 and K207-K217) (Figure 40 B). Site1 of TIPIN was linked to the αβ-domain of CRY1 and other downstream residues located in the N-terminal half of CRY1 as well as to the C-terminal positive patch and helix (K442-K485, Figure 41 B) and the CRY1 tail (S555-K579). The

positive patch and C-terminal helix showed an accumulation of crosslinks in CRY1. Site2 of TIPIN showed links to the same regions within CRY1.

To visualize the distribution of crosslinks inside CRY1, we calculated a 3D model of human CRY1 (Figure 41) using the Swissmodel server (Waterhouse *et al*, 2018). It uses crystal structures of homologous mouse CRY proteins as template for modeling. Labeling the crosslinked residues in the CRY1 model structure showed a one-sided accumulation of links in CRY1, around the FAD binding pocket. Crosslinked residues were accumulated in that area indicating that this side of CRY1 might be oriented towards TTP.

Crosslinked residues within the TIM1-463 crystal structure (Holzer *et al*, 2017) were labeled (Figure 42). It showed that the linked residues were located on the side of TIM that harbors the TIM loop and the secondary loop. K427 was the only non-loop residue within TIM1-463 crosslinked to CRY1.

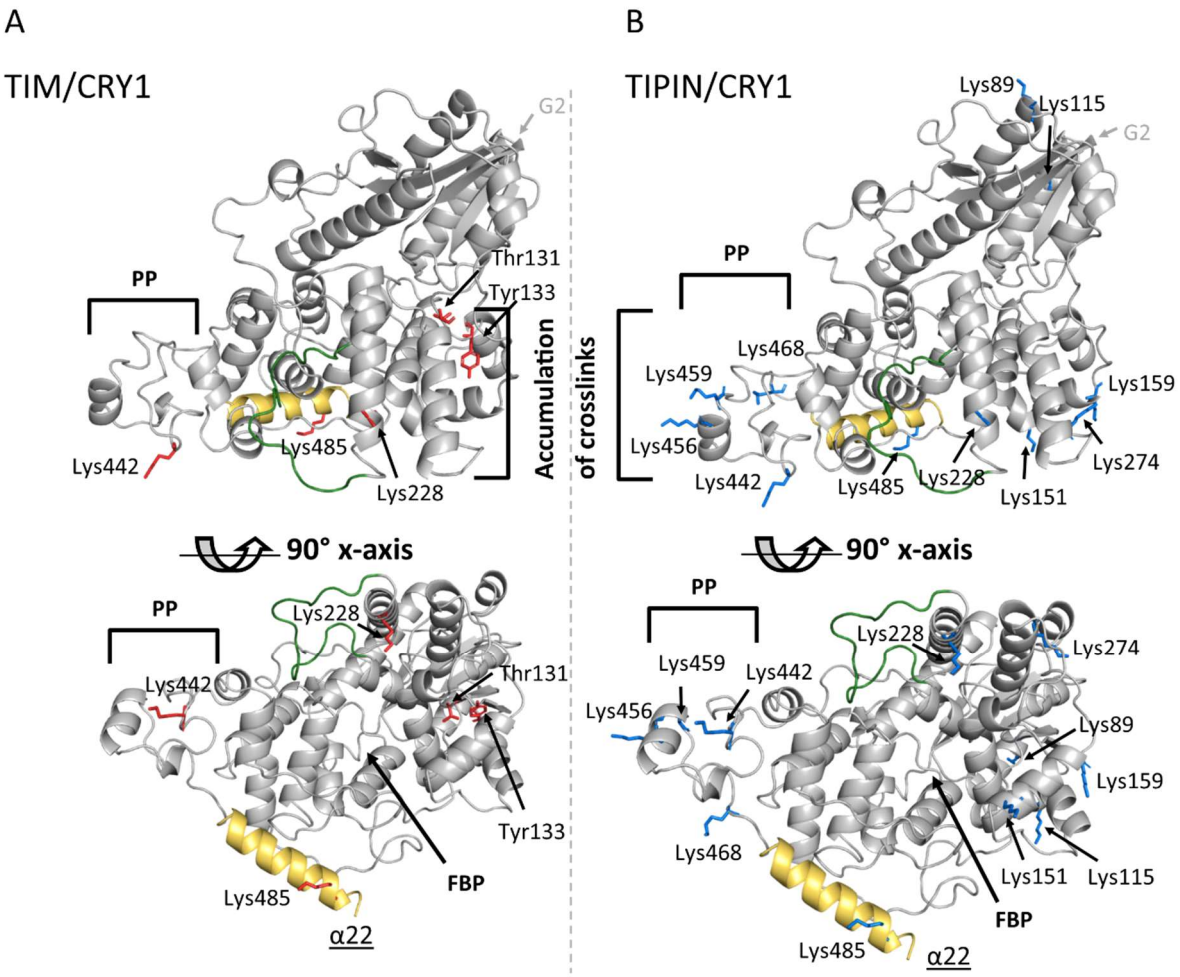

Figure 41: Distribution of crosslinks within the PHR of CRY1. A) Crosslinked residues to TIM within a CRY1 model. B) Crosslinked residues to TIPIN. A 3D model of human CRY1 was calculated using the Swissmodel server (Waterhouse *et al*, 2018), which uses homologous structures as templates for modeling. The crosslinked residues within CRY1 are depicted as sticks. Red: Crosslinks to TIM, Blue: Crosslinks to TIPIN. C-terminal helix22 (α22) is colored in gold and the PBL is colored green. FBP – FAD binding pocket; PP – positively charged patch, PBL – Phosphate binding loop.

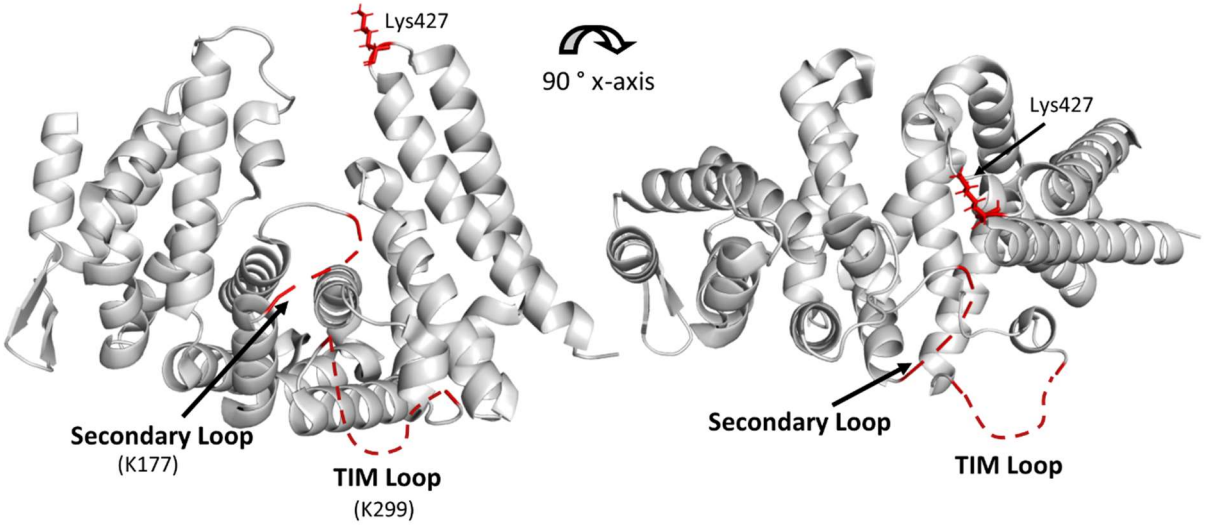

Figure 42: Crosslinks to CRY1 within TIM1-463. TIM1-463 contains two flexible loops (TIM Loop, Secondary loop), that were not resolved structurally. Therefore, the loops are represented as dashed lines in this figure. The residues in brackets indicate the crosslinked residue within the loops. The crosslinked residues of TIM are colored in red. PDB ID: 5MQI (Holzer *et al*, 2017).

5.6.3 Crosslink MS Analysis of TTP/CRY2

5.6.3.1 Intramolecular crosslinks in the TTP/CRY2 complex

The intramolecular crosslinks of TIM, TIPIN and CRY2 within TTP/CRY2 were similar to the TTP and TTP/CRY1 complex (Figure 36, Figure 38, Figure 39). As observed before, the TIM loop was most intimately linked to the TIM C-Terminus. The C-Terminus harbored many links to the PCT region located upstream (S685-S962). The PCT region had links to the TIM loop and centrally located residue K528. The N-Terminus did not contain many links, there were a few links to the TIM loop and one link to the C-Terminus. TIPIN displayed the same two sites of crosslinking (K66-K141, S194-T233) which were seen before (see 5.6.1 and 5.6.2).

CRY2 contained intramolecular links within three prominent regions (Figure 44). The flexible tail was linked to the positive patch, C-terminal helix and also contained links to the PBL and residues next to it (K242, K247, K293). In addition, it harbored links to the αβ-domain and residues downstream of the αβ-domain (K164, K184). The positively charged patch and helix22 were linked to the αβ-domain, to the PBL (S262) and had links to helices adjacent to the PBL (K242, K247) (Figure 44).

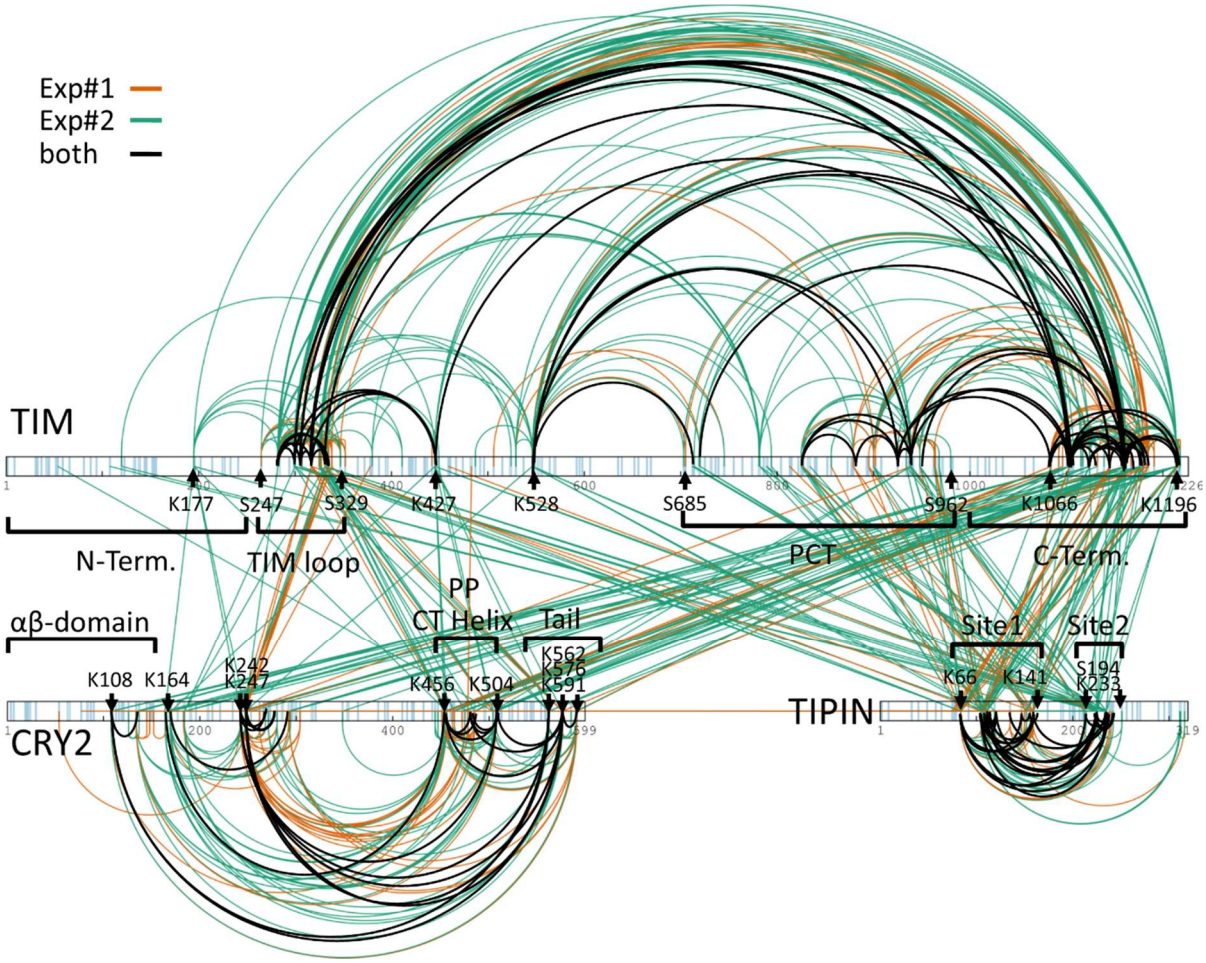

Figure 43: Crosslinks of the TTP/CRY2 complex. The TTP/CRY2 complexes was crosslinked with BS3 and analyzed MS (Figure 35). Crosslinks of two experiments are shown. Experiment #1: orange, Experiment #2: green, Crosslinks found in both experiments: black. For better visibility, here only the reproducible intramolecular links are highlighted in black. Highlighted intermolecular links can be found in Figure 45 and Figure 47. Blue bars indicate the crosslinkable residues. Note: For database search and data analysis of TIM and TIPIN, amino acid sequences that include a N-terminal 6xHis tag and 3C site were used, which lead to an 18 amino acid shift in residue number in the figure. The residue labels and highlights were corrected by the shift and refer to the wild-type residue numbers.

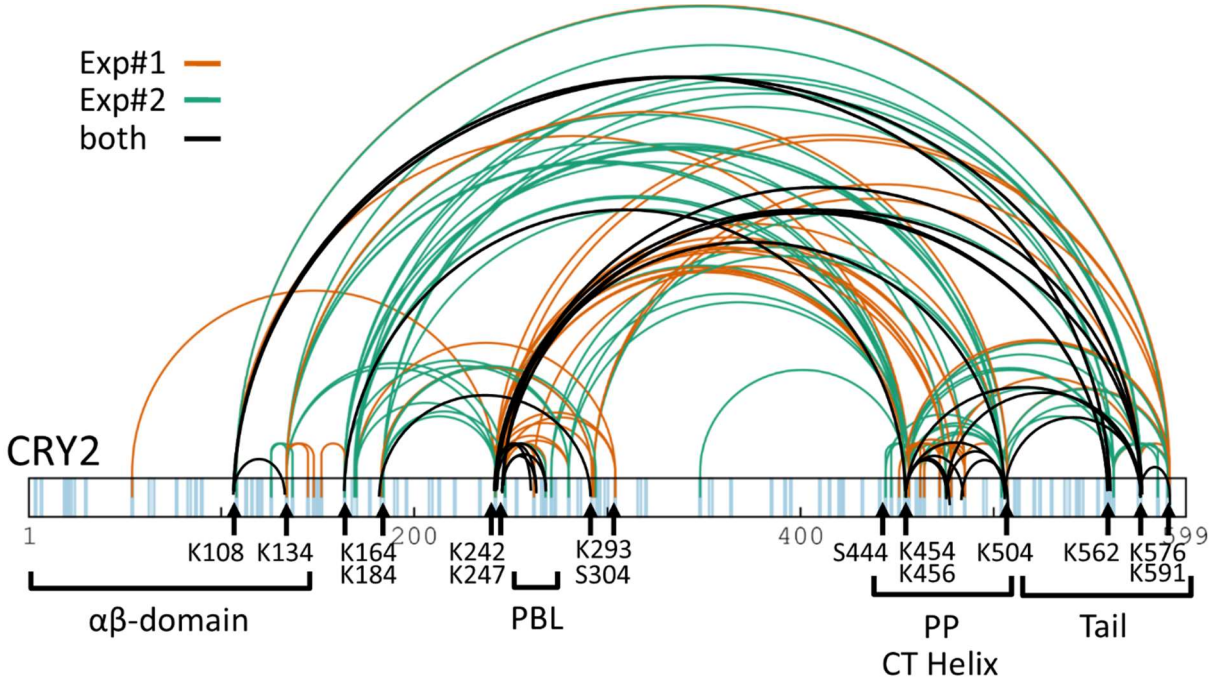

Figure 44: Intramolecular Crosslinks of CRY2 within the TTP/CRY2 complex. Crosslinks from two experiments are shown (orange, green). Blue bars indicate crosslinkable residues within the CRY2 amino acid sequence. A list of reproducible crosslinks can be found in the appendix.

5.6.3.2 Intermolecular Crosslinks of the TTP/CRY2 complex

Crosslinks of TIM and CRY2

In the N-terminus of TIM, K177 of the secondary loop was linked to several parts of CRY2 (Figure 45). The TIM Loop was more densely linked to CRY2. It was linked to CRY2 residues located between the αβ-domain and the PBL (K164, K184, K242, K247), to the PP, the C-terminal helix and the tail. In addition, the C-Terminus of TIM was very tightly linked to CRY2. It had links to the N-terminal half of CRY2, to the PP, the C-terminal helix and the tail. In the central part of TIM (residues ~500-1000), including the PCT region, crosslinks were almost completely absent.

Visualization of the crosslinks in a crystal structure of TIM1-463 (Holzer *et al*, 2017) revealed that most links were located on one side of the TIM1-463 (Figure 46). Crosslinks were accumulated within the two flexible loops (TIM Loop, secondary Loop) that are not resolved in the crystal structure. Labeling of the crosslinked residues within a structure of CRY2 (Figure 48), showed an accumulation of crosslinks around the FAD binding pocket (FBP), a one-sided

accumulation of links. This indicates that the side of CRY2 harboring the FBP and the side of TIM which contains both flexible loops could be oriented towards each other.

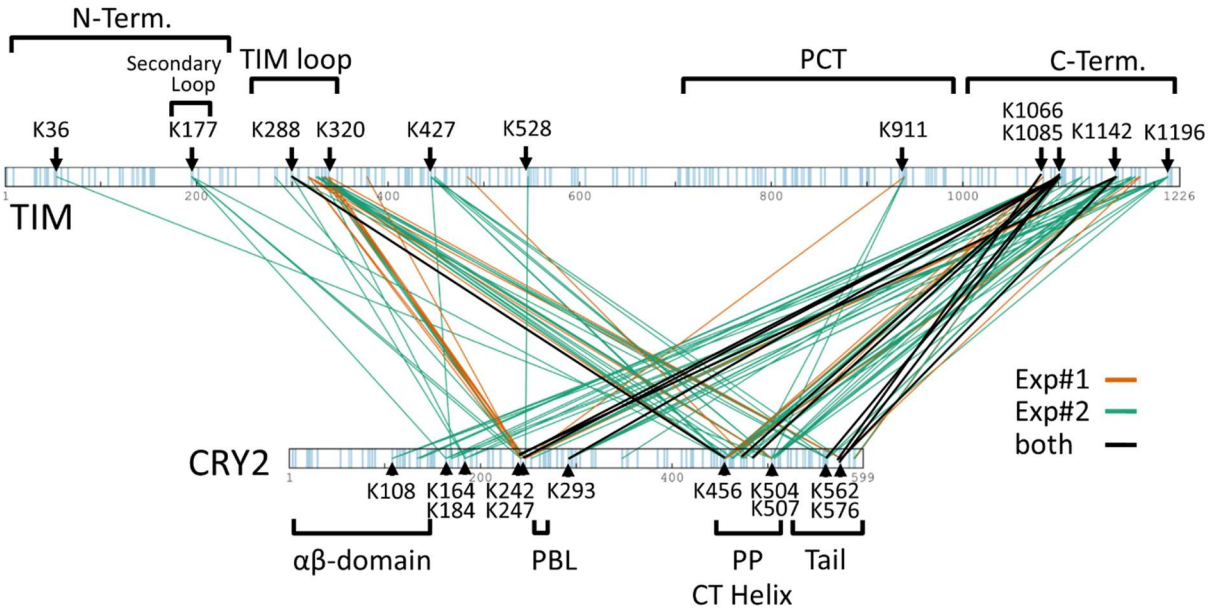

Figure 45: Intermolecular Crosslinks of TIM to CRY2 within the TTP/CRY2 complex. The TTP/CRY2 complex was crosslinked with BS3 and the crosslinks were identified by MS. Crosslinks form two experiments are shown (colored orange and green). Exactly reproduced links are colored black. Blue bars indicate crosslinkable residues. PCT – preceding C-Terminus; PBL – phosphate binding loop; PP – Positively charged patch. Note: For database search and data analysis of TIM, amino acid sequences that include a N-terminal 6xHis tag and 3C site were used, which lead to an 18 amino acid shift in residue number in the figure. The residue labels and highlights were corrected by the shift and refer to the wild-type residue numbers.

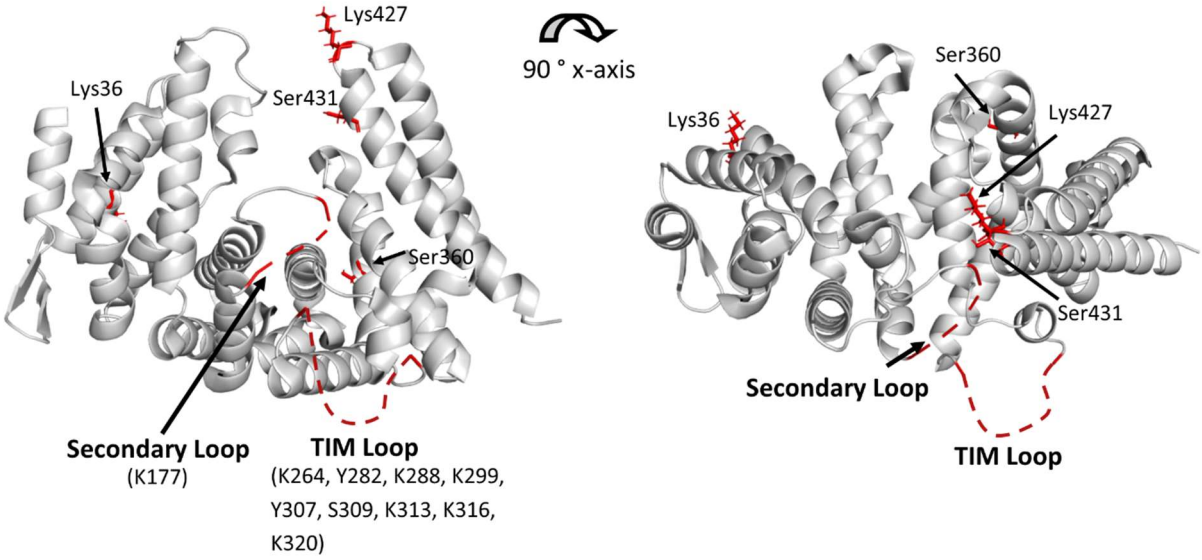

Figure 46: Intermolecular crosslinks within TIM1-463 to CRY2. TIM1-463 contains two flexible loops (TIM Loop, Secondary loop), that were not resolved structurally. Therefore, the loops are represented as dashed lines in this figure. The residues in brackets indicate the crosslinked residues within the loops. The crosslinked residues of TIM are colored in red. PDB ID: 5MQI (Holzer *et al*, 2017).

Intermolecular crosslinks between TIPIN and CRY2

The crosslinks between TIPIN and CRY2 were distributed as follows: The N-terminal half of CRY2, including the αβ-domain, was evenly linked to TIPIN (Figure 47). There was a slight accumulation of links close to the αβ-domain (T145 – Y152) and in the helix next to the PBL (K242, K247). Those residues were linked to both crosslinking sites of TIPIN. The PP, the C-terminal helix and the tail of CRY2 had an accumulation of crosslinks and were linked to site1 and site2 of TIPIN. Visualizing the links to TIPIN within a CRY2 model (Figure 48) showed that the links were accumulated around the FBP, similar to the crosslinks of CRY2 to TIM. This indicated, that the FBP of CRY2 might be oriented to TIPIN.

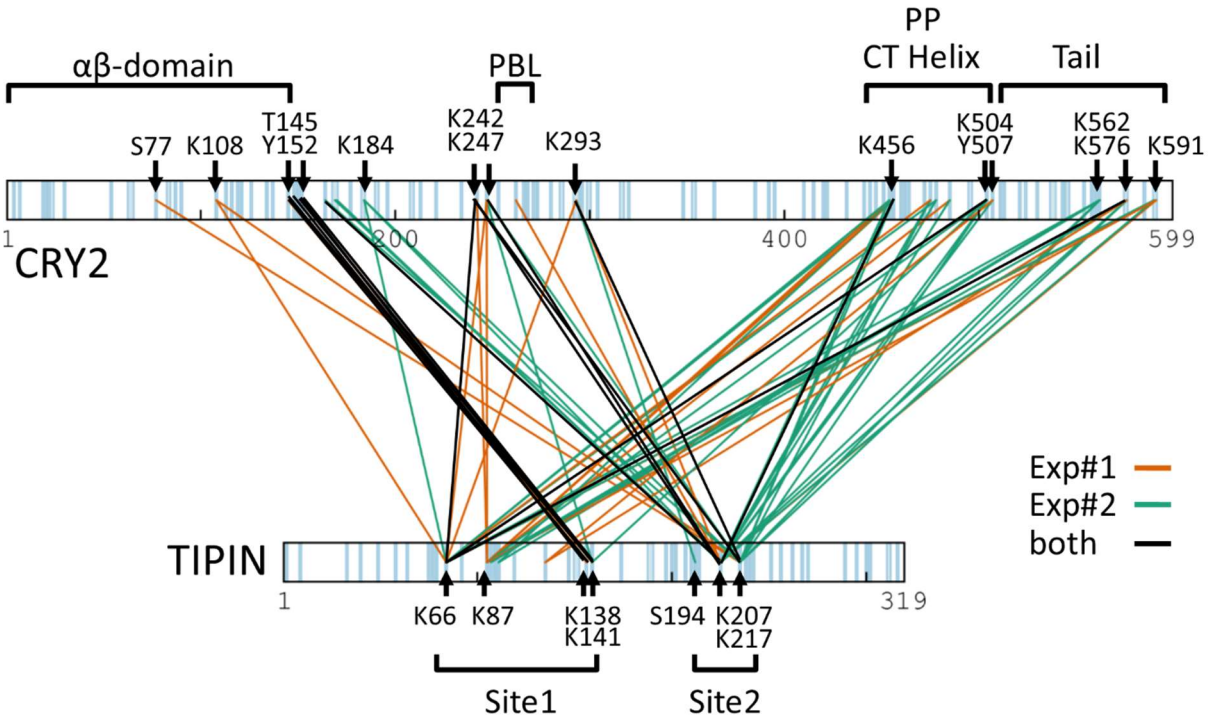

Figure 47: Intermolecular crosslinks between CRY2 and TIPIN, in the TTP/CRY2 complex. The complex was reconstituted in SEC and was crosslinked with BS3. The crosslinks in the complex were analyzed by MS. Crosslinks of two independent experiments are shown (orange, green) Blue bars indicate linkable residues. Note: For database search and data analysis of TIPIN, amino acid sequences that include the 6xHis tag and 3C site were used, which leads to

an 18 residue shift in TIPIN residue numbers. The residue labels were corrected by the shift and refer to the wild-type residue numbers.

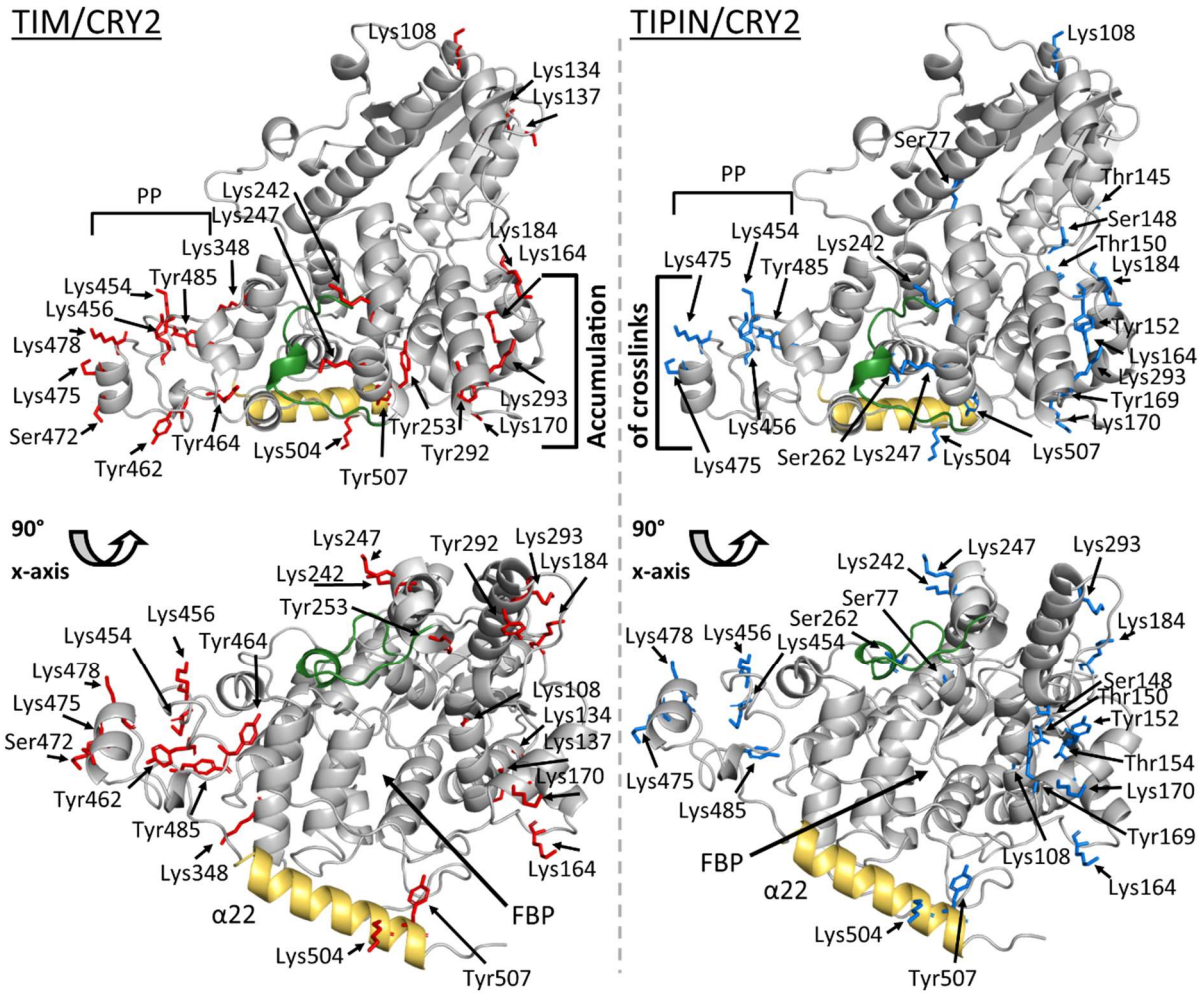

Figure 48: Crosslinked residues within CRY2. A 3D model of human CRY2 was calculated using the Swissmodel server (Waterhouse *et al*, 2018), which uses homologous structures as templates for modeling. The crosslinked residues of CRY2 are shown as sticks. Red: Crosslinks to TIM, Blue: Crosslinks to TIPIN. The C-terminal helix22 is colored in gold and the PBL is colored green. FBP – FAD binding pocket; PP – Positively charged patch.

5.6.4 Comparison of TTP/CRY1 and TTP/CRY2

TIM/CRY

Overall the XLMS results for CRY1/TIM and CRY2/TIM were very similar. The same functional sites within CRY (αβ-domain, positive patch and C-terminal helix, CRY tail) were linked to TIM (Figure 40 A, Figure 45). The αβ-domain of CRY1 was linked to the C-Terminus and the PCT of TIM. The αβ-domain of CRY2 showed only links to the C-Terminus of TIM. Positional equivalents K228 of CRY1 and K247 of CRY2 were crosslinked in a similar way. Both residues showed links to the secondary loop, the PCT and the C-Terminus of TIM, but K228 of CRY1 was not linked to the TIM Loop. The region containing the PP and the C-terminal helix of CRY1 was linked to the TIM C-Terminus. This region in CRY2 showed additional links to the TIM Loop and to other residues in the N-terminal half of TIM. The crosslinking of the tails of CRY1 and CRY2 was similar, both were linked to the TIM C-Terminus, the TIM loop and K427 in the middle of the TIM sequence. Within the C-Terminus, the CRY1 tail was linked to a residue located further upstream (S1039) than the CRY2 tail (K1066). The main differences were that the PP/C-terminal helix of CRY1 was not linked to the TIM loop and that it was linked to other, upstream residues within the C-Terminus of TIM. But as the number of identified crosslinks between CRY1 and TIM was low, it was difficult to make an exact comparison between TTP/CRY1 and TTP/CRY2.

TIPIN/CRY

The crosslinked sites of TIPIN/CRY1 and TIPIN/CRY2 were very similar. The links to TIPIN within CRY1 and CRY2 were distributed mainly around the FAD binding pocket (Figure 40 B, Figure 47). The regions (αβ-domain, PP and C-terminal helix, tail) within CRY1 and CRY2 were crosslinked to the same sites within TIPIN (site1, site2). There were only slight differences in how widely a region was crosslinked. For example, the tail of CRY2 showed links to a wider site2 within TIPIN (K207, K217), whereas the tail of CRY1 only had links to K207. K247 in CRY2 was more widely linked to site2 as it showed links to K207 and K217, whereas the positional equivalent in CRY1 (K228) only showed a link to K207. However, these difference can be due to different numbers of identified crosslinks. For TIPIN/CRY1 39 intermolecular

crosslinks were identified and for TIPIN/CRY2 71 crosslinks. Overall there was no clear difference between the crosslinking of CRY1 and CRY2 to TIPIN.

5.7 SEC Interaction studies to validate binding sites suggested by XLMS

5.7.1 SEC to assess protein oligomeric state

To analyze whether the crosslinked regions of TIM, TIPIN and CRY directly interact or were only closely located, we conducted a series of SEC experiments with various constructs. First, we used single proteins to judge the migration pattern and oligomeric state by analytical SEC (Figure 49).

The CRY proteins showed narrow peaks with tailing to the right side in the SEC run (Figure 49 A, B). The MW_{SEC} of CRY1 was 31 kDa, as its retention volume was ~1 mL larger compared to CRY2, which had a MW_{SEC} of 58 kDa. MW_{PREP} and MW_{MALS} clearly indicated that both CRYs were monomers.

mTIPIN showed a wide peak with tailing and fast migration through the column (Figure 49 C). The MW_{SEC} was 295 kDa, which corresponded to a 9-mer. An exact oligomeric state for hTIPIN could not be determined as the protein showed wide peaks (Figure 16), but it was oligomeric.

The N-terminal TIM constructs (TIM-N-Sumo, TIM-N-ΔL) did not migrate as monomers (Figure 49 D, E). TIM-N-Sumo showed a wide peak with tailing to the left and right side. Its MW_{SEC} was 250 kDa, corresponding to a tetramer. The MW_{PREP} of TIM-N-Sumo was 590 kDa. TIM-N-ΔL, on the other hand, had a sharp peak with a MW_{SEC} of 97 kDa, corresponding to a dimer. This was consistent with its MW_{PREP} and the MW_{MALS} of 94 kDa and 92 kDa.

TIM 520-680 migrated as a sharp, symmetric peak which was assigned to a monomer (Figure 49 F). TIM 827-935 showed a MW_{SEC} and MW_{PREP} in between monomers and dimers (Figure 49 G). The sample quality was not ideal and the results were likely influenced by impurities.

TIM 997-1207 showed different protein species (Figure 49 H). The MW_{SEC} estimation of the two dominant peaks resulted in tetramers and dimers based on MW_{SEC} of 117 kDa and 49 kDa.

The protein peaks showed tailing to the left, which indicated that there were larger TIM997-1207 oligomers as well.

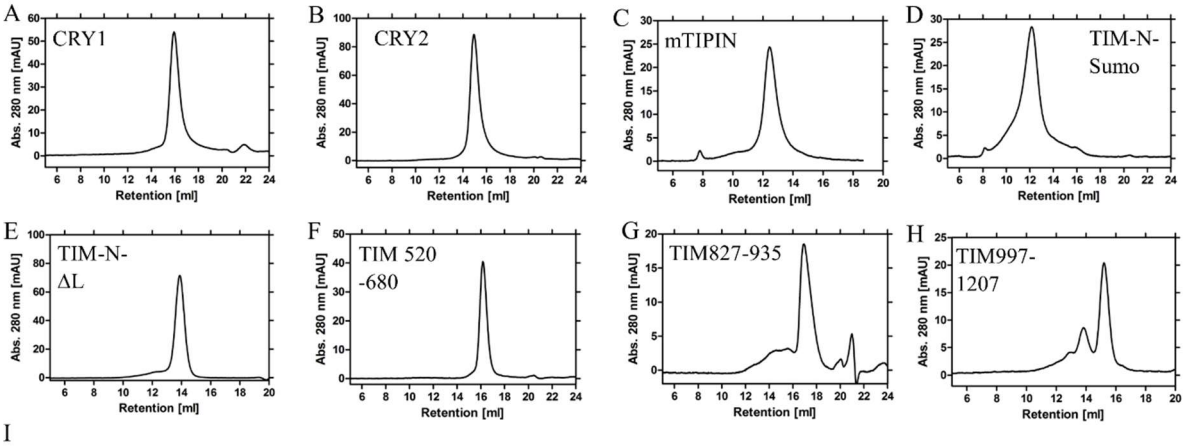

I

Protein	MW_{THEO} [kDa]	MW_{SEC} [kDa]	MW_{PREP} [kDa]	MW_{MALS} [kDa]	Oligomeric state
CRY1	67.2	31	67	80	Monomer
CRY2	67.7	58	82	85	Monomer
hTIPIN	34.5	-	200-500	-	Oligomer
mTIPIN	31.6	295	-	-	9 mer
TIM-N-Sumo	65.1	250	590	-	Tetra-/Oligomer
TIM-N-ΔL	43.3	98	94	92	Dimer
TIM 520-680	19.8	26	17	-	Monomer
TIM 827-935	12.6	16	19	-	Monomer
TIM 997-1207	23.8	117/49	120/70	-	Tetramer/Dimer

Figure 49: Analytical SEC of single proteins to determine MW and oligomeric state. Proteins were run on a calibrated S200 10/300 GL column. A-H) Chromatograms of analytical SECs. I) Table summarizing the MWs and the assigned oligomeric states. MW_{THEO} – MW calculated by Expasy Protparam and the respective amino acid sequences; MW_{SEC} – MW based on analytical SEC; MW_{PREP} – MW estimate based on preparative scale column S200 16/600; MW_{MALS} – MW determined by MALS analysis parallel to SAXS data collection at DESY, Hamburg (Table 26).

5.7.2 Interaction analysis within the TTP complex

5.7.2.1 Interaction of the N-terminal TIM-loop and the TIM C-Terminus

XLMS showed many crosslinks between the TIM loop (239-330) and the C-Terminus of TIM. This indicated structural closeness or association. To asses direct interaction of those sites, we purified C-terminal TIM 997-1207 (Figure 18) and analyzed the interaction with TIM-N-Sumo and TIM-N-ΔL.

TIM-N-ΔL did not show binding to the TIM997-1207 (Figure 50, A). Both proteins were not well separated in the SEC run and the peaks overlapped, but there was no clear shift in retention

volume, and no additional peak, that indicated a complex. TIM997-1207 formed oligomers (red curve) that overlapped with peak1 of the TIM-N-ΔL+TIM997-1207 sample (black curve).

TIM-N-Sumo, that includes the TIM loop, did not show binding to TIM997-1207 either (Figure 50, B). There, a better separation of peaks was observed. The chromatogram contained three peaks. Peak1 contained TIM-N-Sumo, peak3 contained TIM997-1207, peak2 contained oligomers of TIM997-1207 and a little amount of TIM-N-Sumo. But the presence of TIM-N-Sumo in peak2 was likely caused by tailing of TIM-N-Sumo as was seen by the large overlap of the curves (blue and red curve) in peak2. Based on this results, we did not observe a direct interaction of the N-Terminus and C-Terminus of TIM.

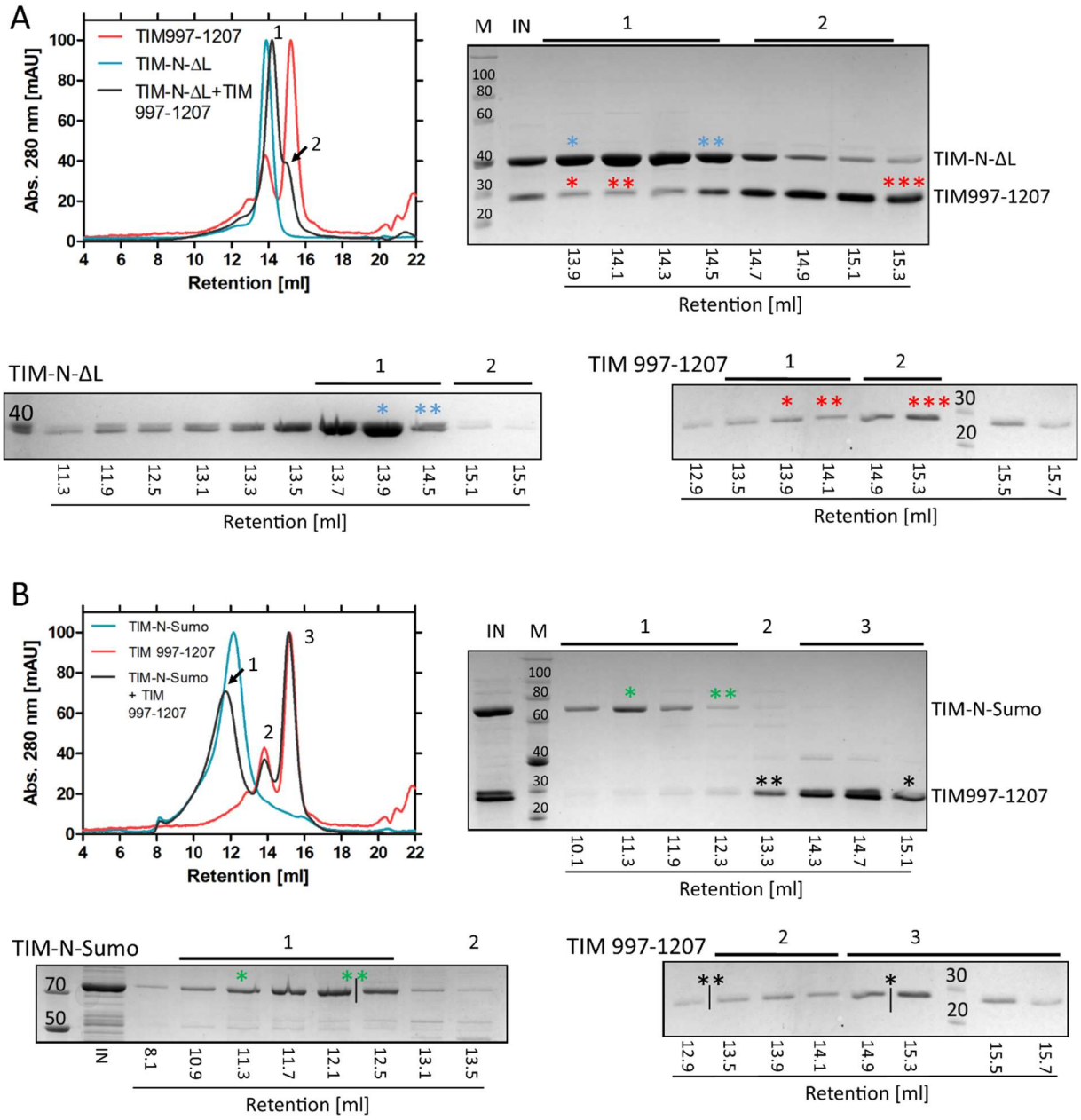

Figure 50: Interaction analysis of TIM-N-ΔL (A), and TIM-N-Sumo (B) with TIM 997-1207 by SEC. After 30 min incubation on ice, the protein species were separated on SEC. Left: Superposition of chromatograms of the protein mix SEC analysis (black) and SEC analysis of single proteins (red, blue). Numbers inside the chromatogram indicate different peaks. Right: SEC fractions analyzed on SDS-PAGE. The numbers below the SDS-PAGE indicate retention volumes in mL. M – protein standard with MW in kDa. The Absorbance at 280 nm was normalized for better comparison of retention volumes. (B) was corrected for shift as whole migration was shifted. Uncorrected curve can be found in appendix. Colored asterisks indicate fractions that have comparable retention volumes.

5.7.2.2 SEC analysis of the TIM 520-680 (TIM BD) with TIM-N-ΔL and TIM C-Terminus

The residue K528 of TIM was crosslinked to the N-terminal half and C-Terminus (Figure 36, Figure 38, Figure 43). To test whether there would be a binding between these regions, we analyzed interaction of TIM520-680 with TIM-N-ΔL and TIM997-1207 (Figure 51). TIM520-680 did not show interaction and co-migration with either of the two constructs. TIM520-680 showed a slight shift in retention with TIM-N-ΔL (Figure 51 A), however, there was no TIM520-680 present in the TIM-N-ΔL fractions, therefore the shift is likely due to experimental variation. The peaks in the SEC of TIM520-680 and TIM997-1207 showed the same retention volumes as their single proteins in separate SECs (Figure 51 B), so there was no binding, but the peaks did partially overlap.

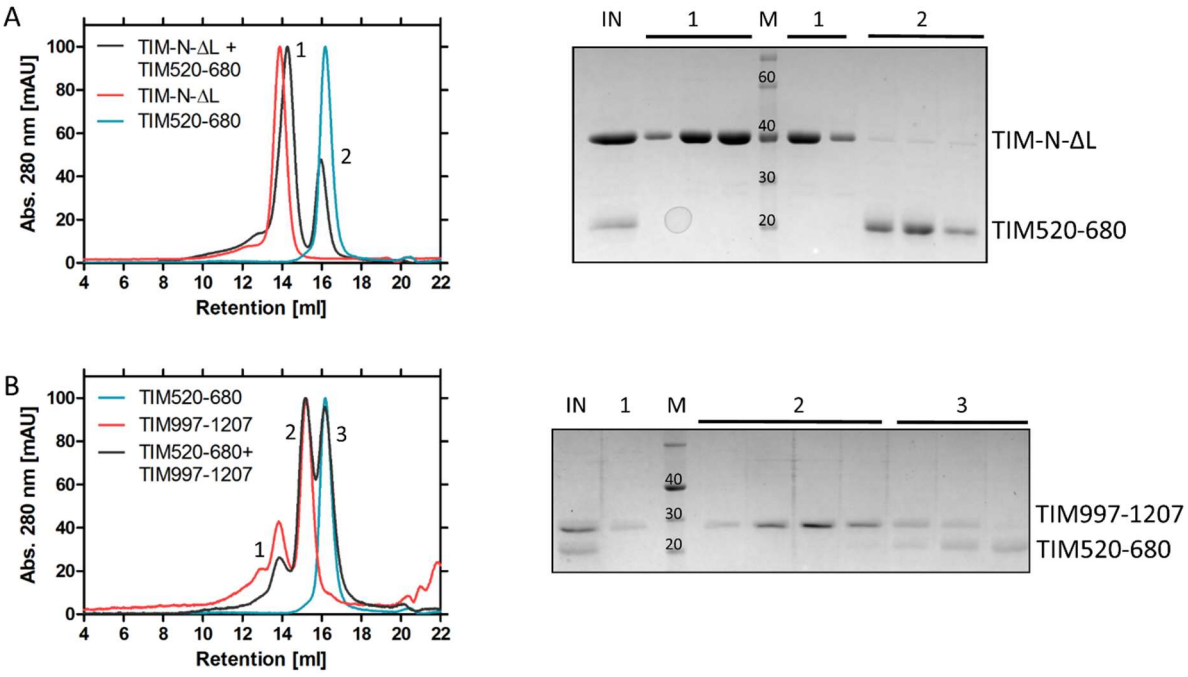

Figure 51: Interaction analysis of the TIM520-680 domain with TIM-N-ΔL (A) and TIM997-1207 (B). A 1.2x excess of TIM520-680 was added to TIM-N-ΔL and TIM997-1207. After 30 min incubation the samples were analyzed by SEC. Left: overlay of chromatograms of the combined SEC run (black curve) and the runs of the single proteins (red curve, blue curve). Right: SDS-PAGE of representative SEC fractions. Numbers indicate the analyzed peak fractions. M – Marker proteins, IN – Input sample. The abs. 280 nm was normalized. (B) was corrected for shifts as the whole retention was shifted. Uncorrected curve can be found in appendix (Figure 73).

5.7.2.3 Binding of TIPIN to the TIM C-Terminus

TIM showed an accumulation of crosslinks between its C-Terminus and TIPIN (Figure 37). To test direct binding, we analyzed a mixture of mTIPIN and TIM997-1207 on SEC (Figure 52). mTIPIN (peak1, blue curve) and TIM997-1207 (peak3, red curve) showed the same retention volumes in the combined SEC compared to the individual SECs. Peak2 contained both proteins, but this was due to tailing of mTIPIN (blue curve) and the presence of TIM997-1207 oligomers, as was seen in the single TIM997-1207 SEC run (red curve). In the individual mTIPIN SEC run (Figure 52, blue curve) a fraction containing peak2 in the combined run (13.7 mL and 14.1 mL) was not analyzed by SDS-PAGE, but the closest fraction at 13.5 mL contained a strong mTIPIN signal which indicates that the presence of mTIPIN in peak2 was due to tailing of the protein. Therefore, TIM997-1207 and mTIPIN likely did not interact.

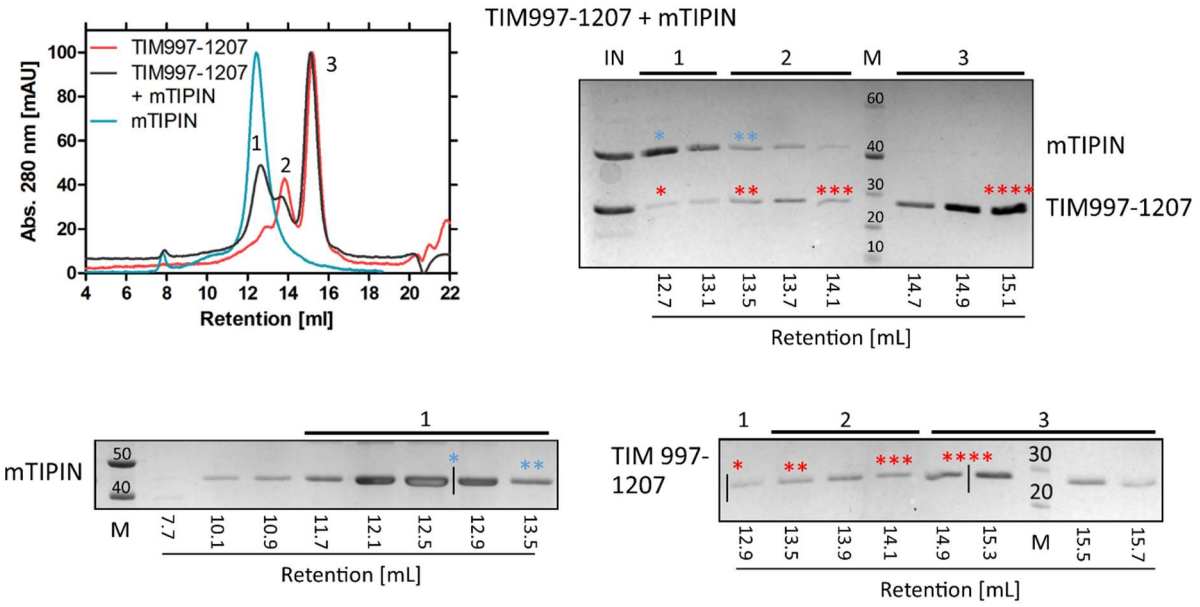

Figure 52: SEC interaction analysis of mTIPIN and TIM997-1207. TIM997-1207 and mTIPIN were mixed in a 1:1 ratio and were analyzed on SEC after 30 min incubation. Left: Overlay of

chromatograms of the combined run of TIM997-1207 with mTIPIN (black) and the single SEC runs of mTIPIN (blue) and TIM997-1207 (red). Numbers inside chromatogram indicate different peaks. Right: SDS-PAGE of SEC fractions. Numbers below the SDS-PAGE indicate retention volumes of the analyzed fractions. The bottom gels show the SDS-PAGE of the single protein SEC runs of mTIPIN and TIM997-1207. IN – Input sample; M - protein standard with MW in kDa; the asterisks * highlight the fractions of comparable retention volumes.

5.7.3 Interaction analysis of CRY with the TIM C-Terminus

Both CRY tails showed crosslinks to the C-Terminus of TIM and the CRY1-PHR was linked to the TIM C-Terminus as well (Figure 38). Therefore, we analyzed a direct interaction of TIM997-1207 and CRY1/2 (Figure 53 A, B). In both SEC analyses the peaks were not resolved well. In the CRY1 + TIM997-1207 SEC (Figure 53 A, black curve), the single peaks of CRY1 (red curve, peak3) and TIM997-1207 (blue curve, peak2) showed a strong overlap. Peak1 contained TIM997-1207 tetramers, as seen before (Figure 49), but also a little CRY1. The presence of CRY1 was caused by tailing of CRY1, rather than interaction, as in the single CRY1 SEC (red curve), CRY1 is present at 14.5 mL as well. There was no increase in CRY1 amount at those retention volumes in combination with TIM997-1207.

In the CRY2 + TIM997-1207 sample (Figure 53, B, black curve), SEC did not separate the different proteins. The proteins in the combined SEC samples (black curve) showed the same migration pattern as in SEC of single proteins (blue and red curve). CRY2 was present at 13.9 mL, but was also present at this retention volume in the single CRY2 SEC (red curve). The was no retention shift for any peak. Therefore, the co-migration was related to the low separation of both proteins and protein tailing. In summary, neither CRY1 nor CRY2 showed a direct interaction with the TIM C-Terminus.

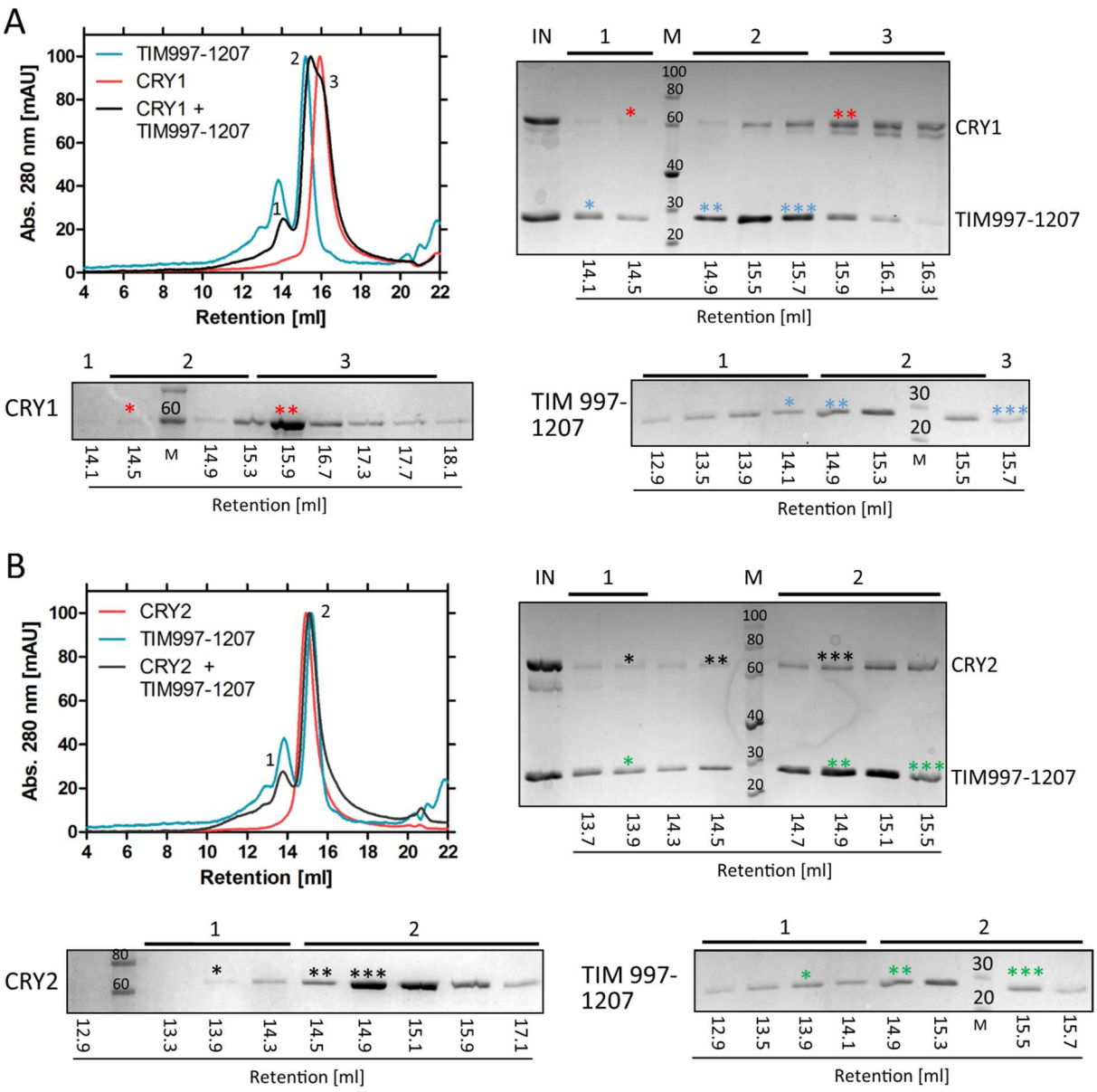

Figure 53: SEC interaction analysis of CRY1 (A) and CRY2 (B) with TIM997-1207. A 1:3 molar excess of TIM997-1207 was mixed with CRY and after 30 min incubation on ice, it was analyzed by SEC. Overlays of chromatograms show the SEC runs of mixed protein (black curve) and individual SEC runs of CRY1/2 (red) and TIM997-1207 (blue). A) SEC of CRY1 and TIM997-1207 B) SEC of CRY2 with TIM997-1207. Numbers inside chromatogram indicate main peaks. Numbers below the SDS-PAGE show the retention volume of analyzed fractions in mL. Bottom: SDS-PAGE of single protein SECs. Asterisks indicate the fractions of similar retention volumes. IN - Input sample, M – protein MW standard in kDa. The abs. 280 nm was normalized. Interaction analysis of CRY tails with TIM and TTP.

5.7.3.1 SEC Analysis of CRY tails with TIM997-1207

In XLMS, many crosslinks of the CRY tails to the TIM C-Terminus were observed (Figure 40, Figure 45). To test whether the tails can bind directly to TIM997-1207, we analyzed the interaction by SEC (Figure 54 A, B).

In SEC, the CRY1 tail (peak3) migrated separately from TIM997-1207 (peak1, peak2) and therefore did not bind to it (Figure 54 A).

The CRY2 tail was faintly present in peak3 and peak2 (Figure 54 B) that contained TIM997-1207 dimers and tetramers (14.0-15.6 mL). Peaks 3 and 4 (black curve) were not completely separated, which might indicate tailing of the CRY2 tail. The intensity CRY2 tail bands showed a steady decrease from the central peak fraction (16.6 mL) to fractions with a lower retention (15.6-14 mL), which indicates tailing as well. At the retention volume of peak3 (~15 mL), the CRY2 tail abs. 280 was not at baseline level (blue curve), supporting tailing of the CRY2 tail. The intensity of the CRY2 tail was not increased in the main fraction of peak3 (15 mL) and peak2 (14 mL). Further, in individual SEC, the CRY2 tail showed migration at a low retention volume of 10.9 mL, indicating oligomerization or aggregation. But directly comparable fractions from the individual CRY2 tail SEC were not analyzed.

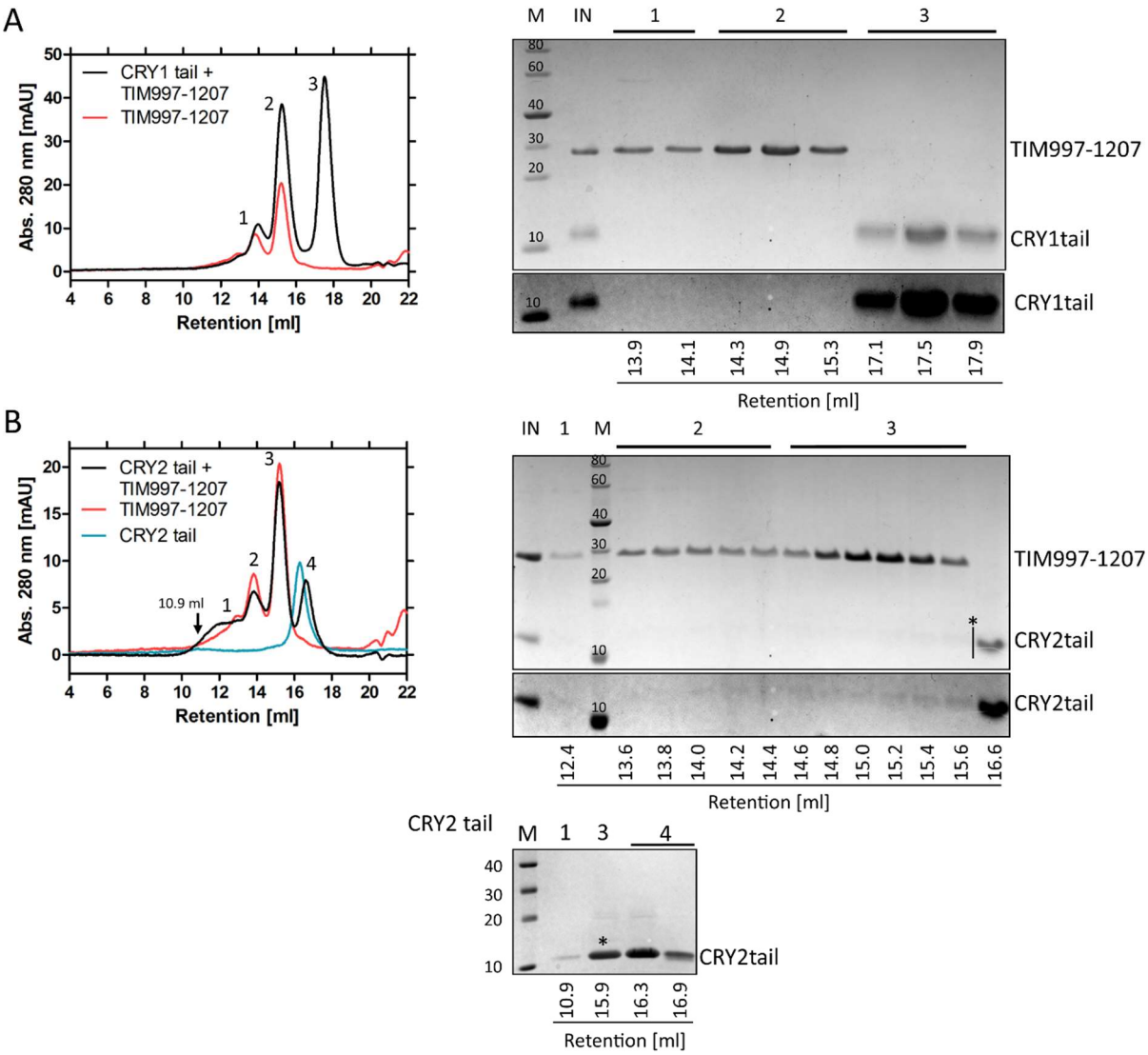

Figure 54: SEC analysis of TIM997-1207 with CRY tails. A 1:2.5x excess of CRY1 tail and CRY2 tail was mixed with TIM997-1207 and after 30 min incubation on ice, it was analyzed by SEC. A) SEC of CRY1 tail with TIM997-1207 B) SEC of CRY2 tail with TIM997-1207. Left: Chromatograms show the absorbance at 280 nm, numbers next to peaks indicate different protein species, that were analyzed on SDS-PAGE. Right: SDS-PAGE of representative fractions; bottom right: same SDS-PAGE with adjusted brightness, contrast for better visibility of weak signals. IN - Input sample, M – MW standard in kDa; bars indicate different proteins species as seen in the chromatogram. (B) was corrected for systematic shifts as the whole migration was shifted (Figure 75).

5.7.3.2 SEC Analysis of CRY tails with TIM-N-ΔL

As the CRY tails had crosslinks to the TIM 1-463 region (Figure 40, Figure 45), we tested the interaction of the CRY tails and TIM-N-ΔL by SEC (Figure 55 A, B). The CRY1 tail showed light co-migration with TIM-N-ΔL in peak2 (Figure 55 A, black curve, 14.1 mL/14.3 mL). In

other SECs with the CRY1 tail it was not present at this volume (Figure 54 A, Figure 56 A), indicating an effect related to Tim-N-ΔL. There was no CRY1 tail in peak1.

The CRY2 tail on the other hand, showed bands in peak2 and peak1, together with TIM-N-ΔL (Figure 55 B). In an individual SEC, the CRY2 tail showed presence at a retention volume of 10.9 mL (Figure 55 B, bottom gel), indicating that the CRY2 tail presence in peak1 was due to oligomerization of the CRY2 tail. The co-migration in peak2 (13.1-14.5 mL) could have been caused by oligomerization as well or, tailing of the main CRY2 tail peak (peak3), as its individual SEC (blue curve) showed some overlap (14.5-15.5 mL) with peak2. An enrichment of the CRY2 tail with TIM-N-ΔL in the central fraction of peak2 (13.9 mL) was not observed, indicating that migration of the CRY2 tail was not affected by TIM-N-ΔL.

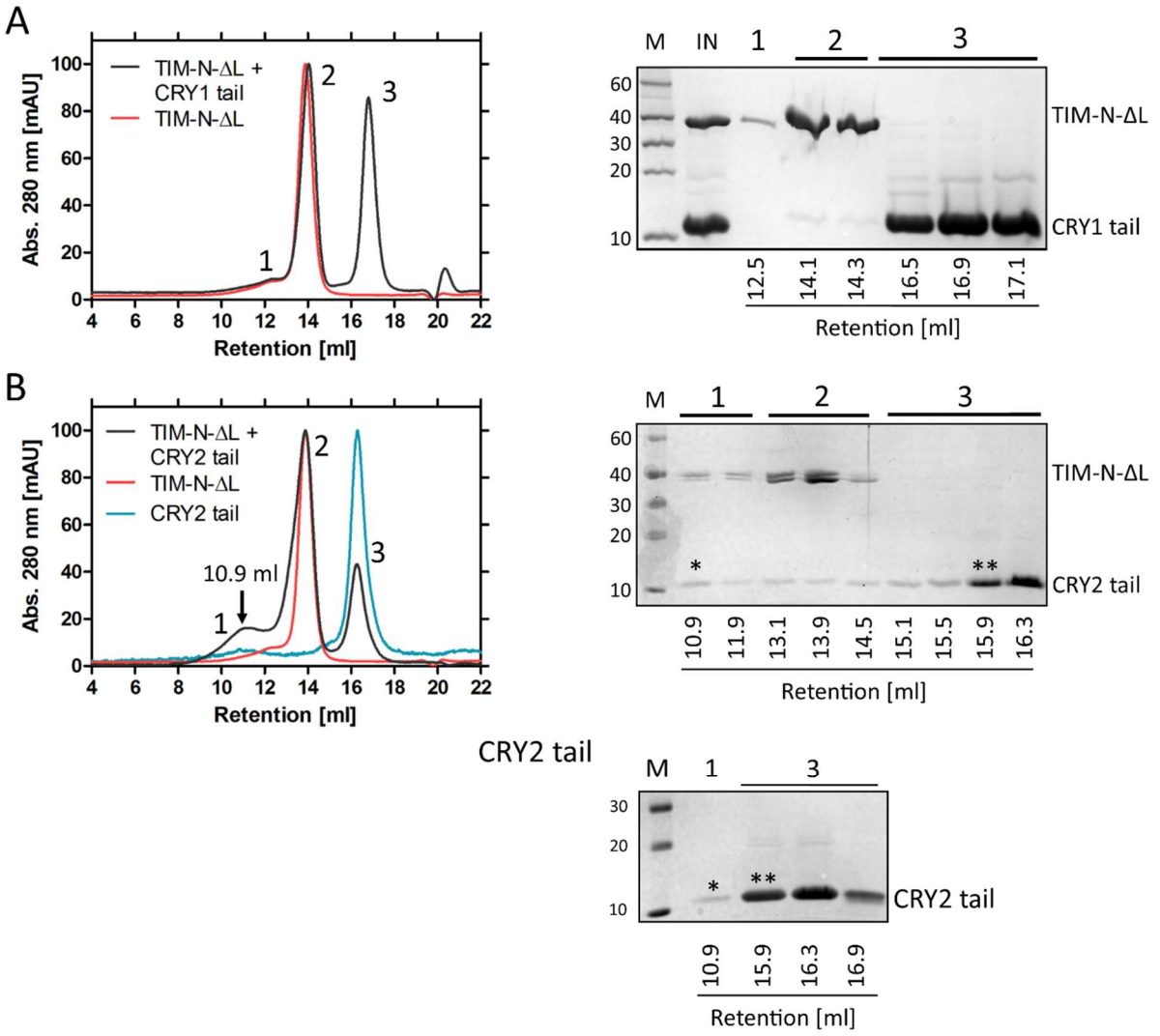

Figure 55: Interaction analysis of TIM-N-ΔL with the CRY tails. An excess of CRY tail (2:1 molar ratio) was mixed with TIM-N-ΔL and was analyzed by SEC after 30 min incubation. SEC runs of the TIM-N-ΔL + CRY1/2 tails are superposed with SEC run of single TIM-N-ΔL, and CRY2 tail. A) SEC of TIM-N-ΔL and CRY1 tail and SDS-PAGE of corresponding

fractions. B) SEC of TIM-N-ΔL with CRY2 tail. Numbers inside chromatogram indicate peaks that were analyzed on SDS-PAGE. M – protein MW standard in kDa; IN – input sample before SEC.

5.7.3.3 SEC Analysis of CRY tails with TIM-N-SL

The interaction of the CRY tail with TIM-N-SL was analyzed by SEC (Figure 56). TIM-N-SL and the CRY1 tail showed well separated peaks. There was no co-migration of the CRY1 tail with TIM-N-SL, indicating no binding. This was in contrast to the SEC with TIM-N-ΔL (Figure 55 A) and indicated a negative effect of the shortened TIM loop on the interaction of CRY1 tail.

In SEC of the CRY2 tail with TIM-N-SL the CRY2 tail was present in peak1, which contained TIM-N-SL (Figure 56 B). There was no enrichment of the CRY2 tail with TIM-N-SL in the central fraction of peak1 (13.9 mL). The CRY2 tail bands were more intense on the left side of peak1 (13.1-13.5 mL), indicating that the presence of the CRY2 tail in peak2 might not be caused by TIM-N-SL. Fractions of an individual SEC of the CRY2 tail at 13.1-13.5 mL were not analyzed by SDS-PAGE. The CRY2 tail showed migration at 10.9 mL in an individual SEC run, indicating oligomerization, which could have caused the presence at 13.1-13.5 mL in the combined run with TIM-N-SL.

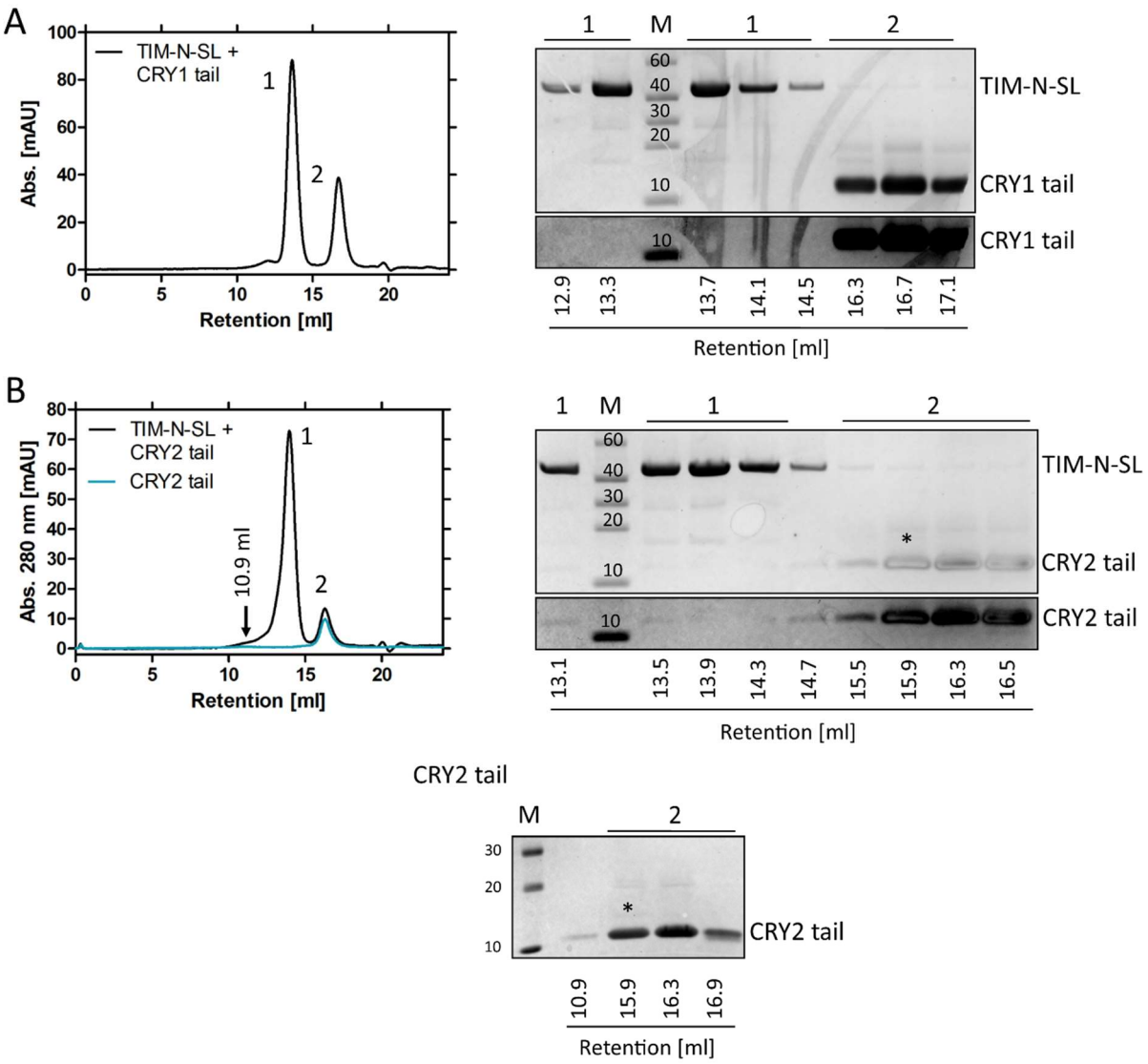

Figure 56: Interaction analysis of TIM-N-SL with the CRY tails. An excess of CRY tail (5:1 molar ratio) was mixed with TIM-N-SL and was analyzed by SEC after 30 min incubation. SEC runs of the TIM-N-SL + CRY1/2 tails are superposed with SEC run of single TIM-N-SL, and CRY2 tail. A) SEC of TIM-N-SL and CRY1 tail and SDS-PAGE of corresponding fractions. B) SEC of TIM-N-SL with CRY2 tail. C) Fractions of SDS-PAGE corresponding to individual CRY2 tail SEC (corresponding to blue curve in B). Numbers inside chromatogram indicate peaks that were analyzed on SDS-PAGE. M – protein MW standard in kDa; IN – input sample before SEC.

5.7.3.4 SEC Analysis of CRY tails with TIM-N-Sumo

To analyze the effect of the full TIM loop on the CRY tails, SECs with TIM-N-Sumo and the CRY tails were done (Figure 57). The CRY1 tail (peak2) and TIM-N-Sumo (peak1) showed a separated migration pattern. There was a very faint band of the CRY1 tail present at 11.3 mL (Figure 57 A). Migration of the CRY1 tail at 11.3 mL was not observed in other SEC experiments (Figure 58, Figure 59), possibly indicating a weak interaction with TIM-N-Sumo. But the 11.3 mL fraction was not analyzed in an individual CRY1 tail SEC.

The CRY2 tail showed co-migration with TIM-N-Sumo (peak 1). In peak1, the CRY2 tail was most dominant at 10.9 mL, a fraction where the maximum of TIM-N-Sumo migrated. Individual SEC of CRY2 tail showed presence of the CRY2 tail at this retention volume as well, therefore the co-migration at 10.9 mL was likely not caused by binding of the CRY2 tail to TIM-N-Sumo. The migration pattern of the CRY2 tail with TIM-N-Sumo was similar to the pattern observed in SEC with TIM-N-ΔL, indicating no difference of the CRY2 tail towards TIM-N-ΔL and TIM-N-Sumo.

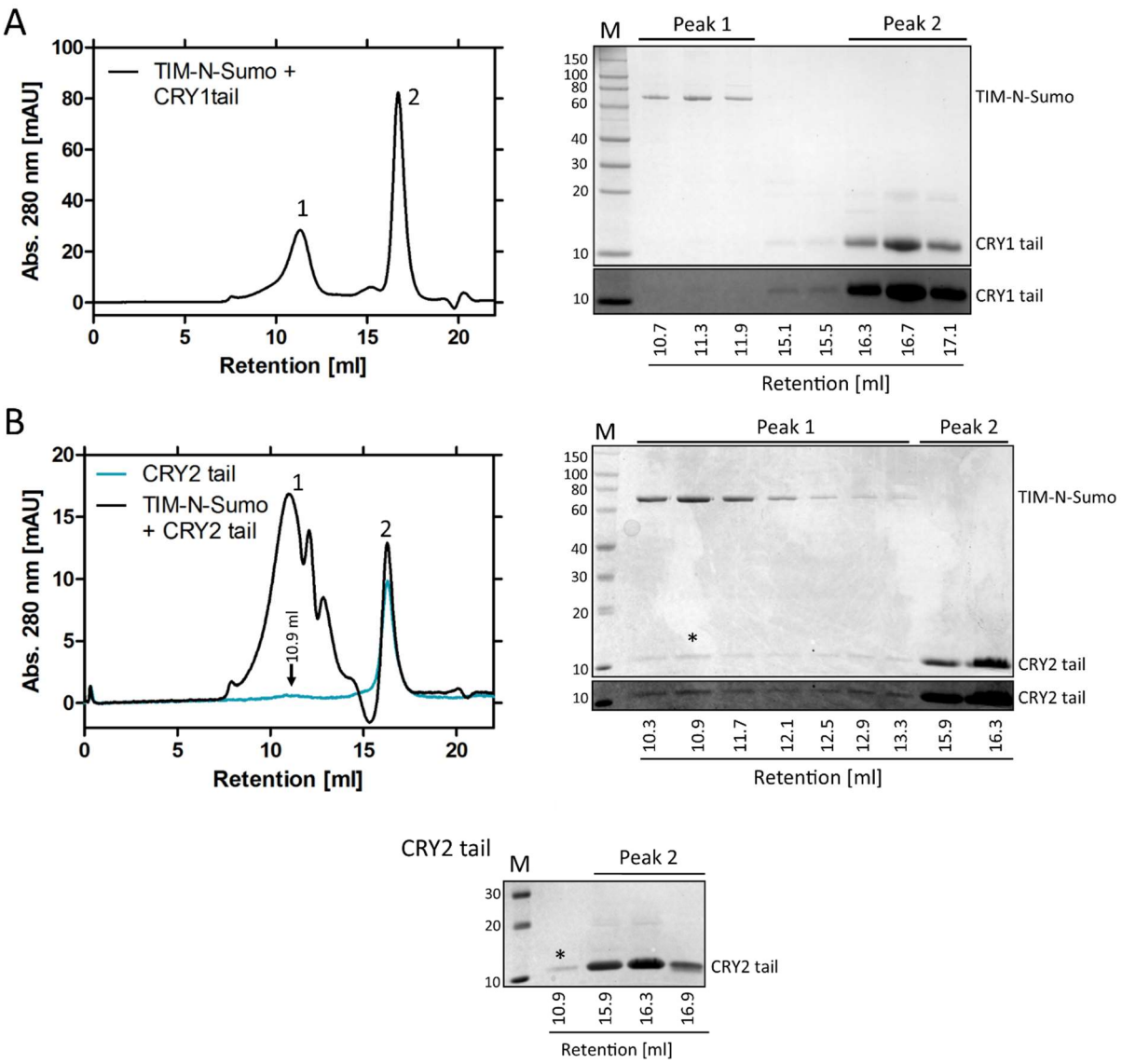

Figure 57: Interaction analysis of TIM-N-Sumo with CRY tails. An excess of CRY tail (4:1 molar ratio) was mixed with TIM-N-Sumo and was analyzed by SEC after 30 min incubation. A) SEC of TIM-N-Sumo and the CRY1 tail and SDS-PAGE of corresponding fractions. B) SEC of TIM-N-Sumo with the CRY2 tail. Numbers inside chromatogram indicate peaks that were analyzed on SDS-PAGE. M – Protein MW standard in kDa.

5.7.3.5 SEC Analysis of the CRY tails with TTP-ΔL

To test if the co-migration of the CRY1 tail with TIM-N-ΔL (Figure 55 A) was related to the dimerization of the TIM-N-ΔL construct, we analyzed whether the effect would persist with TTP-ΔL (Figure 58). Here, the CRY1 tail did not co-migrate with TTP-ΔL (Figure 58 A, peak1), both proteins were well separated in SEC. Therefore, the co-migration of the CRY1 tail with TIM-N-ΔL, was likely due to the homodimerization of the TIM-N-ΔL construct.

The CRY2 tail co-migrated with TTP-ΔL in peak1 (Figure 58 B), but the co-migration could be due to oligomerization of the CRY2 tail, as its presence at a similar retention volume (10.9 mL) was observed in an individual SEC of the CRY2 tail as well (Figure 58 B, blue curve, right gel). The band intensity of the CRY2 tail in the SDS-PAGE was not enhanced in the central TTP-ΔL peak fraction (11.5 mL, peak1).

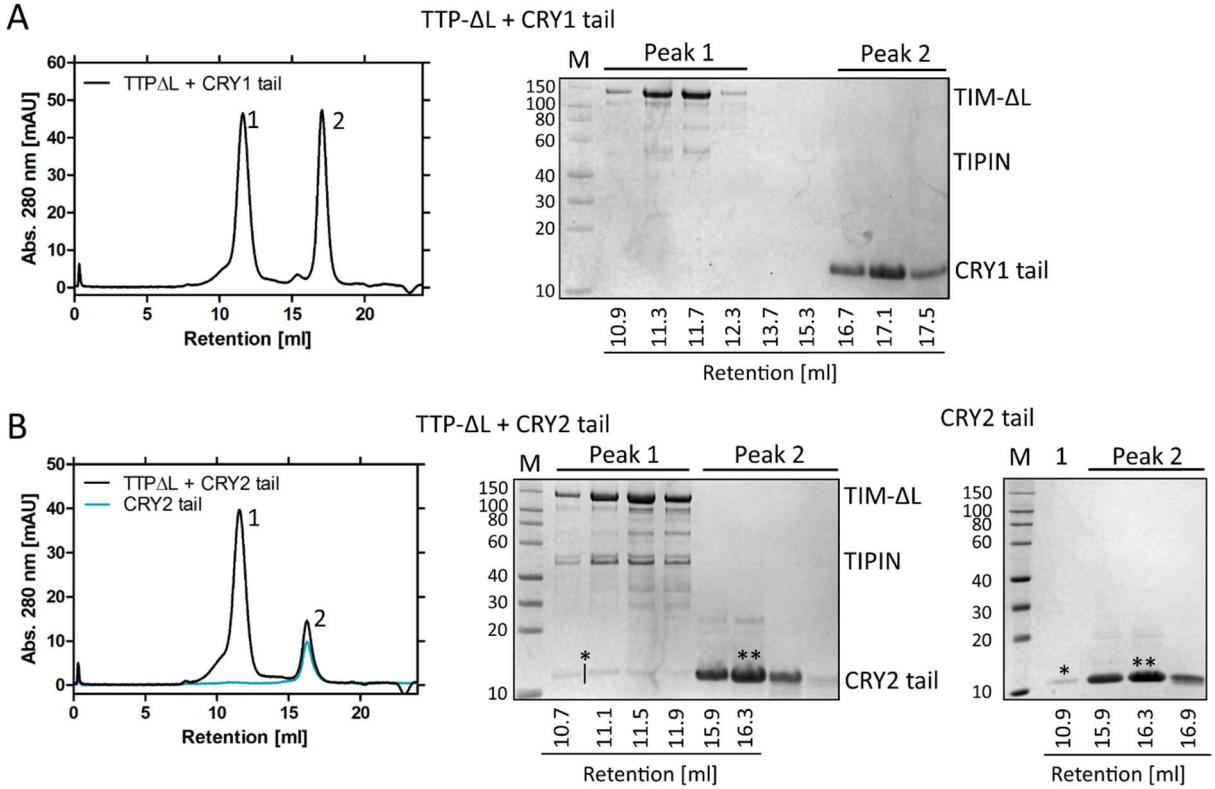

Figure 58: Analytical SEC with of TTP-ΔL with the CRY1 tail and the CRY2 tail. A molar excess of CRY tail (1:17) was mixed with TTP-ΔL and after 30 min incubation, it was analyzed by SEC. A) SEC of CRY1 and TTP-ΔL. B) SEC of CRY2 and TTP-ΔL. Numbers inside chromatogram indicate fractions that were analyzed on SDS-PAGE. M – protein MW standard in kDa.

5.7.3.6 SEC Analysis of the CRY tails with TTP

To assess the effect, the full length TTP complex has on the CRY tails, the interaction was analyzed by SEC (Figure 59). The CRY1 tail did not show co-migration with full length TTP in SEC (Figure 59 A). This was consistent with the SEC of the CRY1 tail with TTP-ΔL (Figure 58), indicating that the co-migration of the CRY1 tail with TIM-N-ΔL and TIM-N-Sumo was likely an effect of the partial TIM constructs used.

The CRY2 tail showed co-migration with TTP (Figure 59 B) at 10.9 mL. The CRY2 tail migrated at 10.9 mL in an individual SEC as well (blue curve, right gel), therefore, the co-migration was likely not caused by TTP.

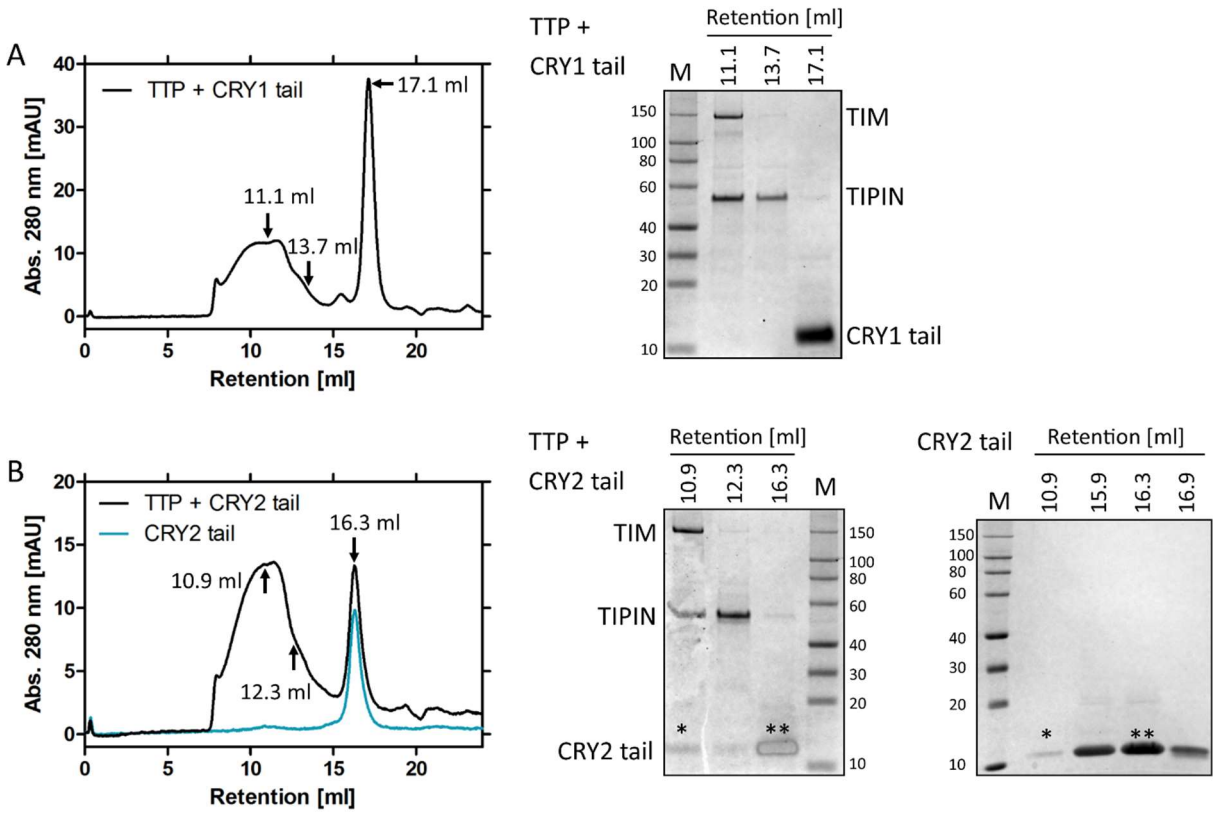

Figure 59: Interaction analysis of TTP and the CRY tails by SEC. A molar excess of CRY tail (1:17) was mixed with TTP and after 30 min incubation, it was analyzed on a S200 10/300 column. A) SEC of CRY1 and TTP. B) SEC of CRY2 and TTP. Numbers inside chromatogram (left) indicate retention volumes of fractions that were analyzed on SDS-PAGE (right). M – protein standard in kDa. Asterisks indicate comparable fractions of the SEC runs.

In summary, the CRY1 tail did not directly interact with TIM997-1207, TIM-N-SL, but showed some co-migration/interaction with TIM-N-ΔL and TIM-N-Sumo. This was likely an effect of the partial TIM constructs, as it was not reproducible with TTP-ΔL and full length TTP. In individual SEC, the CRY2 tail showed migration at a retention volume, that was similar to the retention volumes of the tested TIM and TTP constructs. Further, there was likely some tailing of the main CRY2 tail peak. Therefore, it was unclear whether the observed co-migrations were caused by interaction of the CRY2 tail or by oligomerization and tailing.

5.7.4 Interaction analysis of CRY and TIM827-935

XLMS identified crosslinks of CRY1 and CRY2 to residues in the PCT region of TIM (CRY1: K838, K882; CRY2: K911). To test an interaction, we purified TIM 827-935, mixed it with CRY1/2 and analyzed it by SEC (Figure 60 A, B). In both SECs the CRYs were present in peak2, where TIM827-935 migrated, but the presence of CRY was due to tailing of CRY1 and CRY2 as the individual CRY peaks (peak1, red curves) showed overlap with peak2 in both experiments. Therefore, CRY1 and CRY2 did not bind to TIM827-935.

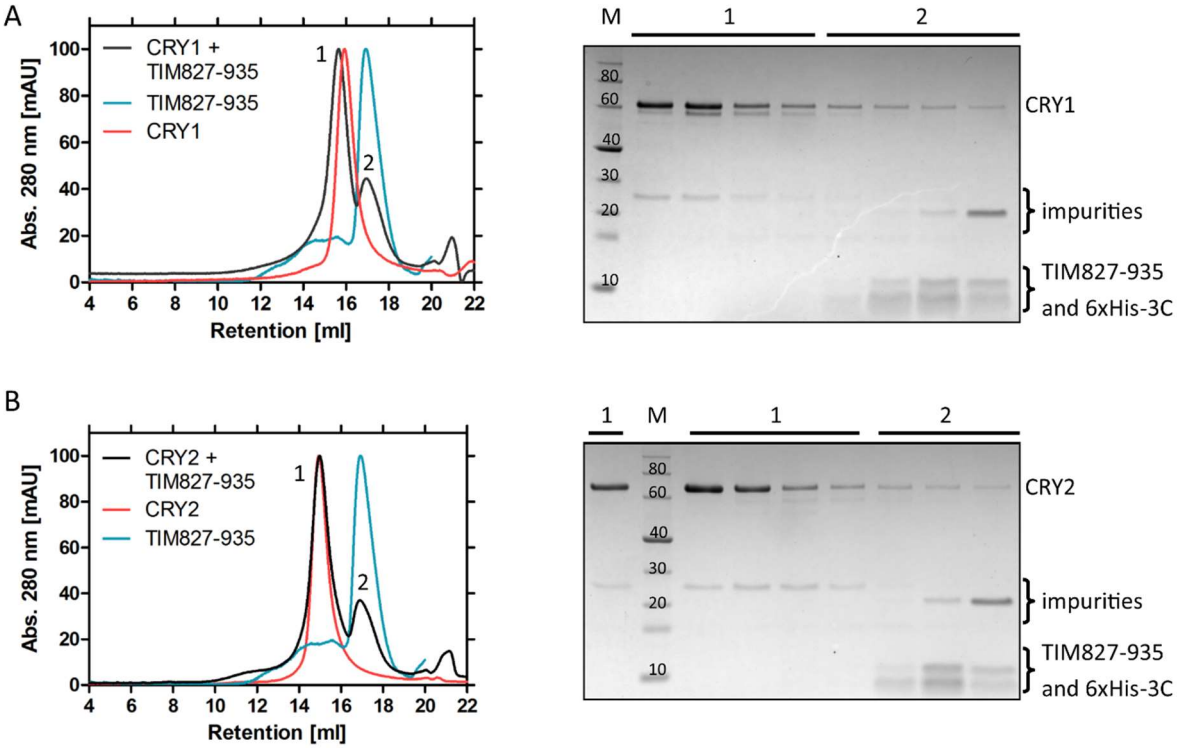

Figure 60: Interaction analysis of TIM827-935 with CRY1 (A) and CRY2 (B) by SEC. CRY1/CRY2 was mixed with a 1:5 excess of TIM 827-935. After incubation for 30 min on ice the protein was analyzed by SEC. Left: Numbers next to peaks indicate different protein species, that were analyzed on SDS-PAGE. Right: SDS-PAGE of peak fractions. IN: Input sample, M: MW protein standard; bars indicate different proteins species as seen in the chromatogram. For better comparability of protein retention, the Abs. 280 nm was normalized. The Chromatogram of CRY-TIM827-935 was superposed with the single chromatograms of CRY (red) and TIM827-935 (blue).

5.7.5 Interaction analysis of CRY with TIPIN

To assess whether TIPIN binds to CRY directly, independently of TIM, we mixed mTIPIN with CRY1 and CRY2 and analyzed the sample by SEC (Figure 61). The mTIPIN + CRY1 SEC contained three peaks (Figure 61 A). Peak1 contained the single mTIPIN and peak3 contained CRY1 as the retention volumes matched the retention of mTIPIN and CRY1 in single protein SECs (blue and red curve). There was an additional peak at a retention volume of 14.6 mL (peak2), which contained CRY1 as well as mTIPIN. A comparable fraction in the single CRY1 SEC showed that a CRY1 band was present at 14.9 mL, 14.5 mL and faintly at 14.1 mL. This indicated that the presence of CRY1 at the retention volume of 14.6 mL (peak2) could be due to tailing of CRY1. mTIPIN showed tailing to larger retention volumes as well (blue curve). A fraction of the single mTIPIN SEC at a retention volume around 14.6 mL was not analyzed. The SDS-PAGE showed impurities of 20-30 kDa (black °) within peak2, which might have attributed to the formation of an additional peak. But in interaction could not be excluded.

The CRY2 + mTIPIN SEC showed a similar pattern (Figure 61 B). There were two dominant peaks (peak1, peak3), that contained mTIPIN and CRY2 (blue and red curve). In between, there was an additional little bump at 13.9 mL (peak2), which contained both proteins according to SDS-PAGE. In the individual SEC CRY2 migrates at 13.9 mL as well, due to tailing. A mTIPIN fraction at 13.9 mL was not analyzed on SDS-PAGE, but in the single mTIPIN SEC, the mTIPIN peak (peak1, blue curve) showed wide tailing in the range of peak2. The increase in abs. 280 nm could have been affected by impurities between 20-30 kDa as well (black °). There was a small amount of CRY2 migrating with mTIPIN in peak1. But there was no increase in band intensity of CRY2 in the main mTIPIN fractions at 12.5 and 12.7 mL, indicating an overlap of the peaks rather than interaction, even though the single CRY2 SEC did not show CRY2 at 12.9 mL. The SEC of the protein mix (black curve) showed wide migration and low separation of peaks and the abs. 280 nm did not return to the baseline after 20 mL, this was in contrast to the individual SECs of mTIPIN and CRY2 (blue and red curve).

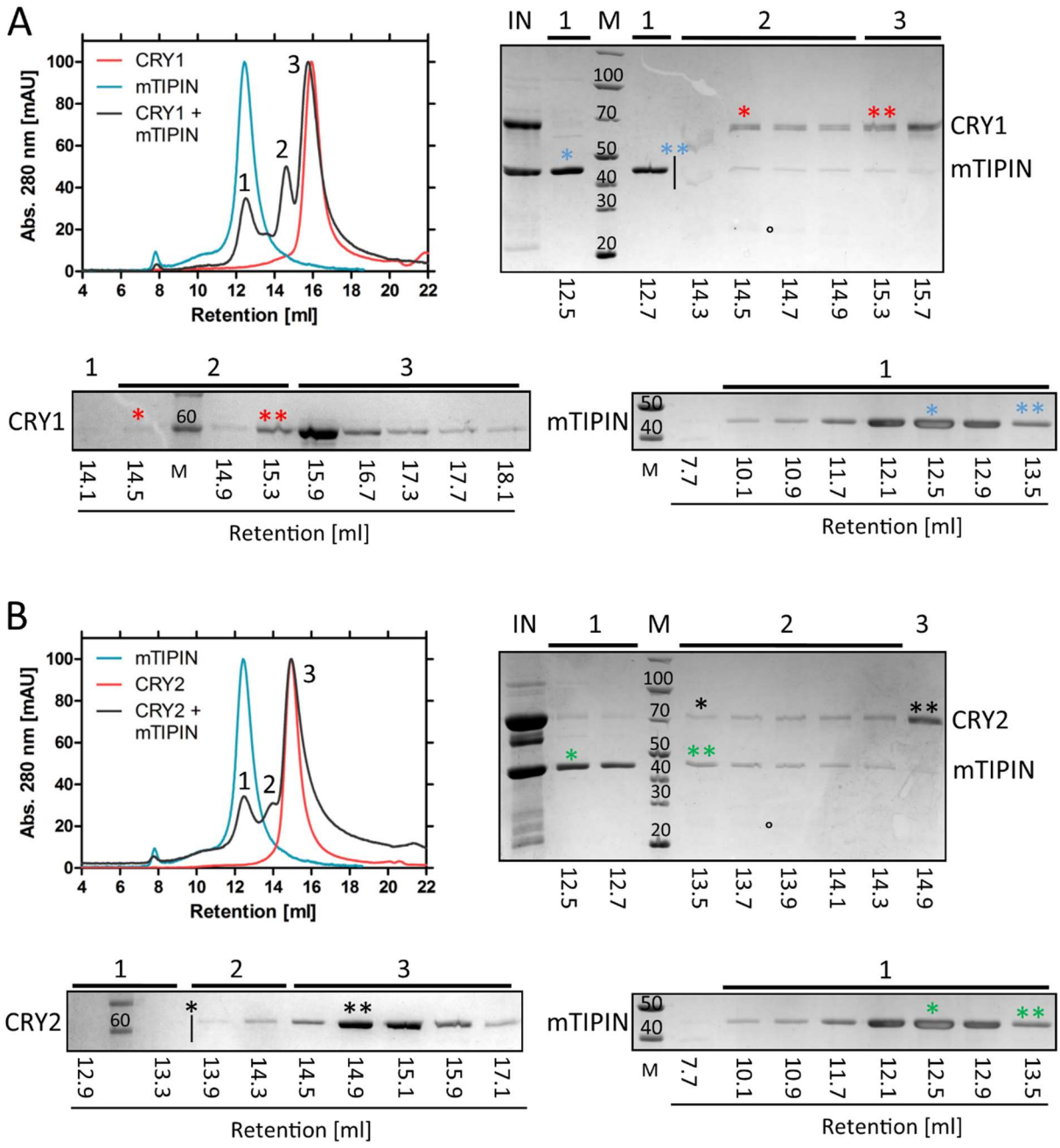

Figure 61: Interaction analysis of CRY1/2 and mTIPIN. A, B) Overlay of SECs and SDS-PAGE of mTIPIN with CRY1/2. An excess of mTIPIN (1:2.5) was mixed with CRY and after 16 h incubation at 4 °C the samples were analyzed by SEC. Numbers inside chromatogram indicate different peaks. Numbers below the SDS-PAGE indicate the retention volumes of the analyzed fractions in mL. IN - Input sample before the SEC run; M - Protein MW standard in kDa; bars indicate the analyzed species visible as peaks in the chromatogram. Colored asterisks * indicate comparable SEC fractions. ° indicates impurities between 20-30 kDa. Abs. 280 nm was normalized.

5.8 Pulldown analysis of TTP and TTP-ΔL

So far, the TIM loop has not been functionally described. In order to obtain information about its function, by interactors of the loop, we conducted pulldown experiments. Purified 6xHis-tagged TTP and TTP-ΔL were bound to Ni^{2+}-NTA beads. SILAC labeled cell extracts were prepared, that were used as prey in the pulldown. The beads were washed and the eluted proteins were identified by MS. The pulldown was done in triplicates with three different combinations of labels for each pulldown (Figure 62 A-C). For the identified proteins, ratios of labels (SILAC log2 ratios) in each experiment were calculated. These ratios were plotted against the protein intensities. For each combination we created a scatterplot in which the proteins formed a cloud-like distribution between log2 ratios of +/-1. This indicated that the same amount of differently labeled protein was detected and therefore there was no enrichment of the protein by either of the TTP or TTP-ΔL. Proteins localized outside of the threshold were enriched with one of the bait complexes. There were few proteins enriched with the same bait in all three replicates (Figure 62 D). With TTP as bait, the proteins SLC39A6, SLC39A7, RBM12B, APOBEC3B and YLPM1 were enriched. SLC39A6 and SLC39A7 are described as zinc transporters (Taylor *et al*, 2003; Huang *et al*, 2005), RBM12B is identified as RNA binding protein without further biochemical characterization (Castello *et al*, 2012) and APOBEC3B is a reported DNA deaminase that acts as inhibitor of retroviral replication (Rose *et al*, 2005). YLPM1, which was enriched with TTP bait as well has a role in the regulation of the telomerase activity during differentiation of embryonic stem cells (Armstrong *et al*, 2004). This is a function potentially connected to TTP, as TTP is involved in regulation of telomere length (Leman *et al*, 2012).

AZI1 (also known as CEP131) was enriched with TTP-ΔL and has a reported function related to TTP, since both proteins are associated with centromers (Andersen *et al*, 2003; Dheekollu *et al*, 2011). AZI1 was also enriched in a former test experiment (not shown). The protein Q8TCX0, that showed enrichment with both bait proteins, was likely a contaminant of the recombinantly expressed TTP and TTP-ΔL or of the sample preparation as it was only present in 'light' samples and did not show consistent enrichment with either TTP or TTP-ΔL.

CRY1 was found enriched in two experiments as well, but as it was enriched with TTP in one experiment and with TTP-ΔL in another, no conclusion regarding binding preference for TTP or TTP-ΔL was made (Figure 62 B, C).

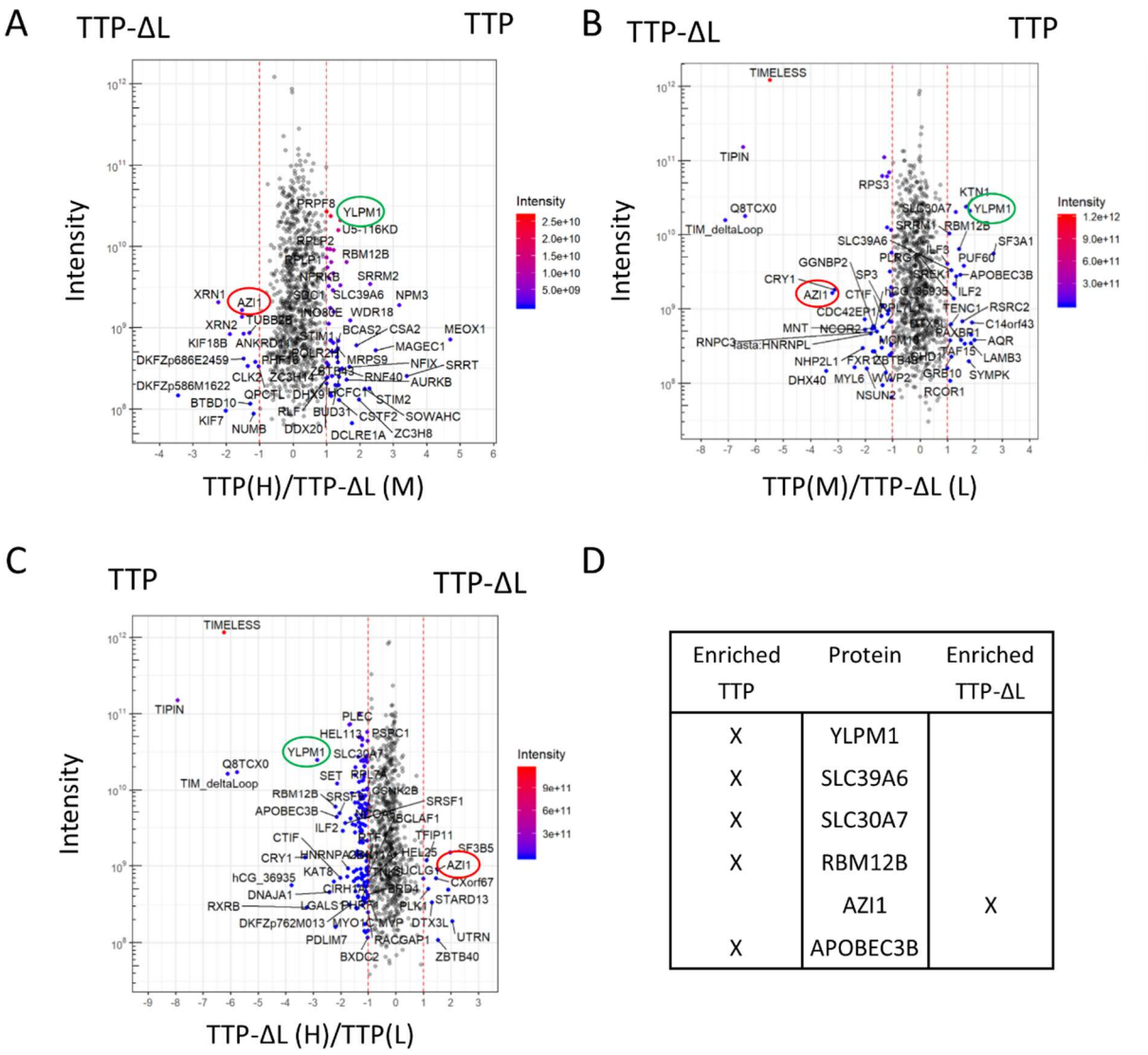

Enriched TTP	Protein	Enriched TTP-ΔL
X	YLPM1	
X	SLC39A6	
X	SLC30A7	
X	RBM12B	
	AZI1	X
X	APOBEC3B	

Figure 62: Protein pulldowns using TTP and TTP-ΔL as bait with SILAC labeled human cell extract. U2OS cells were grown in medium supplemented with isotopically labeled Arg and Lys. Whole cell extract was prepared and used for the pulldowns. A-C) Scatterplots of SILAC log2 ratios of identified proteins in pulldowns using TTP and TTP-ΔL as bait. Dashed red lines indicate a threshold of log2 +/-1 as indicator of enrichment. The proteins AZI1 and YLPM1 are highlighted as TIM has functions related to them. D) Proteins that were enriched in all three experiments are shown. MS analysis was done by the Proteomics core facility at IMB Mainz.

6 Discussion

6.1 TIM, TIPIN and CRY formed a trimeric complex

The first aim of this thesis was to confirm interactions between TIM and CRY1/2 that were observed by Co-IP experiments (Unsal-Kaçmaz *et al*, 2005; Kang & Leem, 2014). A limitation of Co-IP experiments is that it cannot be distinguished between a direct protein-protein interaction and an indirect interaction, as part of a larger complex containing multiple proteins. By expressing TTP and CRY in a recombinant system and by purifying the proteins, we aimed to prove direct interactions.

CRY1 and CRY2 bound directly to the TTP and formed a complex (Figure 20). They formed equimolar 1:1:1 trimeric complexes according to SAXS and MALS MW analysis (Figure 20, Table 26). This is consistent with former observations of TTP and the TTP-RPA complex forming stoichiometric complexes as well (Holzer *et al*, 2017; Witosch *et al*, 2014). A complex of TTP and CRY suggests a connection of the circadian clock and TTP functions, such as DNA replication and DNA damage signaling. This is supported by the observation that genotoxic stress increases interaction of TIM to CRY1 (Kang & Leem, 2014), which indicates that detection of replication stress might trigger feedback to the circadian clock.

Indeed, DNA damage induces a phase advancing of the circadian clock, which is dependent on the signaling kinase ATM (Oklejewicz *et al*, 2008). ATM depends on TTP in its function to induce the CHK2 and the G2/M checkpoint (Yang *et al*, 2010). Interestingly, DNA damage does not lead to increased transcription or translation of core clock genes, suggesting a posttranslational mechanism (Oklejewicz *et al*, 2008). PER1, for example, is a phosphorylation target of ATM/ATR (Matsuoka *et al*, 2007). Modifications on clock proteins could affect their activity, stability and localization, thereby altering the circadian phase. In a similar manner, a TIM mutant lacking 128 amino acids at the C-Terminus (TIM1-1081X), has a reduced CRY2 affinity, which causes destabilization of CRY1/2 and of PER1/2 and leads to the familial advanced sleep phase (FASP) phenotype (Kurien *et al*, 2019). Destabilization of CRY shortens the repressive phase and leads to a phase advance. This is consistent with the period shortening effect observed following TIM RNAi knockdown (Engelen *et al*, 2013). Therefore, wild type TIM and TTP on the other hand, would have a stabilizing effect on CRY, explaining longer circadian periods.

DNA repair processes, such as nucleotide excision repair (NER), show a circadian pattern of activity. NER coincides with high BMAL1 levels and is anti-phase with CRY1 and PER2 levels in mouse fibroblasts (Kang *et al*, 2009). This consistent with another finding, describing that not only DNA repair efficiency is dependent on the circadian phase, but also DNA damage induction. UV photoproduct formation and most efficient NER occurred at the same time when chromatin was most relaxed, which suggests regulation of DNA sensitivity and efficient NER by controlling chromatin condensation (Bee *et al*, 2015). And indeed, the intensity of a circadian phase shift differed dependent on the time after synchronization at which irradiation occurred in rat fibroblasts (Oklejewicz *et al*, 2008).

Upon occurrence of DNA damage, the replication fork is stalled and TTP is involved in damage signaling (Leman & Noguchi, 2012). TTP recruits the signaling kinase ATR/ATRIP, which further activates the kinase CHK1 that induces cell cycle arrest and DNA repair processes. The association of CRY1 with TIM is enhanced after DNA damage and CRY1 is needed for a clock dependent activation of ATR (Kang & Leem, 2014). In addition to that, CRY2 interaction with TIM affects the ATR dependent phosphorylation of CHK1 and cell cycle arrest (Unsal-Kaçmaz *et al*, 2005). This indicates that CRY1/CRY2 may be recruited by TTP upon DNA damage, form a direct complex and assist with downstream signaling and activation of ATR and CHK1. Association with TTP may stabilize CRY which could contribute to the circadian phase shift observed after DNA damage.

However, the effect of DNA damage differs between CRY1 and CRY2. While DNA damage leads to stabilization of CRY1, it reduces stability of CRY2 (Papp *et al*, 2015). This is consistent with the observation that the CRY1/CRY2 ratio controls the circadian period (Li *et al*, 2016). The TIM1-1081X mutant causes a reduction of CRY1 and CRY2 half-life, but shows a shortened period as well (Kurien *et al*, 2019). These conflicting results suggest, that there are additional mechanisms that control CRY stability in response to DNA damage and thereby the phase shift.

It is not known whether the binding site for CRY on TTP is exclusive, and how complex formation with CRY affects TTP in the replisome. Due to the large size of the Polymerases-δ and ε, of the MCM2-7 complex and of the GINS complex and, in general, to the crowdedness of the replisome, it is possible that TTP binding to the replisome, and to CRY1/2 could be mutually exclusive, and that, in case of DNA damage and replication stress, CRY1/2 binding might cause rearrangements of TTP in the replisome. On the other hand, TIM1-309 was reported to bind to CHK1 in Co-IP experiments (Engelen *et al*, 2013). TIM1-309 also binds to

CRY1, which may indicate a competition for TIM. However, in Co-IP it cannot be distinguished between and direct interaction of TIM1-309 and CHK1 and an interaction with a protein complex containing CHK1, the interaction might be indirect or both proteins may bind at different non-overlapping sides within TIM1-309. However, the parallel binding of CHK1 and CRY to TIM1-309 has not been tested. Another possibility would be a dissociation of CRY from TIM after ATR activation.

Many unknowns subsist about the TTP/CRY interaction and how this interaction mediates the coupling between the circadian clock and TIM related functions remains unclear. It is further unclear, how DNA damage increases association with CRY. Perhaps, TTP may be post-translationally modified upon DNA damage or replication stress thereby altering its interactions. For example, phosphorylation of TIM plays a role DNA damage response, as the phosphorylation mimicking mutation T1078D in the TIM C-Terminus affects the interaction with PARP1, a key protein in DNA damage response (Young *et al*, 2015).

6.2 CRY1 and CRY2 showed different affinities for TTP, that may be affected by variable CRY tails

To further characterize the interaction between TTP and CRY1/2, we determined K_D values for the TTP/CRY1 and TTP/CRY2 complexes. CRY2 had a 6-fold higher affinity to TTP compared to CRY1. Located in the nanomolar range, these values were in a similar range as other circadian clock and replication fork associated interactions (Table 27).

Table 27: Overview of K_D values for circadian clock and TIM associated protein complexes. For TTP/CRY interactions, K_D values from NanoSPR experiments are shown.

K_D values of Circadian clock and replication associated interactions

Complex	K_D	Reference
TTP/CRY1	0.78 ± 0.11 µM	This study
TTP/CRY2	0.13 ± 0.01 µM	This study
TTP/CRY1-PHR	0.48 ± 0.08 µM	This study
mCRY1-PHR/mPER2-CBD	0.028 µM	(Schmalen *et al*, 2014)
mCRY1/mBMAL1 577-625	1.4 ± 0.2 µM	(Czarna *et al*, 2013)

mCRY1-PHR/mCLOCK:mBMAL1-PAS	0.065 ± 0.06 µM	(Fribourgh *et al*, 2019)
mCRY2-PHR/mCLOCK:mBMAL1-PAS	1.2 ± 0.2 µM	(Fribourgh *et al*, 2019)
TIM1000-1098/PARP1 661-1041	0.026 ± 0.0015 µM	(Xie *et al*, 2015)
TIM/DNAP-ε	0.068 µM	(Aria *et al*, 2013)
RPA32/TIPIN	0.5 ± 0.19 µM	(Ali *et al*, 2010)

The deletion of helix22 in CRY1 abolishes the interaction between TIM and CRY1 in Co-IP, and therefore this helix probably is the main binding site (Engelen *et al*, 2013). Helix22, as well as the rest of the PHR of CRY1 and CRY2 are very similar (Figure 64). The C-terminal CRY tail on the other hand is variable between CRY1 and CRY2. This suggested that the CRY tails might be involved in the binding to TTP and could affect binding affinities. And indeed, deletion of the CRY1 tail led to an increase in binding affinity for the CRY1-PHR compared to full length CRY1. The binding affinity for CRY1-PHR was intermediate between full length CRY1 and CRY2. This also shows that the CRY1 tail was not essential for binding to TTP, which is consistent with former studies (Engelen *et al*, 2013). We analyzed the binding of the CRY tails to various TIM and TTP constructs by SEC (5.7.3). No binding of the CRY1 tail alone to TTP was observed, consistent with a negative effect of the CRY1 tail on TTP binding. In contrast, the CRY1 tail showed light co-migration with N-terminal TIM fragments (Figure 55, Figure 57). But this might have been an effect restricted to the N-terminal constructs, that formed dimers and oligomers (Figure 49) and does not clearly indicate the role of the CRY1 tail with TTP. SECs of the CRY2 tail with TTP, TTP-ΔL and TIM (TIM997-1207, TIM-N-ΔL, Tim-N-Sumo) constructs showed co-migration. However, the SEC migration pattern of the individual CRY2 tail was unclear due to possible oligomerization and tailing that caused potential overlapping with other peaks (Figure 54). Hence, we cannot say whether the CRY2 tail bound to TTP and whether it behaves in a similar way to the CRY1 tail.

It can be plausible that the CRY tails could be responsible for different affinities of CRY towards TTP. Several functional CRY1 and CRY2 differences are related to their diverging tails, such as difference in nuclear import, transcriptional repression and period length. The CRY tails control the nuclear import rate of the CRYs, which directly affects the nuclear CRY1/CRY2 ratio. CRY2 is imported more quickly into the nucleus compared to CRY1 (Li *et al*, 2016). On the other hand, CRY1 is a more potent circadian transcriptional repressor than CRY2 (Khan *et al*, 2012). A $CRY1^{-/-}$ $CRY2^{-/-}$ double knockout cell line rescued with a chimera of the CRY1-PHR and the CRY2 tail, shows a shortened period, similar to a $CRY1^{-/-}$ knockout, suggesting a role for the CRY tail in period determination (Li *et al*, 2016; Van Der Horst *et al*,

1999). Furthermore, phosphorylation of the tails has an opposite effect on CRY stability and affects the period length. Phosphorylation of the CRY1 tail leads to stabilization, phosphorylation of the CRY2 tail leads to destabilization (Harada *et al*, 2005; Gao *et al*, 2013). The different binding affinity of CRY1 and CRY2 to the deubiquitinase HAUSP is related to the diverging CRY tails. A hybrid of the CRY1-PHR with the CRY2 tail shows a reduced affinity, similar to CRY2 (Papp *et al*, 2015). It is interesting to note that the human CRY1 tail has an opposite net charge compared to the CRY2 tail (pI = 9.2 vs. pI = 5.8) that could give an explanation about the diverging effects of the CRY tails.

In contrast, the tails are not the only component differentiating CRY1/CRY2 functions. A discriminatory effect between CRY1-PHR and CRY2-PHR for the CLOCK/BMAL1 PAS domains was described recently. The serine loop within the PHR at the secondary pocket was reported to be more dynamic in CRY1 compared to CRY2. This resulted in a higher affinity of CRY1 to the CLOCK/BMAL1 PAS domains compared to CRY2 (Fribourgh *et al*, 2019; Michael *et al*, 2017). However, in our XLMS data, we did not observe TIM crosslinks to the serine loop or closely located residues in the CRY PHRs, suggesting the serine loop may not be in contact with TIM. Based on our model (Figure 63), the serine loop is located on the opposing side (opposite of the FBP) of the hypothetical TIM/CRY interface, pointing away from TIM.

But to assess contributions of the PHR on the CRY binding to TTP, a K_D measurement of the CRY2-PHR with TTP would be necessary. Due to difficulties in the purification of CRY2-PHR, this has not been done yet. If both CRY PHRs bound to TTP with similar affinities, this would confirm the tails as modulator of binding affinity. NanoSPR experiments using chimeras of the CRY1-PHR and the CRY2 tail or *vice versa,* could further support this hypothesis. To analyze how the diverging CRY tails could modify CRYs binding affinities, the SEC binding studies with the CRY2 tail could be repeated with optimized CRY2 tail samples.

The tails could modify the binding affinities by having different interactions with TTP. The CRY1 tail could decrease the affinity by negatively interfering with TTP, whereas the CRY2 tail may not. Perhaps the tails may compete with TTP for binding to the CRY-PHR, as it was observed that the CRY tails can fold back bind to their own PHR (Parico *et al*, 2019). Different affinities of the tails for their own PHR could have an effect on TTP binding. The possibility of back folding of the tail to the CRY-PHR is supported by our XLMS data, that showed numerous crosslinks of the CRY tails to the CRY-PHR (Figure 39, Figure 44).

Furthermore, the *in vitro* differences in binding affinity between CRY1 and CRY2 should be investigated in the context of the cell, to determine their functional implications. Multiple questions remain. Do TIM/CRY1 and TIM/CRY2 complexes serve different functions? Is there functional redundancy? Are the interactions further regulated, e.g. by PTMs? Is the interaction of either CRY1 or CRY2 specific to a certain type of stress? It would be interesting to see how the observed affinity difference between CRY1 and CRY2 would relate to different functions in context of TTP.

6.3 A secondary interaction site for CRY on TIM?

We observed that TIM-N-ΔL bound to CRY1 and CRY2 (Figure 24, Figure 25). This is consistent with literature, describing the TIM N-Terminus and the C-terminal CRY helix to be essential for the interaction of CRY and TIM (Engelen *et al*, 2013). Interestingly, in XLMS experiments, we found many crosslinks to CRY outside of the TIM N-terminal region, especially in the C-Terminus of TIM (Figure 38, Figure 43). Additional association of CRY with the TIM C-Terminus can be plausible, as a TTP/RPA structure has a U-shape conformation (Witosch *et al*, 2014), in which the N-Terminus and the C-Terminus could be located closely. Testing the direct interactions of CRY1/CRY2 to TIM997-1207 by SEC, however, did not show an interaction (Figure 53). This was consistent with previous studies in which no interaction was found between full length mCRY1 and C-terminal mTIM1079-1198 in Co-IP experiments (Engelen *et al*, 2013).

A reason for not observing interaction in SEC analysis of CRY1/CRY2 with TIM997-1207 might have been the oligomerization of TIM997-1207 (Figure 49, Figure 53). Oligomerization of the TIM C-terminus was observed before on the shorter TIM construct TIM1000-1098 (Xie *et al*, 2015). However, the dimerization of TIM1000-1098 is broken upon binding to PARP1, which is underlined by their high binding affinity (Table 27). This indicates that a hypothetical interaction of CRY with TIM997-1207 would be weak, too weak to dissolve TIM997-1207 oligomers or too weak to maintain a stable interaction in absence of the main binding site in the N-Terminus of TIM. Another possibility is that the CRY tail could fold back to the CRY-PHR, which might interfere with binding. XLMS revealed many crosslinks of the CRY tails with their own PHR (Figure 39, Figure 44). Backfolding was also described recently in the pre-print literature (Parico *et al*, 2019). However, the CRY1-PHR and CRY2-PHR were not analyzed

with TIM997-1207 by SEC. The CRY tails, that were crosslinked to the TIM C-Terminus as well, did not indicate binding to TIM997-1207 in SEC (Figure 54). The observed crosslinks of the CRY tails to TIM997-1207 could have been a result of the structural closeness and structural flexibility.

In the literature an effect of the TIM C-Terminus on CRY2 was described before (Kurien *et al*, 2019). A C-terminally truncated TIM R1081X mutant has a weakened interaction with CRY2, which results in reduced CRY stability. This suggests that the TIM C-Terminus may be involved in the interaction with CRY. However, the mutant reduces the half-life of CRY1 as well. It is unclear, if this is a direct effect of altered binding, as the binding of CRY1 to TIM R1081X was not tested (Kurien *et al*, 2019). The observed FASP (familial advanced sleep phase) phenotype, however, might have been caused by the lack of the C-terminal NLS, leaving TIM1081X to be mainly cytoplasmic (Kurien *et al*, 2019).

The wide spread crosslinks of the TIM C-Terminus to CRY and the absence of direct binding might be explained by high flexibility of the TIM C-Terminus. The C-terminal flexibility is supported by two recent depositions in the *BioRxiv* pre-print server that show that two structures of TTP homologs (Tof1/Csm3) from *Chaetomium thermophilum* and *Saccharomyces. cerevisiae* could only be solved without the C-Terminus (Grabarczyk, 2020; Baretić *et al*, 2019).

To clarify the role of a potential interaction of CRY with the C-Terminus of TIM, K_D measurements with a C-terminally truncated construct of TIM could be done. A reduced CRY binding affinity to a truncated TIM construct would indicate a stabilizing effect of the TIM C-Terminus on the TTP/CRY interaction. Affinity differences between CRY1 and CRY2 towards truncated TTP could also reveal further information about the differences responsible for the K_D differences between TTP/CRY1 and TTP/CRY2. To fully exclude the possibility that the CRY tails might interfere with CRY binding to the TIM997-1207, an interaction could be tested by using the PHRs of CRY1 and CRY2 instead of full length proteins.

XLMS revealed crosslinks of the TIM loop to the CRY tails (Figure 40, Figure 45). The TIM loop however was not essential for the interaction of TTP with CRY as SEC and pulldown experiments showed (Figure 24, Figure 25). The individual CRY1 tail did not bind to TTP (Figure 59) and removal of the TIM loop in TTP-ΔL suggested a negative interference of the CRY1 tail and the TIM loop, as the binding affinity was increased in NanoSPR (Figure 27). The absence of the TIM loop and the CRY1 tail (TTP-ΔL with CRY1-PHR) at the same time

did not seem to have an additional effect, although the replicates were not perfectly reproducible. This was consistent with the binding affinities between CRY1-PHR and TTP-SL as shortening of the TIM loop did not seem have a clear effect in CRY1-PHR. Therefore, the CRY1 tail and the TIM loop could be involved in a negative interference.

The CRY2 tail on the other hand, might not negatively interfere with the full TIM loop, as CRY2 showed the highest affinity to TTP full length compared to TTP-ΔL and TTP-SL (Figure 27). Perhaps, a potential interaction of the CRY2 tail with the full TIM loop could even have a strengthening effect on the binding, as after shortening of the TIM loop, the affinity appeared reduced, although, the replicates showed variation. The effect of the TIM loop deletion (TTP-ΔL) on the binding of CRY2 was not clear, as replicate #1 showed a reduced affinity, but replicate #2 did not show a difference compared to TTP (Figure 27). Additional SEC experiments did not clarify whether affinity of CRY2 to TTP was affected by an interaction of the CRY2 tail with the TIM loop. In SEC, no migration differences between TIM-N-ΔL/TIM-N-Sumo (Figure 55 B, Figure 57 B) and TTP-ΔL/TTP (Figure 58 B, Figure 59 B) were observed. However, the interpretation of the CRY2 tail SEC results is difficult and needs to be treated with caution, because of the oligomerization, the tailing of CRY2 tail and the limitation of comparable fractions from an individual CRY2 tail SEC.

In order to clarify the effect of the TIM loop on CRY2 tail binding, the SEC experiments could be repeated with an improved CRY2 tail sample. By optimizing the purification of the CRY2 tail and the buffer conditions, e.g. by a Thermal shift assay (Reinhard *et al*, 2013), a non-oligomerizing sample might be obtained. To further assess whether the TIM loop affects CRY2 binding to TTP independently of the CRY2 tail, NanoSPR experiments could be conducted using the CRY2-PHR as well (6.2).

6.4 Binding of CRY and TIPIN?

After observing a trimeric complex of TTP with CRY, we investigated whether TIPIN and CRY could also form a complex independently of TIM. The interaction of CRY and TIPIN was tested in SEC (Figure 61), but did not have a clear results proving or disproving a CRY/TIPIN complex.

In the mixed TIPIN/CRY1, TIPIN/CRY2 samples there was an additional peak present between the individual CRY and TIPIN peak. This additional peak contained CRY and TIPIN, but also

an impurity, therefore it cannot be clearly concluded, that the additional peak stems from a CRY/TIPIN complex because of the possibility that CRY bound to the impurity. XLMS on the other hand, identified many crosslinks between TIPIN and CRY (Figure 40, Figure 47). TIPIN showed crosslinks to the CRY N-Terminus, the C-terminal helix and the tail.

However, crosslinks do not confirm direct protein binding, as proteins can be crosslinked if they have reactive residues in the right distance from each other. But the large number of links between the CRY and TIPIN indicates structural closeness. In two recent structures of TTP homologs (Tof1/Csm3), the TIPIN (Csm3) binds to a region within TIM (Tof1), which is adjacent to the C-terminal region (Grabarczyk, 2020; Baretić *et al*, 2019). This is consistent with the observation that CRY was heavily crosslinked to the TIM C-Terminus as well (Figure 40, Figure 45), indicating that TIPIN, CRY and the TIM C-Terminus could be closely located. As crosslinks over a wide range in the CRY sequence were identified, TIPIN and the TIM C-Terminus might by dynamic and flexible. This supported by the absence of structural information about the C-Terminus of TIM (Tof1) and only the resolution of short Tof1 binding segments of TIPIN (Csm3) in recent structures (Baretić *et al*, 2019; Grabarczyk, 2020).

So far, there are no reports that describe a TIM-independent complex of TIPIN and CRY. Due to the tight association of TIPIN and TIM and the strong stabilizing effect they have on each other, it seems unlikely. Depletion of either TIM or TIPIN leads to a strong reduction of the other partner (Chou & Elledge, 2006). TIPIN and TIM have distinct functions within the TTP complex. TIPIN is responsible for binding to RPA (Nakaya *et al*, 2010), whereas TIM binds to the MCM2-7 and DNA-P-ε (Cho *et al*, 2013; Aria *et al*, 2013).

In order to analyze a direct interaction between TIPIN and CRY, an approach with purified protein seems to be the best possibility. In order to do so, the sample quality of TIPIN needs to be improved. To improve the conditions for the TIPIN purification and stability, a Thermal-shift assay (TSA) can be performed to screen for better buffer conditions (Reinhard *et al*, 2013). Better buffer conditions might lead to a more stable TIPIN that can be purified more readily and that might not oligomerize. Alternatively, a protein pulldown can be performed.

6.5 Structural analysis of the TTP complex

In order to confirm existing XLMS data (Holzer *et al*, 2017) and to compare it to the trimeric TTP/CRY complexes, we analyzed the TTP complex by XLMS. The overall distribution of crosslinks was very similar to TTP/CRY. We found a large number of intramolecular crosslinks from the N-terminal TIM loop to the TIM C-Terminus. SEC analysis of interactions of the TIM N-terminal constructs (TIM-N-ΔL, TIM-N-Sumo) and the C-Terminus (TIM997-1207) did not confirm direct binding (Figure 50). XLMS identified links of central TIM residues (K427, K528) to its C-Terminus. A similar experiment analyzed the links of a TTP complex in which the TIM loop was deleted (Holzer *et al*, 2017). However, in that study long range crosslinks from K427 and K528 to the C-Terminus of TIM were observed as well, indicating closeness.

The C-Terminus of TIM was highly crosslinked to TIPIN (Figure 37). But those crosslinks did not correlate to direct binding of TIPIN to TIM997-1207 in SEC (Figure 52). The absence of a binding site for TIPIN in the TIM C-Terminus is consistent with the observation that TIM1-814 is able to bind TIPIN and even purified N-terminal TIM1-463 shows weak binding (Holzer *et al*, 2017). The heavy linkage between TIPIN and the C-Terminus of TIM (Figure 37) was also not confirmed in another XLMS experiment (Holzer *et al*, 2017). However, in that study, only exact crosslink matches of two replicates were reported, whereas we refer to crosslinks present within the same protein regions (Figure 37).

An earlier study reported that the N-terminal TIM constructs 1-267 and 267-573 bind TIPIN (Yoshizawa-Sugata & Masai, 2007). In the same study TIM1-603 binds to TIPIN, whereas TIM573-904, TIM903-1082 and TIM1082-1208 do not, suggesting that residues 1 to 573 of TIM likely harbor the TIPIN binding site. Consistent with this study, our XLMS data revealed several crosslinks to TIPIN within the N-terminal half of TIM (Figure 37), including the TIM loop, the secondary loop and the centrally located residues K427 and K528.

Unexpectedly, two recently published partial 3D structures of the Tof1/Csm3 complex from *S. cerevisiae* (Tof1(13-781)/Csm3(46-139)) and from *Chaetonium thermophilium* (Tof1(1-728)/Csm3(48-157)) revealed a tight interaction of Csm3 (roughly corresponding to TIPINs site1 in this study) and a portion corresponding to residues 745-804 in human TIM (Baretić *et al*, 2019; Grabarczyk, 2020). This contradicts the before mentioned study that did not report binding of the TIM573-904 construct to TIPIN (Yoshizawa-Sugata & Masai, 2007). A possible

explanation for the difference may be structural rearrangements in the TIM fragment that was used for Co-IP in that study.

The analyzed partial TIM constructs (TIM-N-ΔL, TIM-N-Sumo, TIM997-1207, TIM520-680) did not directly interact with each other in SEC (Figure 50, Figure 51). The presence of crosslinks indicates closeness of those TIM regions and they likely do not interact apart from being covalently bound as part of the same protein. The observation of tight crosslinking between the N-Terminus and the C-Terminus is indicative of structural proximity and is consistent with a reported CryoEM structure of a TIM/TIPIN/RPA complex, that reported a U-shaped conformation (Witosch *et al*, 2014).

The function of the TIM loop is unknown. Association of the TIM loop with the TIM C-Terminus could indicate a regulatory effect on the C-Terminus. Post-translational modifications (PTMs) could alter the association or dissociation of the TIM loop to the TIM C-Terminus as both sites can be modified by PTMs (Figure 71). Since there is a NLS located in the TIM C-Terminus (Engelen *et al*, 2013), the TIM loop might affect the nuclear translocation of TIM. Perhaps it might engage in C-terminal interactions, thereby affecting the accessibility of the NLS and regulating nuclear translocation. To analyze this, the cellular localization of the TTP-ΔL construct could be tested. Additionally, a pulldown using the TIM C-Terminus as prey could provide information about C-terminal interactors that could be influenced by the TIM loop.

6.6 The TIM loop

In SEC and pulldown experiments we found the TIM loop to be dispensable for the interaction with CRY (Figure 24, Figure 25, Figure 26), but it affected the binding affinities of CRY1 and CRY2 in NanoSPR (Figure 27). Deletion of the TIM loop (TTP-ΔL) caused the CRY constructs to bind with similar affinities (Figure 27). It appears that the differentiating effect was abolished. This was consistent in both replicates, although, the exact K_D values were variable. TIM loop deletion caused CRY1 to bind with the same affinity as CRY1-PHR, indicating that the TIM loop may have a negative interference with the CRY1 tail. This is consistent with XLMS data, that identified a crosslink between the CRY1 tail and the TIM loop (Figure 39, Figure 40) and the SAXS model of CRY1/TIM-N-SL indicating closeness of the CRY1 tail and the TIM loop (Figure 32). If the CRY1-PHR was affected by TIM loop deletion itself was not

clear, because the replicates were variable. This was the case for CRY2 as well. The second replicates (#2, for TTP-ΔL and TTP-SL) differed by roughly 50%, indicating a systematic effect, perhaps related to the batch of nanoparticles used for the measurements.

The shortened TIM loop (TTP-SL) caused CRY1 and CRY2 to bind with similar affinities. The affinity of CRY1 was enhanced compared to TTP (Figure 27). Interestingly, in contrast to the TTP-ΔL measurement, the affinities for CRY1 were lower than for CRY1-PHR. This suggests, that the shortened loop may still cause a negative interference with the CRY1 tail, but it could be reduced compared to a full TIM loop. The affinity for CRY2 seemed somewhat reduced, although, the two replicates were not consistent, suggesting a potential negative effect of the shortened TIM loop on CRY2. The hypothesis of the TIM loop affecting the CRY2 affinity is supported by XLMS analysis, that identified several links of the TIM loop and CRY2 (Figure 45). There were many links of the TIM loop to the CRY2 tail, the C-terminal helix and positive patch and the PHR, especially residues K184, K242 and K247.

The complexes of TIM-N-ΔL/CRY2 and TIM-N-SL/CRY2 were not analyzed by SAXS. But as the SAXS structural parameters of TTP/CRY1 and TTP/CRY2 were very similar (Table 26) and CRY1/CRY2 are similar as well (Figure 64), it is likely, that the complexes assemble in the same way. Therefore, it is likely, that the TIM loop and the CRY2 tail would be located in vicinity in a TIM-N-SL/CRY2 complex as well. But in contrast to CRY1 it cannot be said, whether the potential effect TIM loop deletion on CRY2 affinity was related to the CRY2 tail, as the CRY2-PHR was not tested in NanoSPR, due to purification difficulties.

To further clarify how a deletion or shortening of the TIM loop affects CRY2 binding, additional replicates of NanoSPR measurements with TTP-ΔL/TTP-SL could be done. To understand whether a potential effect on CRY2 binding is related to its tail, the CRY2-PHR construct should be analyzed as well.

In a bigger picture, it would be interesting to understand, how the TIM loop is involved in fulfilling the functions of TIM. For example, how does TIM loop deletion affect TIM in stress signaling and stabilization of the replication fork. Is the activation of cell cycle checkpoints affected? Is DNA damage repair induced in a similar manner? To understand the effect on CRY interactions, it would be interesting to analyze, whether TIM-ΔL can interact with CRY in a similar way and whether there is an effect on downstream processes like CHK1 phosphorylation in which CRY2 was reported to have an enhancing effect (Unsal-Kaçmaz *et al*, 2005). As DNA

damage leads to a circadian phase shift in cells (Oklejewicz *et al*, 2008), it could be tested, whether the phase shift is affected by a TIM-ΔL mutant.

6.7 SAXS modeling of the TIM-N-ΔL/SL dimers and their complexes with CRY1

In order to understand how CRY associates with the TIM N-Terminus, we collected SAXS data to extract structural parameters and to create *ab initio* models of TIM-N-ΔL/SL and their complexes with CRY1. The SAXS models of TIM-N-ΔL and TIM-N-SL were dimeric and the dimers associated in a symmetric way (Figure 30). Dimerization was consistent with data from SEC, MALS and the Bayesian MW (Figure 49, Table 26) and was reported in the literature before (Holzer *et al*, 2017). The SAXS model of TIM-N-ΔL could be overlaid very well with an *in silico* dimer of TIM-N-ΔL (Figure 30 C, D) and the scattering profiles fitted as well. In the dimer, the TIM-N-ΔL monomers were positioned towards each other in an angled position and the dimer contact was established by a bundle of four helices.

The TIM-N-SL SAXS model had a similar shape, which is consistent with similar structural parameters, indicating a only slight increase in size due to 70 additional residues of the partial TIM loop (Table 26). It was clearly dimeric as well. There were two additional bulks in the envelope, which likely contain the loops (Figure 29 A, D). The TIM-N-ΔL *in silico* dimer did not fit to the SAXS envelope, as in the SAXS model of the dimer, the TIM-N-SL monomers did appear oriented towards each other in an angled position (Figure 30 D). In the TIM-N-SL dimer, the TIM loops would be positioned close to each other at the dimer interface (Figure 30 B). This positioning might lead to interference of the loops positioning the TIM-N-SL monomers in a different, more straight position.

The models of TIM-N-ΔL/TIM-N-SL with CRY1 showed association of TIM-N-ΔL/TIM-N-SL dimers with a monomer of CRY1. A 2:1 association is consistent with MW obtained by MALS and Bayesian interference (Figure 25, Table 26). Asymmetry of the CRY1 SAXS model allowed to allocate the CRY1-PHR and the CRY1 tail within the model (Figure 28). By comparing the individual CRY1 model to the TIM-N-ΔL/TIM-N-SL models it can be stated that the bottom part of the CRY1-PHR, which is the position of the C-terminal helix, associated

with the TIM-N-Δ/SL dimers. This is consistent with literature that identified the C-terminal helix as essential for interaction of CRY1 and TIM (Engelen *et al*, 2013).

In the TIM-N-ΔL/SL/CRY1 models, the CRY1 tail appeared attached to TIM (Figure 32). By SEC, a light co-migration of the CRY1 tail with TIM-N-ΔL was seen (Figure 55 A, peak2), which would be consistent with the model. However, this co-migration was not confirmed in SEC with TTP-ΔL (Figure 56, Figure 58) indicating this was an effect related to the partial TIM-N-ΔL construct. In the TIM-N-SL model, the CRY1 tail was attached to TIM-N-SL as well, but it did not bind in SEC (Figure 56). The localization of the CRY1 tail to TIM-N-SL was likely caused by the modelling software, which is based on the DAMMIN algorithm, that favors compact models (Franke & Svergun, 2009).

In the TIM-N-SL/CRY1 model (Figure 32 B, F, Figure 30 D), the TIM loop and the CRY1 tail would be positioned close to each other, which is consistent with the potential negative interference of the TIM loop and the CRY1 tail that were concluded from K_D values (Figure 27).

A limitation to the SAXS models is, that they are based on complexes of CRY1 with partial TIM constructs. It is possible that the orientation of CRY towards the N-Terminus of TIM is changed in a full length TTP complex. The U-shape of TTP/RPA (Witosch *et al*, 2014), with the TIM C-Terminus that is close to CRY could lead to a reorientation of CRY within TTP/CRY complex. Another limitation of these results is the low resolution that *ab initio* modeling by SAXS can provide. Typically, the maximum resolution is about 10-20 Å (Mertens & Svergun, 2010). Detailed information of the CRY1/TIM-N and the TIM-N dimer interface could not be obtained. For SAXS modeling, the sample quality is of primary importance as the scattering data is the average scattering of all the molecules in solution. Sample heterogeneity has a strong effect on the final model. In some cases, our collected scattering data had to be cut, which shortened the Guinier region and the data used for analysis. This was due to non-ideal buffer background subtraction and/or slight sample aggregation. Cutting the data can reduce the accuracy of the obtained structural parameters and models. Therefore, the samples could be further optimized for SAXS by screening different buffer conditions and optimizing purification conditions. However, it is unlikely that a lot more details can be extracted from new optimized SAXS models as the maximum resolution is limited. In order to obtain detailed structural data, high-resolution methods such as CryoEM or X-ray crystallography could give further information about the complex.

6.8 Hypothetical structure of TIM1-463/CRY complex

In order to build a model of the TTP-CRY complex, we combined information from literature with data collected in this study. The essential binding site for TIM within CRY is reported to be the C-terminal helix22 of CRY (Engelen *et al*, 2013). The site of interaction is located within the first 309 N-terminal residues of TIM (Engelen *et al*, 2013). We could confirm that the N-terminal TIM construct (1-463) bound to CRY and that the TIM loop (residues 239-330) was not essential for binding of CRY (Figure 24, Figure 25). This means that the binding site might be located within residues 1-238 of TIM. XLMS analysis of the TTP/CRY2 complex showed an accumulation of crosslinked residues around the FAD binding pocket of CRY (Figure 48), the opposite side did not show substantial crosslinking. This indicates that the FAD binding pocket may be directed towards TIM. The TIM loop was linked to residues surrounding the FAD binding pocket, and the C-terminal helix as well as the positive patch (Figure 45), which indicates that those parts of TIM may be accessible to the TIM loop. Based on this we created a model of the CRY/TIM1-463 complex (Figure 63). In the model, we placed CRY with its C-terminal helix within the N-terminal TIM region, reported to be sufficient for CRY binding (blue). TIM1-463 was oriented in a way in which the TIM loop could be close to the FAD binding pocket of CRY, but could access the C-terminal CRY helix as well as the positively charged patch.

XLMS identified many links of the TIM C-Terminus to CRY as well as to the TIM loop (Figure 37, Figure 45). This indicates that the TIM C-Terminus may be positioned close by. This is consistent with the U-shape of a TIM/TIPIN/RPA complex in CryoEM (Witosch *et al*, 2014).

The SAXS models of TIM-N-ΔL/SL and CRY are in agreement with the model, as both indicated an association of the CRY C-Terminus with TIM-N-ΔL/SL and that the TIM loop may be located in vicinity (Figure 30). However, due to limited resolution of ab initio SAXS models, a precise determination of binding sites or relative orientations of the molecules could not be done. In order to obtain more precise information about the exact binding site, shortened constructs of the TIM N-Terminus could be tested for interaction with CRY. But most information would be obtained from a high resolution crystal or CryoEM structure of the complex. Mutagenesis of the amino acids involved in the interaction could confirm their contribution in binding.

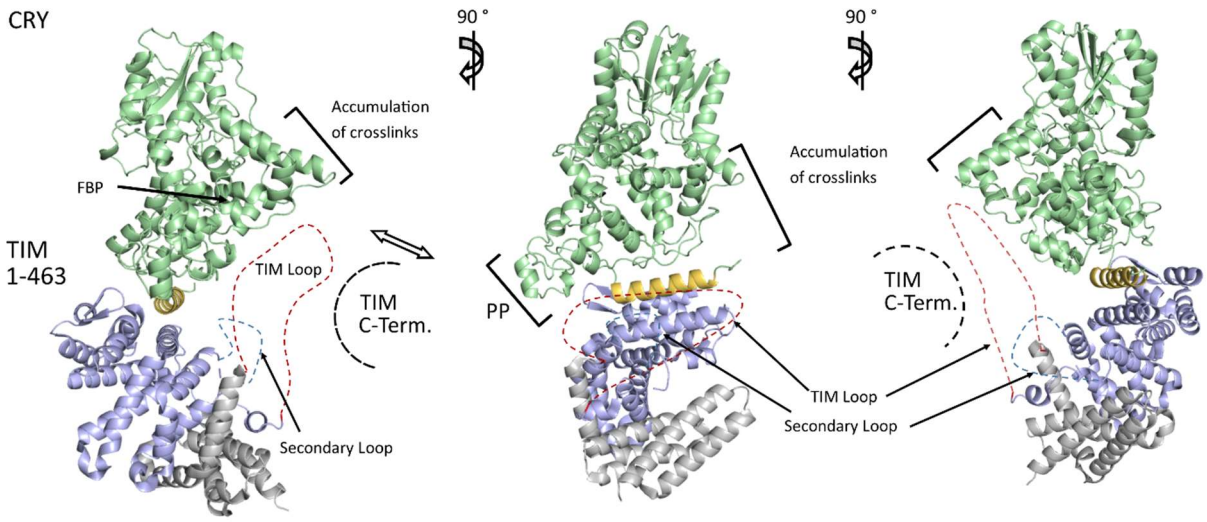

Figure 63: Hypothetical model of the TIM1-463/CRY2 complex. Different perspectives of the putative TIM1-463/CRY2 model are shown. CRY is depicted in light green, the C-terminal helix is colored yellow, TIM1-463 is depicted in light blue/gray. TIM1-309, that is sufficient to bind CRY is colored in light-blue, TIM 310-563 is colored in gray. The flexible TIM loops are indicated as dashed lines (red – TIM loop, blue – second loop). The localization of the TIM C-Terminus is indicated by a dashed line. For modeling Swissprot model of hCRY2 (Waterhouse *et al*, 2018) was used and the crystal structure of TIM1-463 (Holzer *et al*, 2017), PDB ID:5MQI. PP – Positively charged patch in CRY, FBP – FAD binding pocket.

6.9 Protein pulldown with TTP/TTP-ΔL

Since the TIM loop has not been functionally described yet, we were interested in finding interactors which could give information about functions of the TIM loop. We performed a pulldown screen using purified TTP and TTP-ΔL as bait and human cell extracts as prey. CEP131 (AZI1) was specifically enriched with TTP-ΔL and YLPM1 (ZAP3) was enriched with TTP (Figure 62).

CEP131 is found in centriolar satellites (CS), which are important for protein trafficking to the centrosome, and are involved in regulation of centrosome maintenance, ciliogenesis and neurogenesis (Tollenaere *et al*, 2015). Together with other partner proteins, CEP131 organizes the recruitment of CDK2 to the centromers in S-phase (Kodani *et al*, 2015). CDK2 triggers centriole duplication which is essential for the formation of the mitotic spindles, but also has other distinctive roles in cell cycle progression. During mitosis, CS are dissolved and some of their proteins are located to the centromers until the CS are re-assembled after mitosis (Blagden & Glover, 2003). Depletion of CEP131 leads to multipolar mitotic spindles, which causes mis-

segregation of chromosomes during mitosis. After mitosis, these cells show increased levels of DNA damage markers such as phosphorylated H2AX (γ-H2AX), phosphorylated ATM and phosphorylated CHK2, representing post-mitotic DNA damage (Staples *et al*, 2012). Interestingly, CS are sensitive to cellular stresses, such as UV radiation. This leads to dismissal of CEP131 from CS (Villumsen *et al*, 2013).

An interaction of TTP with CEP131 allows speculation about a functional connection of both proteins. TTP as checkpoint signaling protein could influence CEP131 functions in centriole replication and assembly of the mitotic spindle. TTP is involved in organizing sister chromatid cohesion, by interacting with Smc1, Smc3, SA1 as members of the cohesin complex (Leman *et al*, 2010). Both proteins could work together in orchestrating responses to replication stress.

YMPL1 was enriched with TTP (Figure 62). It is a nuclear protein, that plays a role in downregulation of telomerase activity during *in vitro* differentiation. This is achieved by downregulation of the telomerase mTert subunit, by binding of several regulatory proteins, including YLPM1, to the promotor region of the *mTert* gene (Armstrong *et al*, 2004). TIM was reported to be involved in regulation of telomere length as well, by interaction with TRF1 and TRF2 (Leman *et al*, 2012). In addition to that, TIM is essential for embryonic development (Gotter *et al*, 2000). This could indicate a functional connection between TIM and YLPM1.

Confirmation of both pulldowns is necessary, for example by Co-IP. To analyze, whether the interactions are direct, the proteins could be purified and tested by pulldown or SEC.

6.10 Purification and characterization of individual proteins

Recombinant expression and purification of human CRY1 and CRY2 was successfully established using similar methods as described for the mouse homologs (Schmalen *et al*, 2014; Czarna *et al*, 2013). CRY1 and CRY2 were monomeric as determined by MW_{SEC}, MW_{PREP}, MW_{MALS}, and Bayesian MW (Table 26, Figure 49). The MW_{SEC} of CRY1 was 31 kDa, approximately half its MW_{THEO} (Figure 49). This might be explained by an interaction with the column material in analytical SEC, which caused a longer protein retention and a different MW_{SEC} estimation.

Human TTP and the variations TTP-ΔL and TTP-SL were purified under similar conditions as mouse TTP (Witosch *et al*, 2014). TTP showed a MW_{MALS} of almost twice its MW_{THEO} indicating a TTP dimer (tetramer of 2xTIM, 2xTIPIN) (Figure 13). This is in contrast with previous reports of human and mouse TTP indicating TTP monomers (Holzer *et al*, 2017; Witosch *et al*, 2014). The buffer used for the MALS measurement by Holzer et al. contained additional 50 mM Arginine and 50 mM Glutamate, which are commonly used for protein stabilization (Baynes *et al*, 2005; Blobel *et al*, 2011). Arginine and Glutamate were reported to collapse flexible loops to the protein core, thereby preventing protein oligomerization and aggregation (Blobel *et al*, 2011). The absence of Arginine and Glutamate in our buffer could have caused association of two TTP monomers. This also indicates that the MWs of TTP-ΔL and TTP-SL were closer to their monomeric form (Figure 13) because the TIM loop was deleted or shortened.

Human and mouse TIPIN formed large oligomers in the SEC (Figure 16, Figure 49), indicating protein instability. Difficulties in obtaining TIPIN are known, as it is challenging to express and purify or could be purified only in large oligomers (Holzer *et al*, 2017; Witosch, 2014).

TIM-N-ΔL and TIM997-1207 were readily purified and formation of oligomers was observed for both proteins before (Holzer *et al*, 2017; Xie *et al*, 2015). However, we could observe even larger oligomers of TIM997-1207, such as tetramers. This could be due to the TIM997-1207 construct, that was about 100 residues larger than TIM1000-1098, which was analyzed in the literature.

To further improve protein stability, a thermal shift assay could be done, to screen for better buffer conditions (Reinhard *et al*, 2013). This could improve the behavior of proteins in terms of aggregation and oligomerization. Especially oligomerization of TIM997-1207, TIPIN and the CRY2 tail could be improved by that.

6.11 Conclusion

In this study we showed the direct binding of the TTP complex to CRY1 and CRY2. This supports the hypothesis of a direct coupling of both processes by key proteins. In addition, there still might be a serial coupling, which is achieved by factors that regulate the threshold for

occurrence of certain properties, for example the cell growth (c-Myc) and the cell cycle (Wee1) (Unsal-Kaçmaz *et al*, 2005).

CRY1 and CRY2 showed different affinities for the TTP complex, which may be caused by the interference or interaction of the CRY tails with the newly described flexible TIM loop. This interplay adds another layer of functional control to the coupling of the cell cycle and the circadian clock, especially since the CRY tails as well as the TIM loop appear to be hotspots for regulatory post-translational modifications. The differences in binding to TTP may help to understand the individual roles of CRY1 and CRY2. Using SAXS and XLMS data, we created initial models for a CRY/TIM complex, that could help to understand the association of CRY with TIM.

A protein pulldown identified potential interactors of TTP that might be influenced by the TIM loop. This could serve as a starting point to explore the functional roles of the TIM loop in regulation of TTP functions.

7 References

Ahijado-Guzmán R, Menten J, Prasad J, Lambertz C, Rivas G & Sönnichsen C (2017) Plasmonic Nanosensors for the Determination of Drug Effectiveness on Membrane Receptors. *ACS Appl. Mater. Interfaces* **9:** 218–223

Ahijado-Guzmán R, Prasad J, Rosman C, Henkel A, Tome L, Schneider D, Rivas G & Sönnichsen C (2014) Plasmonic Nanosensors for Simultaneous Quantification of Multiple Protein–Protein Binding Affinities. *Nano Lett.* **14:** 5528–5532

Akamatsu Y & Kobayashi T (2015) The Human RNA Polymerase I Transcription Terminator Complex Acts as a Replication Fork Barrier That Coordinates the Progress of Replication with rRNA Transcription Activity. *Mol. Cell. Biol.* **35:** 1871–1881

Akashi M, Tsuchiya Y, Yoshino T & Nishida E (2002) Control of Intracellular Dynamics of Mammalian Period Proteins by Casein Kinase I (CKI) and CKI in Cultured Cells. *Mol. Cell. Biol.* **22:** 1693–1703

Ali SI, Shin J-SS, Bae S-HH, Kim B & Choi B-SS (2010) Replication protein A 32 interacts through a similar binding interface with TIPIN, XPA, and UNG2. *Int. J. Biochem. Cell Biol.* **42:** 1210–1215

Andersen JS, Wilkinson CJ, Mayor T, Mortensen P, Nigg EA & Mann M (2003) Proteomic characterization of the human centrosome by protein correlation profiling. *Nature* **426:** 570–574

Aria V, De Felice M, Di Perna R, Uno S, Masai H, Syväoja JE, van Loon B, Hübscher U & Pisani FM (2013) The Human Tim-Tipin Complex Interacts Directly with DNA Polymerase ϵ and Stimulates Its Synthetic Activity. *J. Biol. Chem.* **288:** 12742–12752

Armstrong L, Lako M, van Herpe I, Evans J, Saretzki G & Hole N (2004) A role for nucleoprotein Zap3 in the reduction of telomerase activity during embryonic stem cell differentiation. *Mech. Dev.* **121:** 1509–1522

Aryal RP, Kwak PB, Tamayo AG, Gebert M, Chiu P-L, Walz T & Weitz CJ (2017) Macromolecular Assemblies of the Mammalian Circadian Clock. *Mol. Cell* **67:** 770-782.e6

Auclair Y, Rouget R & Drobetsky EA (2009) ATR kinase as master regulator of nucleotide excision repair during S phase of the cell cycle. *Cell Cycle* **8:** 1865–1871

Bakkenist CJ & Kastan MB (2003) DNA damage activates ATM through intermolecular autophosphorylation and dimer dissociation. *Nature* **421:** 499–506

Balsalobre A, Damiola F & Schibler U (1998) A Serum Shock Induces Circadian Gene Expression in Mammalian Tissue Culture Cells. *Cell* **93:** 929–937

Baretić D, Jenkyn-Bedford M, Aria V, Cannone G, Skehel M, Yeeles JTP, Baretic D, Jenkyn-Bedford M, Aria V & Cannone G (2019) Cryo-EM Structure of the Fork Protection Complex Bound to CMG at a Replication Fork. *bioRxiv***:** 2019.12.18.880690

Barnes JW (2003) Requirement of Mammalian Timeless for Circadian Rhythmicity. *Science (80-.).* **302:** 439–442

Bass J (2012) Circadian topology of metabolism. *Nature* **491:** 348–356

Baynes BM, Wang DIC & Trout BL (2005) Role of Arginine in the Stabilization of Proteins against Aggregation. *Biochemistry* **44:** 4919–4925

Bee L, Marini S, Pontarin G, Ferraro P, Costa R, Albrecht U & Celotti L (2015) Nucleotide excision repair efficiency in quiescent human fibroblasts is modulated by circadian clock. *Nucleic Acids Res.* **43:** 2126–2137

Benna C, Bonaccorsi S, Wülbeck C, Helfrich-Förster C, Gatti M, Kyriacou CP, Costa R & Sandrelli F (2010) Drosophila timeless2 Is Required for Chromosome Stability and Circadian Photoreception. *Curr. Biol.* **20:** 346–352

Bermejo R, Doksani Y, Capra T, Katou Y-M, Tanaka H, Shirahige K & Foiani M (2007) Top1- and Top2-mediated topological transitions at replication forks ensure fork progression and stability and prevent DNA damage checkpoint activation. *Genes & Dev.* **21:** 1921–1936

Bermejo R, Lai MS & Foiani M (2012) Preventing Replication Stress to Maintain Genome Stability: Resolving Conflicts between Replication and Transcription. *Mol. Cell* **45:** 710–718

Bianco JN, Bergoglio V, Lin Y-L, Pillaire M-J, Schmitz A-L, Gilhodes J, Lusque A, Mazières J, Lacroix-Triki M, Roumeliotis TI, Choudhary J, Moreaux J, Hoffmann J-S, Tourrière H & Pasero P (2019) Overexpression of Claspin and Timeless protects cancer cells from replication stress in a checkpoint-independent manner. *Nat. Commun.* **10:** 910

Blagden SP & Glover DM (2003) Polar expeditions — provisioning the centrosome for mitosis. *Nat. Cell Biol.* **5:** 505–511

Blobel J, Brath U, Bernadó P, Diehl C, Ballester L, Sornosa A, Akke M & Pons M (2011) Protein loop compaction and the origin of the effect of arginine and glutamic acid mixtures on solubility, stability and transient oligomerization of proteins. *Eur. Biophys. J.* **40:** 1327–1338

Brown SA (2005) PERIOD1-Associated Proteins Modulate the Negative Limb of the Mammalian Circadian Oscillator. *Science (80-.).* **308:** 693–696

Brown SA, Zumbrunn G, Fleury-Olela F, Preitner N & Schibler U (2002) Rhythms of Mammalian Body Temperature Can Sustain Peripheral Circadian Clocks. *Curr. Biol.* **12:** 1574–1583

Budini M, Jacob G, Jedlicki A, Pérez C, Allende CC & Allende JE (2009) Autophosphorylation of carboxy-terminal residues inhibits the activity of protein kinase CK1α. *J. Cell. Biochem.* **106:** 399–408

Buhr ED, Yoo S-H & Takahashi JS (2010) Temperature as a Universal Resetting Cue for Mammalian Circadian Oscillators. *Science (80-.).* **330:** 379–385

Bunger MK, Wilsbacher LD, Moran SM, Clendenin C, Radcliffe LA, Hogenesch JB, Simon MC, Takahashi JS & Bradfield CA (2000) Mop3 Is an Essential Component of the Master Circadian Pacemaker in Mammals. *Cell* **103:** 1009–1017

Burns JL, Guzder SN, Sung P, Prakash S & Prakash L (1996) An Affinity of Human Replication Protein A for Ultraviolet-damaged DNA. *J. Biol. Chem.* **271:** 11607–11610

Camacho F, Cilio M, Guo Y, Virshup DM, Patel K, Khorkova O, Styren S, Morse B, Yao Z &

Keesler GA (2001) Human casein kinase Iδ phosphorylation of human circadian clock proteins period 1 and 2. *FEBS Lett.* **489:** 159–165

Castello A, Fischer B, Eichelbaum K, Horos R, Beckmann BM, Strein C, Davey NE, Humphreys DT, Preiss T, Steinmetz LM, Krijgsveld J & Hentze MW (2012) Insights into RNA Biology from an Atlas of Mammalian mRNA-Binding Proteins. *Cell* **149:** 1393–1406

Chapman RD, Heidemann M, Albert TK, Mailhammer R, Flatley A, Meisterernst M, Kremmer E & Eick D (2007) Transcribing RNA Polymerase II Is Phosphorylated at CTD Residue Serine-7. *Science (80-.).* **318:** 1780–1782

Chaves I, Yagita K, Barnhoorn S, Okamura H, van der Horst GTJ & Tamanini F (2006) Functional Evolution of the Photolyase/Cryptochrome Protein Family: Importance of the C Terminus of Mammalian CRY1 for Circadian Core Oscillator Performance. *Mol. Cell. Biol.* **26:** 1743–1753

Chen R, Schirmer A, Lee Y, Lee H, Kumar V, Yoo S-H, Takahashi JS & Lee C (2009) Rhythmic PER Abundance Defines a Critical Nodal Point for Negative Feedback within the Circadian Clock Mechanism. *Mol. Cell* **36:** 417–430

Chen R & Wold MS (2014) Replication protein A: Single-stranded DNA's first responder. *BioEssays* **36:** 1156–1161

Cho W-H, Kang Y-H, An Y-Y, Tappin I, Hurwitz J & Lee J-K (2013) Human Tim-Tipin complex affects the biochemical properties of the replicative DNA helicase and DNA polymerases. *Proc. Natl. Acad. Sci.* **110:** 2523–2527

Chou DM & Elledge SJ (2006) Tipin and Timeless form a mutually protective complex required for genotoxic stress resistance and checkpoint function. *Proc. Natl. Acad. Sci.* **103:** 18143–18147

Cimprich KA & Cortez D (2008) ATR: an essential regulator of genome integrity. *Nat. Rev. Mol. Cell Biol.* **9:** 616–627

Cortese MS, Uversky VN & Keith Dunker A (2008) Intrinsic disorder in scaffold proteins: Getting more from less. *Prog. Biophys. Mol. Biol.* **98:** 85–106

Curtis AM, Seo S, Westgate EJ, Rudic RD, Smyth EM, Chakravarti D, FitzGerald GA & McNamara P (2004) Histone Acetyltransferase-dependent Chromatin Remodeling and the Vascular Clock. *J. Biol. Chem.* **279:** 7091–7097

Czarna A, Berndt A, Singh HR, Grudziecki A, Ladurner AG, Timinszky G, Kramer A & Wolf E (2013) XStructures of drosophila cryptochrome and mouse cryptochrome1 provide insight into circadian function. *Cell* **153:** 1394–1405

Czarna A, Breitkreuz H, Mahrenholz CC, Arens J, Strauss HM & Wolf E (2011) Quantitative analyses of cryptochrome-mBMAL1 interactions: Mechanistic insights into the transcriptional regulation of the mammalian circadian clock. *J. Biol. Chem.* **286:** 22414–22425

Czeisler CA, Shanahan TL, Klerman EB, Martens H, Brotman DJ, Emens JS, Klein T & Rizzo JF (1995) Suppression of Melatonin Secretion in Some Blind Patients by Exposure to Bright Light. *N. Engl. J. Med.* **332:** 6–11

Damiola F (2000) Restricted feeding uncouples circadian oscillators in peripheral tissues from the central pacemaker in the suprachiasmatic nucleus. *Genes Dev.* **14:** 2950–2961

Davidson AJ, Sellix MT, Daniel J, Yamazaki S, Menaker M & Block GD (2006) Chronic jet-lag increases mortality in aged mice. *Curr. Biol.* **16:** R914–R916

Dheekollu J, Wiedmer A, Hayden J, Speicher D, Gotter AL, Yen T & Lieberman PM (2011) Timeless Links Replication Termination to Mitotic Kinase Activation. *PLoS One* **6:** e19596

Dibner C, Schibler U & Albrecht U (2010) The Mammalian Circadian Timing System: Organization and Coordination of Central and Peripheral Clocks. *Annu. Rev. Physiol.* **72:** 517–549

Doi M, Hirayama J & Sassone-Corsi P (2006) Circadian Regulator CLOCK Is a Histone Acetyltransferase. *Cell* **125:** 497–508

Eide EJ, Woolf MF, Kang H, Woolf P, Hurst W, Camacho F, Vielhaber EL, Giovanni A & Virshup DM (2005) Control of Mammalian Circadian Rhythm by CKI -Regulated Proteasome-Mediated PER2 Degradation. *Mol. Cell. Biol.* **25:** 2795–2807

Engelen E, Janssens RC, Yagita K, Smits VAJ, van der Horst GTJ & Tamanini F (2013) Mammalian TIMELESS Is Involved in Period Determination and DNA Damage-Dependent Phase Advancing of the Circadian Clock. *PLoS One* **8:**

Etchegaray J-P, Yang X, DeBruyne JP, Peters AHFM, Weaver DR, Jenuwein T & Reppert SM (2006) The Polycomb Group Protein EZH2 Is Required for Mammalian Circadian Clock Function. *J. Biol. Chem.* **281:** 21209–21215

Fan J & Pavletich NP (2012) Structure and conformational change of a replication protein A heterotrimer bound to ssDNA. *Genes Dev.* **26:** 2337–2347

Feng W, Collingwood D, Boeck ME, Fox LA, Alvino GM, Fangman WL, Raghuraman MK & Brewer BJ (2006) Genomic mapping of single-stranded DNA in hydroxyurea-challenged yeasts identifies origins of replication. *Nat. Cell Biol.* **8:** 148–155

Field MD, Maywood ES, O'Brien JA, Weaver DR, Reppert SM & Hastings MH (2000) Analysis of Clock Proteins in Mouse SCN Demonstrates Phylogenetic Divergence of the Circadian Clockwork and Resetting Mechanisms. *Neuron* **25:** 437–447

Filipski E & Lévi F (2009) Circadian Disruption in Experimental Cancer Processes. *Integr. Cancer Ther.* **8:** 298–302

Fischer L & Rappsilber J (2017) Quirks of Error Estimation in Cross-Linking/Mass Spectrometry. *Anal. Chem.* **89:** 3829–3833

Fischer L & Rappsilber J (2018) False discovery rate estimation and heterobifunctional cross-linkers. *PLoS One* **13:** e0196672

Foley LE, Gegear RJ & Reppert SM (2011) Human cryptochrome exhibits light-dependent magnetosensitivity. *Nat. Commun.* **2:** 356

Franke D, Petoukhov M V., Konarev P V., Panjkovich A, Tuukkanen A, Mertens HDT, Kikhney AG, Hajizadeh NR, Franklin JM, Jeffries CM & Svergun DI (2017) ATSAS 2.8 : a comprehensive data analysis suite for small-angle scattering from macromolecular solutions. *J. Appl. Crystallogr.* **50:** 1212–1225

Franke D & Svergun DI (2009) DAMMIF , a program for rapid ab-initio shape determination in small-angle scattering. *J. Appl. Crystallogr.* **42:** 342–346

Fribourgh JL, Srivastava A, Sandate CR, Michael AK, Hsu PL, Nguyen LT, Torgrimson MR,

Parico GCG, Tripathi S, Zheng N, Lander GC, Partch CL, Rakers C, Nguyen LT, Torgrimson MR, Parico GCG, Tripathi S, Zheng N, Lander GC, Hirota T, et al (2019) Protein dynamics regulate distinct biochemical properties of cryptochromes in mammalian circadian rhythms. *bioRxiv***:** 740464

Fu L, Pelicano H, Liu J, Huang P & Lee CC (2002) The Circadian Gene Period2 Plays an Important Role in Tumor Suppression and DNA Damage Response In Vivo lates Bmal1 transcription through PAS-mediated reac-tions with other transcription factors. In the best-known negative feedback loop, cytoplasmic CRY1 . *Cell* **111:** 41–50

Gallego M, Kang H & Virshup DM (2006) Protein phosphatase 1 regulates the stability of the circadian protein PER2. *Biochem. J.* **399:** 169–175

Gao P, Yoo S-HH, Lee K-JJ, Rosensweig C, Takahashi JS, Chen BP & Green CB (2013) Phosphorylation of the Cryptochrome 1 C-terminal Tail Regulates Circadian Period Length. *J. Biol. Chem.* **288:** 35277–35286

Gasteiger E (2003) ExPASy: the proteomics server for in-depth protein knowledge and analysis. *Nucleic Acids Res.* **31:** 3784–3788

Gekakis N (1998) Role of the CLOCK Protein in the Mammalian Circadian Mechanism. *Science (80-.).* **280:** 1564–1569

Gery S, Komatsu N, Baldjyan L, Yu A, Koo D & Koeffler HP (2006) The Circadian Gene Per1 Plays an Important Role in Cell Growth and DNA Damage Control in Human Cancer Cells. *Mol. Cell* **22:** 375–382

Golombek DA & Rosenstein RE (2010) Physiology of circadian entrainment. *Physiol. Rev.* **90:** 1063–1102

Gotoh T, Vila-Caballer M, Liu J, Schiffhauer S & Finkielstein C V. (2015) Association of the circadian factor Period 2 to p53 influences p53's function in DNA-damage signaling. *Mol. Biol. Cell* **26:** 359–372

Gotter AL (2003) Tipin, a Novel Timeless-Interacting Protein, is Developmentally Co-expressed with Timeless and Disrupts its Self-association. *J. Mol. Biol.* **331:** 167–176

Gotter AL, Manganaro T, Weaver DR, Kolakowski LF, Possidente B, Sriram S, MacLaughlin DT & Reppert SM (2000) A time-less function for mouse Timeless. *Nat. Neurosci.* **3:** 755–756

Gotter AL, Suppa C & Emanuel BS (2007) Mammalian TIMELESS and Tipin are Evolutionarily Conserved Replication Fork-associated Factors. *J. Mol. Biol.* **366:** 36–52

Grabarczyk DB (2020) Crystal structure of the Tof1-Csm3 (Timeless-Tipin) fork protection complex. *bioRxiv* **3:** 2020.01.24.918474

Graewert MA, Franke D, Jeffries CM, Blanchet CE, Ruskule D, Kuhle K, Flieger A, Schäfer B, Tartsch B, Meijers R & Svergun DI (2015) Automated Pipeline for Purification, Biophysical and X-Ray Analysis of Biomacromolecular Solutions. *Sci. Rep.* **5:** 10734

Graham MJ, Combe C, Kolbowski L & Rappsilber J (2019) xiView: A common platform for the downstream analysis of Crosslinking Mass Spectrometry data. *bioRxiv***:** 1–5

Grant T, Rohou A & Grigorieff N (2018) cisTEM, user-friendly software for single-particle image processing. *Elife* **7:** e35383

Guillaumond F, Dardente H, Giguère V & Cermakian N (2005) Differential Control of Bmal1

Circadian Transcription by REV-ERB and ROR Nuclear Receptors. *J. Biol. Rhythms* **20:** 391–403

Güler AD, Ecker JL, Lall GS, Haq S, Altimus CM, Liao H-W, Barnard AR, Cahill H, Badea TC, Zhao H, Hankins MW, Berson DM, Lucas RJ, Yau K-W & Hattar S (2008) Melanopsin cells are the principal conduits for rod–cone input to non-image-forming vision. *Nature* **453:** 102–105

Gustafson CL & Partch CL (2015) Emerging models for the molecular basis of mammalian circadian timing. *Biochemistry* **54:** 134–149

Hajizadeh NR, Franke D, Jeffries CM & Svergun DI (2018) Consensus Bayesian assessment of protein molecular mass from solution X-ray scattering data. *Sci. Rep.* **8:** 7204

Harada Y, Sakai M, Kurabayashi N, Hirota T & Fukada Y (2005) Ser-557-phosphorylated mCRY2 Is Degraded upon Synergistic Phosphorylation by Glycogen Synthase Kinase-3β. *J. Biol. Chem.* **280:** 31714–31721

He Z, Henricksen LA, Wold MS & Ingles CJ (1995) RPA involvement in the damage-recognition and incision steps of nucleotide excision repair. *Nature* **374:** 566–569

Hirano A, Braas D, Fu Y-H & Ptáček LJ (2017) FAD Regulates CRYPTOCHROME Protein Stability and Circadian Clock in Mice. *Cell Rep.* **19:** 255–266

Hirano A, Fu Y-H & Ptáček LJ (2016) The intricate dance of post-translational modifications in the rhythm of life. *Nat. Struct. Mol. Biol.* **23:** 1053–1060

Hirayama J, Sahar S, Grimaldi B, Tamaru T, Takamatsu K, Nakahata Y & Sassone-Corsi P (2007) CLOCK-mediated acetylation of BMAL1 controls circadian function. *Nature* **450:** 1086–1090

Hirota T, Lee JW, St. John PC, Sawa M, Iwaisako K, Noguchi T, Pongsawakul PY, Sonntag T, Welsh DK, Brenner DA, Doyle FJ, Schultz PG & Kay SA (2012) Identification of Small Molecule Activators of Cryptochrome. *Science (80-.).* **337:** 1094–1097

Hirota T, Lee JW, Lewis WG, Zhang EE, Breton G, Liu X, Garcia M, Peters EC, Etchegaray J-P, Traver D, Schultz PG & Kay SA (2010) High-Throughput Chemical Screen Identifies a Novel Potent Modulator of Cellular Circadian Rhythms and Reveals CKIα as a Clock Regulatory Kinase. *PLoS Biol.* **8:** e1000559

Hoang N, Schleicher E, Kacprzak S, Bouly JP, Picot M, Wu W, Berndt A, Wolf E, Bittl R & Ahmad M (2008) Human and Drosophila cryptochromes are light activated by flavin photoreduction in living cells. *PLoS Biol.* **6:** 1559–1569

Holman JD, Tabb DL & Mallick P (2014) Employing ProteoWizard to Convert Raw Mass Spectrometry Data. *Curr. Protoc. Bioinforma.* **46:** 13.24.1-13.24.9.

Holzer S, Degliesposti G, Kilkenny ML, Maslen SL, Matak-Vinkovíc D, Skehel M & Pellegrini L (2017) Crystal structure of the N-terminal domain of human Timeless and its interaction with Tipin. *Nucleic Acids Res.* **45:** 5555–5563

Hornbeck P V., Zhang B, Murray B, Kornhauser JM, Latham V & Skrzypek E (2015) PhosphoSitePlus, 2014: mutations, PTMs and recalibrations. *Nucleic Acids Res.* **43:** D512–D520

Van Der Horst GTJ, Muijtjens M, Kobayashi K, Takano R, Kanno SI, Takao M, De Wit J, Verkerk A, Eker APM, Van Leenen D, Buijs R, Bootsma D, Hoeijmakers JHJ & Yasui A

(1999) Mammalian Cry1 and Cry2 are essential for maintenance of circadian rhythms. *Nature* **398:** 627–630

Hosoda H, Kato K, Asano H, Ito M, Kato H, Iwamoto T, Suzuki A, Masushige S & Kida S (2009) CBP/p300 is a cell type-specific modulator of CLOCK/BMAL1-mediated transcription. *Mol. Brain* **2:** 34

Huang L, Kirschke CP, Zhang Y & Yu YY (2005) The ZIP7 Gene (Slc39a7) Encodes a Zinc Transporter Involved in Zinc Homeostasis of the Golgi Apparatus. *J. Biol. Chem.* **280:** 15456–15463

Huang N, Chelliah Y, Shan Y, Taylor CA, Yoo S-H, Partch C, Green CB, Zhang H & Takahashi JS (2012) Crystal Structure of the Heterodimeric CLOCK:BMAL1 Transcriptional Activator Complex. *Science (80-.).* **337:** 189–194

Huber A-LL, Papp SJ, Chan AB, Henriksson E, Jordan SD, Kriebs A, Nguyen M, Wallace M, Li Z, Metallo CM & Lamia KA (2016) CRY2 and FBXL3 Cooperatively Degrade c-MYC. *Mol. Cell* **64:** 774–789

Johnson A & O'Donnell M (2005) CELLULAR DNA REPLICASES: Components and Dynamics at the Replication Fork. *Annu. Rev. Biochem.* **74:** 283–315

Jones DT (1999) Protein secondary structure prediction based on position-specific scoring matrices 1 1Edited by G. Von Heijne. *J. Mol. Biol.* **292:** 195–202

Jones JC, Phatnani HP, Haystead TA, MacDonald JA, Alam SM & Greenleaf AL (2004) C-terminal Repeat Domain Kinase I Phosphorylates Ser2 and Ser5 of RNA Polymerase II C-terminal Domain Repeats. *J. Biol. Chem.* **279:** 24957–24964

Kang T-H, Lindsey-Boltz LA, Reardon JT & Sancar A (2010) Circadian control of XPA and excision repair of cisplatin-DNA damage by cryptochrome and HERC2 ubiquitin ligase. *Proc. Natl. Acad. Sci.* **107:** 4890–4895

Kang T-H, Reardon JT, Kemp M & Sancar A (2009) Circadian oscillation of nucleotide excision repair in mammalian brain. *Proc. Natl. Acad. Sci. U. S. A.* **106:** 2864–2867

Kang TH & Leem SH (2014) Modulation of ATR-mediated DNA damage checkpoint response by cryptochrome 1. *Nucleic Acids Res.* **42:** 4427–4434

Katada S & Sassone-Corsi P (2010) The histone methyltransferase MLL1 permits the oscillation of circadian gene expression. *Nat. Struct. Mol. Biol.* **17:** 1414–1421

Kelman Z (1997) PCNA: structure, functions and interactions. *Oncogene* **14:** 629-640.

Kemp MG, Akan Z, Yilmaz S, Grillo M, Smith-Roe SL, Kang T-H, Cordeiro-Stone M, Kaufmann WK, Abraham RT, Sancar A & Ünsal-Kaçmaz K (2010) Tipin-Replication Protein A Interaction Mediates Chk1 Phosphorylation by ATR in Response to Genotoxic Stress. *J. Biol. Chem.* **285:** 16562–16571

Khan SK, Xu H, Ukai-Tadenuma M, Burton B, Wang Y, Ueda HR & Liu AC (2012) Identification of a Novel Cryptochrome Differentiating Domain Required for Feedback Repression in Circadian Clock Function. *J. Biol. Chem.* **287:** 25917–25926

Kim JY, Kwak PB & Weitz CJ (2014) Specificity in Circadian Clock Feedback from Targeted Reconstitution of the NuRD Corepressor. *Mol. Cell* **56:** 738–748

Kim S-T, Lim D-S, Canman CE & Kastan MB (1999) Substrate Specificities and Identification of Putative Substrates of ATM Kinase Family Members. *J. Biol. Chem.* **274:** 37538–37543

Kodani A, Yu TW, Johnson JR, Jayaraman D, Johnson TL, Al-Gazali L, Sztriha L, Partlow JN, Kim H, Krup AL, Dammermann A, Krogan NJ, Walsh CA & Reiter JF (2015) Centriolar satellites assemble centrosomal microcephaly proteins to recruit CDK2 and promote centriole duplication. *Elife* **4:** 1–27

Koike N, Yoo S-H, Huang H-C, Kumar V, Lee C, Kim T-K & Takahashi JS (2012) Transcriptional Architecture and Chromatin Landscape of the Core Circadian Clock in Mammals. *Science (80-.).* **338:** 349–354

Kolbowski L, Mendes ML & Rappsilber J (2017) Optimizing the Parameters Governing the Fragmentation of Cross-Linked Peptides in a Tribrid Mass Spectrometer. *Anal. Chem.* **89:** 5311–5318

Konarev P V., Volkov V V., Sokolova A V., Koch MHJ & Svergun DI (2003) PRIMUS : a Windows PC-based system for small-angle scattering data analysis. *J. Appl. Crystallogr.* **36:** 1277–1282

Krissinel E & Henrick K (2007) Inference of Macromolecular Assemblies from Crystalline State. *J. Mol. Biol.* **372:** 774–797

Kume K, Zylka MJ, Sriram S, Shearman LP, Weaver DR, Jin X, Maywood ES, Hastings MH & Reppert SM (1999) mCRY1 and mCRY2 Are Essential Components of the Negative Limb of the Circadian Clock Feedback Loop. *Cell* **98:** 193–205

Kurabayashi N, Hirota T, Sakai M, Sanada K & Fukada Y (2010) DYRK1A and Glycogen Synthase Kinase 3 , a Dual-Kinase Mechanism Directing Proteasomal Degradation of CRY2 for Circadian Timekeeping. *Mol. Cell. Biol.* **30:** 1757–1768

Kurien P, Hsu PK, Leon J, Wu D, McMahon T, Shi G, Xu Y, Lipzen A, Pennacchio LA, Jones CR, Fu YH & Ptáček LJ (2019) TIMELESS mutation alters phase responsiveness and causes advanced sleep phase. *Proc. Natl. Acad. Sci. U. S. A.* **116:** 12045–12053

Kutta RJ, Archipowa N, Johannissen LO, Jones AR & Scrutton NS (2017) Vertebrate Cryptochromes are Vestigial Flavoproteins. *Sci. Rep.* **7:** 44906

Lamia KA, Sachdeva UM, DiTacchio L, Williams EC, Alvarez JG, Egan DF, Vasquez DS, Juguilon H, Panda S, Shaw RJ, Thompson CB & Evans RM (2009) AMPK Regulates the Circadian Clock by Cryptochrome Phosphorylation and Degradation. *Science (80-.).* **326:** 437–440

Langmesser S & Albrecht U (2006) Life time - Circadian clocks, mitochondria and metabolism. *Chronobiol. Int.* **23:** 151–157

Langston LD & O'Donnell M (2006) DNA Replication: Keep Moving and Don't Mind the Gap. *Mol. Cell* **23:** 155–160

Lea WA & Simeonov A (2012) Fluorescence Polarization Assay. *Expert Opin Drug Discov.* **6:** 17–32

Lee C, Etchegaray J-P, Cagampang FRA, Loudon ASI & Reppert SM (2001) Posttranslational Mechanisms Regulate the Mammalian Circadian Clock. *Cell* **107:** 855–867

Lee C, Weaver DR & Reppert SM (2004) Direct Association between Mouse PERIOD and CKI Is Critical for a Functioning Circadian Clock. *Mol. Cell. Biol.* **24:** 584–594

Lehman IR & Kaguni LS (1989) DNA polymerase α. *J. Biol. Chem.* **264:** 4265–4268

Leitner A, Reischl R, Walzthoeni T, Herzog F, Bohn S, Förster F & Aebersold R (2012)

Expanding the Chemical Cross-Linking Toolbox by the Use of Multiple Proteases and Enrichment by Size Exclusion Chromatography. *Mol. Cell. Proteomics* **11:** M111.014126

Leman AR, Dheekollu J, Deng Z, Lee SW, Das MM, Lieberman PM & Noguchi E (2012) Timeless preserves telomere length by promoting efficient DNA replication through human telomeres. *Cell Cycle* **11:** 2337–2347

Leman AR, Noguchi C, Lee CY & Noguchi E (2010) Human Timeless and Tipin stabilize replication forks and facilitate sister-chromatid cohesion. *J. Cell Sci.* **123:** 660–670

Leman AR & Noguchi E (2012) Local and global functions of Timeless and Tipin in replication fork protection. *Cell Cycle* **11:** 3945–3955

Li Y, Xiong W & Zhang EE (2016) The ratio of intracellular CRY proteins determines the clock period length. *Biochem. Biophys. Res. Commun.* **472:** 531–538

Li Z, Stuart RO, Qiao J, Pavlova A, Bush KT, Pohl M, Sakurai H & Nigam SK (2000) A role for Timeless in epithelial morphogenesis during kidney development. *Proc. Natl. Acad. Sci.* **97:** 10038–10043

Lowrey PL (2000) Positional Syntenic Cloning and Functional Characterization of the Mammalian Circadian Mutation tau. *Science (80-.).* **288:** 483–491

MacNeill SA (2010) Structure and function of the GINS complex, a key component of the eukaryotic replisome. *Biochem. J.* **425:** 489–500

Madeira F, Park Y mi, Lee J, Buso N, Gur T, Madhusoodanan N, Basutkar P, Tivey ARN, Potter SC, Finn RD & Lopez R (2019) The EMBL-EBI search and sequence analysis tools APIs in 2019. *Nucleic Acids Res.* **47:** W636–W641

Maiolica A, Cittaro D, Borsotti D, Sennels L, Ciferri C, Tarricone C, Musacchio A & Rappsilber J (2007) Structural Analysis of Multiprotein Complexes by Cross-linking, Mass Spectrometry, and Database Searching. *Mol. Cell. Proteomics* **6:** 2200–2211

Matsuda T, Saijo M, Kuraoka I, Kobayashi T, Nakatsu Y, Nagai A, Enjoji T, Masutani C, Sugasawa K, Hanaoka F, Yasui A & Tanaka K (1995) DNA Repair Protein XPA Binds Replication Protein A (RPA). *J. Biol. Chem.* **270:** 4152–4157

Matsuoka S, Ballif BA, Smogorzewska A, McDonald ER, Hurov KE, Luo J, Bakalarski CE, Zhao Z, Solimini N, Lerenthal Y, Shiloh Y, Gygi SP & Elledge SJ (2007) ATM and ATR Substrate Analysis Reveals Extensive Protein Networks Responsive to DNA Damage. *Science (80-.).* **316:** 1160–1166

Mendes ML, Fischer L, Chen ZA, Barbon M, O'Reilly FJ, Giese SH, Bohlke-Schneider M, Belsom A, Dau T, Combe CW, Graham M, Eisele MR, Baumeister W, Speck C & Rappsilber J (2019) An integrated workflow for crosslinking mass spectrometry. *Mol. Syst. Biol.* **15:** e8994

Meng QJ, Logunova L, Maywood ES, Gallego M, Lebiecki J, Brown TM, Sládek M, Semikhodskii AS, Glossop NRJ, Piggins HD, Chesham JE, Bechtold DA, Yoo SH, Takahashi JS, Virshup DM, Boot-Handford RP, Hastings MH & Loudon ASI (2008) Setting Clock Speed in Mammals: The CK1ε tau Mutation in Mice Accelerates Circadian Pacemakers by Selectively Destabilizing PERIOD Proteins. *Neuron* **58:** 78–88

Merbitz-Zahradnik T & Wolf E (2015) How is the inner circadian clock controlled by interactive clock proteins? *FEBS Lett.* **589:** 1516–1529

Mertens HDT & Svergun DI (2010) Structural characterization of proteins and complexes using small-angle X-ray solution scattering. *J. Struct. Biol.* **172:** 128–141

Michael AK, Fribourgh JL, Chelliah Y, Sandate CR, Hura GL, Schneidman-Duhovny D, Tripathi SM, Takahashi JS & Partch CL (2017) Formation of a repressive complex in the mammalian circadian clock is mediated by the secondary pocket of CRY1. *Proc. Natl. Acad. Sci.* **114:** 1560–1565

Mistlberger RE (1994) Circadian food-anticipatory activity: Formal models and physiological mechanisms. *Neurosci. Biobehav. Rev.* **18:** 171–195

Miyazaki K, Nagase T, Mesaki M, Narukawa J, Ohara O & Ishida N (2004) Phosphorylation of clock protein PER1 regulates its circadian degradation in normal human fibroblasts. *Biochem. J.* **380:** 95–103

Moore RY & Eichler VB (1972) Loss of a circadian adrenal corticosterone rhythm following suprachiasmatic lesions in the rat. *Brain Res.* **42:** 201–206

Müller F, Fischer L, Chen ZA, Auchynnikava T & Rappsilber J (2018) On the Reproducibility of Label-Free Quantitative Cross-Linking/Mass Spectrometry. *J. Am. Soc. Mass Spectrom.* **29:** 405–412

Müller M & Carell T (2009) Structural biology of DNA photolyases and cryptochromes. *Curr. Opin. Struct. Biol.* **19:** 277–285

Nagelhus TA, Haug T, Singh KK, Keshav KF, Skorpen F, Otterlei M, Bharati S, Lindmo T, Benichou S, Benarous R & Krokan HE (1997) A Sequence in the N-terminal Region of Human Uracil-DNA Glycosylase with Homology to XPA Interacts with the C-terminal Part of the 34-kDa Subunit of Replication Protein A. *J. Biol. Chem.* **272:** 6561–6566

Nagoshi E, Saini C, Bauer C, Laroche T, Naef F & Schibler U (2004) Circadian Gene Expression in Individual Fibroblasts. *Cell* **119:** 693–705

Nakaya R, Takaya J, Onuki T, Moritani M, Nozaki N & Ishimi Y (2010) Identification of proteins that may directly interact with human RPA. *J. Biochem.* **148:** 539–547

Nangle SN, Rosensweig C, Koike N, Tei H, Takahashi JS, Green CB & Zheng N (2014) Molecular assembly of the period-cryptochrome circadian transcriptional repressor complex. *Elife* **3:** 1–14

Nogales E & Scheres SHW (2015) Cryo-EM: A Unique Tool for the Visualization of Macromolecular Complexity. *Mol. Cell* **58:** 677–689

Noguchi E, Noguchi C, McDonald WH, Yates JR & Russell P (2004) Swi1 and Swi3 Are Components of a Replication Fork Protection Complex in Fission Yeast. *Mol. Cell. Biol.* **24:** 8342–8355

Numata Y, Ishihara S, Hasegawa N, Nozaki N & Ishimi Y (2010) Interaction of human MCM2-7 proteins with TIM, TIPIN and Rb. *J. Biochem.* **147:** 917–927

Oklejewicz M, Destici E, Tamanini F, Hut RA, Janssens R & van der Horst GTJ (2008) Phase Resetting of the Mammalian Circadian Clock by DNA Damage. *Curr. Biol.* **18:** 286–291

Ong S (2003) Mass spectrometric-based approaches in quantitative proteomics. *Methods* **29:** 124–130

Otterlei M (1999) Post-replicative base excision repair in replication foci. *EMBO J.* **18:** 3834–3844

Padmanabhan K, Robles MS, Westerling T & Weitz CJ (2012) Feedback Regulation of Transcriptional Termination by the Mammalian Circadian Clock PERIOD Complex. *Science (80-.).* **337:** 599–602

Panjkovich A & Svergun DI (2018) CHROMIXS: automatic and interactive analysis of chromatography-coupled small-angle X-ray scattering data. *Bioinformatics* **34:** 1944–1946

Papp SJ, Huber AL, Jordan SD, Kriebs A, Nguyen M, Moresco JJ, Yates JR & Lamia KA (2015) DNA damage shifts circadian clock time via Hausp-dependent Cry1 stabilization. *Elife* **4:** 1–19

Parico GCG, Perez I, Fribourgh JL, Hernandez BN, Lee H-W & Partch CL (2019) The CRY1 tail controls circadian timing by regulating its association with CLOCK:BMAL1. *bioRxiv***:** 758714

Park MS, Ludwig DL, Stigger E & Lee S-H (1996) Physical Interaction between Human RAD52 and RPA Is Required for Homologous Recombination in Mammalian Cells. *J. Biol. Chem.* **271:** 18996–19000

Pasero P & Tourrière H (2019) Overexpression of the Fork Protection Complex: a strategy to tolerate oncogene-induced replication stress in cancer cells. *Mol. Cell. Oncol.* **6:** 1–3

Petrotchenko E V. & Borchers CH (2010) Crosslinking combined with mass spectrometry for structural proteomics. *Mass Spectrom. Rev.* **29:** 862–876

Pettersen EF, Goddard TD, Huang CC, Couch GS, Greenblatt DM, Meng EC & Ferrin TE (2004) UCSF Chimera-A visualization system for exploratory research and analysis. *J. Comput. Chem.* **25:** 1605–1612

Preitner N, Damiola F, Luis-Lopez-Molina, Zakany J, Duboule D, Albrecht U & Schibler U (2002) The Orphan Nuclear Receptor REV-ERBα Controls Circadian Transcription within the Positive Limb of the Mammalian Circadian Oscillator. *Cell* **110:** 251–260

Pukkala E, Auvinen A & Wahlberg G (1995) Incidence of cancer among Finnish airline cabin attendants, 1967-92. *BMJ* **311:** 649–652

Ralph M, Foster R, Davis F & Menaker M (1990) Transplanted suprachiasmatic nucleus determines circadian period. *Science (80-.).* **247:** 975–978

Rappsilber J (2011) The beginning of a beautiful friendship: Cross-linking/mass spectrometry and modelling of proteins and multi-protein complexes. *J. Struct. Biol.* **173:** 530–540

Rappsilber J, Mann M & Ishihama Y (2007) Protocol for micro-purification, enrichment, pre-fractionation and storage of peptides for proteomics using StageTips. *Nat. Protoc.* **2:** 1896–1906

Ray Chaudhuri A & Nussenzweig A (2017) The multifaceted roles of PARP1 in DNA repair and chromatin remodelling. *Nat. Rev. Mol. Cell Biol.* **18:** 610–621

Receveur-Brechot V & Durand D (2012) How Random are Intrinsically Disordered Proteins? A Small Angle Scattering Perspective. *Curr. Protein Pept. Sci.* **13:** 55–75

Reddy AB, Maywood ES, Karp NA, King VM, Inoue Y, Gonzalez FJ, Lilley KS, Kyriacou CP & Hastings MH (2007) Glucocorticoid signaling synchronizes the liver circadian transcriptome. *Hepatology* **45:** 1478–1488

Reinhard L, Mayerhofer H, Geerlof A, Mueller-Dieckmann J & Weiss MS (2013) Optimization

of protein buffer cocktails using Thermofluor. *Acta Crystallogr. Sect. F Struct. Biol. Cryst. Commun.* **69:** 209–214

Rose KM, Marin M, Kozak SL & Kabat D (2005) Regulated Production and Anti-HIV Type 1 Activities of Cytidine Deaminases APOBEC3B, 3F, and 3G. *AIDS Res. Hum. Retroviruses* **21:** 611–619

Rosensweig C & Green CB (2018) Periodicity, repression, and the molecular architecture of the mammalian circadian clock. *Eur. J. Neurosci.***:** 1–27

Sancar A, Lindsey-Boltz LA, Ünsal-Kaçmaz K & Linn S (2004) Molecular Mechanisms of Mammalian DNA Repair and the DNA Damage Checkpoints. *Annu. Rev. Biochem.* **73:** 39–85

Sangoram AM, Saez L, Antoch MP, Gekakis N, Staknis D, Whiteley A, Fruechte EM, Vitaterna MH, Shimomura K, King DP, Young MW, Weitz CJ & Takahashi JS (1998) Mammalian Circadian Autoregulatory Loop. *Neuron* **21:** 1101–1113

Sato TK, Panda S, Miraglia LJ, Reyes TM, Rudic RD, McNamara P, Naik KA, FitzGerald GA, Kay SA & Hogenesch JB (2004) A Functional Genomics Strategy Reveals Rora as a Component of the Mammalian Circadian Clock. *Neuron* **43:** 527–537

Schalbetter SA, Mansoubi S, Chambers AL, Downs JA & Baxter J (2015) Fork rotation and DNA precatenation are restricted during DNA replication to prevent chromosomal instability. *Proc. Natl. Acad. Sci. U. S. A.* **112:** E4565–E4570

Schmalen I, Reischl S, Wallach T, Klemz R, Grudziecki A, Prabu JR, Benda C, Kramer A & Wolf E (2014) Interaction of circadian clock proteins CRY1 and PER2 is modulated by zinc binding and disulfide bond formation. *Cell* **157:** 1203–1215

Schneider M, Belsom A & Rappsilber J (2018) Protein Tertiary Structure by Crosslinking/Mass Spectrometry. *Trends Biochem. Sci.* **43:** 157–169

Scholz J, Besir H, Strasser C & Suppmann S (2013) A new method to customize protein expression vectors for fast, efficient and background free parallel cloning. *BMC Biotechnol.* **13:** 12

Scoma HD, Humby M, Yadav G, Zhang Q, Fogerty J & Besharse JC (2011) The De-Ubiquitinylating Enzyme, USP2, Is Associated with the Circadian Clockwork and Regulates Its Sensitivity to Light. *PLoS One* **6:** e25382

Serçin Ö & Kemp MG (2011) Characterization of functional domains in human Claspin. *Cell Cycle* **10:** 1599–1606

Shanware NP, Hutchinson JA, Kim SH, Zhan L, Bowler MJ & Tibbetts RS (2011) Casein Kinase 1-dependent Phosphorylation of Familial Advanced Sleep Phase Syndrome-associated Residues Controls PERIOD 2 Stability. *J. Biol. Chem.* **286:** 12766–12774

Sheward WJ, Naylor E, Knowles-Barley S, Armstrong JD, Brooker GA, Seckl JR, Turek FW, Holmes MC, Zee PC & Harmar AJ (2010) Circadian Control of Mouse Heart Rate and Blood Pressure by the Suprachiasmatic Nuclei: Behavioral Effects Are More Significant than Direct Outputs. *PLoS One* **5:** e9783

Shieh SY, Ahn J, Tamai K, Taya Y & Prives C (2000) The human homologs of checkpoint kinases Chk1 and Cds1 (Chk2) phosphorylate, p53 at multiple DNA damage-inducible sites. *Genes Dev.* **14:** 289–300

Shostak A (2017) Circadian clock, cell division, and cancer: From molecules to organism. *Int. J. Mol. Sci.* **18:** 873

Smith KD, Fu MA & Brown EJ (2009) Tim-Tipin dysfunction creates an indispensible reliance on the ATR-Chk1 pathway for continued DNA synthesis. *J. Cell Biol.* **187:** 15–23

So AY-L, Bernal TU, Pillsbury ML, Yamamoto KR & Feldman BJ (2009) Glucocorticoid regulation of the circadian clock modulates glucose homeostasis. *Proc. Natl. Acad. Sci.* **106:** 17582–17587

Sogo JM (2002) Fork Reversal and ssDNA Accumulation at Stalled Replication Forks Owing to Checkpoint Defects. *Science (80-.).* **297:** 599–602

Sommariva E, Pellny TK, Karahan N, Kumar S, Huberman JA & Dalgaard JZ (2005) Schizosaccharomyces pombe Swi1, Swi3, and Hsk1 Are Components of a Novel S-Phase Response Pathway to Alkylation Damage. *Mol. Cell. Biol.* **25:** 2770–2784

Staples CJ, Myers KN, Beveridge RDD, Patil AA, Lee AJX, Swanton C, Howell M, Boulton SJ & Collis SJ (2012) The centriolar satellite protein Cep131 is important for genome stability. *J. Cell Sci.* **125:** 4770–4779

Stark H (2010) GraFix: Stabilization of Fragile Macromolecular Complexes for Single Particle Cryo-EM. In pp 109–126.

Stephan FK (2002) The 'Other' Circadian System: Food as a Zeitgeber. *J. Biol. Rhythms* **17:** 284–292

Stephan FK, Swann JM & Sisk CL (1979) Entrainment of circadian rhythms by feeding schedules in rats with suprachiasmatic lesions. *Behav. Neural Biol.* **25:** 545–554

Stephan FK & Zucker I (1972) Circadian Rhythms in Drinking Behavior and Locomotor Activity of Rats Are Eliminated by Hypothalamic Lesions. *Proc. Natl. Acad. Sci.* **69:** 1583–1586

Stratmann M, Stadler F, Tamanini F, van der Horst GTJ & Ripperger JA (2010) Flexible phase adjustment of circadian albumin D site-binding protein (Dbp) gene expression by CRYPTOCHROME1. *Genes Dev.* **24:** 1317–1328

Sugiyama T, New JH & Kowalczykowski SC (1998) DNA annealing by Rad52 Protein is stimulated by specific interaction with the complex of replication protein A and single-stranded DNA. *Proc. Natl. Acad. Sci.* **95:** 6049–6054

Suloway C, Pulokas J, Fellmann D, Cheng A, Guerra F, Quispe J, Stagg S, Potter CS & Carragher B (2005) Automated molecular microscopy: The new Leginon system. *J. Struct. Biol.* **151:** 41–60

Svergun D, Barberato C & Koch MHJ (1995) CRYSOL – a Program to Evaluate X-ray Solution Scattering of Biological Macromolecules from Atomic Coordinates. *J. Appl. Crystallogr.* **28:** 768–773

Svergun DI, Petoukhov M V. & Koch MHJ (2001) Determination of Domain Structure of Proteins from X-Ray Solution Scattering. *Biophys. J.* **80:** 2946–2953

Taylor BL & Zhulin IB (1999) PAS domains: internal sensors of oxygen, redox potential, and light. *Microbiol. Mol. Biol. Rev.* **63:** 479–506

Taylor KM, Morgan HE, Johnson A, Hadley LJ & Nicholson RI (2003) Structure–function analysis of LIV-1, the breast cancer-associated protein that belongs to a new subfamily of

zinc transporters. *Biochem. J.* **375:** 51–59

Tei H, Okamura H, Shigeyoshi Y, Fukuhara C, Ozawa R, Hirose M & Sakaki Y (1997) Circadian oscillation of a mammalian homologue of the Drosophila period gene. *Nature* **389:** 512–516

Toh KL (2001) An hPer2 Phosphorylation Site Mutation in Familial Advanced Sleep Phase Syndrome. *Science (80-.).* **291:** 1040–1043

Tollenaere MAX, Mailand N & Bekker-Jensen S (2015) Centriolar satellites: Key mediators of centrosome functions. *Cell. Mol. Life Sci.* **72:** 11–23

Di Tommaso P, Moretti S, Xenarios I, Orobitg M, Montanyola A, Chang J-M, Taly J-F & Notredame C (2011) T-Coffee: a web server for the multiple sequence alignment of protein and RNA sequences using structural information and homology extension. *Nucleic Acids Res.* **39:** W13–W17

Tsuchiya Y, Akashi M, Matsuda M, Goto K, Miyata Y, Node K & Nishida E (2009) Involvement of the Protein Kinase CK2 in the Regulation of Mammalian Circadian Rhythms. *Sci. Signal.* **2:** ra26–ra26

Ueda HR, Chen W, Adachi A, Wakamatsu H, Hayashi S, Takasugi T, Nagano M, Nakahama K, Suzuki Y, Sugano S, Iino M, Shigeyoshi Y & Hashimoto S (2002) A transcription factor response element for gene expression during circadian night. *Nature* **418:** 534–539

Ukai-Tadenuma M, Yamada RG, Xu H, Ripperger JA, Liu AC & Ueda HR (2011) Delay in Feedback Repression by Cryptochrome 1 Is Required for Circadian Clock Function. *Cell* **144:** 268–281

Unsal-Kacmaz K, Chastain PD, Qu P-P, Minoo P, Cordeiro-Stone M, Sancar A & Kaufmann WK (2007) The Human Tim/Tipin Complex Coordinates an Intra-S Checkpoint Response to UV That Slows Replication Fork Displacement. *Mol. Cell. Biol.* **27:** 3131–3142

Unsal-Kaçmaz K, Mullen TE, Kaufmann WK & Sancar A (2005) Coupling of human circadian and cell cycles by the timeless protein. *Mol. Cell. Biol.* **25:** 3109–16

Urtishak KA, Smith KD, Chanoux RA, Greenberg RA, Johnson FB & Brown EJ (2009) Timeless maintains genomic stability and suppresses sister chromatid exchange during unperturbed DNA replication. *J. Biol. Chem.* **284:** 8777–8785

Vanselow K, Vanselow JT, Westermark PO, Reischl S, Maier B, Korte T, Herrmann A, Herzel H, Schlosser A & Kramer A (2006) Differential effects of PER2 phosphorylation: molecular basis for the human familial advanced sleep phase syndrome (FASPS). *Genes Dev.* **20:** 2660–2672

Vermeulen K, Van Bockstaele DR & Berneman ZN (2003) The cell cycle: a review of regulation, deregulation and therapeutic targets in cancer. *Cell Prolif.* **36:** 131–149

Villumsen BH, Danielsen JR, Povlsen L, Sylvestersen KB, Merdes A, Beli P, Yang Y-G, Choudhary C, Nielsen ML, Mailand N & Bekker-Jensen S (2013) A new cellular stress response that triggers centriolar satellite reorganization and ciliogenesis. *EMBO J.* **32:** 3029–3040

Vitaterna MH, Selby CP, Todo T, Niwa H, Thompson C, Fruechte EM, Hitomi K, Thresher RJ, Ishikawa T, Miyazaki J, Takahashi JS & Sancar A (1999) Differential regulation of mammalian Period genes and circadian rhythmicity by cryptochromes 1 and 2. *Proc. Natl. Acad. Sci.* **96:** 12114–12119

Wahl GM & Carr AM (2001) The evolution of diverse biological responses to DNA damage: insights from yeast and p53. *Nat. Cell Biol.* **3:** E277–E286

Waterhouse A, Bertoni M, Bienert S, Studer G, Tauriello G, Gumienny R, Heer FT, de Beer TAP, Rempfer C, Bordoli L, Lepore R & Schwede T (2018) SWISS-MODEL: homology modelling of protein structures and complexes. *Nucleic Acids Res.* **46:** W296–W303

Witosch J (2014) Structural Characterization of the Timeless-Tipin-RPA Complex and its Interaction with ssDNA. *Diss. - LMU Munich*

Witosch J, Wolf E & Mizuno N (2014) Architecture and ssDNA interaction of the Timeless-Tipin-RPA complex. *Nucleic Acids Res.* **42:** 12912–12927

Wu X, Shell SM, Liu Y & Zou Y (2007) ATR-dependent checkpoint modulates XPA nuclear import in response to UV irradiation. *Oncogene* **26:** 757–764

Xie S, Mortusewicz O, Ma HT, Herr P, Poon RRY, Helleday T & Qian C (2015) Timeless Interacts with PARP-1 to Promote Homologous Recombination Repair. *Mol. Cell* **60:** 163–176

Xing W, Busino L, Hinds TR, Marionni ST, Saifee NH, Bush MF, Pagano M & Zheng N (2013) SCF FBXL3 ubiquitin ligase targets cryptochromes at their cofactor pocket. *Nature* **496:** 64–68

Yamamoto T, Nakahata Y, Tanaka M, Yoshida M, Soma H, Shinohara K, Yasuda A, Mamine T & Takumi T (2005) Acute physical stress elevates mouse Period1 mRNA expression in mouse peripheral tissues via a glucocorticoid-responsive element. *J. Biol. Chem.* **280:** 42036–42043

Yang X, Wood PA & Hrushesky WJM (2010) Mammalian TIMELESS is required for ATM-dependent CHK2 activation and G2/M checkpoint control. *J. Biol. Chem.* **285:** 3030–3034

Yang Y, Duguay D, Bedard N, Rachalski A, Baquiran G, Na CH, Fahrenkrug J, Storch K-F, Peng J, Wing SS & Cermakian N (2012) Regulation of behavioral circadian rhythms and clock protein PER1 by the deubiquitinating enzyme USP2. *Biol. Open* **1:** 789–801

Ye R, Selby CP, Ozturk N, Annayev Y & Sancar A (2011) Biochemical analysis of the canonical model for the mammalian circadian clock. *J. Biol. Chem.* **286:** 25891–25902

Ye W, Celiksoy S, Jakab A, Khmelinskaia A, Heermann T, Raso A, Wegner S V., Rivas G, Schwille P, Ahijado-Guzmán R & Sönnichsen C (2018) Plasmonic Nanosensors Reveal a Height Dependence of MinDE Protein Oscillations on Membrane Features. *J. Am. Chem. Soc.* **140:** 17901–17906

Ye X, Gao Y, Chen J, Reifsnyder DC, Zheng C & Murray CB (2013) Seeded Growth of Monodisperse Gold Nanorods Using Bromide-Free Surfactant Mixtures. *Nano Lett.* **13:** 2163–2171

Yoo S-H, Yamazaki S, Lowrey PL, Shimomura K, Ko CH, Buhr ED, Siepka SM, Hong H-K, Oh WJ, Yoo OJ, Menaker M & Takahashi JS (2004) PERIOD2::LUCIFERASE real-time reporting of circadian dynamics reveals persistent circadian oscillations in mouse peripheral tissues. *Proc. Natl. Acad. Sci.* **101:** 5339–5346

Yoo SH, Mohawk JA, Siepka SM, Shan Y, Huh SK, Hong HK, Kornblum I, Kumar V, Koike N, Xu M, Nussbaum J, Liu X, Chen Z, Chen ZJ, Green CB & Takahashi JS (2013) Competing E3 ubiquitin ligases govern circadian periodicity by degradation of CRY in nucleus and cytoplasm. *Cell* **152:** 1091–1105

Yoshizawa-Sugata N & Masai H (2007) Human Tim/Timeless-interacting Protein, Tipin, Is Required for Efficient Progression of S Phase and DNA Replication Checkpoint. *J. Biol. Chem.* **282:** 2729–2740

Young LM, Marzio A, Perez-Duran P, Reid DA, Meredith DN, Roberti D, Star A, Rothenberg E, Ueberheide B & Pagano M (2015) TIMELESS Forms a Complex with PARP1 Distinct from Its Complex with TIPIN and Plays a Role in the DNA Damage Response. *Cell Rep.* **13:** 451–459

Zhang R, Lahens NF, Ballance HI, Hughes ME & Hogenesch JB (2014) A circadian gene expression atlas in mammals: Implications for biology and medicine. *Proc. Natl. Acad. Sci.* **111:** 16219–16224

Zhang Y & Hunter T (2014) Roles of Chk1 in cell biology and cancer therapy. *Int. J. Cancer* **134:** 1013–1023

Zheng B, Larkin DW, Albrecht U, Sun ZS, Sage M, Eichele G, Lee CC & Bradley A (1999) The mPer2 gene encodes a functional component of the mammalian circadian clock. *Nature* **400:** 169–173

Zoltowski BD, Vaidya AT, Top D, Widom J, Young MW & Crane BR (2011) Structure of full-length Drosophila cryptochrome. *Nature* **480:** 396–399

Zylka MJ, Shearman LP, Weaver DR & Reppert SM (1998) Three period Homologs in Mammals: Differential Light Responses in the Suprachiasmatic Circadian Clock and Oscillating Transcripts Outside of Brain. *Neuron* **20:** 1103–1110

8 Appendix

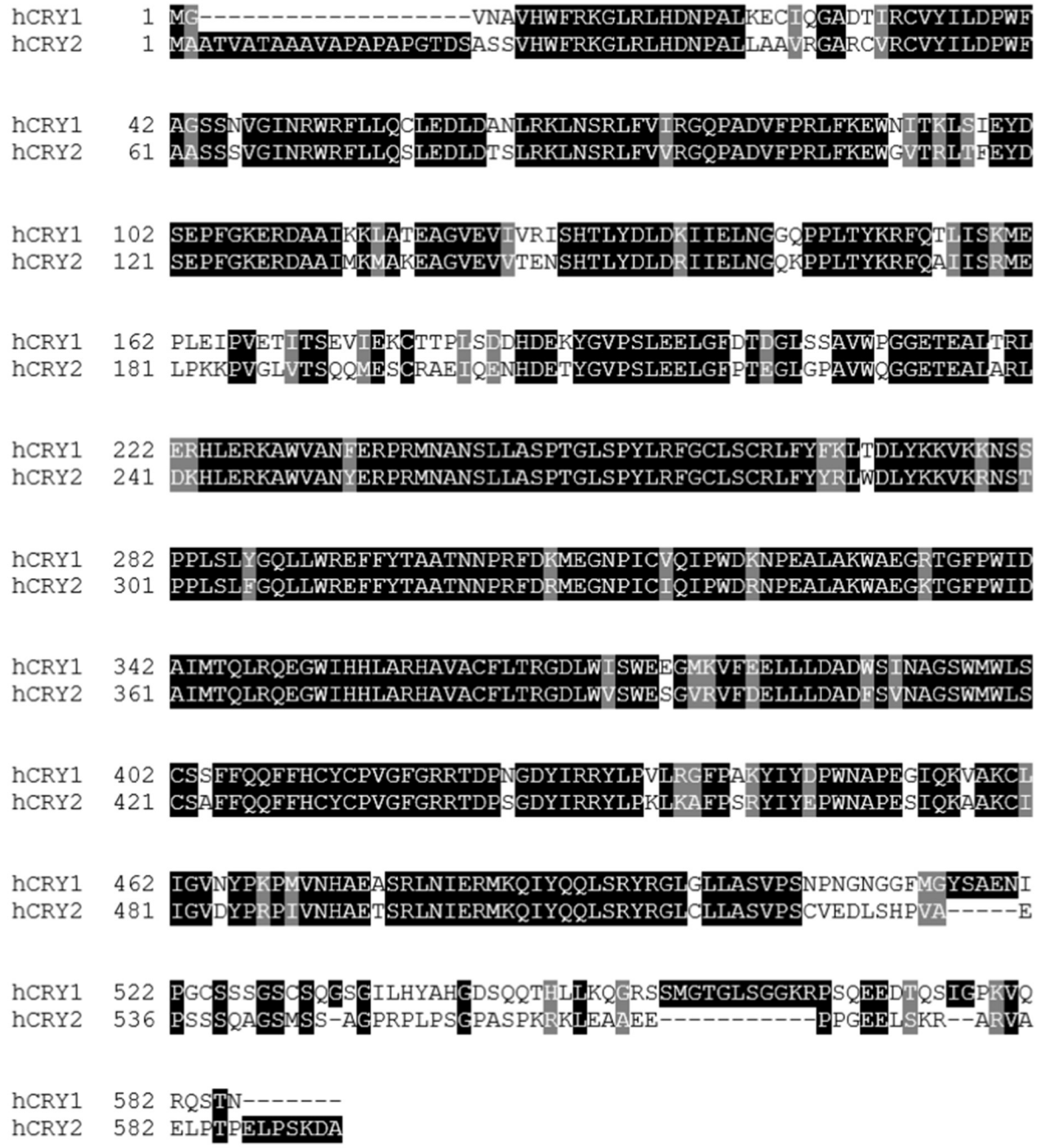

Figure 64: Alignment of human CRY1 and CRY2. The alignment was created using the T-Coffee service (Di Tommaso *et al*, 2011).

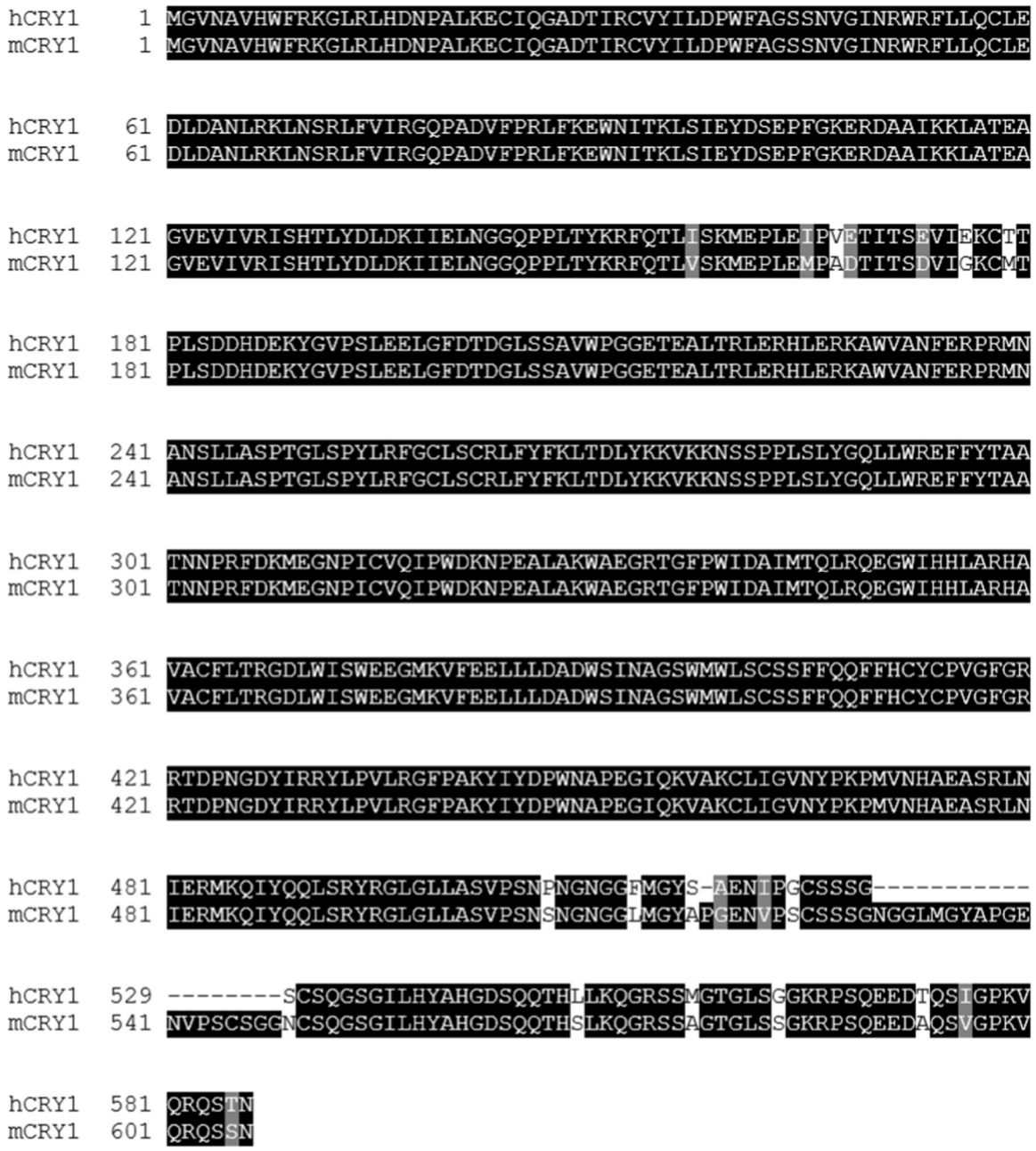

Figure 65: Alignment of human and mouse CRY1. Alignment was generated by T-Coffee (Di Tommaso *et al*, 2011).

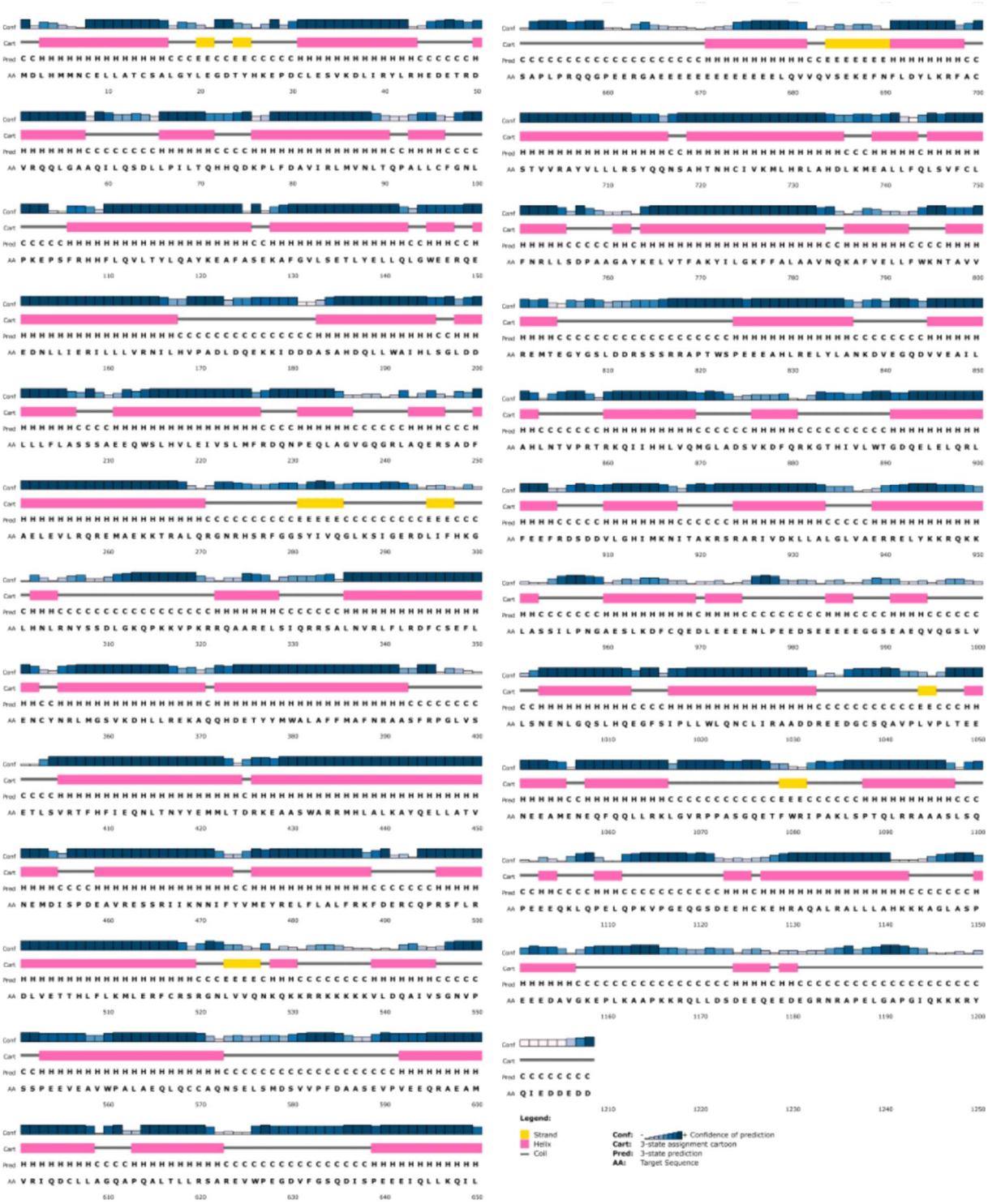

Figure 66: Secondary structure prediction of human TIM by PSIPRED (Jones, 1999).

Figure 67: Secondary structure prediction of human TIPIN. Prediction was calculated using PSIPRED (Jones, 1999).

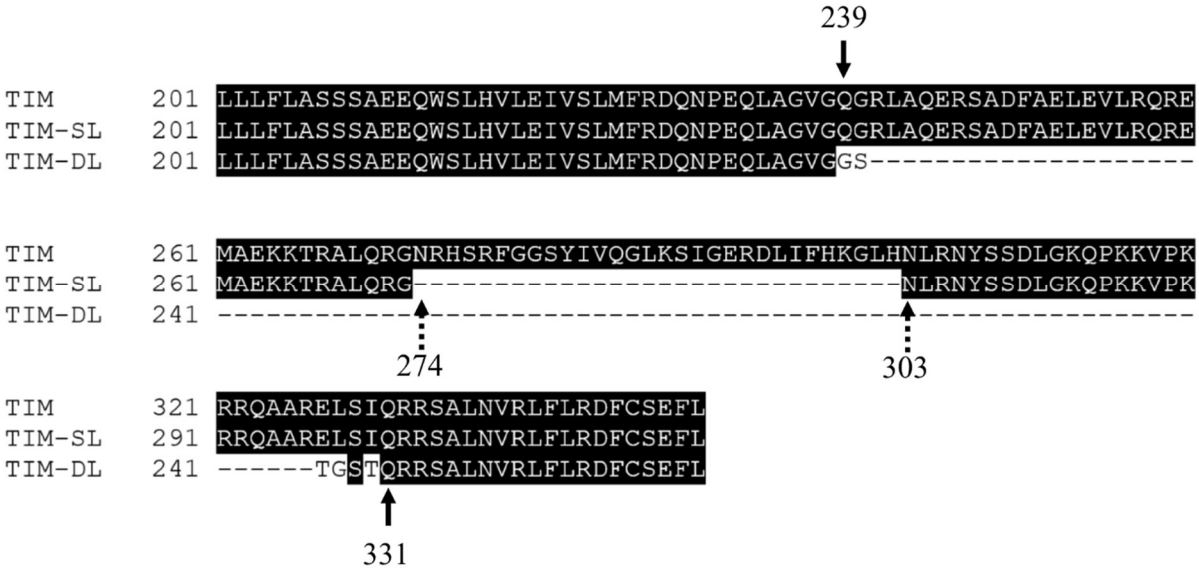

Figure 68: Alignment of the TIM loops. In this thesis three different variants of the TIM loop were used. TIM-SL refers to the shortened loop which was shortened by 30 residues. In TIM-DL (ΔL), the loop was deleted and replaced by the residues GSTGST as a linker. Arrows indicate start and end positions of the modified fragments. Sequences were aligned using the T-Coffee server (Di Tommaso *et al*, 2011).

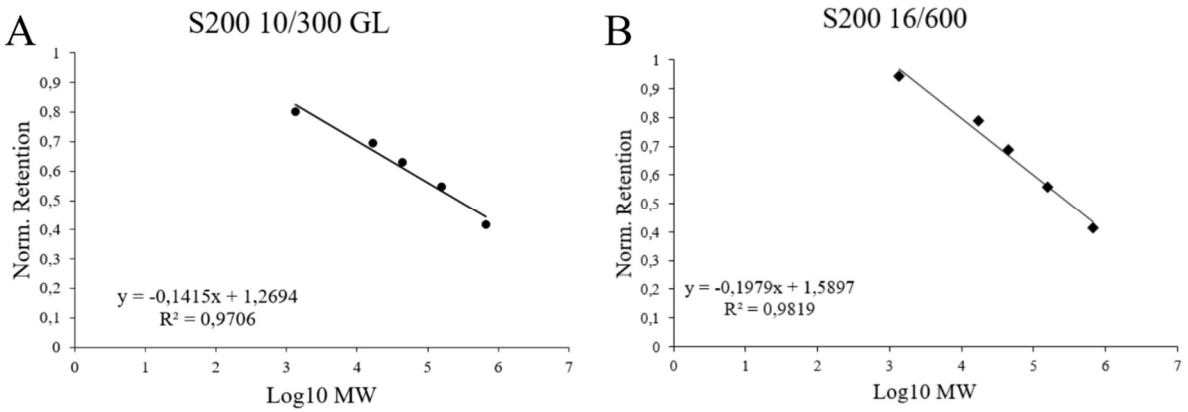

Figure 69: Calibration curves that were used to calculate MW_{SEC} and MW_{PREP} values. A) Calibration curve of the analytical S200 10/300 GL column. B) Calibration curve of the preparative S200 16/600 column.

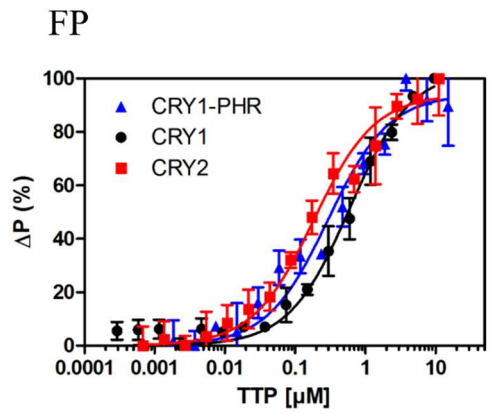

	FP	FP (Lig. Depl.)
CRY1	0.6 ± 0.09 μM	0.71 ± 0.11 μM
CRY2	0.18 ± 0.04 μM	0.18 ± 0.05 μM
CRY1-PHR	0.29 ± 0.06 μM	0.36 ± 0.1 μM

Figure 70: FP data analysis of TTP and CRY with binding model adjusted for ligand depletion and no ligand depletion.

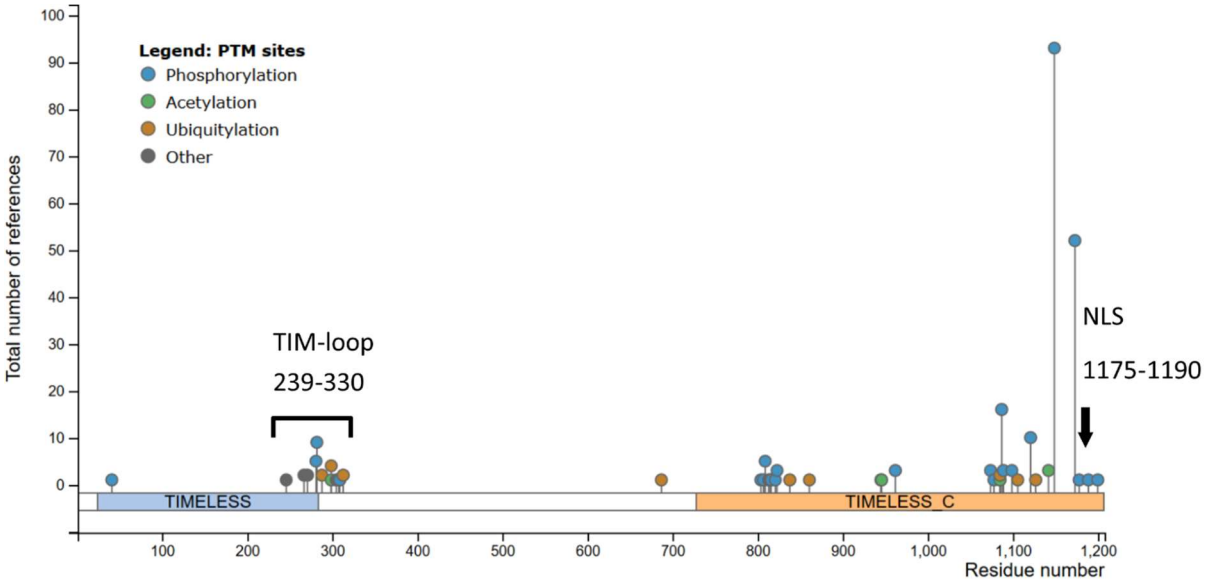

Figure 71: Overview of PTMs in human TIM. The TIM loop and the C-Terminus of TIM are highly modified. Figure was derived from PhosphositePlus (Hornbeck *et al*, 2015). Database was accessed 3rd March, 2020.

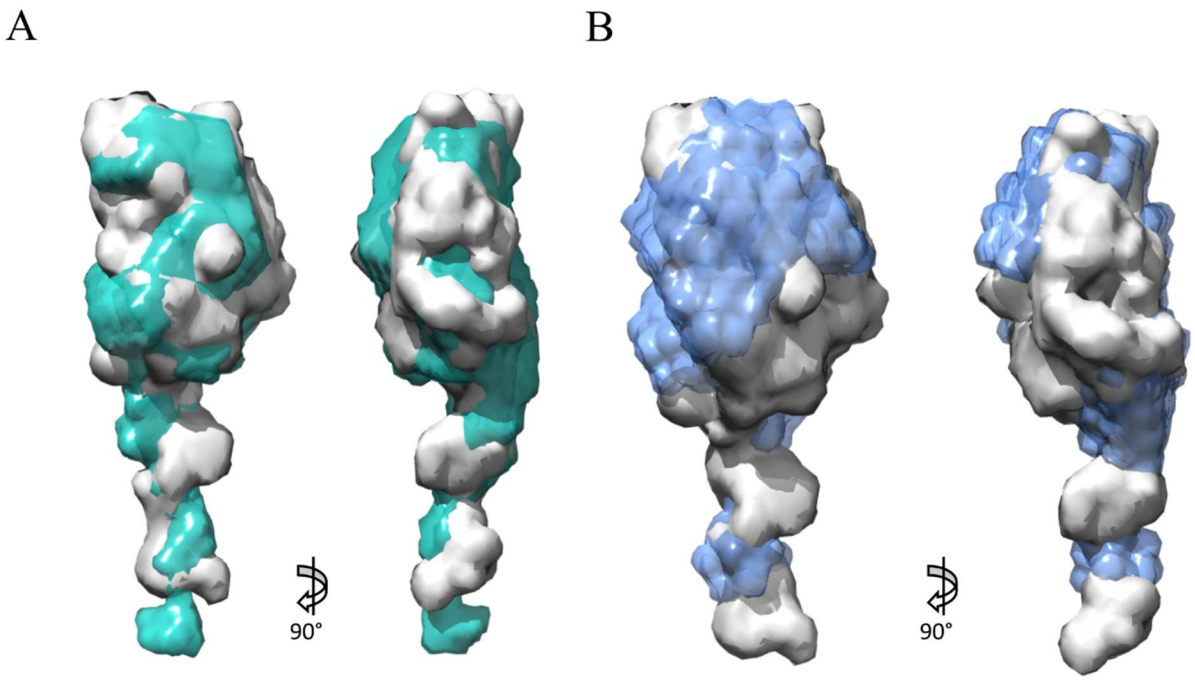

Figure 72: Overlay of SAXS models of CRY1 as monomer and in complex with TIM-N-ΔL (A) and TIM-N-SL (B). TIM-N-ΔL is shown in green, CRY1 as monomer is shown in grey and TIM-N-SL is shown in blue.

Tables with reproducible Crosslinks

Table 28: Reproducible intramolecular crosslinks of the TIM/TIPIN complex. Crosslinks are highlighted as black lines in Figure 36.

Protein1	SeqPos1	LinkedRes1	Protein2	SeqPos2	LinkedRes2
TIM	264	K	TIM	313	K
TIM	264	K	TIM	288	K
TIM	264	K	TIM	727	K
TIM	281	S	TIM	1085	K
TIM	299	K	TIM	313	K
TIM	299	K	TIM	1144	K
TIM	299	K	TIM	1106	K
TIM	307	Y	TIM	316	K
TIM	309	S	TIM	1144	K
TIM	309	S	TIM	317	K
TIM	313	K	TIM	1144	K
TIM	313	K	TIM	1142	K
TIM	313	K	TIM	1143	K

TIM	313	K	TIM	1085	K
TIM	313	K	TIM	1162	K
TIM	313	K	TIM	1127	K
TIM	313	K	TIM	317	K
TIM	511	K	TIM	1144	K
TIM	528	K	TIM	1144	K
TIM	528	K	TIM	687	K
TIM	528	K	TIM	916	K
TIM	528	K	TIM	1166	K
TIM	528	K	TIM	727	K
TIM	809	S	TIM	861	K
TIM	861	K	TIM	930	K
TIM	930	K	TIM	1144	K
TIM	930	K	TIM	1085	K
TIM	1066	K	TIM	1144	K
TIM	1066	K	TIM	1106	K
TIM	1066	K	TIM	1143	K
TIM	1066	K	TIM	1162	K
TIM	1066	K	TIM	1158	K
TIM	1074	S	TIM	1144	K
TIM	1085	K	TIM	1144	K
TIM	1085	K	TIM	1142	K
TIM	1085	K	TIM	1158	K
TIM	1085	K	TIM	1196	K
TIM	1085	K	TIM	1143	K
TIM	1085	K	TIM	1127	K
TIM	1085	K	TIM	1162	K
TIM	1085	K	TIM	1114	K
TIM	1085	K	TIM	1149	S
TIM	1085	K	TIM	1099	S
TIM	1089	T	TIM	1142	K
TIM	1099	S	TIM	1144	K
TIM	1106	K	TIM	1144	K
TIM	1106	K	TIM	1127	K
TIM	1127	K	TIM	1142	K
TIM	1127	K	TIM	1144	K
TIM	1127	K	TIM	1196	K

TIM	1127	K	TIM	1158	K
TIM	1142	K	TIM	1149	S
TIM	1142	K	TIM	1158	K
TIM	1142	K	TIM	1196	K
TIM	1142	K	TIM	1162	K
TIM	1142	K	TIM	1144	K
TIM	1142	K	TIM	1166	K
TIM	1143	K	TIM	1166	K
TIM	1144	K	TIM	1196	K
TIM	1144	K	TIM	1166	K
TIM	1144	K	TIM	1197	K
TIM	1158	K	TIM	1196	K
TIM	1158	K	TIM	1166	K
TIM	1162	K	TIM	1196	K
TIM	1166	K	TIM	1196	K
TIPIN	66	K	TIPIN	87	K
TIPIN	66	K	TIPIN	134	K
TIPIN	66	K	TIPIN	93	K
TIPIN	66	K	TIPIN	101	K
TIPIN	66	K	TIPIN	217	K
TIPIN	66	K	TIPIN	141	K
TIPIN	66	K	TIPIN	91	K
TIPIN	66	K	TIPIN	207	K
TIPIN	66	K	TIPIN	222	S
TIPIN	66	K	TIPIN	129	Y
TIPIN	66	K	TIPIN	89	K
TIPIN	66	K	TIPIN	117	K
TIPIN	87	K	TIPIN	194	S
TIPIN	87	K	TIPIN	207	K
TIPIN	87	K	TIPIN	141	K
TIPIN	87	K	TIPIN	101	K
TIPIN	87	K	TIPIN	91	K
TIPIN	87	K	TIPIN	217	K
TIPIN	87	K	TIPIN	294	S
TIPIN	89	K	TIPIN	194	S
TIPIN	89	K	TIPIN	141	K
TIPIN	89	K	TIPIN	217	K

TIPIN	91	K	TIPIN	101	K
TIPIN	91	K	TIPIN	207	K
TIPIN	91	K	TIPIN	217	K
TIPIN	93	K	TIPIN	134	K
TIPIN	93	K	TIPIN	207	K
TIPIN	93	K	TIPIN	141	K
TIPIN	93	K	TIPIN	217	K
TIPIN	93	K	TIPIN	194	S
TIPIN	101	K	TIPIN	217	K
TIPIN	101	K	TIPIN	194	S
TIPIN	101	K	TIPIN	207	K
TIPIN	101	K	TIPIN	141	K
TIPIN	117	K	TIPIN	217	K
TIPIN	133	K	TIPIN	217	K
TIPIN	133	K	TIPIN	141	K
TIPIN	133	K	TIPIN	207	K
TIPIN	134	K	TIPIN	217	K
TIPIN	134	K	TIPIN	207	K
TIPIN	138	T	TIPIN	207	K
TIPIN	141	K	TIPIN	207	K
TIPIN	141	K	TIPIN	217	K
TIPIN	207	K	TIPIN	217	K
TIPIN	207	K	TIPIN	224	T

Table 29: Reproducible intermolecular crosslinks of the TIM/TIPIN complex. Crosslinks are highlighted as black lines in Figure 37.

Protein1	**SeqPos1**	**LinkedRes1**	**Protein2**	**SeqPos2**	**LinkedRes2**
TIM	313	K	TIPIN	207	K
TIM	313	K	TIPIN	217	K
TIM	427	K	TIPIN	66	K
TIM	427	K	TIPIN	217	K
TIM	427	K	TIPIN	207	K
TIM	528	K	TIPIN	93	K
TIM	528	K	TIPIN	207	K
TIM	861	K	TIPIN	134	K

TIM	861	K	TIPIN	207	K
TIM	916	K	TIPIN	141	K
TIM	921	K	TIPIN	207	K
TIM	921	K	TIPIN	93	K
TIM	930	K	TIPIN	217	K
TIM	1085	K	TIPIN	66	K
TIM	1085	K	TIPIN	217	K
TIM	1085	K	TIPIN	93	K
TIM	1085	K	TIPIN	87	K
TIM	1106	K	TIPIN	87	K
TIM	1106	K	TIPIN	89	K
TIM	1127	K	TIPIN	134	K
TIM	1127	K	TIPIN	66	K
TIM	1142	K	TIPIN	141	K
TIM	1142	K	TIPIN	134	K
TIM	1142	K	TIPIN	66	K
TIM	1144	K	TIPIN	87	K
TIM	1144	K	TIPIN	207	K
TIM	1144	K	TIPIN	194	S
TIM	1144	K	TIPIN	93	K
TIM	1144	K	TIPIN	66	K
TIM	1144	K	TIPIN	134	K
TIM	1144	K	TIPIN	141	K
TIM	1158	K	TIPIN	87	K
TIM	1162	K	TIPIN	66	K
TIM	1166	K	TIPIN	87	K
TIM	1196	K	TIPIN	207	K
TIM	1196	K	TIPIN	93	K
TIM	1196	K	TIPIN	66	K
TIM	1196	K	TIPIN	87	K
TIM	1196	K	TIPIN	134	K
TIM	1196	K	TIPIN	133	K

TTP/CRY2 – Intermolecular Links

Table 30: Reproducible intermolecular crosslinks of the TTP/CRY2 complex. Crosslinks are highlighted as black lines in Figure 45 and Figure 47.

Protein1	SeqPos1	LinkedRes1	Protein2	SeqPos2	LinkedRes2
TIM	288	K	CRY2	456	K
TIM	1066	K	CRY2	576	K
TIM	1085	K	CRY2	562	K
TIM	1085	K	CRY2	576	K
TIM	1085	K	CRY2	247	K
TIM	1085	K	CRY2	293	K
TIM	1085	K	CRY2	485	Y
TIM	1085	K	CRY2	242	K
TIM	1085	K	CRY2	475	K
TIM	1142	K	CRY2	576	K
TIM	1142	K	CRY2	242	K
TIPIN	66	K	CRY2	576	K
TIPIN	66	K	CRY2	504	K
TIPIN	66	K	CRY2	242	K
TIPIN	138	T	CRY2	150	T
TIPIN	138	T	CRY2	148	S
TIPIN	138	T	CRY2	145	T
TIPIN	141	K	CRY2	152	Y
TIPIN	141	K	CRY2	150	T
TIPIN	141	K	CRY2	148	S
TIPIN	207	K	CRY2	164	K
TIPIN	207	K	CRY2	247	K
TIPIN	207	K	CRY2	456	K
TIPIN	207	K	CRY2	242	K
TIPIN	217	K	CRY2	242	K
TIPIN	217	K	CRY2	293	K
TIM	427	K	TIPIN	66	K
TIM	511	K	TIPIN	207	K
TIM	771	K	TIPIN	93	K
TIM	809	S	TIPIN	141	K
TIM	816	S	TIPIN	141	K
TIM	861	K	TIPIN	141	K
TIM	861	K	TIPIN	66	K
TIM	882	K	TIPIN	207	K
TIM	882	K	TIPIN	66	K
TIM	882	K	TIPIN	141	K

TIM	882	K	TIPIN	87	K
TIM	921	K	TIPIN	207	K
TIM	921	K	TIPIN	91	K
TIM	921	K	TIPIN	87	K
TIM	921	K	TIPIN	141	K
TIM	921	K	TIPIN	66	K
TIM	930	K	TIPIN	66	K
TIM	930	K	TIPIN	141	K
TIM	930	K	TIPIN	134	K
TIM	930	K	TIPIN	207	K
TIM	945	K	TIPIN	93	K
TIM	1085	K	TIPIN	66	K
TIM	1085	K	TIPIN	217	K
TIM	1085	K	TIPIN	207	K
TIM	1127	K	TIPIN	134	K
TIM	1142	K	TIPIN	207	K
TIM	1142	K	TIPIN	141	K
TIM	1142	K	TIPIN	217	K
TIM	1142	K	TIPIN	66	K
TIM	1144	K	TIPIN	207	K
TIM	1144	K	TIPIN	87	K
TIM	1158	K	TIPIN	66	K
TIM	1158	K	TIPIN	141	K
TIM	1162	K	TIPIN	66	K
TIM	1166	K	TIPIN	87	K
TIM	1167	K	TIPIN	87	K
TIM	1196	K	TIPIN	207	K

TTP/CRY2 – Intramolecular crosslinks

Table 31: Reproducible intramolecular crosslinks of the TTP/CRY2 complex. Crosslinks are highlighted as black lines in Figure 43 and Figure 44.

Protein1	SeqPos1	LinkedRes1	Protein2	SeqPos2	LinkedRes2
CRY2	108	K	CRY2	576	K
CRY2	108	K	CRY2	134	K
CRY2	108	K	CRY2	562	K
CRY2	164	K	CRY2	456	K

CRY2	184	K	CRY2	293	K
CRY2	242	K	CRY2	266	S
CRY2	242	K	CRY2	576	K
CRY2	242	K	CRY2	262	S
CRY2	242	K	CRY2	271	S
CRY2	242	K	CRY2	562	K
CRY2	242	K	CRY2	504	K
CRY2	247	K	CRY2	271	S
CRY2	247	K	CRY2	266	S
CRY2	247	K	CRY2	576	K
CRY2	247	K	CRY2	562	K
CRY2	454	K	CRY2	478	K
CRY2	454	K	CRY2	485	Y
CRY2	454	K	CRY2	504	K
CRY2	456	K	CRY2	478	K
CRY2	456	K	CRY2	576	K
CRY2	475	K	CRY2	504	K
CRY2	475	K	CRY2	576	K
CRY2	478	K	CRY2	504	K
CRY2	504	K	CRY2	576	K
CRY2	576	K	CRY2	590	S
TIM	264	K	TIM	313	K
TIM	264	K	TIM	288	K
TIM	264	K	TIM	727	K
TIM	281	S	TIM	1085	K
TIM	299	K	TIM	313	K
TIM	299	K	TIM	1144	K
TIM	299	K	TIM	1106	K
TIM	307	Y	TIM	316	K
TIM	309	S	TIM	1144	K
TIM	309	S	TIM	317	K
TIM	313	K	TIM	1144	K
TIM	313	K	TIM	1142	K
TIM	313	K	TIM	1143	K
TIM	313	K	TIM	1085	K
TIM	313	K	TIM	1162	K
TIM	313	K	TIM	1127	K

TIM	313	K	TIM	317	K
TIM	511	K	TIM	1144	K
TIM	528	K	TIM	1144	K
TIM	528	K	TIM	687	K
TIM	528	K	TIM	916	K
TIM	528	K	TIM	1166	K
TIM	528	K	TIM	727	K
TIM	809	S	TIM	861	K
TIM	861	K	TIM	930	K
TIM	930	K	TIM	1144	K
TIM	930	K	TIM	1085	K
TIM	1066	K	TIM	1144	K
TIM	1066	K	TIM	1106	K
TIM	1066	K	TIM	1143	K
TIM	1066	K	TIM	1162	K
TIM	1066	K	TIM	1158	K
TIM	1074	S	TIM	1144	K
TIM	1085	K	TIM	1144	K
TIM	1085	K	TIM	1142	K
TIM	1085	K	TIM	1158	K
TIM	1085	K	TIM	1196	K
TIM	1085	K	TIM	1143	K
TIM	1085	K	TIM	1127	K
TIM	1085	K	TIM	1162	K
TIM	1085	K	TIM	1114	K
TIM	1085	K	TIM	1149	S
TIM	1085	K	TIM	1099	S
TIM	1089	T	TIM	1142	K
TIM	1099	S	TIM	1144	K
TIM	1106	K	TIM	1144	K
TIM	1106	K	TIM	1127	K
TIM	1127	K	TIM	1142	K
TIM	1127	K	TIM	1144	K
TIM	1127	K	TIM	1196	K
TIM	1127	K	TIM	1158	K
TIM	1142	K	TIM	1149	S
TIM	1142	K	TIM	1158	K

TIM	1142	K	TIM	1196	K
TIM	1142	K	TIM	1162	K
TIM	1142	K	TIM	1144	K
TIM	1142	K	TIM	1166	K
TIM	1143	K	TIM	1166	K
TIM	1144	K	TIM	1196	K
TIM	1144	K	TIM	1166	K
TIM	1144	K	TIM	1197	K
TIM	1158	K	TIM	1196	K
TIM	1158	K	TIM	1166	K
TIM	1162	K	TIM	1196	K
TIM	1166	K	TIM	1196	K
TIPIN	66	K	TIPIN	87	K
TIPIN	66	K	TIPIN	134	K
TIPIN	66	K	TIPIN	93	K
TIPIN	66	K	TIPIN	101	K
TIPIN	66	K	TIPIN	217	K
TIPIN	66	K	TIPIN	141	K
TIPIN	66	K	TIPIN	91	K
TIPIN	66	K	TIPIN	207	K
TIPIN	66	K	TIPIN	222	S
TIPIN	66	K	TIPIN	129	Y
TIPIN	66	K	TIPIN	89	K
TIPIN	66	K	TIPIN	117	K
TIPIN	87	K	TIPIN	194	S
TIPIN	87	K	TIPIN	207	K
TIPIN	87	K	TIPIN	141	K
TIPIN	87	K	TIPIN	101	K
TIPIN	87	K	TIPIN	91	K
TIPIN	87	K	TIPIN	217	K
TIPIN	87	K	TIPIN	294	S
TIPIN	89	K	TIPIN	194	S
TIPIN	89	K	TIPIN	141	K
TIPIN	89	K	TIPIN	217	K
TIPIN	91	K	TIPIN	101	K
TIPIN	91	K	TIPIN	207	K
TIPIN	91	K	TIPIN	217	K

TIPIN	93	K	TIPIN	134	K
TIPIN	93	K	TIPIN	207	K
TIPIN	93	K	TIPIN	141	K
TIPIN	93	K	TIPIN	217	K
TIPIN	93	K	TIPIN	194	S
TIPIN	101	K	TIPIN	217	K
TIPIN	101	K	TIPIN	194	S
TIPIN	101	K	TIPIN	207	K
TIPIN	101	K	TIPIN	141	K
TIPIN	117	K	TIPIN	217	K
TIPIN	133	K	TIPIN	217	K
TIPIN	133	K	TIPIN	141	K
TIPIN	133	K	TIPIN	207	K
TIPIN	134	K	TIPIN	217	K
TIPIN	134	K	TIPIN	207	K
TIPIN	138	T	TIPIN	207	K
TIPIN	141	K	TIPIN	207	K
TIPIN	141	K	TIPIN	217	K
TIPIN	207	K	TIPIN	217	K
TIPIN	207	K	TIPIN	224	T

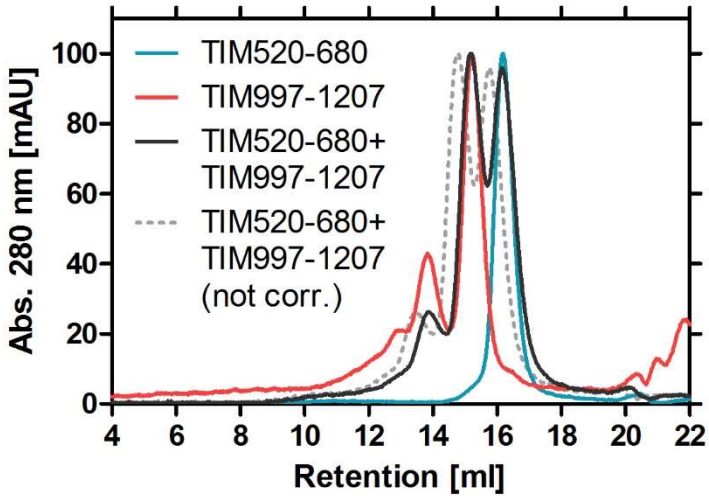

Figure 73: Uncorrected Chromatogram of the SEC interaction analysis of TIM520-680 with TIM997-1207.

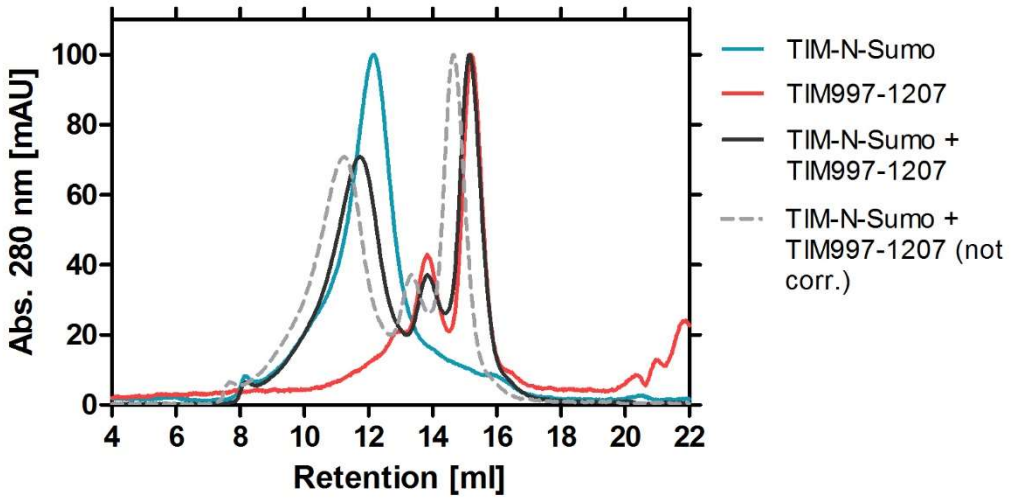

Figure 74: Uncorrected chromatogram of the SEC interaction analysis of TIM-N-Sumo with TIM997-1207.

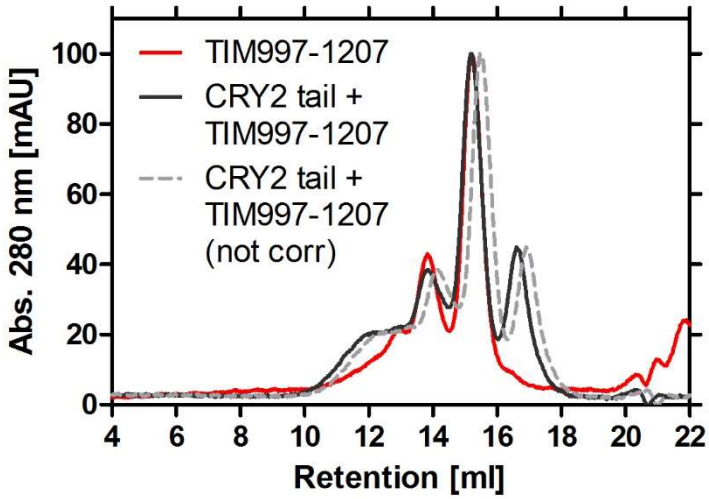

Figure 75: Uncorrected migration curve of the SEC interaction analysis of TIM997-1207 with the CRY2 tail.

9 Danksagung

The content of this section was removed for privacy.